Faculty of Engineering Aswan University

Design and Techno-economic Analysis of Different Gasifiers for Bioenergy Application

By

Hoda Abd El-Sattar Hemaid Ibrahim

M.Sc., Electrical Engineering, Aswan University

A Thesis Submitted to the Faculty of Engineering

Aswan University (ASWU)

In Partial Fulfillment of the Requirements for the Degree of

Doctor of Philosophy

In

Electrical Engineering

October 2022

Design and Techno-economic Analysis of Different Gasifiers for Bioenergy Application

Submitted By

Hoda Abd El-Sattar Hemaid Ibrahim

M.Sc., Electrical Engineering, Aswan University

For the degree of

Doctor of Philosophy

In

Electrical Engineering

Supervision Committee

Title/Name	Affiliation	Signature
Prof. Loai Saad Eldeen Nasrat	Elec. Eng. Dept., ASWU, Aswan, Egypt	
Prof. Francisco Jurado Melguizo	Elec. Eng. Dept., Jaen University, Spain	
Assoc. Prof. Salah Mohamed Kamel	Elec. Eng. Dept., ASWU, Aswan, Egypt	

Examination Committee

Title/Name	Affiliation	Signature
Prof. Walid Aly Seif El-Islam El-Khattam	Ain Shams University, Cairo, Egypt	
Prof. Abdalla Ahmed Ibrahiem	Aswan University, Aswan, Egypt	
Prof. Loai Saad Eldeen Nasrat	Aswan University, Aswan, Egypt	

Declaration and Certificate of Originality

I certify that in the preparation of this thesis, I have observed the provisions of the scientific code of ethics. Further, I certify that this work is free of plagiarism and all materials appearing in this thesis have been properly quoted and attributed.

I certify that all copyrighted material incorporated into this thesis is in compliance with the international copyright law and that I have received written permission from the copyright owners for my use of their work, which is beyond the scope of the law.

I agree to indemnify and save harmless Faculty of Engineering, Aswan University from any and all claims that may be asserted or that may arise from any copyright violation.

I hereby certify that the research work in this thesis is my original work and it does not include any copied parts without the appropriate citation.

Hoda Abd El-Sattar,

October, 2022

ABSTRACT

Exploration and exploitation of renewable energy resources are of particular importance for enhancing energy security to reduce dependence on fossil fuels and to decrease the effects of global warming (reduce carbon emissions). Biomass is one of the few renewable energy sources whose availability is not dependent on weather conditions and can be stored in accordance with demand and, as so, electricity generation from it can be highly predictable. Biomass can be converted into different forms of energy using various processes such as the gasification process. Biomass tri-generation is a relatively new concept, which has the potential to improve the bioenergy economics for areas with warm climate. This concept can be applied with various energy conversion technologies.

In addition, this thesis optimal performance assessment is performed on two different small scales combined cooling, heat and power systems (CCHP) to comparatively assess the highly integrated system. the first CCHP system consists of the integration of a downdraft fixed bed gasifier with externally fired gas turbine (EFGT) (power generation system), a heat recovery device, and the absorption cooling cycle using Corn Stover (CS) as the biomass feedstock, while the second system consists of a direct burning combustor unit, an EFGT, an organic Rankine cycle (ORC) as bottoming unit for maximizing the electrical efficiency, and an absorption refrigeration unit for cooling power production using sugarcane bagasse as the biomass feedstock.

Despite considerable development on a global scale in the technologies associated with the renewable energy sources, electricity shortage and cost is still a problem in remote isolated regions and on islands with abundant renewable resources of energy. So that, this thesis also presents a techno-economic design of different stand-alone hybrid power system scenarios for different case study areas in Egypt, these different models for optimal techno-economic models are based on integrating the biomass gasifier units with other sustainability sources such as solar, wind energy, etc.

The design simulations performed using Cycle-Tempo thermodynamics software for solving the optimal performance design for small-scale CCHP system. A recent and modified optimization algorithms based on utilizing MATLAB software for solving the techno-economic analysis of an isolated hybrid micro grid that consists of biomass gasifier, photovoltaic panels, wind turbines, and batteries or fuel cell for satisfying the electricity demands in a small villages or remote areas in Egypt.

RESUMEN

La exploración y explotación de recursos de energía renovable son de particular importancia para mejorar la seguridad energética para reducir la dependencia de los combustibles fósiles y disminuir los efectos del calentamiento global (reducir las emisiones de carbono). La biomasa es una de las pocas fuentes de energía renovable cuya disponibilidad no depende de las condiciones climáticas y puede almacenarse de acuerdo con la demanda, por lo que la generación de electricidad a partir de ella puede ser altamente predecible. La biomasa se puede convertir en diferentes formas de energía mediante varios procesos, como el proceso de gasificación. La trigeneración de biomasa es un concepto relativamente nuevo, que tiene el potencial de mejorar la economía de la bioenergía para áreas con clima cálido. Este concepto se puede aplicar con varias tecnologías de conversión de energía.

Además, la evaluación del rendimiento óptimo de esta tesis se realiza en dos sistemas combinados diferentes de refrigeración, calor y energía a pequeña escala para evaluar comparativamente el sistema altamente integrado. El sistema combinado de refrigeración, calor y energía consiste en la integración de un gasificador de lecho fijo de tiro descendente con turbina de gas alimentada externamente (sistema de generación de energía), un dispositivo de recuperación de calor y el ciclo de refrigeración por absorción utilizando Corn Stover como materia prima de biomasa, mientras que el segundo El sistema consta de una unidad de combustión de combustión directa, una turbina de gas de combustión externa, un ciclo Rankine orgánico como unidad de fondo para maximizar la eficiencia eléctrica y una unidad de refrigeración por absorción para enfriar la producción de energía utilizando bagazo de caña de azúcar como materia prima de biomasa.

A pesar del considerable desarrollo a escala mundial de las tecnologías asociadas a las fuentes de energía renovable, la escasez y el coste de la electricidad sigue siendo un problema en regiones remotas y aisladas y en islas con abundantes recursos renovables de energía. Por lo tanto, esta tesis también presenta un diseño tecno económico de diferentes escenarios de sistemas de energía híbridos autónomos para diferentes áreas de estudio de casos en Egipto, estos diferentes modelos para modelos tecno económicos óptimos se basan en la integración de las unidades de gasificación de biomasa con otras fuentes de sostenibilidad. como la energía solar, eólica, etc.

Las simulaciones de diseño se realizaron con el software de termodinámica Cycle-Tempo para resolver el diseño de rendimiento óptimo para sistemas combinados de refrigeración,

calor y energía a pequeña escala. Algoritmos de optimización recientes y modificados basados en la utilización del software MATLAB para resolver el análisis tecno económico de una microrred híbrida aislada que consiste en un gasificador de biomasa, paneles fotovoltaicos, turbinas eólicas y baterías o celdas de combustible para satisfacer la demanda de electricidad en pequeños pueblos. o áreas remotas en Egipto.

*'This thesis is dedicated to the memory of my deceased niece '**Rahma Eid**', whose support, attention, and perseverance inspired me throughout the duration of my studies.'*

To all who have been great support and encouragement for me,

I dedicate this work.

ACKNOWLEDGEMENT

First of all, my gratitude and thanks for "**ALLAH**" of giving me patience and ability to complete this thesis. I would like to take this opportunity to extend my heartfelt appreciation to this following persons whose have contribute directly or indirectly towards the completion of the thesis.

I would say thanks to my supervisors **Prof. Loai Saad Eldeen Nasrat** and **Prof. Francisco Jurado** to guide me well throughout the research work. Their immense knowledge, motivation and patience have given me more power and spirit to excel in the research writing. They are my mentor and better advisors for my doctorate study beyond the imagination. It would not have been possible to conduct this research without their precious support.

No words of thanks can express my feeling toward my supervisor **Assoc. Prof. Salah Mohamed Kamel,** who supported me, encouraged me, and advanced me always. Without his guidance and challenging, I would never have been able to achieve this work. Moreover, I want to point to his humanism, and his higher level of manners. I feel honored to have been given the opportunity to work under his supervision.

My special thanks go out to **Dr.Hamdy Sultan,** Faculty of Engineering, Minia University, Egypt, for his valuable guidance's, suggestions, generous assistance and continuous encouragement during my study.

My appreciation also goes to my colleagues in Advanced Power Systems Research Laboratory (APSR Lab), Faculty of Engineering, Aswan University, & "Sala de Investigadores", University of Jaen, Spain, for the friendly academic atmosphere, the useful discussions, and their encouragement.

No words of thanks can express my feeling towards **my family**, especially **my parents**. They always stand beside me, encourage me and present the advices to me. Without their guidance, I would never be able to do this thesis. Finally, I would like to thank all my friends who have given me so much attention and support during my study.

Eng. Hoda Abd El-Sattar

October. 2022

Table of Contents

Table of Contents

List of Figures

List of Tables

Nomenclature

Acronyms

ABC	Artificial Bee Colon Algorithm
AHA	Artificial Hummingbird Algorithm
ALO	Antlion Optimizer
ANNs	Artificial Neural Networks
AO	Aquila Optimizer
ASC	Annualized System Cost
ATC	Annual Total Cost
BG	Biomass Gasifier
BSA	Backtracking Search Algorithm
CCHP	Combining Cooling, Heat, and Power
CD	Critical Density
CEC	Congress on Evolutionary Computation
CFA	Franklin's and Coulomb's Algorithm
CHP	Combined Heat and Power
CP	Critical Pressure
CPR	System Cooling to Power Ratio
CR	Circulation Ratio
CRH	Hierarchy of Corporate Rank
CS	Corn Stover
CSA	Cuckoo Search Algorithm
CT	Critical Temperature
DG	Diesel Generator
DPSP	Deficiency of Power Supply Probability
EC	Energy Cost
EDE	Enhanced Differential Evolution
EFGT	Externally Fired Gas Turbine
ELE	Electrolyzer
ELF	Equivalent Loss Factor
ESQ	Enhanced Solution Quality Mechanism

FC	Fuel Cells
FFA	Firefly algorithm
FPA	Flower Pollination Algorithm
GA	Genetic Algorithm
GAHA	Gradient Artificial Hummingbird Algorithm
GBO	Gradient Based Optimizer
GHG	Greenhouse Gas Emissions
GIS	Geographic Information System
GOA	Grasshopper Optimization Algorithm
GWO	Gray Wolf Optimizer
GWP	Global Warming Potential
HBA	Honey Badger Algorithm
HBO	Heap-Based Optimizer
HE	Heat Exchanger
HHO	Harris Hawks Optimizer
HOMER	Multiple Energy Sources Hybrid Optimization Model
HRPS	Hybrid Renewable Power Systems
HRS	Recovery Vapor Generator
HSA	Harmony Search Algorithm
HT	Hydrogen Tank
HTHE	High Temperature Heat Exchanger
IHOGA	Improved Hybrid Optimization by Genetic Algorithms
IHSA	Improved Harmony Search Algorithm
IRENA	International Renewable Energy Agency
LCC	Life Cycle Cost
LEO	Local Escaping Operator
LOEE	Loss of Energy Expected
LOLE	Loss of Load Expected
LOLH	Loss of Load Hours
LPSP	loss of power supply probability
MAE	Mean Absolute Error
MFO	Moth-Flame Optimizer

MGT	Micro Gas Turbine
Mha	Million Hectares
MOA	Mayfly Optimization Algorithm
MOOP	Multi-Objective Optimization Problem
MOSaDE	Multi-Objective Self-Adaptive Differential Evolution
MPPT	Maximum Power Point Tracking
MVO	Multi-Verse Optimizer
NASA	National Aeronautics and Space Administration
NBP	Normal Boiling Point
NPC	Net Present Cost
ODP	Ozone Depletion Potential
ORC	Organic Rankine Cycle
PC	Performance Coefficient
PEMFC	Polymer Electrolyte Membrane
PPTD	Pinch Point Temperature Difference
PSO	Particle Swarm Optimization
PSOGSA	Hybrid Particle Swarm-Gravitational Search Algorithm
PV	Solar Photovoltaic
RE	Relative Error
REF	Renewable Energy Fraction
RES	Renewable Energy Sources
RK	Runge Kutta Search Mechanism
RMSE	The root mean square error
RUN	RUNge Kutta Algorithm
SA	Simulated Annealing
SCA	Sine Cosine Algorithm
SD	Standard Deviation
SDO	Supply Demand-Based Optimization
SHO	Selfish Herd Optimizer
SMA	Slime Mould Algorithm
SOA	Seagull Optimization Algorithm
SOC	State of Charge

SOFC	Solid Oxide Fuel Cell
SSA	Salp Swarm Algorithm
SSO	Social Spider Optimizer
STOA	Sooty Tern Optimization Algorithm
TIT	Turbine Inlet Temperature
TLBO	Teaching-Learning Based Optimization
TLO	Teaching Learning Based Optimization
TRNSYS	Transient Energy System Software Program
TSO	Transient Search Optimization Algorithm
UL	Unmet Load
VAC	Vapor Absorption Cooling
WCA	Water Cycle Algorithm
WHO	Wild Horse Optimizer
WOA	Whale Optimization Algorithm
WT	Wind Turbine

Symbols

η_{Hg}	The hot syngas efficiency
(r)	A random value between $[0,1]$
(t)	The current iteration
$\overrightarrow{S_c}$	The search agent location
$\overrightarrow{S_p}$	The present location of the search agent
$\overrightarrow{v_b}$	A parameter that is randomly lying between $[-a, a]$
$\overrightarrow{v_c}$	A parameter that decreases linearly from one to zero
$\overrightarrow{X_A}$ and $\overrightarrow{X_B}$	Two individuals randomly selected from the swarm
$\overrightarrow{X_b}$	The position of individuals with the highest order concentration that is currently found
B_{CH}	The charging energy
B_{DIS}	The discharging energy
BE_T	The total biomass consumption

B_{rated}	The biomass consumption rate per hour (kg/h)
C_A^{cap}	The capital cost annual interest
C_A^{fuel}	The feedstock's annual fuel cost
C_B	A uniformly distributed arbitrary coefficient
C_f	Parameter to control the frequency of employing variable (A)
$C_{O\&M,r}$	The components operation and maintenance cost
C_{pg}	The specific heat capacity of syngas
cp_w	The specific heat capacity of water (kJ kg^{-1} K^{-1})
$C_{rep,r}$	The components replacement cost
c_ω	The walk coefficient
D_A	The movement of the sooty tern in the search field
E_{Con}	The energy consumption (kWh)
$F_{Cons_{BG}}(t)$	The average fuel consumption per hour
F_0	The no-load fuel consumption
FC_P	The generated electrical power from PEMFC
F_m	The marginal fuel consumption
G_i	The distance between the search agent and the best one
HHV_H	The higher heat value of the stored hydrogen gas (kWh/kg)
H_p	The specific enthalpy of the pipes
$HT_E(t)$	The stored hydrogen energy in the HT at time step (t)
HT_m	The stored hydrogen mass in the HT
$HT_m(t)$	The stored hydrogen mass at time step (t)
ite_{max}	The maximum iteration number
k_1 and k_2	Attraction constants for evaluating the cognitive and social behaviors
LHV_B	The lower heat value of the biomass feedstock
LHV_{pg}	The lower heat value of syngas
m_{air}	The mass ratio of air
m_{air}	The air mass flow rate (kg/s)
m_B	The mass flow of the biomass feedstock

m_{fuel}	The mass ratio of fuel
m_{ORC}	The working fluid mass flow
m_{pg}	The mass flow of syngas
m_{w}	The water mass flow (kg/s)
N_{BG}	The number of biomass generators
N_{pv}	The number of PV modules
N_{wt}	The number of WTs in the wind farm
$P_{EL_{th}}$	The thermal power
P_{aux}	The additional electrical consumption of other components
$pbest_{ij}$	The best position reached by the i-th mayfly in the i-th dimension
$P_{BG}(t)$	The generator output power
P_{c}	The EFGT compressor work consumption (kW)
P_{dum}	The dummy load
P_{EL}	The net electrical power
$P_{ELE/HT}$	The energy transferred to the hydrogen tank from electrolyzer
P_{ex}	The excess power
P_{FP}	The power consumption of feed pump
PG_{rated}	The rated power of biomass generators
$P_{HT/FC}(t)$	The power supplied towards the FC from the HT

Chapter 1

Introduction

Chapter 1

Introduction

1.1. Introduction of Energy

The increased use of fossil fuels has led to rise in the atmospheric CO_2 levels, which has led to a rise in the temperature of the globe, which is known as the phenomenon of climate change [1]. This phenomenon is considered one of the most serious environmental challenges facing the world during the modern century. In addition, the growing in population density around the world and the increase in the level of energy consumption to provide for basic needs and the high level of well-being led to an increase in the amount of need for energy and this is what led most developed countries to search for alternative energy solutions. Where the use of renewable energies is the best solution to provide the need for energy and reduce as much as possible dependence on traditional energy sources and decrease the GHG [2].

The sustainable energy trade has recently increased, which is considered one of the businesses that intervene in converting renewable energies into sources of income and promote them. In recent decades, many countries have increased their interest in exploiting and investing in renewable energy sources (RES) to contribute to electricity production and curb climate change [3]. According to the International Energy Agency (IEA), with the increase in renewable energy projects until the end of 2019, renewable energy generation increased by about 3% and the share of sustainable energy in global electricity generation has jumped to nearly 28% [4].

Energy is not represented as electricity only; energy is the pillar of the economy and a source of sustainable development. It can be said that the energy problem in the world still lies in the required diversity, and despite the improvement in the utilization of RES, the growth in the use of renewable energy is still below the required level. This indicates that fossil energy is still dominant in the production of energy, and the reason can be attributed to the fact that generating renewable energy is still relatively expensive. However, it is planned that by the year 2030, RES, which include hydropower, WT, PV, bio-energy, geothermal energy, and marine energy, will contribute approximately 40% of the electricity supply [5].

1.2. State of Energy in Egypt

Egypt is one of the countries that work to promote the utilization of RES, encourage and develop its technologies, and exploit its resources to maximize the efficient utilization of various sources to contribute to promoting economic growth, preserving the environment, and achieving leadership in the area of sustainable power for resources [6]. Egypt is one of a few countries that have huge potential to exploit renewable energy. It has the ability to generate renewable energy from all sources: hydropower, wind, solar energy, and biomass, in addition to the fact that the vast desert areas make it well suited for the development of renewable energy projects.

In recent years, Egypt has been striving to create and develop different projects for increasing the share of RES. Solar, wind, and hydro energies are the most widely used RES in Egypt that contribute in the production of electricity [7]. The energy sector in Egypt plays an important role in economic development, as it presents around 13.1% of the gross domestic product [8]. Therefore, the Egyptian government is working on setting the necessary policies and strategies to develop the energy sector, diversify energy sources, and encourage investment in renewable energies sources in order to meet the increasing energy demand, to enhance the role of renewable energy and energy efficiency in order to ensure the continuity of security and energy supplies [9]. According to IRENA, the goal of this strategy is to obtain 20% of the total electric energy through renewable energies (wind energy contributes about 12%, 6% hydro and 2% solar) by 2022 and 42% by 2035 [9]. The objective of this strategy is to provide the necessary energy supplies for development needs, including identifying the optimal mix of energy, developing reliance on its renewable sources, and raising the efficiency of its use [10]. According to the data from IRENA in 2018, Figure 1.1, presented the renewable sources generation statues (GWh) in Egypt.

Although Egypt has large potential for biomass resources, especially from agricultural waste and wood, biomass energy is used in Egypt on a limited scale Annually, approximately twenty-one million tons of agricultural waste are discarded [11]. Still, latest technological developments provide important opportunities to expand the use of biomass energy in Egypt. [12]. Biomass is converted into many usable and versatile forms of energy such as biofuels or syngas, which are one of the most important biomass product, which are obtained through many primary treatment technologies and the most widely used is gasification technology which is used in small scale range [13].

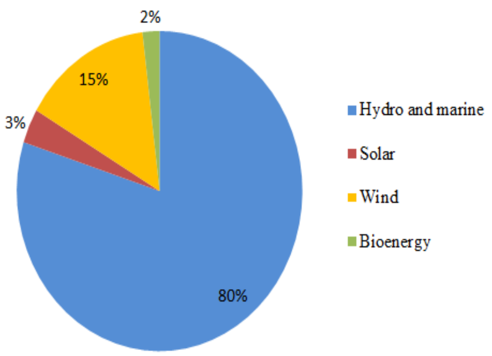

Figure 1. 1: The status of renewable sources generation in Egypt

Hybrid renewable power systems (HRPS) are used to reduce the problem of the changing nature of sustainable power sources and to secure continuous electrical supply to the loads. This can be achieved by combining sustainable and traditional forms of energy, or by combining sustainable sources together using an appropriate strategy so that now when one of these renewable sources is powerful, it is used to cover the failure of other sources. Currently, there are many papers related to studying the performance of HRPSs and studying different optimization algorithms. The purpose of such studies is to assess the system components' maximum capacity and improve the main economic and technical indicators in the design of these systems. In prior researches, several algorithms and software tools have been designed and used in order to improve and determine the optimal design size for an HRPS, these sizing methods, and tools are presented in Figure 1.2.

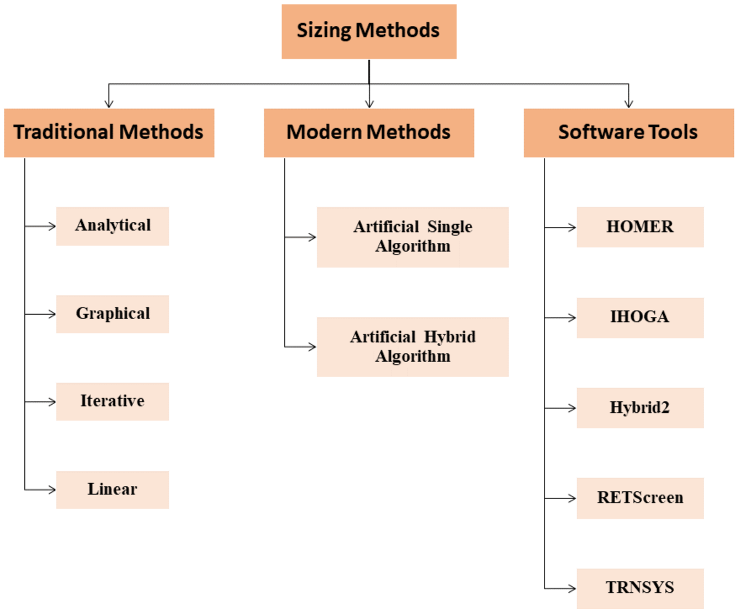

Figure 1. 2: Overview of sizing methods, and tools for HRPS [14], [15].

1.3. Main Objectives of the Thesis

The main objectives of this thesis can be summarized in the following points:

- Study the optimal performance parameters including the operating conditions (maximum pressure, maximum temperature) and the system configuration for a theoretical model combining cooling, heat, and power production (CCHP).
- Optimal performance assessment on two different small scale CCHP systems to comparatively assess the highly integrated system. the first CCHP system consists of the integration of a downdraft fixed bed gasifier with EFGT (power generation system), a heat recovery device, and the absorption cooling cycle using CS as the biomass feedstock, while the second system consists of a direct burning combustor unit, an EFGT, an ORC as bottoming unit for maximizing the electrical efficiency, and an absorption refrigeration unit for cooling power production using sugarcane bagasse as the biomass feedstock.
- Study four working fluids (cyclohexane, benzene, toluene and R113) with the entire system to analyze the optimal ORC working fluid. The simulation has been carried out using the thermodynamics software Cycle-Tempo ("Cycle-Tempo"). NIST Chemistry Web Book ("Thermo physical Properties of Fluid Systems") has been used to study the thermo physical properties of the working fluids.
- Develope different stand-alone HRPSs scenarios have been developed for the optimal sizing performance of integrated biomass units with other renewable energy systems such as PV, WT, Batteries, and Fuel cells (FC).
- The optimal size of the proposed stand-alone HRPSs is solved using different recent optimization algorithms namely, SMA, SOA, HBO, CFA, STOA, RUN, MOA, and AHA.
- The proposed design algorithms are implemented with the aim of resolving the multi-objective optimization under the constraints issue of minimizing the system energy cost (EC), excess energy, the LPSP, and determining the best optimal size of the components, i.e., the number of PV modules, number of WTs, number of biomass generators, number of battery banks, the rated power of the FC, the rated power of the water electrolyzer (ELE), and the mass of the hydrogen gas tank (HT).

- Study the development of the original RUN algorithm, by applying quantum mechanics to the original RUN, and this quantum model called here the QRUN algorithm.
- An enhanced hybrid algorithm called a Gradient Artificial Hummingbird Algorithm (GAHA) based on the combination between a bio-inspired AHA and Gradient based optimizer (GBO) methods.
- Assessing the performance of the proposed algorithms using different standards and several benchmark function tests.
- Comparing and evaluating the results applying the proposed algorithms to the recent and well-known optimization algorithms such as AO algorithm, GWO, WOA, and SCA.

1.4. Thesis Organization

This thesis is structured as follows:

Chapter 1: Introduction

This chapter presents a general overview, the background and the motivation of the study.

Chapter 2: Literature Review.

This chapter discusses the different renewable energy resources (especially biomass), distributed generation, and optimization methods. In addition, this chapter gives a comprehensive survey of the previous solutions that have been suggested to solve the optimal techno economic solution of different HRPSs.

Chapter 3: Development of CCHP System Based on Biomass Gasification

This chapter discusses the modeling of a tri-generation system for converting biomass into electrical, cooling and heat power. This target is achieved by developed two different systems, the first configuration is based on the integration of a downdraft fixed bed gasifier with EFGT (power generation system), a heat recovery device, and the absorption cooling cycle, while the second system consists of direct burning of biomass using a combustor chamber, at atmospheric pressure, connected with EFGT, ORC and absorption cooling system.

Chapter 4: Techno Economic Design of Hybrid Systems with Biomass Gasifier

In this chapter, different stand-alone HRPSs scenarios have been developed for the optimal sizing performance for techno-economic optimization models of integrated biomass units with other renewable energy systems such as PV, WT, Batteries, and FC. The main constraints and objective functions are described in this chapter.

Chapter 5: Recent and Developed Optimization Techniques for Optimal Techno Economic Design

In this chapter, different optimization techniques are proposed to solve optimal sizing problem of HRPSs. In addition, different enhancements and improvements are proposed to improve the performance of the conventional optimization algorithms, which theses algorithms can be summarized as follows; QRUN and GAHA.

Chapter 6: Results and Discussion

This chapter presents the results and discussion of obtaining the optimal sizing of various HRPSs scenarios using different methods. Different test systems are used to validate the performance of the proposed techniques. The results show the power of the proposed techniques to find the best optimal components size and minimize the EC with increasing the reliability of LPSP, which fulfills the required load of isolated societies. The obtained results prove the effectiveness of the proposed techniques compared with well-known and recent optimization algorithms.

Chapter 7: Conclusions and Future Works

This chapter gives a summary of the conclusions and highlights the achievement of this work. In addition, some topics for future work related to the subject of the thesis are also proposed

Chapter 2

Literature Review

Chapter 2

Literature Review

2.1. Overview of Renewable Energy

Energy is not represented as electricity only; energy is the pillar of the economy and a source of sustainable development. It can be said that the energy problem in the world still lies in the required diversity and despite the improvement in the utilization of renewable energy sources. The growth in the use of renewable energy is still below the required level. Egypt is one of a few countries that have huge potential to exploit renewable energy. It has the ability to generate renewable energy from all sources: hydropower, wind, solar energy, and biomass, in addition to the fact that the vast desert areas make it well suited for the development of renewable energy projects. Therefore, the government has created a comprehensive, long-term energy plan in order to ensure the security and continuity of energy supplies. This strategy aims to improve the use and development of clean energy sources in the power sector so that the contribution of renewable energy to electrical energy production is reached about 42% by 2035 [8].

The likelihood of rising energy distribution disparity due to the use of renewable energy sources is significant, ensuring long-term continuous energy distribution while simultaneously reducing emits GHG. This is why most researchers are working on the design and development of distributed energy resources based on the use of renewable sources (PV, WT, Diesel generator (DG), Biomass gasifier (BG), Battery bank, and FC, etc.), especially in rural areas, to be utilized in feeding the required loads [16].

2.1.1. Solar Energy

For the solar energy field, Egypt enjoys direct solar radiation with an intensity that varies from 2000 to 3200 kWh/m^2/year from north to south [17]. The average daily sunshine ranges between 9.3 to 10.8 hours/day. This average ranges from 6 to 8 hours/day in the north, while it rises in the south to range from 8 to 10 hours/day. The number of hours of sunshine increases in summer, especially in June and July to reach a maximum of 12 hours/day [17], [18]. Currently, solar energy projects in Egypt have become one of the strategic axes of the plan to expand reliance on renewable energy, as solar energy represented about 2% of the total energy generated in Egypt during the period from 2012 to 2017 [17]. During 2019-2020, the electricity generated through solar energy reached about 3655 GWh [10].

2.1.2. Wind Energy

Wind energy has a lot of importance because it is one of the important sources of renewable and clean energy. WTs convert the kinetic energy in the wind into usable electrical or mechanical energy. Thus, it is possible to use this energy in homes, dwellings, farms, and many other places. Hence, it is possible to save a lot of money spent on importing other energy sources from abroad, such as oil. The reliance on wind energy in recent years is very large and Wind energy is one of the technological breakthroughs that have brought about a great change in the world. Investment in this energy source is very promising and that is why many countries of the world are interested in it.

Egypt is one of the most important countries with good potential for wind energy, as the average wind speed along the Gulf of Suez is about 10.5 m/s [17]. Egypt is well aware of the importance of wind energy, and in order to exploit it optimally, it follows a long-term strategy, as it is expected that the capacity of wind-generated energy in Egypt will reach 7 GW by 2022. There are many projects based on wind energy in the Gulf of Suez, one project with a capacity of 540 MW is under construction, and another project with a capacity of 580 MW. In addition, there are feasibility studies for several projects in cooperation with external companies such as the French Development Agency, the European Investment Bank, and the European Union [18].

2.1.3. Biomass Energy

Egypt is a country in northern Africa with a stable area size of around 100 Mha (995,450 km^2) [19]. The share of agricultural land (the total cultivated area), which includes the area of arable land, permanent crops, and permanent pastures, in 2018, was about 3.8 Mha (38,360 km^2), while there is no forest area in Egypt [20]. Egypt's arable land for 2018 was about 2.9 million hectares [21]; approximately 75 percent of the agricultural land is arable, while permanent crops covered the remaining area. Egypt is considered one of the poorest countries in the exploitation of biomass in energy production despite the availability of many sources of biomass which are disposed by ways that affect the environment negatively [6]. Agricultural residues are considered the most important biomass sources (each ton of crops produces 5 to 6 tons of waste) [22]. The farmers usually dispose of the residues of crops by burning which has a bad effect on the biological components and organic soil due to its environmental impact on the properties of natural and chemical soil [23]. The total annual production of the remains of Egyptian agriculture is between 45 and 50 million tons (about 12.57 million tons of these remains can produce 189.76 PJ/year of potential energy) [24].

Biomass resources can be considered a suitable solution for addressing the energy shortage by establishing decentralized bioenergy stations based on biomass-specific resources [25]. Biomass can be also used in gas or diesel plants by adding some modern and appropriate equipment. In spite of the electrical benefits of these plants, they also work to reduce the harmful effects of wastes burning on the environment and create new jobs [26]. Biomass sources can be converted into fuel based on many thermodynamics conversion techniques such as gasification technology and direct firing [13].

In an effort to utilize Egypt's biomass usage to generate bioenergy, the Ministry of Environment in co-operation with the Ministry of Electricity has submitted to the Cabinet of Ministries all the necessary studies for the feed-in tariff for electricity generated from waste. In return, the Cabinet of Ministries has issued a decree in 2015 to form a ministerial committee to study all electricity from waste projects. A feed-in tariff will allow the private sector to feed electricity generated by any kind of waste to the grid in exchange for money [23].

In addition, the Ministry of Environment in cooperation with the United Nations Development Programme (UNDP) has taken an off-grid approach to biogas production under the "Bio-energy for Sustainable Rural Development" project, which founded 30 startups that built 1.300 small-scale biogas units. Although biomass is one of the oldest known energy sources of humankind, its current contribution to primary energy consumption in the world is small [24].

2.2. Off Grid Hybrid System

The world's need is increasing every day to reduce dependence on the use of fossil fuels, so finding means, solutions, and alternatives for how to produce the required energy has become of paramount importance. Thus, the push to develop and produce renewable energy globally increases every year, many countries have managed to develop renewable energy projects based on solar and wind energy on a large scale. This progress is essential to the plan to replace renewable energy sources that depend on fossil fuels and establish a solid foundation for a sustainable society [27].

An off-grid power generation is a viable option for supplying electricity to small communities in developing countries that do not have enough money to spend on a continuous connection to the public electric grid and places that are very remote and cannot be easily connected to the grid due to their distance from basic infrastructure; In such circumstances, the utilization of renewable energies can help these places develop more quickly [28]. The most common methods of generating renewable energy are solar and wind energy solutions. Nevertheless, it often depends on the area to decide which resources will be used to get the best results. This could include hydropower and/or biomass energy, as additional means of producing renewable energy. Hybrid Renewable Energy System stations are generally characterized as a combination of two or more various power sources to supply the electrical power required for the loads, it can be a mixture of either traditional and renewable sources or only renewable sources.

An off-grid power generation system causes reliability issues because of the unavailability of electricity backup from the utility grid. Moreover, solar and wind energy's variable nature causes non-linear and erratic energy production, which leads to a power mismatch where the load requirements of the consumer are not satisfied by the capacity production [29]. To overcome this, a hybrid renewable energy system is used with an energy backup unit to meet consumer demand. Where the energy storage system consists of FCs, batteries, etc., thereby the wind and solar energy complementary characteristics are integrated with the energy storage system backup unit to make the system credible and sustainable [30].

2.3. Techno-Economic Issues and Optimization Tools

In order to optimize the hybrid energy systems, many techno-economic issues have been taken into account. Examples of costs taken into account in hybrid systems optimal sizing study include NPC, EC, ASC, and LCC. Most research investigations examine the question of whether energy production can meet load demands [31]. The technical indices used as a result are the LPSP, the LOLE, LOEE, DPSP, LOLH, UL, ELF, and REF [31].

Different methods have been proposed to solve the optimal sizing of isolated hybrid renewable systems; these methods are based on classical software and metaheuristic techniques. The most famous of these software tools used in the optimization process are the Multiple Energy Sources Hybrid Optimization Model (HOMER), Improved Hybrid Optimization by Genetic Algorithms (IHOGA), TRNSYS, and RET Screen [32]. Recently, researchers have used artificial intelligence algorithms (metaheuristic) such as PSO [33], GA

[34], [35], ABC [36], Harmony Search Algorithm (HSA) [37], and GOA [38], and hybrid metaheuristic optimization algorithms such as TLBO + EDE, and TLBO + SSA [39].

2.4. Optimization Algorithms

The optimization field has become widespread everywhere. The optimization method is an important mathematical paradigm that has many uses [40]. It is a general term for some applications (especially engineering and commercial disciplines) that study how to obtain the minimum or maximum of certain factors (such as reducing costs and energy use or increasing revenue, production, performance, and efficiency) under the limitations of certain to make all or some of the indicators are the optimal solution [40].

The general formulation of the optimization problem in engineering design is the selection of a set of parameters (variables) to achieve the optimum value of the design index (target) within a series of related constraints. Therefore, optimization problems can often be expressed as problems in the form of mathematical programming. When implementing engineering optimization design, the engineering design problem should be expressed as a mathematical formula. Optimization algorithms can be divided into two main types, which are old or traditional algorithms and modern or non-traditional algorithms, and these two divisions include four subsections:

1. Classical optimization algorithms; these are the well-known old algorithms such as the Newton-Raphson algorithm, linear programming algorithm, and nonlinear programming algorithm, etc. This type of algorithm falls under the category of traditional algorithms.

2. Meta-heuristic optimization algorithms; they are random or stochastic optimization algorithms, which can come with several names and classifications, such as evolutionary algorithms and natural-inspired algorithms, and population-based algorithms, etc. This type of algorithm falls under the category of modern algorithms.

3. Artificial intelligence based optimization algorithms; these are algorithms that include in their structure either artificial neural networks, or support vector machines, or fuzzy systems, etc. This type of algorithm falls under the category of modern algorithms.

4. Hybrid optimization algorithms; in this type, two or more algorithms are combined together. This combination could be between two classical algorithms, or classical and

meta-heuristic algorithms, or classical and meta-heuristic algorithms, or two meta-heuristic algorithms, etc. This type of algorithm falls under the category of modern algorithms.

2.4.1. Advantages and Disadvantages of Modern Algorithms

Features of modern algorithms

1. These algorithms are easier to learn than the classical algorithms, which is based on pure and complex mathematical methods.
2. They are very powerful algorithms that can reach the area in which the optimal possible result is located, so they are widely used in many recent applications and fields.
3. These algorithms can solve the most difficult problems and programmatically move from one problem to another with the least effort and the best possible results.
4. These algorithms use penalty functions, which make it possible to design a generic optimizer more easily.

Drawbacks of the modern algorithms

1. These algorithms are not construct on the gradient-based like the classical algorithms, but rather on the process of probability and stochastic processes, so a new rounded answer is obtained every time we run these algorithms.
2. To get a quasi-uniform solution in each run, the algorithms must then be run with very large iterations.
3. To understand the philosophy of running these algorithms, some materials and phenomena in biology, physics, astronomy, and chemistry must be studied.

2.4.2. Examples of Recent Algorithms

In this section, a brief explanation of some of the modern optimization algorithms used in this thesis are presented and explained.

2.4.2.1. Slime Mould Algorithm (SMA)

SMA is a new stochastic mathematical model inspired by the behavior of Physarum polycephalum (acellular slime mould or myxomycete) [41]. This algorithm is based on simulating the fluctuation of the slime mould. It uses adaptive weights to imitate the process of producing positive and negative reactions to the wave propagation of slime mould based on the bio-oscillator to create the optimal track to deliver food in a comparatively more significant way [42]. The SMA is mathematically designed and applied to solve engineering problems based on how Slime Mold creates the optimal food pathway to attach food in a relatively XX way. The mathematical model of the SMA is briefly explained in the following subsections:

A. Approach Food

To imitate the constriction position to model the approaching behavior of slime mould, the following formula is used:

$$\overrightarrow{X(t+1)} = \begin{cases} \overrightarrow{X_b(t)} + \overrightarrow{v_b} \cdot \left(\overrightarrow{W} \cdot \overrightarrow{X_A(t)} - \overrightarrow{X_B(t)}\right), r < p \\ \overrightarrow{v_c} \cdot \overrightarrow{X(t)}, r \geq p \end{cases} \tag{2.1}$$

Where, $\overrightarrow{v_b}$ represents a parameter that is randomly lying between $[-a, a]$, $\overrightarrow{v_c}$ decreases linearly from one to zero, (t) is the current iteration, $\overrightarrow{X_b}$ represents the position of individuals with the highest odor concentration that is currently found, $\overrightarrow{X}$ is the slime mould position, $\overrightarrow{X_A}$ and $\overrightarrow{X_B}$ represent two individuals randomly selected from the swarm, $\overrightarrow{W}$ represents the weight of slime mould and (r) is a random value between [0,1]. $p, \overrightarrow{v_b}$ and $\overrightarrow{W}$ are represented as follows:

$$p = \tanh|S(i) - DF| \tag{2.2}$$

$$\overrightarrow{v_b} = [-a, a] \tag{2.3}$$

$$a = \operatorname{arctanh}(-\left(\frac{t}{max\_t}\right) + 1) \tag{2.4}$$

$$\overrightarrow{W}(SmellIndex(i)) = \begin{cases} 1 + r \cdot \log\left(\frac{bF - S(i)}{bF - wF} + 1\right), condition \\ 1 - r \cdot \log\left(\frac{bF - S(i)}{bF - wF} + 1\right), others \end{cases} \tag{2.5}$$

$$SmellIndex = sort(S) \tag{2.6}$$

where, $i = 1,2, \ldots, n$, $S(i)$ represents the fitness of $\overrightarrow{X}$ and ranks first half of the population, DF represents the best fitness obtained in all iterations, bF indicates the optimal fitness obtained in the current iterative process, wF presents the worst fitness value obtained in the current iterative process, SmellIndex stands for the sequence of the sorted fitness values.

B. Wrap Food

The location of the slime mould is updated according to the following mathematical expression:

$$\overrightarrow{X^*} = \begin{cases} \text{rand} \cdot (UB - LB) + LB, \text{rand} < z \\ \overrightarrow{X_b(t)} + \overrightarrow{v_b} \cdot \left(W \cdot \overrightarrow{X_A(t)} - \overrightarrow{X_B(t)} \right), r < p \\ \overrightarrow{v_c} \cdot \overrightarrow{X(t)}, r \geq p \end{cases} \tag{2.7}$$

Where, LB and UB indicate the lower and upper boundaries, rand and r present a random value between [0,1].

C. Grabble Food

The value of $\overrightarrow{v_b}$ fluctuates randomly between $[-a, a]$ and the more the iterations, the value of $\overrightarrow{v_b}$ tends to be zero. The value of $\overrightarrow{v_c}$ is between [-1,1] and becomes zero eventually. The flowchart that indicates the steps of the SMA is illustrated in Figure 2.1.

In a recently published paper [43], SMA has been applied for estimating the parameters of three different mathematical models of solar cells; single diode model (SDM), double diode model (DDM), and triple diode model (TDM). The obtained results from SMA have been compared with the corresponding ones obtained from the application of different well-known optimization algorithms such as CSA, ABC, TLO, and PSO. Statistical results based on the operation of the SMA-based mathematical models for 30 individual runs showed decent and applicable performance in terms of accuracy, stability, and reliability of SMA compared with the other optimization techniques.

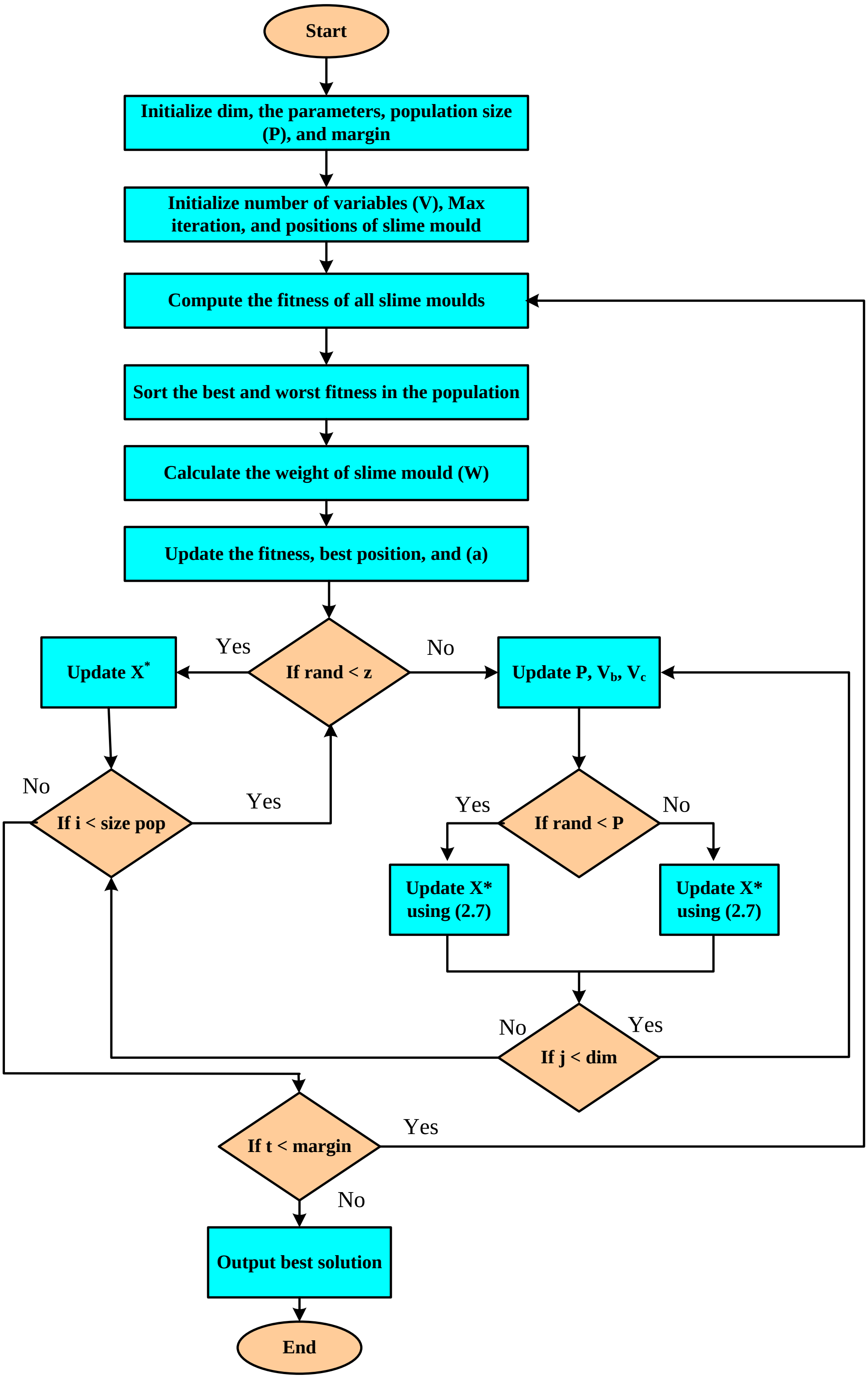

Figure 2. 1: Flowchart of SMA method [42], [43]

2.4.2.2. Seagull Optimization Algorithm (SOA)

SOA is one of the newest bio-inspired algorithms that is presented by Dhiman and Kumar [44]. SOA is based on studying the behavior of gulls in finding the most abundant food sources during the migration season and studying the behavior of attacking used to obtain their prey [45]. One of the ways for seagulls to get food is to use breadcrumbs to attract fishes and emit rain sounds on their feet to attract worms hiding underground. As for migratory behavior, it is known that gulls move in groups, so it is extremely necessary to meet the following conditions: avoiding collisions, moving towards the direction of nearest neighbors, and staying near the best search agent.

To prove the efficiency and performance of the SOA algorithm, it has been tested and compared with other well-known algorithms for solving 44 well-known benchmark test functions consisting of unimodal, multimodal, fixed-dimension multimodal, Congress on Evolutionary Computation 2005 functions (CEC 2005) [46], and CEC 2015 special session test functions [47]. The obtained results on the unimodal and multimodal test functions showed the exploration and exploitation capabilities of the proposed SOA. Also, the results of the CEC 2005 and CEC 2015 benchmark test functions illustrated the capabilities of the SOA in solving challenging and high dimensionality bound-constrained real problems. The statistical test has been also performed to demonstrate the statistical significance of SOA over benchmark test functions [44].

In order to prove the good performance and the superiority of the SOA algorithm over other optimization techniques, the SOA developer [44], applied it for solving the optimization problems for seven real-life industrial problems. These optimization problems are Optical buffer design, Pressure vessel design, Speed reducer design, Welded beam design, Tension/compression spring design, 25-bar truss design, and rolling element-bearing design. The obtained results based on SOA have been compared with recently developed nine advanced algorithms, namely SHO, DE Algorithm, PSO, GA, GSA, SCA, MFO, MVO, and GWO. By comparing the statistical results of these different algorithms, the SOA provided the best performance within all algorithms. The mathematical formulation of the immigration and the prey attack is explained in the following subsections.

1. Immigration (Exploration)

At this stage, the algorithm imitates how a swarm of seagulls moves from one location to another. The seagulls have to satisfy three cases.

A. Avoiding Collisions

To obviate collisions with other seagulls, an extra variable (A) is used to calculate the position of the new search agent. The search agent movement mechanism in a specific search area (A) can be mathematically described in the following formulas:

$$\overrightarrow{S_c} = A * \overrightarrow{S_p}(x) \tag{2.8}$$

$$A = C_f - (x * (\frac{C_f}{ite_{max}})) \tag{2.9}$$

where, $\overrightarrow{S_c}$ symbolizes the search agent location which does not collide with other search agents, $\overrightarrow{S_p}$ indicates the present location of the search agent, x indicates the current iteration (x = 0 ,1 ,2 ,…. ite_{max}), ite_{max} denotes the maximum iteration number, and C_f is introduced to control the frequency of employing variable (A) which is reduced linearly from C_f to zero. In this study the value of C_f is set to two.

B. Moving Towards the Direction Of Nearest Neighbors

At this condition, the search agents head towards the best neighbor and this can be represented by the following formula:

$$\overrightarrow{S_M} = B * (\overrightarrow{bS_p}(x) - \overrightarrow{S_p}(x)) \tag{2.10}$$

$$B = 2 * A^2 * Rd \tag{2.11}$$

Where, $\overrightarrow{S_M}$ denotes the position of search agent $\overrightarrow{S_p}$ towards the best-fit search agent $\overrightarrow{bS_p}$. The behaviour of (B) is randomized which is responsible for proper balancing between exploration and exploitation, and (Rd) is a random value in the interval of [0, 1].

C. Staying Near the Best Search Agent.

In the last condition, the search agent can update its location concerning the best search agent. The distance between the search agent and the best-fit search agent ($\overrightarrow{S_D}$) is expressed as follows:

$$\overrightarrow{S_D} = \left| \overrightarrow{S_M} + \overrightarrow{S_c} \right| \tag{2.12}$$

2. Attacking (Exploitation)

The behavior of the gulls' spiral movement occurs in the air in their way of attacking the prey. This behavior can be expressed at the l, m, and n levels as follows:

$$l = r * \cos k \tag{2.13}$$

$$m = r * \sin k \tag{2.14}$$

$$n = r * k \tag{2.15}$$

$$r = j * e^{kv} \tag{2.16}$$

Where r is the radius of the spiral per each turn, k is a random value in the interval of $[0 \leq k \leq 2\pi]$, while j and ν are constants describing the spiral shape. From the abovementioned equations, the updated position of the search agent is expressed according to the following formula:

$$\overrightarrow{S_p}(x) = \overrightarrow{bS_p}(x) + (l * m * n * \overrightarrow{S_D}) \tag{2.17}$$

The flowchart of the SOA is shown in Figure 2.2.

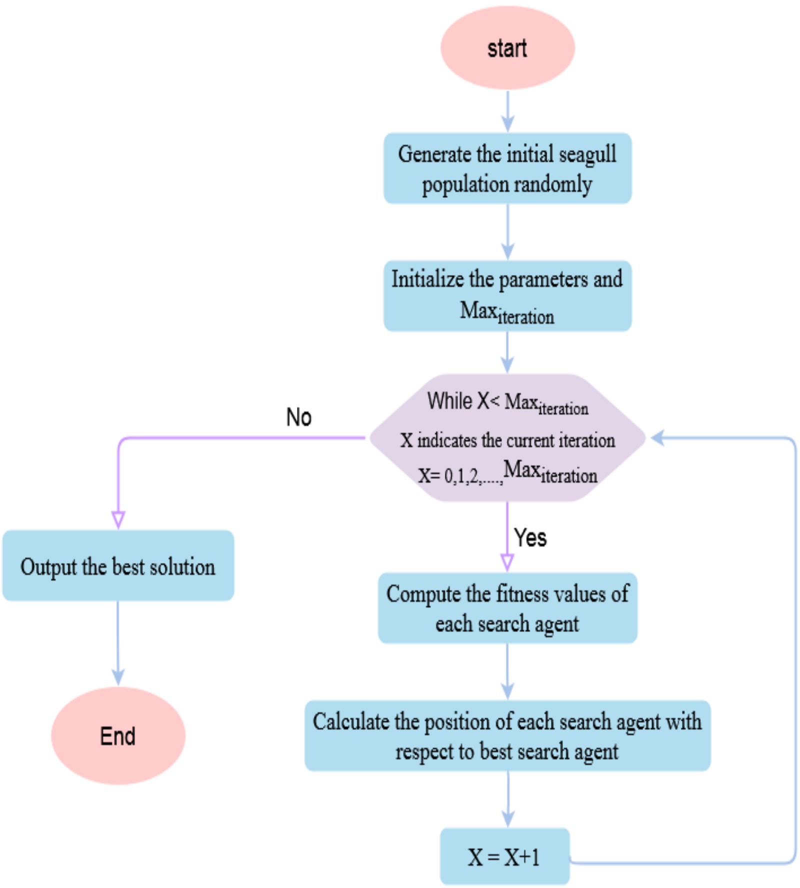

Figure 2. 2: Flowchart of SOA

2.4.2.3. Heap-based optimizer (HBO)

A new meta-heuristic optimization technique based on human-behavior called HBO has been created by Qamar Askari in [48]. HBO technique is based on the hierarchy of corporate rank (CRH) and the interplay of individuals in this hierarchy, HBO's mathematical model is based on three phases, which are interplay between employees and their direct manager, interplay amongst coworkers, and employee self-contribution. Unlike numerous of previous meta-heuristics algorithms, the relative fitness of search agents is used to organize them in a hierarchy, and the notion of minimum or maximum heap is used to allow interplay between them while maintaining their relative difference. Furthermore, a factor termed Gamma (γ) is established to help the algorithm avoid premature convergence without compromising the exploitation capability by allowing it to escape local optima. The pseudo-code of the HBO technique is indicated in Figure 2.3.

To prove the efficiency and performance of the HBO technique, it has been tested and compared with 7 well-known algorithms, and 97 diverse test functions involving 29 CEC-BC-2017 functions. The exploitative and explorative behavior of HBO has assessed from the obtained results of using 24 unimodal and 44 multimodal functions. Experiments and the Friedman mean rank test reveal that HBO outperforms and takes first place.

```
1.  Initialize general parameters, N, D, T_max, and (L_i, U_i)
2.  Generate a random population P of N search agents
3.  Building the heap
Algorithm 1; Heapify_Up (i)
Input: i (the index of the node we are trying to heapify)
➢ Assuming that the rest of the nodes fulfill the heap property
while i≠ root and heap[i].key < heap[ parent (i)].key do
        swap(heap[i], heap[ parent (i)])
        i ← parent (i)
end
Algorithm 2; Build_Heap (P, N)
Input: P, N
for i ← 1 to N do
    heap[i].value ← i
    heap[i].key ← f (x_i)
    Heapify_Up (i)
end
4.  Update Search agents positions repeatedly
Algorithm 3; HBO_Main_Body
for t ← 1 to T_max do
    Compute γ, p_1, p_2
    for I ← N down to 2 do
        i ← heap[I ].value
        bi ← heap[ parent (I )].value
        ci ← heap[colleague(I )].value
        B⃗ ← x⃗_bi
        S⃗ ← x⃗_ci
        for k ← 1 to D do
            p ← rand ()
            x^k_temp ← update x^k_i(t)
         end
         if   f( x⃗_temp ) < f( x⃗_i(t)) then
              x⃗_i(t + 1) ← x⃗_i(t)
         end
         Heapify_Up (I)
    end
end
return x_heap[1].value
```

Figure 2. 3: The pseudo-code of the HBO algorithm

2.4.2.4. Franklin's and Coulomb's algorithm (CFA)

A meta-heuristic optimization algorithm called CFA has been created by Ghasemi et al. [49], is based on the theories of the Coulomb's and Franklin's law. For optimal outcomes, the CFA employs two separate theories. First is the Coulomb's Law, which is based on the attraction and repulsion of electrons. This phenomenon governs the interaction of two independent point charges separated by a certain distance. Second is the Franklin's Law, which is based on that every item has an equal quantity of positive and negative charges, according to this law. CFA's mathematical model is based on four steps: Initialization, Attraction / repulsion, Probabilistic ionization, and Probabilistic contact. The pseudo-code of the CFA technique is indicated in Figure 2.4.

```
Generate the initial point charges (population)
Initialize parameters
Initial fitness evaluation of whole population
While criteria not satisfied do
    for (i = 1: N) do
        The attraction/repulsion phase is applied for point charges of objects.
        Evaluate the fitness values.
        The probabilistic ionization phase is applied for elementary charges (control variables) of
    point charge and fitness evaluation.
        The probabilistic contact phase is applied for objects.
        Selection of the best solution.
    end for
end while
```

Figure 2. 4: The pseudo-code of the CFA technique

2.4.2.5. Sooty Tern Optimization Algorithm (STOA)

STOA is a bio-inspired algorithm that has been validated using 44 benchmark test functions [50]. The results showed that STOA outperforms nine well-known optimization techniques in terms of performance. In addition, the results of the unimodal and multimodal test functions demonstrate the STOA algorithm's exploration and exploitation potencies. On the other hand, the results of CEC 2005 and CEC 2015 standard test functions prove that the STOA is capable of addressing high and challenging dimensionality bound-constrained actual situations. Statistical analysis has been carried out to establish the statistical significance of the STOA over benchmark test functions. Furthermore, to verify and demonstrate the performance of STOA on a given search space, it has been applied in 6 classic engineering structure problems, namely; pressure vessel design, speed reducer design, welded beam design, tension/compression spring design, 25-bar truss design, and rolling element bearing design problems [50].

However, sooty terns are species of birds that are found in all regions of the world and are scientifically called Onychoprion fuscatus. STOA stimulates the attacking and migration behavior of sooty tern birds in nature. Sooty terns generally live in colonies, and they use their natural intelligence in attacking the prey [50]. The following features characterize the migration behavior of the sooty terns:

- During seasonal movements, sooty terns fly in groups while their initial position within the same group is different to prevent collisions in the group,
- In the same group, all individuals can fly in the direction of the fittest sooty tern,
- All individuals in a particular group update their location regarding the best fittest candidate,
- During movement in the air, sooty terns use the spiral-shaped mechanism surrounding the prey and attacking it.

During the migration stage, the sooty terns should satisfy some conditions such as avoidance of collision, flying, and converging towards the best sooty tern in the group, updating location according to the location of the best fittest sooty tern. The mathematical representation of the migration behavior is given in the following equations [50].

$$C_i = D_A * X_i\ (it), \tag{2.18}$$

$$D_A = C_f - (it * {}^{C_f}/_{Max_{it}}), \tag{2.19}$$

Where C_i denotes the location of the search agent, X_i (it) denotes the current location of the sooty tern at the it-th iteration, D_A presents the movement of the sooty tern (search agent) in the search field, C_f is a controlling coefficient that decreases from C_f to zero and used for adjusting the movement in the search field, and Max_{it} denotes the maximum iterations number.

$$R_i = C_B * (X_{best}\ (it) - X_i\ (it)), \tag{2.20}$$

$$C_B = 0.05 * rand\ (0,1), \tag{2.21}$$

Where R_i denotes the various positions of the search agent X_i (it) in the search space in its movement towards the best fittest sooty tern, C_B denotes a uniformly distributed arbitrary coefficient.

$$G_i = C_i * R_i, \tag{2.22}$$

Where G_i denotes the distance between the search agent and the best one.

During migration time, sooty terns have the ability to change the speed and the direction of the attack. During the attack, sooty terns move toward the prey in a spiral shape that can be presented by the following equations [50],

$$x' = Radius * \sin(m), \tag{2.23}$$

$$y' = Radius * \cos(m), \tag{2.24}$$

$$z' = Radius * m, \tag{2.25}$$

$$R = u * e^{kv}, \tag{2.26}$$

Where x', y', and z' denote the angle of attack; Radius denotes the radius of each turn in the spiral; m is a variable that ranges between ($0 \leq k \leq 2\pi$); u and v are factors describing the spiral shape. The updated position of the candidate search agent is computed according to the following equation,

$$X_i\ (t) = (\ R_i\ (it) * (x' + y' + z')) * X_{best}\ (it), \tag{2.27}$$

The flowchart of the proposed STOA algorithm is shown in Figure 2.5.

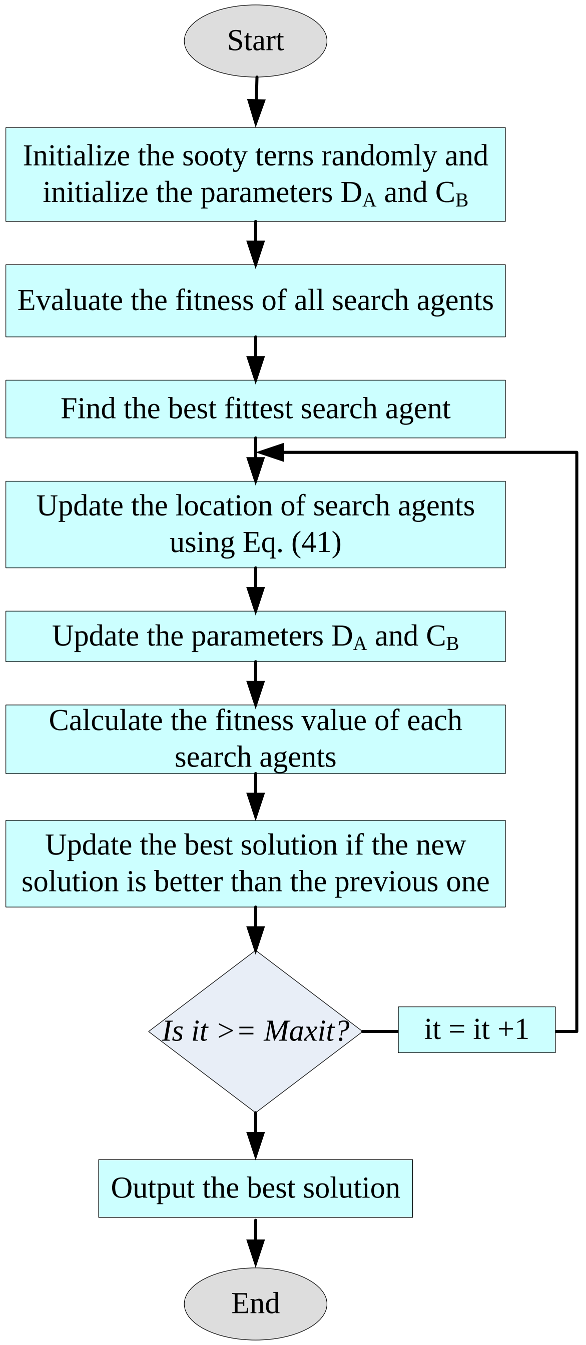

Figure 2. 5: Flowchart of the STOA method.

2.4.2.6. Mayfly Optimization Algorithm (MOA)

Mayflies are a species of insects that belong to the order Ephemeroptera that originated from the so old group named Palaeoptera. The MOA algorithm can be called a modification of the standard PSO [51], [52]. The proposed MOA method combines the merits of the PSO, GA, and FFA. The MOA is inspired by the patterns of the mating process of the mayflies. In the MOA, the males and females are arranged in different groups. In addition, the male mayflies are considered stronger than the female individuals, and then the males will do better in the optimization process. A group of males and another female group are randomly initiated. Each mayfly is considered a candidate solution in the search space of the optimization problem. The position of each individual determines its possibility of obtaining the desired optimal solution. The random location of the individuals in the search space is presented by the position vector p = (p_1, p_2, …….., p_d), the performance of each mayfly is assessed regarding a certain objective function represented by f(x). The social and movement experiences of each individual in the search space determine the new path of the mayfly after updating its position using the velocity vector v = (v_1, v_1, ……., v_d,). Each individual in the swarm decides its direction regarding its best position (pbest), while the best position obtained in the swarm by any individual is the global best position (gbest).

1. Movement of males

Similar to the PSO, the individuals in the swarm update their current position according to the following equation in which the position of certain mayfly i, in the current iteration (t) (p_i(t)) is updated by adding its velocity in the next iteration v_i(t+1) [52],

$$p_i(t+1) = p_i(t) + v_i(t+1), \tag{2.28}$$

The male mayflies continue their nuptial dance up to some meters above the water level, and their velocity is updated as follows [51],

$$v_{ij}(t+1) = v_{ij}(t) + k_1 * e^{-\lambda r_p^2} (pbest_{ij} - p_{ij}(t)) + k_2 * e^{-\lambda r_g^2} (gbest_j - P_{ij}(t)), \tag{2.29}$$

Where k_1 and k_2 are attraction constants for evaluating the cognitive and social behaviors, respectively. λ is used to limit the visibility between individual mayflies. r_p and r_g denote the distance between the position of the individual in the current iteration p_i (t) and its best position (pbest) and the global best position (gbest), respectively. The values of r_p and r_g are calculated according to equations (30) and (31), respectively. v_{ij} and p_{ij} are the velocity and the location of the i-th search agent in the j-th dimension. $pbest_{ij}$ denotes the best position reached by the i-th mayfly in the i-th dimension. The best position of the i-th search agent is determined according to the following formula,

$$pbest_i = \begin{cases} p_i\,(t+1), & f(p_i\,(t+1)) < f\,(pbest_i) \\ pbest_i, & \text{otherwise} \end{cases}, \tag{2.30}$$

Where f(.) is the objective function of the optimization problem. r_p and r_g are evaluated as follows,

$$r_p^2 = \left(\sum_{j=1}^{d}(p_{ij} - pbest_i)\right)^{1/2}, \quad (2.31)$$

$$r_g^2 = \left(\sum_{j=1}^{d}(p_{ij} - gbest_i)\right)^{1/2} \quad (2.32)$$

To ensure the optimization algorithm's best performance, the best candidates should continue their up and down dancing. Therefore, the velocity of the best mayflies should continue to change. The velocity, in this case, is expressed as follows,

$$v_{ij}(t+1) = v_{ij}(t) + c * \varepsilon, \quad (2.33)$$

Where ε is a random number in the range of [-1, 1] and c is a coefficient describing the nuptial dancing of the mayflies.

2. Movement of females

The female mayflies do not fly in swarms like males. For the mating process, female mayflies move toward the location of the males. The position of a certain individual female mayfly in the search area q_i (t) is updated as presented in the following equation [51], [52],

$$q_i(t+1) = q_i(t) + v_i(t+1), \quad (2.34)$$

The authors of the MOA decided to model the attraction between males' and females' mayflies in a deterministic manner. The fittest female is proposed to be attracted to the fittest male, the second female towards the second male, etc. Consequently, the velocity of the female mayflies is determined using the following equation [53],

$$v_{ij}(t+1) = \begin{cases} v_i(t) + k_2 * e^{-\eta r_{fm}^2}\left(p_{ij}(t) - q_{ij}(t)\right), & f(q_i) > f(p_i) \\ u_{ij}(t) + c_\omega * \eta & f(q_i) \le f(p_i) \end{cases} \quad (2.35)$$

Where $q_{ij}(t)$ denotes the location of the i-th female in the j-th dimension during the iteration t. $u_{ij}(t)$ presents the velocity of the i-th female mayfly in the j-th dimension. r_{fm} denotes the distance between the male and female mayflies, and c_ω is the walk coefficient that is randomly selected in the case when a female mayfly is not attracted by any male.

3. Mating process

The way for the selection of the parents is the same as that used for the attraction of females by males' mayflies. The selection might be random or according to a certain objective function. When the mating is based on an objective function, the best fittest female mates with the corresponding best fittest male, the second female in the chain mates with the second fittest male in the swarm, and so on. Finally, two offspring are generated according to the following equation [51], [53],

$$\text{offspring}_1 = \rho * \text{male} + (1 - \rho) * \text{female}, \tag{2.36}$$

$$\text{offspring}_2 = \rho * \text{female} + (1 - \rho) * \text{male}, \tag{2.37}$$

Where ρ is random numbers in Gauss distribution, the flowchart describing the procedure of the proposed MOA algorithm is shown in Figure 2.6, while the block diagram of MOA used for optimizing the proposed hybrid renewable system is illustrated in Figure 5.8.

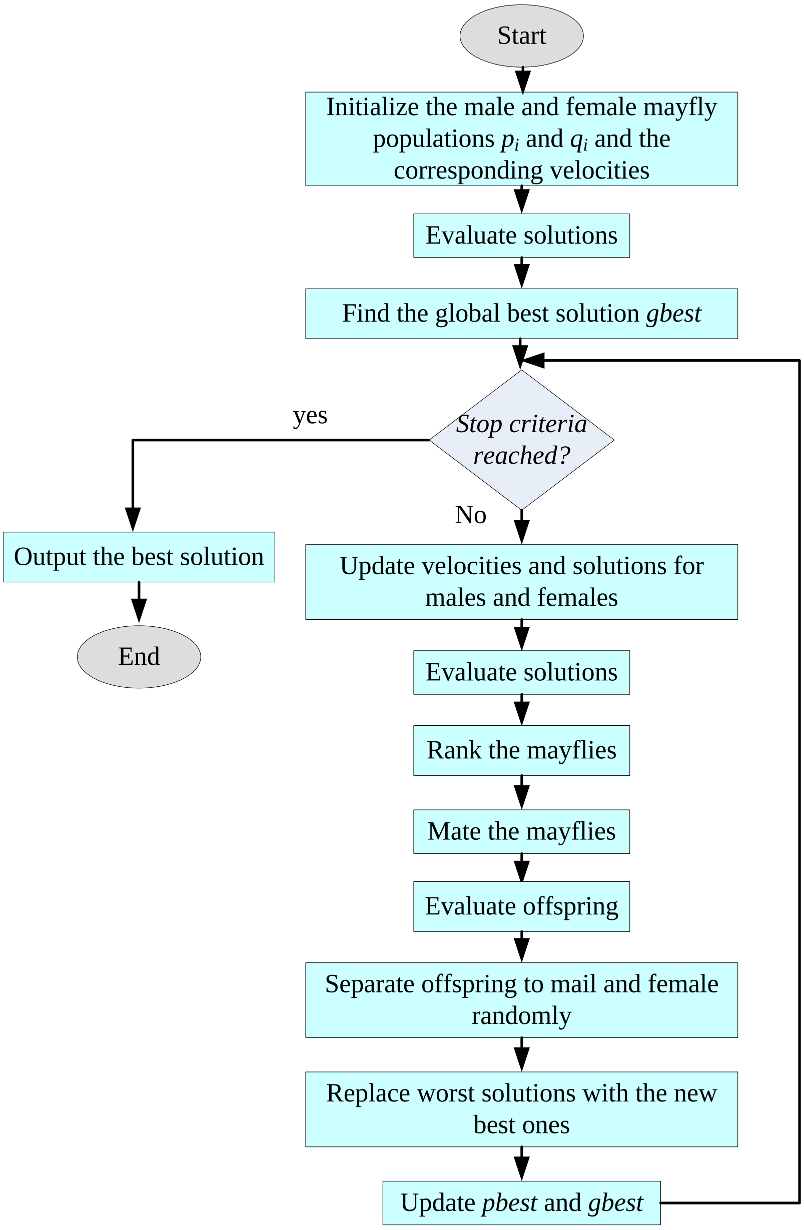

Figure 2. 6: Flowchart of the MOA method.

2.5. Literature Searches

2.5.1. Combined Cooling, Heat and Power (CCHP) System

Biomass source can be converted into fuel based on many thermodynamics conversion techniques such as gasification technology and direct firing. In gasification process, the biomass is converted to a mixture of gases in the presence of a catalyst [54]. In [54]–[56], different types of gasification process have been presented. The direct firing or combustion is the process of burning biomass at high temperatures in the presence of excess air. The direct firing is considered one of the simplest thermodynamics conversion technique which has the lowest cost due to using an internal furnace (combustion chamber) [57], consequently, this type has been used in the current work. Schematic graph of the basic units of biomass system is illustrated in Figure 2. 7.

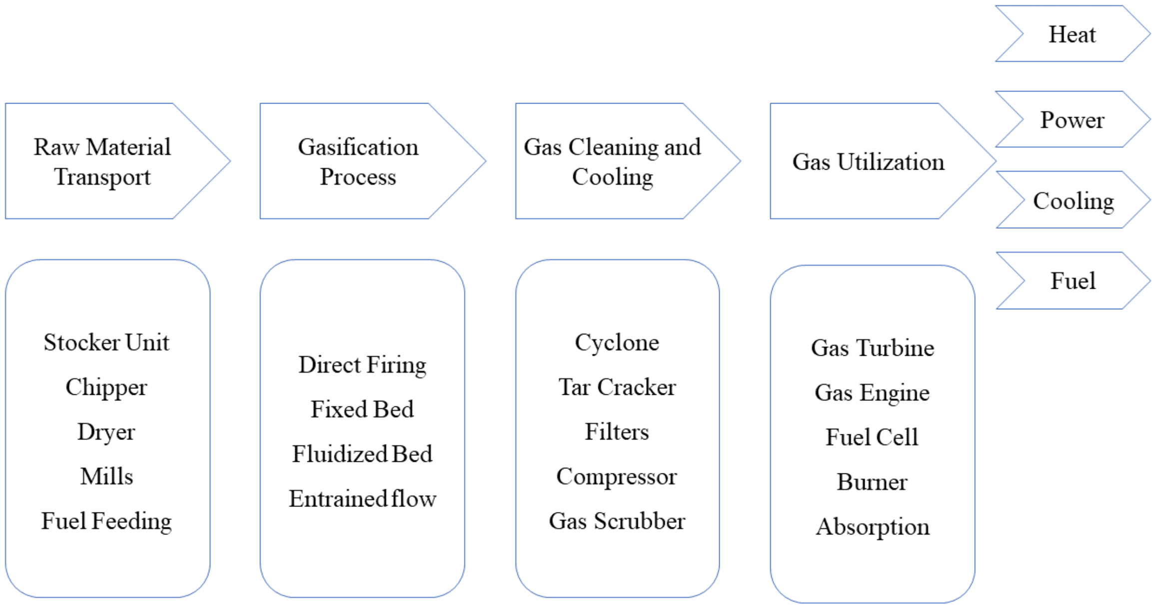

Figure 2. 7: Layout of the Biomass System Units.

Numerous researchers focused on modeling hybrid biomass system for heat and power. In [57], a small-scale biomass CHP based on the gasification technology associated with an EFGT has been proposed to generate about 100 kW. Moreover, the performance of the plant at different values of TIT has been studied. In [58], the performance of a hybrid system consists of the gasification reactor connected to MGT, a SOFC and heat recovery unit has been analyzed. This system has the ability to produce about 262 kW electric power and 405 kW of thermal power, the overall efficiency of CHP is about 88%. In [59], a simulation of CHP plant consists of a gasification unit, EFGT and an ORC have been carried out. The electrical energy produced by this model is more 200 kW and overall electrical efficiency is 20.7%. In [60], the optimum model of a gas turbine coupled to ORC technology has been presented and the obtained results proved that Toluene is the most suitable fluid to increase the net electrical production. In [61], the techno-economic aspects of EFGT and ORC using a direct burning system has been studied and the results proved that the generated energy is 1.3 kW using Toluene as a more suitable working fluid at temperature level (> 300℃). Furthermore, few researchers focused on modeling a tri-generation system. In [62] studied the thermodynamic of tri-generation plant based on biomass combustion connected to ORC and absorption unit. In [63] tri-generation system consists of SOFC with ORC and absorption chiller has been developed, Where 24.6 kW of electric power is obtained, about 69.9 kW of the thermal energy and 22.1 kW from absorption chiller. In [64] studied the performance of biomass gasification combined with indirect heat gas turbine (IHGT) and absorption chiller for a tri-generation system, the system electrical efficiency reached to 27% at 1100 ℃ of turbine temperature. However, the most important hybrid systems presented in the literature could be summarized in Table 2. 1.

Table 2. 1: Overview of combined heat and power systems

Reference	Feedstock Type	Conversion Technology	System	TIT	ORC Working Fluids studied	Power Range	Efficiency
Datta et al. [57]	NA	Gasification	EFGT	1050-1350K	-	100 kW	η_{th} =16-34%
Perna et al. [58]	NA	Gasification	MGT & SOFC	-	-	262 kW_{el} 405 kW_{Th}	η_{CHP} =88%
Vera et al. [59]	Olive tree pruning	Gasification	EFGT ORC	800-950℃ 169-177℃	Isopentane, Benzene, Cyclo-hexane, R113, R245fa	207.3 kW_{el}	η_{el} =20.7%
Yue Cao et al. [60]	NA	Direct Firing	GT&ORC	NA	Toluene, P-Xylene, Ethylbenzene, Steam	NA	η_{th} =23.3% For QD128 GT and using Toluene ORC
Camporeale et al. [61]	NA	Direct Firing	EFGT & ORC	800 ℃ NA	Toluene, MM, MDM and MD2M	1383 kW_{el}	η_{el} =23%
Maraver et al. [62]	NA	Combustion	ORC& Absorption Chiller	NA	n-Pentane, n-Heptane, MDM, D6 and Toluene	NA	from 20.5% to 24.5%
Chattopadhyay and Ghosh [64]	NA	Gasification	IHGT & Absorption Chiller	1100 ℃	-	97.70 kW_{el}	η_{el} =19.6% η_{th} =56.6%
Kalina [65]	Spruce chips	Gasification	ICE& ORC	NA	R123 and R245fa	241.8 kW_{el}	η_{el} =23.8%

2.5.2. Hybrid Renewable Systems

Li et al. [66] used the HOMER simulation software to simulate and perform optimization and techno-economic analysis of an off-grid hybrid system located in a rural area in west China. The proposed system is based on the combination of PV, WT, biogas generator, and battery units. It would have been better if there were comparisons with other optimization techniques. Hassani et al. [67], proposed an off-grid hybrid energy system to supply a house with a consumption of 2,808 kWh/day located in Bejaia, in eastern Algeria using HOMER software to conduct an economic analysis. The configuration of the proposed system is PV with HT production system. This research illustrates that with a good design of the system described by the authors, it can charge the batteries, feed the ELE, and occasionally produce extra power.

In [68], six different configurations of stand-alone hybrid systems based on PV, WT, DG, and battery units in a remote rural area in Bangladesh have been studied and evaluated. The optimum configuration was chosen based on the criterion of minimum cost of energy and reduction of GHG emissions. The optimization technique used in this study is the HOMER software. A techno-economic optimization model for a real case study, 2iE-K1 campus, has been presented by Tsuanyo et al [69]. This system consists of PV and DG generators without using a battery bank as an auxiliary unit. The results obtained from this system were compared with a stand-alone model of DGs of different sizes. HOMER simulation software has been used while considering the minimization of EC as the objective function. Maleki and Pourfayaz [70], proposed an optimal sizing algorithm for stand-alone hybrid systems based on PV, WT, and DG. The authors considered the application of battery and/or FC as energy storage devices. Two optimization algorithms have been used, namely HSA and SA. The obtained results from both algorithms have been compared with the corresponding ones obtained by HOMER simulation software. Simulation results indicated that using the battery as a storage device with the proposed PV/WT and DG system is more cost-effective than using the FC system. Shakti and Subhash [71] have studied the optimal sizing of both stand-alone and grid-connected PV-biomass systems using two optimization techniques ABC optimization technique and HOMER. The results indicated that the grid-connected PV-biomass system has better performance in terms of cost of generated units.

Ref [72], designed a grid-tied hybrid system consisting of PV and wind units with and without energy storage system for the Lafarge cement factory in Al-Tafilah, Jordan. The main objective of this study was to maximize the renewable energy system fraction with the cost of electricity, accounting for the amount of excess energy from the system and the amount of deficit energy met by the grid, lower than the local grid tariff and with 100% renewable energy ratio in order to meet the renewable energy targets. According to the findings, the system using lithium-ion batteries is more economically viable than the system without an energy storage system. The final suggested hybrid system has a capacity of 20.75 MW PV, 26 MW wind systems, and 16.8 MWh Lithium-Ion batteries. Its efficiency is 62.53 %, its cost of energy is 0.203 $/kWh, and its emissions of carbon dioxide by 71,373 tons. In [73], proposed a modeling and simulation process of grid-tied PV and wind systems in the absence and presence of the battery storage for supplying electricity to a residential building in an Italian city, based on using a computational model built-in TRNSYS 17 simulation (Transient Energy System Software Program). The energy reliability-constrained method is used for the multi-objective optimization to achieve the optimum energy reliability of the renewable energy system. The results from the energy reliability-constrained method was compared with the results from the Pareto-front multi objective optimization methods. Ref [74], presented a specific model based on the TRNSYS software used to size a hybrid electrical renewable energy system that might be used to satisfy electrical load requirements. By using an immersed electrical heater to make up for the thermal losses of the bitumen tank, it is possible to keep the temperature of bitumen in storage constant. The created model replicates the yearly performance of several PV-WT-based hybrid system setups. The worst month technique and the annual average month approach are two size deterministic methodologies that are compared in this study.

A renewable hybrid tri-generation system that powers a heat pump, electric office equipment, and an electric car charging station based on using PV, and a wind micro-generator with and without battery storage is presented in Ref [75]. The dynamic interaction between the three electric loads and the renewable hybrid tri-generation system is investigated using the findings of the dynamic simulation. To identify the most modern load in relation to the availability of the renewable source and to assess the system energy dependability, several indices are created and analyzed both with and without a battery storage system. Another paper [76], proposed new weekly deterministic and annual statistical analyses by utilizing a brand-new dynamic simulation tool in the TRNSYS environment. This dynamic simulation for an electric renewable hybrid system (consists of PV, WT, and battery unis) utilized to power heat pumps, the pure electric energy consumption of an office building, and the electric car charging station of the office building is considered to be located in the Mediterranean area.

Ref [77], developed two ANNs For sizing and modeling a clean energy community that uses a PV-wind hybrid system, combined with energy storage systems and electric vehicle charging stations, to fulfill the building district energy demand. The first one is utilized to forecast the energy performance indicators, while the grid energy indication factor is estimated by the other ANN. For the evaluation of each input's influence on each output, the Garson algorithm was used. Optimized ANNs have a single hidden layer with 20 neurons, resulting in very high clean energy community prediction accuracy.

Several recent studies focus on studying the performance of different optimization techniques for optimal sizing and location of hybrid systems. Diab et al. [78] recommended off-grid PV, WT, DG and battery systems for a rural area in Egypt. In this paper, four optimization algorithms have been used and evaluated, mainly WOA, WCA, MFO, and Hybrid particle swarm-gravitational search technique (PSOGSA). Among the suggested optimization methods, the WOA technique proved its superiority in determining the optimal sizing and location of hybrid systems. Minimization of the cost of energy was taken as the objective function. Ramli et al. [79] applied a Multi-Objective Self-Adaptive Differential Evolution (MOSaDE) technique to obtain the optimum size for a hybrid energy system using three different combinations of PV, WT, DG, and battery storage system. The main target of this study is to minimize the cost of energy supplied by the hybrid renewable system and the LPSP. Buker et al. [80] have utilized GOA to obtain the optimal sizing for an off-grid system in Yobe state-Nigeria. The isolated system comprises five housing units. The system consists of PV, WT, DG, and battery units. The obtained results based on the GOA technique were compared with PSO and CSA optimization techniques and the superiority of the proposed GOA method has been proved. The computation time of this study has not been stated.

A hybrid system based on PV, DG, and battery storage system located in a rural village in Algeria has been studied and evaluated by Yahiaoui et al [81]. This paper is based on using the Grey Wolf Optimizer (GWO) method to reduce the total annual cost of the system. The comparison of the results obtained from GWO with the corresponding ones obtained based on the PSO technique showed that GWO performs better in reducing system costs. There is no suggestion for more configurations to confirm the best for this site area. Geleta et al. [82], implemented the GWO algorithm for solving the optimization problem of optimal sizing of a hybrid system including solar panels, WT, and battery units. The objective function of this stand-alone system was to minimize the total annual costs of the system. The results obtained from the GWO algorithm were compared with those obtained based on the PSO algorithm. The GWO provided the best result in terms of the minimum objective function.

Maleki et al. [83] applied an Improved Harmony Search (IHSA) optimization technique to determine the optimal sizing of a hybrid system based on PV and battery units located in Davarzan, Iran. The results obtained from the IHS algorithm were compared with the results obtained from the conventional HSA technique and SA algorithm. Within the completely proposed algorithms, the IHSA method provided the minimum value of the Total LCC.

Fathy et al. [84] developed a recent methodology based on SSO to determine the optimal sizing of a hybrid integrated microgrid system based on PV, WT, battery, and DGs. The obtained results from the proposed SSO are compared with those obtained from other algorithms such as HHO, GWO, MVO, ALO, and WOA. The obtained results showed the effectiveness and superiority of the proposed SSO in designing reliable and costless microgrids.

Eteiba et al. [85] have presented a comparison of four optimization techniques to determine the optimal sizing of a rural stand-alone PV-biomass-battery energy system while utilizing the minimization of the NPC as the objective function for the proposed optimization methods. The used algorithms are the FPA, the HSA, ABC, and the FFA. Besides, three different types of batteries have been studied, namely Flooded lead-acid, Lithium Ferro Phosphate, and Nickel Iron Battery. The results indicated that among the three types of batteries, the Nickel Iron battery presented better performance while in all cases the proposed FFA algorithm generated the optimal solution compared to the other algorithms. An optimization model for a grid-connected hybrid system based on PV, WT and biomass generator has been proposed by Gonzalez et al [86] to improve connectivity to the grid. PV and wind are the main energy source, while the biomass system is used as a standby emergency system. This research paper presented an optimal solution for minimizing LCC in a rural town using GA and PSO algorithm. In other research papers based on environmental and economic criteria, Gonzalez et al [87] performed a grid-connected system consisting of PV, WT, and biomass gasification. The authors used multi-objective optimization based on the GA to provide a set of optimum results for a town in central Catalonia. Serir et al. [88], assessed an energy management control using three MPPT methods (Perturbation and

Observation , Fuzzy Logic Controller and Adaptive Fuzzy Logic Controller) to a hybrid power system based on a photovoltaic array, wind system, a battery bank, and a moto-pump. The simulation achieved using Matlab/Simulink.

In [89] Cai et al. presented an optimization model for reducing the total LCC of a hybrid isolated system located in a remote area in South Khorasan. The off-grid system includes PV and DGs while using batteries as a backup system. This study presented a new hybrid algorithm called IHS-SA-GIS for optimal sizing and location for the proposed hybrid system. The obtained results showed that using a PV energy system with a DG, significantly minimized GHG emissions and supply costs by 59.6% and 22.2%, respectively compared with the case of using a DG system only. Khan and Javaid [30] presented an optimization methodology using three different configurations of stand-alone hybrid systems including PV, WT, and FCs to minimize the total annual cost of energy paid by the consumer using the JAYA algorithm. The results showed that JAYA algorithm has a faster convergence rate compared to three algorithms, which are GA, BSA, and PSO. The results also indicated that PV-FC configuration was the most cost-effective system compared to PV-WT-FC and WT-FC systems while the total annual cost achieved was $1051200 at LPSP = 0% and $790000 at LPSP= 2%. Diab et al. [90] developed and applied Modified Farmland Fertility Algorithm (MFFA) for reducing the EC while satisfying the operational constraints including the LPSP for the proposed hybrid system including PV, WT, and FC units to provide the electricity for Ataka region, Egypt.

Based on the Literature searches, Table 2.2 provides a summary of these cited references depending on their studied systems' configurations based on battery bank. At the same time, a summary of some recent hybrid system research based on FC configuration is presented in Table 2.3.

Table 2. 2: A summary of different hybrid system configurations based on battery bank.

Hybrid System Configuration	Ref.	Location	Technique	Objective function
PV, WTs, DG, and batteries	[78]	Abu-Monqar village in the Western Desert of Egypt	WOA, WCA, PSOGSA, MFO	EC LPSP
	[84]	A remote area in Aljouf region in the north of Saudi Arabia	SSO, HHO, GWO, MVO, ALO	EC
	[91]	Dakhla area in Morocco	EO, HHO, AEFO, GWO, STOA	NPC
	[92]	-	An improved GA	EC, NPC, LPSP, CO_2emissions
	[93]	Rabat, Morocco	MOPSO, PESA II, SPEA2	Total NPC, CO_2 emission
PV, WTs, and batteries	[94]	Ahvaz city in Iran	GWO and PSO	NPC

	[95]	Manipur state in India	FOA	EC
PV, WTs, BG, and batteries	[96]	a faculty building in Karabük University campus, Turkey	GWO, GA, and SA	Total NPC, LPSP, and EC
	[97]	A small rural communit located at latitude 29° 49.794' N and longitude 39° 34.362' E	HSA, JOA, and PSO	lower cost and reduce CO_2 emission
PV, BG, and battery	[71]	-	ABC and HOMER	annual cost
	[98]	Kaidupur village, in Punjab State, India	DF and ABC	TAC
	[85]	Monshaet Taher village in Beni Suef, Egypt	FPA, HS, ABC, and FOA	NPC
PV, WTs, BG, and pumped hydro storage	[99]	Saudi Arabia	WOA, FFA, and PSO	EC
PV, Biogas generator, Battery, and Pumped-storage hydro	[100]	A radio transmitter station in India	WCA and MFO	Total NPC
	[101]	A radio transmitter station in China at Hubei's Three Gorges Dam	DSPBO, WCA, MOA, GA, FOA, and GWO	Reducing the overall LCC

Table 2. 3: FC based on different hybrid energy systems.

Hybrid System Configuration	**Ref.**	**Location**	**Technique**	**Objective function**
PV/WTs/DG/battery PV/WTs/DG/FC	[70]	Iran	HSA HOMER SAA	TAC
PV/WTs/FC	[28]	Suez Gulf in Egypt	IAEO,AEO PSO, SSA, and GWO	EC
PV/WTs/battery/HT	[102]	Zhejiang in China	IACO ACO	Annual Cost LPSP
WT/FC/battery/super-capacitor	[103]	Tanda in Ivory Coast	NSGAII	TAC LPSP
PV/WT/FC PV/FC WT/FC	[30]	Hawksbayin Pakistan	JOA GA, BSA and PSO	TAC
PV/WT/FC	[104]	Turkey	HOMER	EC
PV/DG/FC (off-grid)	[105]	Kerman in Iran	MOCSA	NPC LPSP
PV/DG/FC (grid-connected)	[106]	Kerman in Iran	MOCSA	EC LPSP
PV/WT/FC	[107]	Egypt	MBA, PSO ABC, and CS	Annual Cost
PV/WT/FC PV/FC WT/FC	[108]	Iran	FPA PSO TLBO	Total NPC

Chapter 3

Development of CCHP System Based on Biomass Gasification

Chapter 3

Development of CCHP System Based on Biomass Gasification

3.1. Introduction

This chapter is focused on providing new models of the optimal performance of a small tri-generation power, heat, and cooling plant with two different system configurations using the professional Cycle-Tempo® software tool;

1) The first configuration is based on the integration of a downdraft fixed bed gasifier with EFGT (power generation system), a heat recovery device, and the absorption cooling cycle using CS as the biomass feedstock.

2) The second configuration is based on a direct burning biomass combustor, an EFGT, an ORC as bottoming unit for maximizing the electrical efficiency, and an absorption refrigeration unit for cooling power production using sugarcane bagasse as the biomass feedstock.

Before describing any system, we will start by explaining the biomass feedstock and major units used during this thesis.

3.2. Biomass Feedstock Characteristics

3.2.1. Corn Stover (CS)

CS is the by-product of corn harvesting, plants left in a field after harvest and consists of the residue: stalk, leaves, sheaths, husks, shanks, cobs, tassels, lower ears, and silks. Corn is one of the most widespread crops in Egypt. Its production reached 6.8 million tons in 2018 [109]. In the past, there was a use of corn residues in Upper Egypt as fuel for the furnace or for making Dari (which protects the fields from the sun), but it is now useless and without value, making it a source of undesirable waste. In this study, CS is selected as biomass feedstock as it consists of small amounts of ash and readily available in many areas. The CS samples are ground with a hammer mill to pass through chopping machine to be chopped in form of pieces with length varied from 1 to 15 mm as shown in Figure 3.1. The major ultimate and proximate analysis of CS is presented in Table 3.1.

Figure 3. 1: Sample of the CS pretreatment

Table 3. 1: CS properties [110]

Proximate Analysis (%)		**Method**
Moisture content	4.01	According to ASTM (D3173)
Volatiles matter	75.63	According to ASTM (D3175)
Ash	5.13	According to ASTM (D3174)
Fixed carbon	15.23	Determined by difference
Higher Heat Value of Biomass, HHV (MJ/kg)	17.31	According to ASTM (D5865)
Lower Heat value of Biomass, LHV (MJ/kg)	14.824	According to ASTM (D5865)
Ultimate Analysis (%)		
C	43.92	According to ASTM (D3178)
H	6.01	According to ASTM (D3178)
O	40.44	Determined by difference
N	0.42	According to ASTM (D3179)
S	0.07	According to ASTM (D3177)
Oxygen/Carbon ratio	1.38	-
Hydrogen/Carbon ratio	1.64	-
Other characteristics		
Biomass consumption (Kg/h)		100
Gasification agent type		Air
Operating pressure (bar)		1.013

3.2.2. Sugarcane Bagasse

Sugarcane is an important and strategic agricultural crop. It is an essential source of the sugar industry and used for producing black honey. Reed industrial waste is used in the paper industry and ethanol production [111]. The produced residues during sugarcane processing can be used for producing power and ethanol as shown in Figure 3.2. Bagasse is the remains of reeds (stalks) of sugar cane after de-mixing and extracting sugar juice. This represents about 30% of the weight of cane sugar [24]. The major ultimate and proximate analysis of bagasse is presented in Table 3.2.

Table 3. 2: Main analysis of bagasse.

Ultimate Analysis ^{a} wt.%		**Proximate Analysis wt.%**		**Calorific Values^{a}(dry) MJ/kg**	
Hydrogen	5.87	Moisture content (ar.)	10.39	LHV	17.71
Carbon	48.64	Ash content^{b}	2.44	HHV	18.99
Nitrogen	0.16	Volatile matter	85.61		
Sulphur	0.04	Fixed carbon	11.95		
Oxygen	42.82	Bulk density (kg/m^{3})^{c}	173		

ar. = as received, (the material in its original form)
[a] According to ECN Phyllis classification (#894)
[b] According to ASTM D1102
[c] According to ASTM D1895B

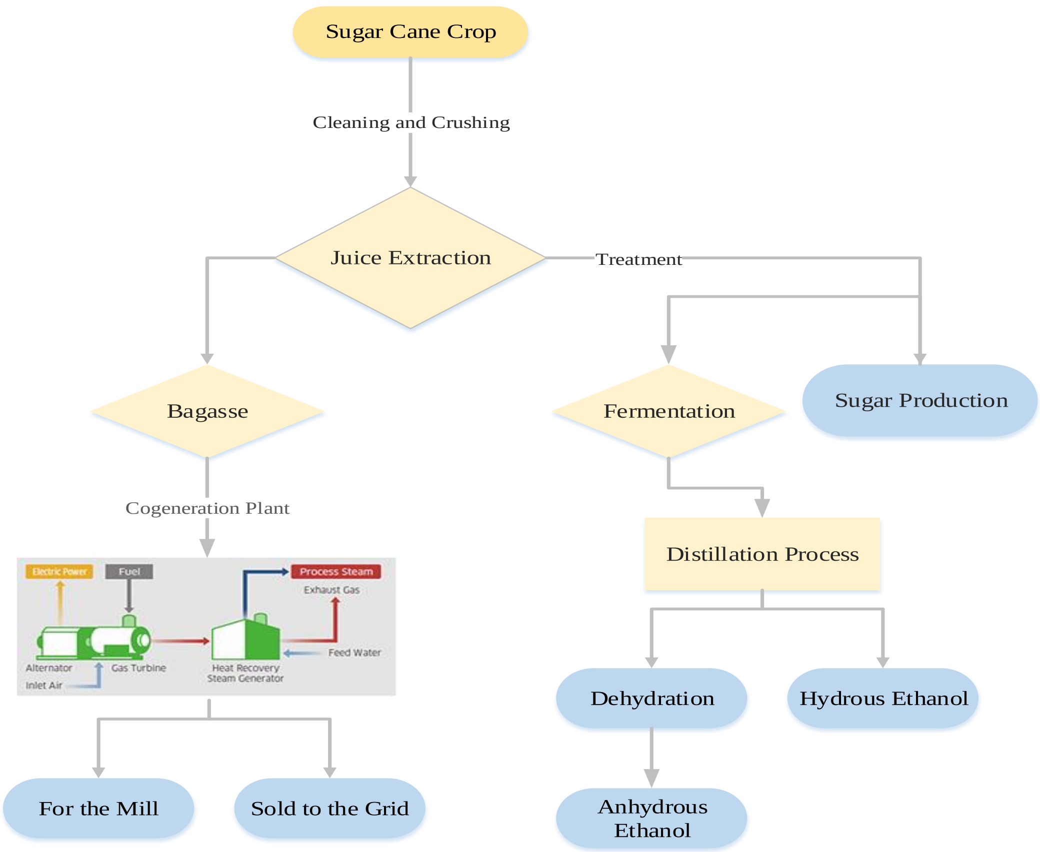

Figure 3. 2: Schematic of the treatment of sugar cane and its residues [112].

3.3. Components Description

3.3.1. Gasification unit

Gasification is a thermochemical process that converts the raw materials (biomass) into a mixture of gases called syngas or product gas which consists mainly of hydrogen, nitrogen, carbon monoxide, carbon dioxide and methane [113]. This method is achieved by breaking the molecules of biomass material at relatively high temperature (greater than 700℃) and control amount of oxygen or air and then recombining them to form a clean fuel (syngas) similar to natural gas [114]. This clean fuel can be converted to methanol, petrol, used directly as an alternative to natural gas, or combined with natural gas for the gas supply network.

Downdraft reactor (Throated gasifier) is an attractive technology due to its possibility of producing mechanical and electrical energy from biomass in small range (≤ 5 MW) with less cost than other gasifiers and it can produce a low BTU Gas (~ 6000 KJ/m^3) with tars [54], [115]. This type is used in the proposed system in the current thesis.

The design of the gasification device depends on the thermodynamic process. According to previous studies [116]–[118], there are two main types of thermodynamic models namely the kinetic model and the equilibrium model, both are depend on different operating conditions. For the kinetic model, research and experiments in [119], have shown that it is more suitable for gasification at high temperatures but becomes more complex at temperatures higher than 1500 ºC [120]. It also requires many numbers of reactions and accurate information for the gasifier device, making it more complex [121]. While the equilibrium model which are based either on the use of equilibrium constants (stoichiometric method) or on the Gibbs free energy minimization (non-stoichiometric method) has been widely used in the design of gasification devices in many studies because this model relies on the second law of thermodynamics [122]. The only inputs needed to calculate the thermal value and composition of the resulting gas are the approximate and ultimate analysis of the feedstock [116], [123]. The used software for design in that research depends on the calculation of a repetitive approach based on the Gibbs free energy minimization method [124]. This thermodynamic method does not require to know precisely the mechanisms of chemical reaction accurately and therefore, it provides acceptable results in the case of complex multi-reactions process like gasification [116], [120].

As shown in Figure 3.3, four phases of reaction occur within the downdraft reactor after biomass enters through it from the top and the gasification agent is entered at both sides, so both the biomass and the agent move in the same direction [125]. These four phases of reactions are described below and the main reactions are clearly presented in Table 3.3:

1) Drying: it is the initial phase of biomass where moisture is removed. It is necessary to remove the moisture from the fuel before any operations above 100 °C. High moisture content fuel is one of the most common reasons for failure to produce clean gas [126].

2) Pyrolysis: it is present an important role in biomass gasification. It is the heating of raw biomass at a temperature below 600°C at a pressure of 0.1-0.5 MPa in the absence of air/oxygen to convert biomass into charcoal and various tar gasses and liquids [127], [128]. It is essentially the process of charring.

3) Combustion: it is considered the gross exothermic method of the four phases and the heat, which drives to other three zones come directly from combustion. Due to the high temperature (1000-1300°C) in this zone, different reactions occur, char and tars are oxidized into water vapor and carbon dioxide as waste products and released heat [127], [128].

4) Reduction: it is the elimination of oxygen from waste products of the combustion zone at high temperature to output flammable gases. Combustion and reduction is equal and opposite the feedback [128].

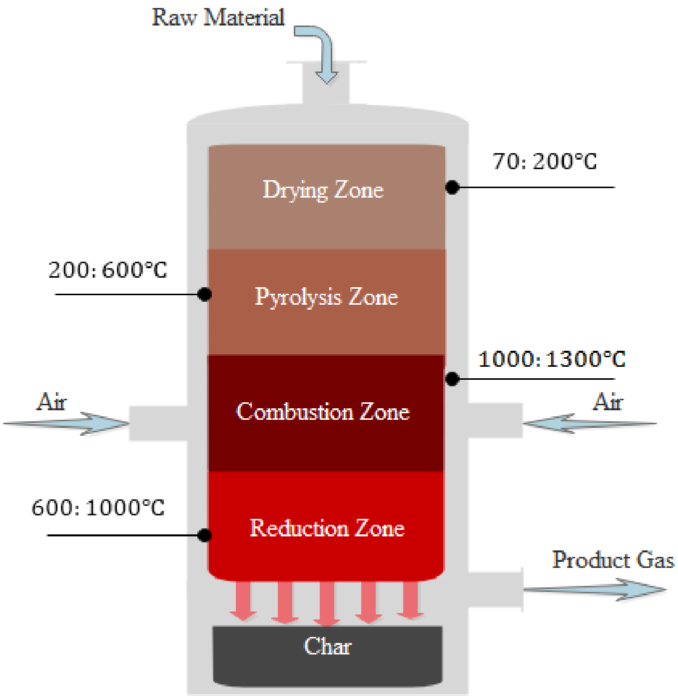

Figure 3. 3: Down draft gasifier scheme [129].

Table 3. 3: Major reactions occur in the down draft reactor.

Method	**Reactions** [122]	**ΔH (KJ/mol)** [130]
Gasification with O_2	$C + 0.5\ O_2 \overset{\Delta}{\leftrightarrow} CO$	-111
Combustion with O_2	$C + O_2 \overset{\Delta}{\leftrightarrow} CO_2$	-393
Gasification with CO_2	$C + CO_2 \overset{\Delta}{\leftrightarrow} 2CO$	172
Gasification with steam	$C + H_2O \overset{\Delta}{\leftrightarrow} CO + H_2$	131
Gasification with H_2	$C + 2H_2 \overset{\Delta}{\leftrightarrow} CH_4$	-75
CO oxidation	$2CO + O_2 \overset{\Delta}{\leftrightarrow} 2CO_2$	-283
Water gas shift	$CO + H_2O \overset{\Delta}{\leftrightarrow} H_2 + CO_2$	-41
Methanation	$CO + 3H_2 \overset{\Delta}{\leftrightarrow} CH_4 + H_2O$	-206
Steam methane reforming	$CH_4 + H_2O \overset{\Delta}{\leftrightarrow} 3H_2 + CO$	206

All biomass materials are similar in their chemical composition since the main chemical constituents are carbon, oxygen and hydrogen. The molecular formulas of CS (biomass used) are estimated as $CH_{1.268}O_{0.603}N_{0.0139}S_{0.00245}$ [131]. According to the above, biomass decomposes after the gasification process to (H_2), (CO_2), (CO), (N_2), (CH_4), char (C) and tar

($CH_{1.55}O_{0.55}$) as described in the following equation, which is called the global CS gasification reaction [131]:

$$CH_aO_bN_cS_d\ (biomass) \xrightarrow{\text{Gasification}} w\,H_2 + k\,CO + m\,CO_2 + n\,CH_4 + r\,H_2S + x\,NH_3 + y\,C\,(char) + z\,CH_{1.55}O_{0.55}(tar) \quad (3.1)$$

Where; a, b, c and d represent the number of atoms of H, O, N and S, and w, k, m, n, r, x, y and z represent the numbers of moles in the product chemical composition.

The higher heating value for CS is estimated based on the ultimate analysis as presented in Table 3.1 using the following empirical correlation equation [132]:

$$HHV\ (kJ/kg) = 349.1C + 1178.3H + 100.5S - 103.4O - 15.1N - 21.1ASH \quad (3.2)$$

Where; C, H, O, S and N are percentages of carbon, hydrogen, oxygen, sulfur and nitrogen, respectively. There are two efficiencies for the product gas namely the hot gas(η_{Hg}) and cold gas efficiencies (η_{Cg}) and they are calculated according to following equations [59].

$$\eta_{Hg} = \frac{LHV_{pg}\,m_{pg} + (\Delta T)m_{pg}\,C_{pg}}{m_B LHV_B} \quad (3.3)$$

$$\eta_{Cg} = \frac{LHV_{pg}\,m_{pg}}{LHV_B\,m_B} \quad (3.4)$$

LHV_{pg}, and LHV_B are the lower heat value of product gas (syngas) and biomass feedstock, respectively. m_{pg}, and m_B are the mass flow of product gas (syngas) and biomass feedstock, respectively. C_{pg} is the specific heat capacity of product gas (syngas) and ΔT is the temperature difference between gas outlet and fuel inlet.

3.3.2. Externally Fired Gas Turbine (EFGT):

EFGT is considered one of the popular conversion technology that used with biomass gasification for generate power from small and medium size plants [133]. EFGT is similar in its components and operation with other gas turbines.

The most important characteristic of this technology is the existence of both key devices: the combustion chamber and the high temperature heat exchanger (HTHE) which replaces the traditional firing system [134]. Many researches have focused on the use of biomass burning directly with EFGT due to its economic benefit, especially for places where biomass resources are available such as mills. This technology does not require any cleaning equipment systems which increase the investment cost [135]. From the perspective of thermodynamics, the Brayton cycle is the basis of EFGT. The main units of EFGT are combustion, compressor, turbine and generator as indicated in Figure 3.4.

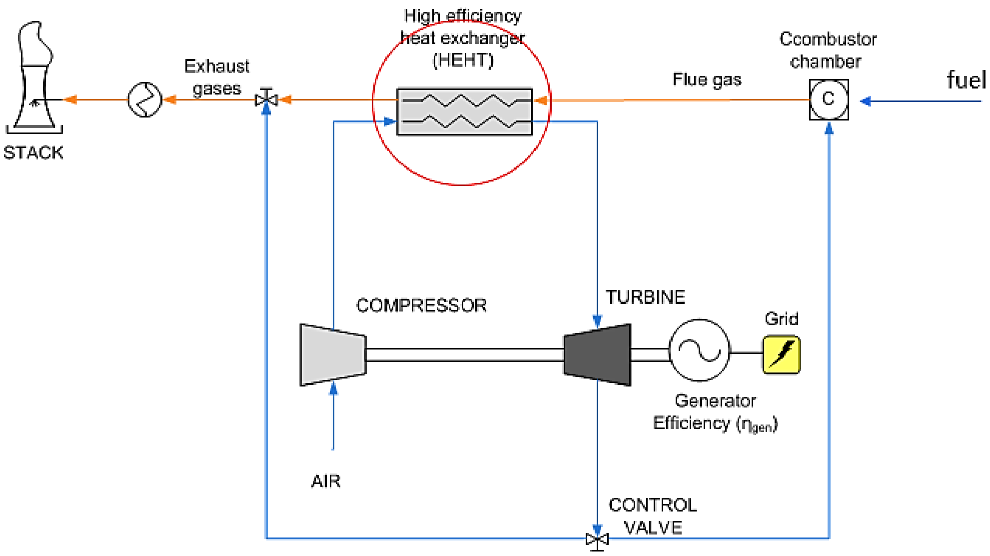

Figure 3. 4: Basic scheme of the EFGT

The combustor is an atmospheric direct-fired unit that burns the biomass feedstock directly, the combustion process requires the availability of three factors; fuel, air and heat. The temperature of combustion chamber can exceed 2000 ℃ (this will require a high cost), depending on the chemical characteristics of fuel, the moisture content of fuel, the amount of air and the construction of furnace [136].

The Air-Fuel Ratio (λ_{air}) and the efficiency of combustion chamber (η_{cc}) [116] are calculated as following:

$$\lambda_{air} = \frac{m_{air}}{\mathrm{m_{fuel}}} \qquad (3.5)$$

$$\eta_{cc} = \frac{\phi_{\mathrm{out}}}{\phi_{in}} \qquad (3.6)$$

Where m_{air} is mass ratio of air, m_{fuel} is mass ratio of fuel, Φ_{out} is the rate of useful energy from combustion and Φ_{in} is the rate of input energy (kW).

EFGT is similar in its components with the traditional gas micro-turbine, but it is characterized by HTHE, which is considered the most important part. HTHE works to increase the enthalpy of ambient air by converting thermal power of flue gas produced from the combustion chamber to rotate the turbine body and increase the temperature of compressed air to turbine inlet conditions [135]. Figure 3.5, shows the T-S layout of EFGT cycle, both of ΔT_h and ΔT_l represent the temperature difference inlet and outlet of HTHE. A small difference in temperature leads to better efficiency but the capital cost will increase because of the need for a larger exchanger [137].

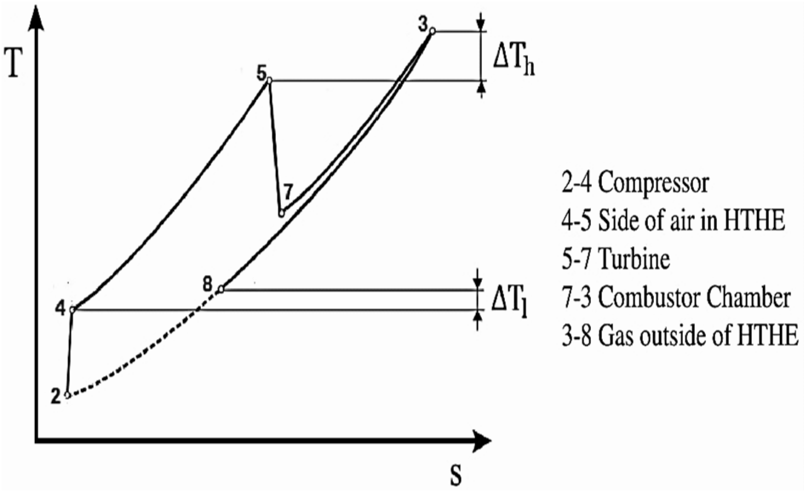

Figure 3. 5: T-S diagram of EFGT [137].

The net electrical power (P_{EL}) and efficiency of EFGT system ($\eta_{EFGT_{EL}}$) can be directly calculated using the following equations [59], [138]:

$$P_{EL} = (P_t - P_c) * \eta_{gen} \quad (3.7)$$

$$\eta_{EFGT_{EL}} = \frac{P_{EL}}{m_B * LHV_B} \quad (3.8)$$

Where P_t is the EFGT work output (kW), P_c is the EFGT compressor work consumption (kW), and η_{gen} is the generator efficiency.

3.3.3. Organic Rankine Cycle (ORC)

ORC is one of the most important economically and technologically attractive technologies to reuse thermal waste heat sources to maximize the electricity generation [139]. This technology is a closed cycle process and similar to the traditional steam turbine but instead of using water, a fluid called organic working fluid is used [140]. This fluid is characterized by a molecular mass higher than water and evaporates at low boiling conditions, which causes regularity of turbine rotation and non-corrosion of metal parts [141]. The ORC system consists of a pump, a condenser, an evaporator and a turbine. Other ORC systems use an internal heat exchanger (regenerator) to interchange heat inter the liquids leaving the turbine and that getting in the evaporator so as to improve system efficiency [142]. The layout diagram of the ORC units is indicated in Figure 3.6.

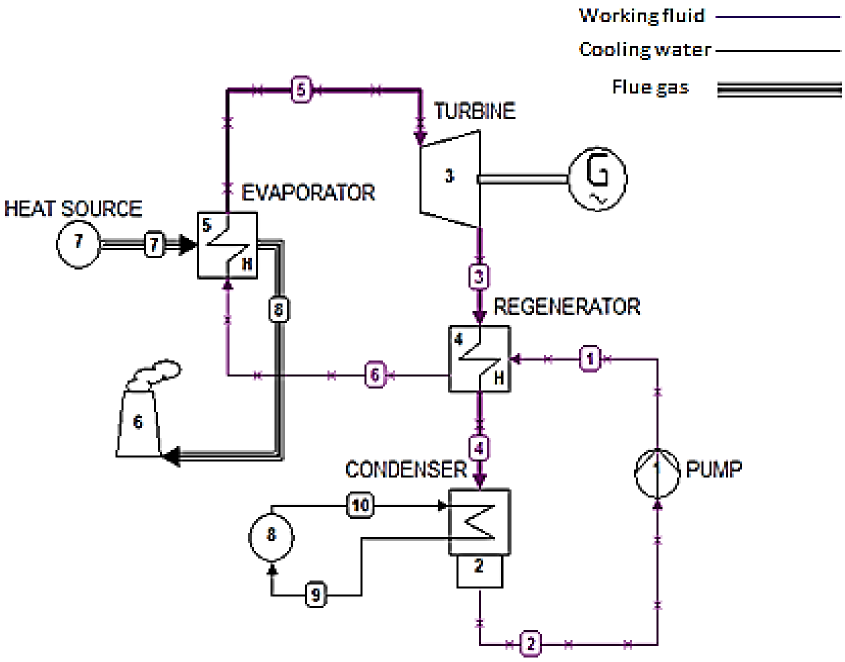

Figure 3. 6: ORC schematic.

The performance of ORC mainly depends on the working fluid. The choice of suitable working fluid for ORC depends on several considerations such as environmental characteristics (ozone depletion potential (ODP) and GWP), thermodynamics properties and safety properties (non-flammable and non-toxic) [142], [143]. In general, the working fluids are classified into three types (wet, dry and isentropic). The saturation curve (T-s) of the three working fluid types is shown in Figure 3.7. Wet working fluids can cause small droplets of water inside the turbine, resulting in decrease in turbine efficiency or damage. To avoid this, the wet fluid must be overheated in the evaporator before entering the turbine body [144]. In case of dry and isentropic fluids, the overheating process is not recommended and these two types are usually used.

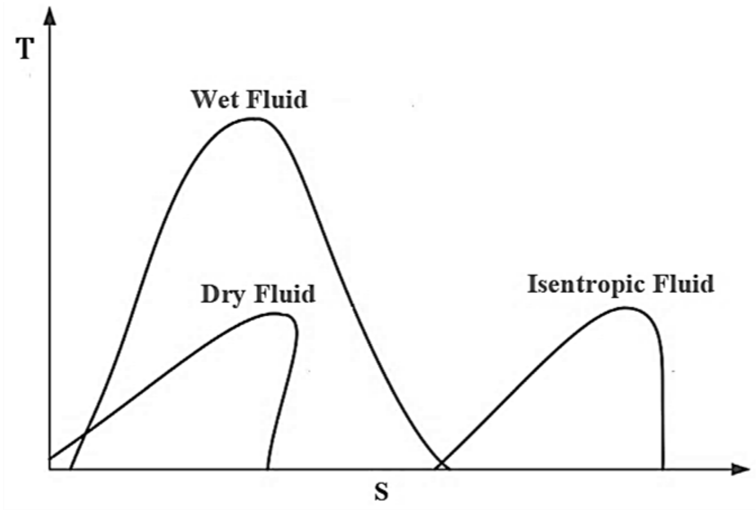

Figure 3. 7: T-s Curve for working fluid types [143].

In this work, four types of dry working fluids are suggested to be used in the ORC generator: cyclohexane, benzene, toluene and R113. The main properties and safety data classifications of these fluids are given in Table 3.4. The thermo-physical properties of used working fluids are given according to NIST Chemistry WebBook.

Table 3. 4: Main Characteristics of used working fluids

Fluid	**Thermodynamic Data**					**Environmental Data**			**Safety data**
	CD (kg/m3)	CT (℃)	CP (bar)	NBP (℃)	Acentric factor	GWP (100 yr)	Flammable	ODP	ASHRAE 34 safety group
Cyclohexane	273	280.49	40.75	80.7	0.21	-	Yes	-	A3
Benzene	309	288.90	48.94	80.1	0.21	-	Yes	-	B2
Toluene	292	318.60	41.26	110.6	0.27	3	Yes	0	A3
R113	560	214.06	33.9	47.6	0.25	6130	No	1000	A1

3.3.4. Absorption Cooling System

This system uses exhaust heat of EFGT or the waste heat from ORC subsystem to generate cooling power. The absorption cooling system consists of two subsystems namely HRS and VAC [145];

1) HRS subsystem, that used water and vapor as the working fluids [145]. During this process, the exhaust heat is treated under low pressure through the evaporator and

drum units to produce the saturated vapor which is used to provide the necessary heat for the generator [62].

2) VAC subsystem. It consists of generator, absorber, condenser, preheater (super heater), solution heat exchanger (HE) and evaporator. The preheater and solution of HE are the most important units because they improve the performance of system (Chattopadhyay and Ghosh, 2018). This subsystem uses water mixed with ammonia as refrigerant instead of conventional refrigerants [145]. Ammonia is more efficient and has a GWP less than 1. In absorber, the ammonia is absorbed in liquid water, so it is called a strong solution.

3.4. Developed CCHP Plant Configuration

This section is for simulating a small-scale CCHP plant using two different configurations and studying the ability of two types of biomass (CS and bagasse) to generate electrical, thermal, and cooling power through this system.

3.4.1. Gasifier, EFGT, and Absorption Units

This CCHP system is based on using the gasification unit (downdraft fixed bed gasifier), EFGT as an electrical generation unit, and heat recovery device with the absorption cooling cycle. This system aims to generate around 70 kW of electric power from 100 Kg/h of the CS. The simulation has been carried out using the thermodynamics software Cycle-Tempo [146].

Figure 3.8, shows the EFGT diagram for syngas conversion process. As we can see, the gas produced by the gasification reactor enters the combustion chamber (pipe 2), which is an internal oven where the gas is heated and oxidized under atmospheric pressure and temperature not exceeding 950 ℃ with the presence of hot air from the turbine and this amount of air is controlled using a control valve (pipe 6), then this flue gas passes through HTHE (pipe 8). In HTHE, the energy in the gas is transferred to a compressed air. This air is considered the working liquid that enters the compressor (pipe 1) and it is compressed under pressure, which is four times the atmospheric pressure and certain temperature, then it passes to HTHE (pipe 3) with flue gas [138]. This hot and clean air expands within the body of the turbine (pipe 4) to produce electricity. The waste heat from the flue gas (pipe 10) (exhaust gas) can be used in heat (stacks) and cooling (chiller) applications.

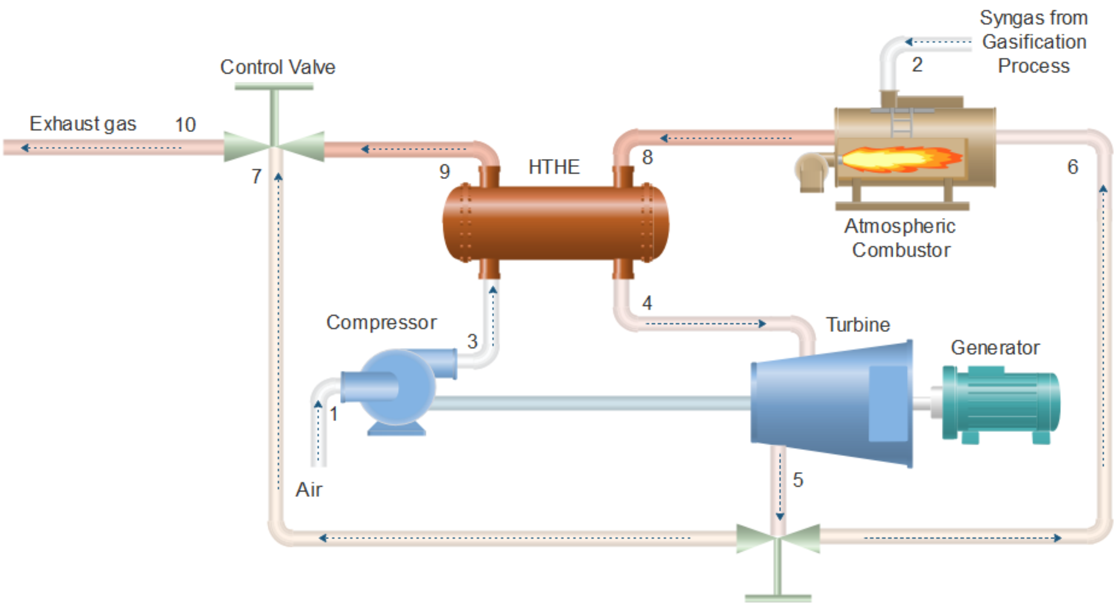

Figure 3. 8: Schematic of EFGT [59]

The HTHE efficiency (η_{HTHE}) is the ratio of the exchanged thermal power to the ideally exchangeable thermal power that can be calculated as [59]:

$$\eta_{HTHE} = \frac{H_{p4} - H_{p3}}{H_{p8} - H_{p9}} \tag{3.9}$$

Where, (H_p) is the specific enthalpy of the pipes involved in the equation.

The power consumption in compressor (P_c) is determined by:

$$P_c = \left(H_{p3} - H_{p1}\right) * m_{air} \tag{3.10}$$

Figure 3.9, indicates the absorption cooling system layout process. During the cooling process, the exhaust heat of EFGT (pipe 10) is treated under low pressure through the evaporator and drum units to produce a saturated vapor (pipe 15) which used to provide the necessary heat for the generator. The working fluids used during this process are water and steam [147].

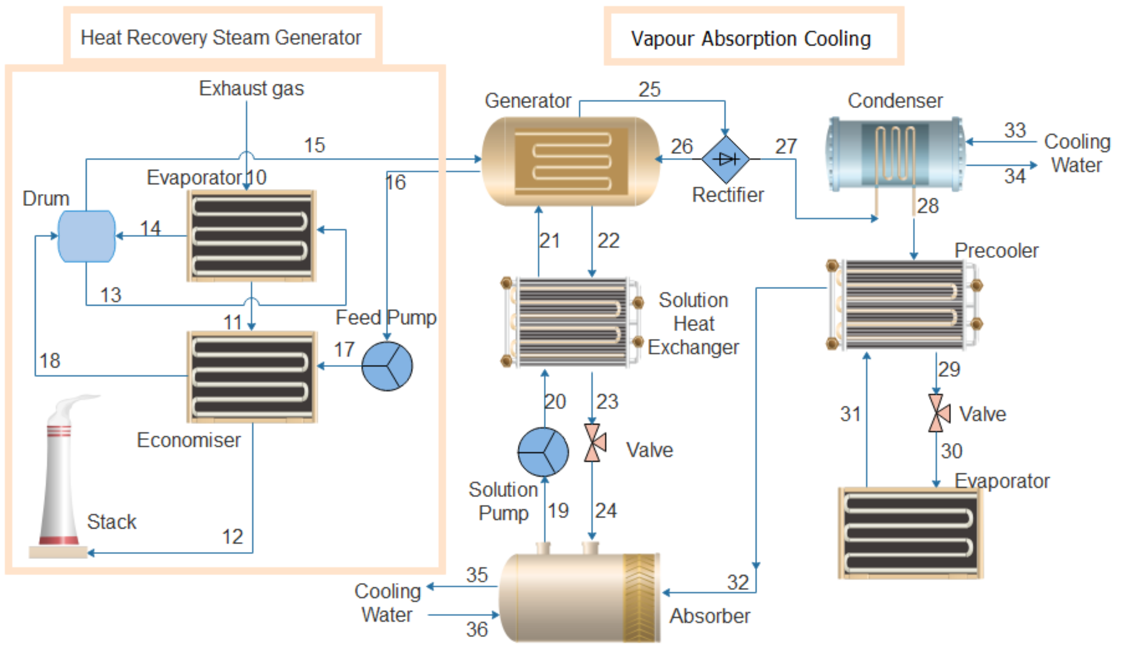

Figure 3. 9: Sketch of absorption cooling system [63], [147].

For the VAC subsystem, the strong solution of the working fluid is supplied to the generator from the absorber (pipe 19) and heat exchanger (pipe 21). With saturated vapor (pipe 15) in the generator at high pressure, ammonia evaporates with steam and produces distilled ammonia which is supplied to rectifier (pipe 25) and then condensed (pipe 27) by cooling tower water in condenser. A weak solution of ammonia flows from generator and return back to the absorber (pipe 24) through the heat exchanger (pipe 23) [63]. The importance of solution heat exchanger is to balance between the strong and the weak solutions of ammonia before combining them in the absorber unit [148].

The condensed liquid (pipe 28) flows to evaporator through precooler and controlled by expansion valve (pipe 30). Liquid refrigerant is sprayed on evaporator tubes to produce chilled water and the ammonia evaporates at low temperature and pressure. After that, the ammonia (pipe 31) returns to precooler and then supplied to the absorber (pipe 32). The absorber unit is cooled by cooling tower water [147]. The main specifications of the CCHP system used are listed in Table 3.5.

Table 3. 5: Main performance properties of the Gasifier, EFGT, and Absorption system

Performance Parameters	Value
Combustion chamber pressure bar	1.013 bar
Combustion chamber efficiency	96 %

Maximum flue gases temperature	938.45 ℃
Hot side temperature difference for HTHE	110 ℃
Maximum TIT	875 ℃
Turbine isentropic efficiency	83 %
Compressor isentropic efficiency	80 %
Turbine and compressor mechanical efficiency	95 %
Electric generator efficiency	97 %
Exhaust gases temperature	252.25 ℃
circulation ratio (CR) of the HR drum	5
Isentropic efficiency of the HR pump	65 %
Mechanical efficiency of the HR pump	60 %
Operating pressure of HR pump ($\wp_{\mathrm{HR_p}}$)	2.7 bar
Isentropic efficiency of the solution pump	65 %
Stack temperature	$>$ 100 ℃
Generator temperature	120 ℃
Operating pressure of valve	2.83 bar
Working fluid in absorption cooling subsystem	Ammonia/water

The power consumption of feed pump ($\mathrm{P_{FP}}$), the system cooling power ($\mathbb{Q}_{eva}$) (kW) and are calculated as follows:

$$\mathrm{P_{FP}} = \left(\mathrm{H_{p17}} - \mathrm{H_{p16}}\right) * \mathrm{m_{15}} \tag{3.11}$$

$$\mathbb{Q}_{eva} = \mathrm{m_{31}H_{31}} - \mathrm{m_{30}H_{30}} \tag{3.12}$$

The overall electrical efficiency ($\eta_{\mathrm{net_{EL}}}$), the overall thermal efficiency (η_{th}), the system cooling to power ratio (CPR) and performance coefficient (PC) of hybrid system are given as [64], [147].

$$\eta_{\mathrm{net_{EL}}} = \frac{\mathrm{P_{EL}} - \mathrm{P_{FP}} - \mathrm{P_{SP}}}{\mathrm{m_B} * \mathrm{LHV_B}} \tag{3.13}$$

$$\mathrm{P_{SP}} = \left(\mathrm{H_{p20}} - \mathrm{H_{p19}}\right) * \mathrm{m_{19}} \tag{3.14}$$

$$\eta_{\mathrm{th}} = \frac{\mathrm{P_{EL}} - \mathrm{P_{FP}} - \mathrm{P_{SP}} + \mathbb{Q}_{eva}}{\mathrm{m_B} * \mathrm{LHV_B}} \tag{3.15}$$

$$\mathrm{CPR} = \frac{\mathbb{Q}_{eva}}{\mathrm{P_{EL}} - \mathrm{P_{FP}} - \mathrm{P_{SP}}} \tag{3.16}$$

$$\mathrm{PC} = \frac{\mathbb{Q}_{eva}}{\mathbb{Q}_{gen} + \mathrm{P_{SP}}} \tag{3.17}$$

$$\mathbb{Q}_{gen} = \left(\mathrm{H_{p15}} - \mathrm{H_{p16}}\right) * \mathrm{m_{15}} \tag{3.18}$$

Where, $\mathrm{P_{SP}}$ is the power consumption of solution pump (kW) and $\mathbb{Q}_{gen}$ is the recovered heat flows to generator ($\mathrm{kW_{th}}$).

3.4.2. EFGT, ORC and Absorption Units

This CCHP system is based on studying the optimal performance parameters including the operating conditions (maximum pressure, maximum temperature) for the developed system, which is based on a direct burning biomass combustor, an EFGT, and an ORC as bottoming unit for maximizing the electrical efficiency. The tri-generation system presents an absorption refrigeration unit for cooling power production. The used biomass type is sugarcane bagasse which is available in various areas of Upper Egypt, especially Qena and Aswan. Four working fluids (cyclohexane, benzene, toluene and R113) have been studied with the entire system to analyze the optimal ORC working fluid. The simulation has been carried out using the thermodynamics software Cycle-Tempo [146]. NIST Chemistry WebBook [149] has been used to study the thermo-physical properties of the working fluids. The selection of more suitable ORC working fluid is mainly depends on the temperature difference between the heat source and its boiling point. This system aims to generate around 170 kW of electric power from 144 kgh^{-1} of bagasse

Figure 3.10, illustrates the layout of the simulation CCHP system, where bagasse is introduced into the combustion chamber (through pipe 1) reaching a reaction temperature of 985 ℃. The biomass is transformed into high-temperature flue gas (the combustion exhaust gas) and inserted into the HTHE (pipe 3). The thermal power of hot flue gas is partially absorbed by the air inside HTHE to start moving the turbine to generate mechanical power. The air is drawn into a compressor (pipe 2), then it enters HTHE (pipe 4) and expands in the turbine (pipe 5). The air produced from the turbine (pipe 6) is reused in the combustor chamber (pipe 7) controlled by the valve. HTHE efficiency (η_{HTHE}), is the ratio of the thermal power exchanged to the ideally exchangeable [59], which is indicated according to the following equation:

$$\eta_{HTHE} = \frac{H_{p5} - H_{p4}}{H_{p3} - H_{p8}} \quad (3.19)$$

The thermal power ($P_{EL_{th}}$), and electrical efficiency of the EFGT ($\eta_{EFGT_{EL}}$) system are directly calculated using the following formulas [138]:

$$P_{EL_{th}} = m_w \times cp_w \times \Delta T_w \quad (3.20)$$

$$\eta_{EFGT_{EL}} = \frac{P_{EL_{th}} + P_{EL}}{m_B \times LHV_B} \quad (3.21)$$

m_w represents the water mass flow (kg/s), cp_w is the specific heat capacity of water (kJ kg^{-1} K^{-1}), ΔT_w is the water temperature.

In the ORC system, the organic working fluid is fed into a closed loop cycle through a pump (pipe 12), then conveyed to the regenerator (pipe 13) where the fluid is reheated. The fluid is then passed through the evaporator (pipe 14). At this point, both of working fluid and waste heat from EFGT (pipe 10) enter in the evaporator. The waste heat increases the fluid's temperature until reaches to the evaporation point. The vaporized fluid passes through the turbine (pipe 15) and expands, causing the turbine to spin and generating electrical power when a generator is connected in the same shaft. The steam out from the turbine passes through the regenerator (pipe 16) to reduce the temperature and preheat the working fluid at a later stage. The organic vapour passes through the condenser to back again to its original liquid form of working fluid. Once this fluid reaches the pump, the process restarts [59], [150].

One of the most important factors when considering the performance of ORC system is the PPTD. PPTD is the temperature difference between the heat source and evaporator temperatures [151]. If the heat source temperature is constant, and the temperature of evaporator is low, this will lead to increase PPTD and heat inside ORC system. This is the reason of larger turbines will be needed and the cost will be increased. Evaporator temperature and pressure should be kept within certain values [152]. Each working fluid has optimal PPTD ratio [150]. In this work, the minimum value of PPTD for the selected working fluids is taken to be 10 ºC.

The heat transferred to the working fluid in the evaporator ($Q_{eva_{orc}}$), the thermal efficiency of ORC ($\eta_{ORC_{th}}$) which depends on the turbine and pump pressure ($P_{turbine}$, P_{pump}), the net electrical efficiency ($\eta_{net_{EL}}$) and CHP efficiency ($\eta_{net_{CHP}}$) of whole system (EFGT and ORC) are calculated using the following equations [59]:

$$Q_{eva_{orc}} = H_{p15} - H_{p14} \tag{3.22}$$

$$\eta_{ORC_{th}} = \frac{P_{turbine} - P_{pump}}{m_{ORC}} \tag{3.23}$$

$$P_{turbine} = m_{ORC} \times (H_{p15} - H_{p16}) \tag{3.24}$$

$$P_{pump} = m_{ORC} \times (H_{p13} - H_{p12}) \tag{3.25}$$

$$\eta_{net_{EL}} = \frac{P_{EL} + P_{ORC_{el}} - P_{aux}}{m_B \times LHV_B} \tag{3.26}$$

$$\eta_{net_{CHP}} = \frac{P_{EL} + P_{EL_{th}} + P_{ORC_{el}}}{m_B \times LHV_B} \tag{3.27}$$

Where m_{ORC} is the working fluid mass flow and P_{aux} is the additional electrical consumption of other components such as pumps and compressors.

During the absorption process, the exhaust heat (pipe 11) is treated under low pressure through the evaporator and drum units to produce the saturated vapor (pipe 16) which is used to provide the necessary heat for the generator [62]. In VAC subsystem, the mixture of ammonia and water is pumped from the absorber (pipe 20) through the HE (pipe 21) and supplied to the generator (pipe 22). The heat is transferred to the generator unit (pipe 16), this waste heat under high pressure makes the ammonia to be separated from the water which called a weak solution. The weak solution of ammonia flows from the generator through HE and expansion valve (pipes 23 and 24) and return to the absorber (pipe 24). It is important to balance the strong and weak ammonia solutions [147]. The high-pressure ammonia from generator unit is condensed in the condenser through the drum (pipe 28). The condensed liquid (pipe 29) is transferred to the drum, HE (pipe 30) and preheater (pipe 31) through the reflux valve. The condensed liquid through preheater is poured into the evaporator (pipe 33) and controlled by an expansion valve (pipe 32). The liquid refrigerant is then sprayed on the evaporator tubes to produce the chilled water and the ammonia, which evaporates at low temperature and pressure. The ammonia (pipe 34) returns to the preheater, supplies to the absorber (pipe 5) and finally is cooled down through the cooling tower. The main specifications of this CCHP are listed in Table 3.6.

The Reflux ratio, which represents the ratio of mass flow rate of liquid refrigerant from reflux valve to the mass flow rate from condenser, The CPR, and the CP are computed according to the following formulas [64], [147]:

$$P_{net_{el}} = P_{EL} + P_{ORC_{el}} - P_{aux} \tag{3.28}$$

$$CPR = \frac{\mathbb{Q}_{eva}}{P_{net_{el}}} \tag{3.29}$$

$$\text{reflux ratio} = \frac{m_{30}}{m_{29}} \tag{3.30}$$

$$P_{SP} = \left(H_{p20} - H_{p19}\right) * m_{20} \tag{3.31}$$

$$\mathbb{Q}_{gen} = \left(H_{p16} - H_{p17}\right) * m_{16} \tag{3.32}$$

$$\mathrm{PC} = \frac{\mathbb{Q}_{eva}}{\mathbb{Q}_{gen} + \mathrm{P_{SP}}} \tag{3.33}$$

Where $\mathrm{P_{net_{el}}}$ is the total output of electrical power (kW), and $\mathrm{Q_{gen}}$ is the recovered heat flow to generator ($\mathrm{kW_{th}}$).

The net electrical and thermal efficiency of CCHP system are defined as follows [64]:

$$\eta_{\mathrm{net}_{el}} = \frac{\mathrm{P}_{\mathrm{net}_{el}}}{\mathrm{m_B} * \mathrm{LHV_B}} \tag{3.34}$$

$$\eta_{\mathrm{net}_{el}} = \frac{\mathrm{P}_{\mathrm{net}_{el}} + \mathbb{Q}_{eva}}{\mathrm{m_B} * \mathrm{LHV_B}} \tag{3.35}$$

Table 3. 6: Main Characteristics of the EFGT, ORC and Absorption system

EFGT		
Variables	**Present Study**	**Source**
Biomass consumption	144 kg/h	-
Pressure of the burning chamber	1.013 bar	[59], [138]
Maximum flue gases temperature	1000 ℃	[59]
TIT	875 ℃	[59]
$\boldsymbol{\eta}_{\mathbf{isentropic}}$ of turbine	83 %	[59]
$\boldsymbol{\eta}_{\boldsymbol{mech}}$ of turbine	95 %	[59]
$\boldsymbol{\eta}_{\mathbf{isentropic}}$ of compressor	80 %	[59]
$\boldsymbol{\eta}_{\boldsymbol{mech}}$ of compressor	95 %	[59]
Generator efficiency	97 %	[59]
Exhaust gases temperature	271 ℃	-
ORC		
$\boldsymbol{\eta}_{\mathbf{isentropic}}$ of the turbine	80 %	[59], [153]
$\boldsymbol{\eta}_{\boldsymbol{mech}}$ of the turbine	95 %	[59]
$\boldsymbol{\eta}_{\mathbf{isentropic}}$ of the pump	80 %	[153], [154]
$\boldsymbol{\eta}_{\boldsymbol{mech}}$ of the pump	80 %	[154]
Operating pressure of pump ($\boldsymbol{p}_{\mathbf{Pump}}$)	25 bar	[154]
Generator efficiency	95 %	[153]

PPTD in evaporator	10 ℃	-
TIT of an ORC	< 310 ℃	-
District heating temperature	98 ℃	-
Working fluids selected	Cyclohexane Benzene Toluene R113	-
Absorption Cooling		
CR of the HRS drum	5	-
Operating pressure of HRS pump	2.7 bar	-
$\eta_{\text{isentropic}}$ and η_{mech} of pumps	75 %	[155]
Generator temperature	120 ℃	[145]
Stack temperature	> 100 ℃	-
Operating pressure of valve	2.83 bar	-
Working fluid in absorption cooling subsystem	Ammonia/water	-

Chapter 4

Techno Economic Design of Hybrid Systems with Biomass Gasifier

Chapter 4

Techno Economic Design of Hybrid Systems with Biomass Gasifier

4.1. Introduction

This chapter provides a description and explains the analysis of the components of different scenarios of a stand-alone hybrid system based on using a biomass system. In addition, the formulation of the optimization problem, the economics, and cost performance of the proposed systems are discussed. These stand-alone hybrid systems are based on utilizing real-time meteorological data for different remote areas located in Egypt.

The suggested off-grid hybrid systems that we discussed in the thesis are as follows;

1) Hybrid Stand-alone PV, WT, Biomass System, and Battery units in Abu-Monqar region, Egypt.
2) Hybrid Stand-alone PV, WT, Biomass System, and Battery units in Alrashda Village in Egypt.
3) Hybrid Stand-alone PV, WT, Biomass , and Battery units for supplying a load in the new Tiba city, north-east of Luxor city in Egypt
4) Hybrid Stand-alone PV, Biomass System, FC, ELE units, and HT units in Abu-Monqar region, Egypt.

4.2. The Hybrid System Components Description

This section explains in detail the description of the major system units, which are PV, WT, Biomass System, Inverter, Batteries, FC, ELE, and HT units. Figure 4.1, illustrated the layout model of the stand-alone hybrid system based on using the PV, WT, Biomass System, and Batteries. While, the graphical diagram of the stand-alone hybrid system based on using the PV, Biomass System, FC, ELE, and HT units is indicated in Figure 4.2.

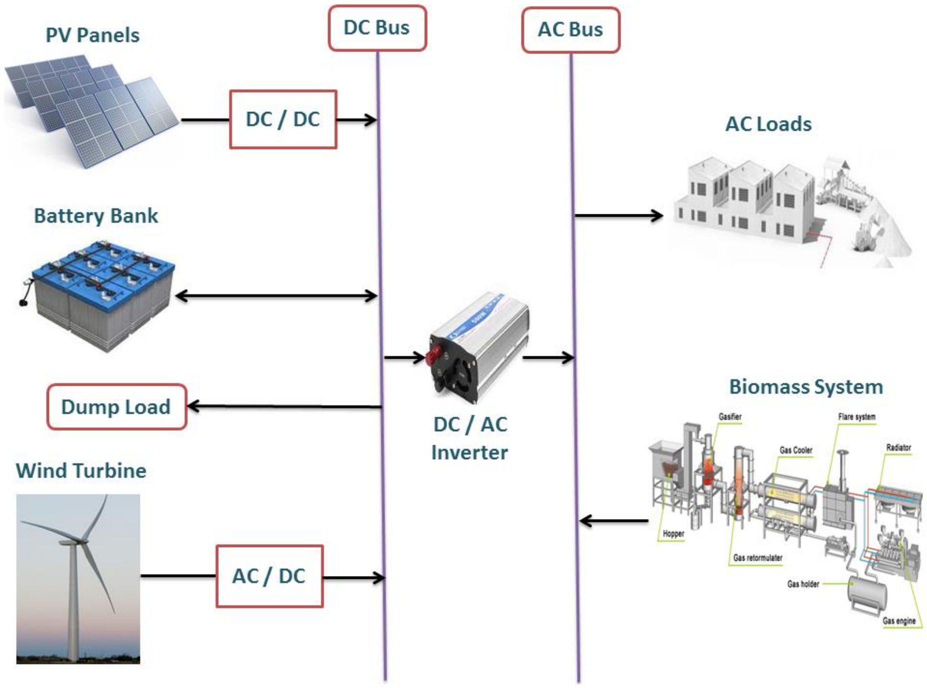

Figure 4. 1: The architecture of the PV, WT, Biomass System, and Batteries stand-alone hybrid system.

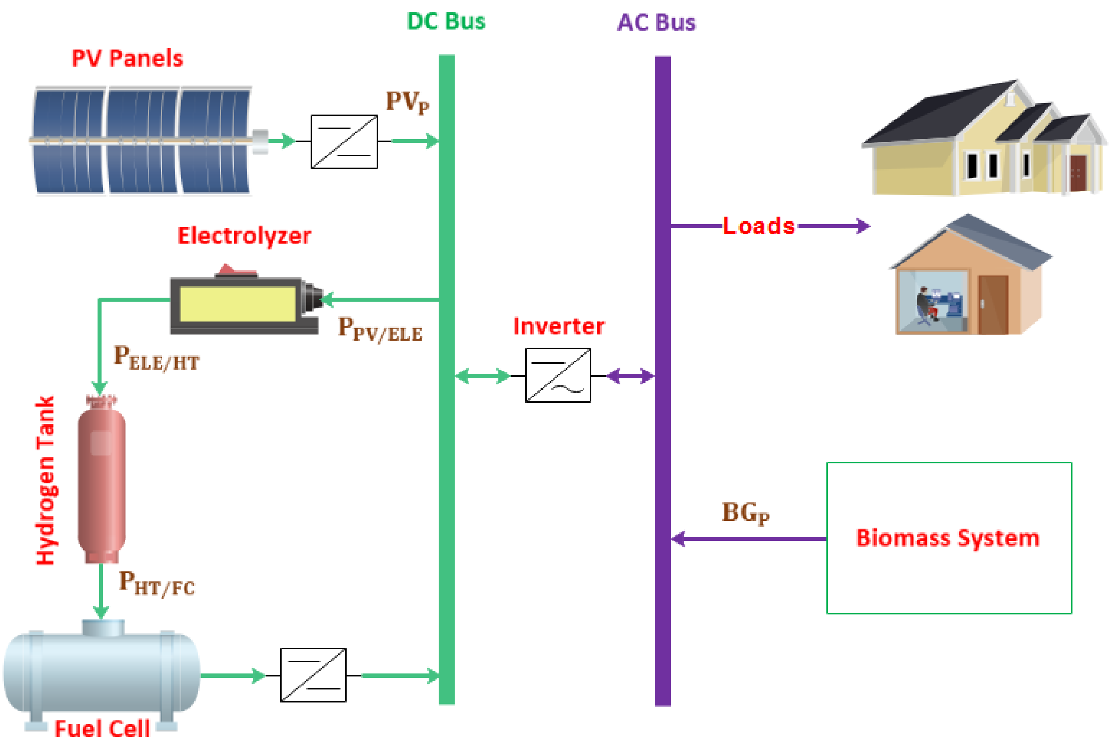

Figure 4. 2: The PV, Biomass System, FC, ELE, and HT hybrid system’s configuration layout.

4.2.1. Photo Voltaic (PV)

The performance of the solar module changes according to the changes in the environmental and weather conditions in the installation site [156]. The generated output power of the PV system (P_{PV}) is calculated using the following equations [78], [157]:

$$T_{cell}(t) = R_{int}(t)\left(\frac{T_{NO} - 20}{0.8}\right) + T_{amb} \tag{4.1}$$

$$P_{pv}(t) = \left(N_{pv}\, p_{rated}^{PV}\, \eta_w\, \eta_{PV}\right)\left(\frac{R_{int}(t)}{R_{nom}}\right)\left(1 - \gamma_T(T_{cell}(t) - T_r)\right) \tag{4.2}$$

Where, $T_{cell}(t)$ and T_r are the cell temperature at time t and under standard operating conditions, respectively; T_{NO} is the cell temperature at normal operating conditions; N_{pv} is the number of PV modules included in the PV system; η_{pv} and η_w are the PV system efficiency and wiring efficiency, respectively; p_{rated}^{PV} is the PV rated power at normal conditions; R_{int} and R_{nom} are the intensity of solar radiation at time t and under standard conditions, respectively; and γ_T is the temperature coefficient of power for the PV module.

4.2.2. Wind Turbine (WT)

The WT consists of three basic parts, namely the tower, the blades, and the generator that converts the kinetic energy into electrical energy [158], [159]. The amount of electrical energy generated from a WT depends on the wind speed and the design of the blades [160]. The wind speed increases with height above the ground level. Hence, the wind speed at a certain height H2 is calculated according to the following equation [161]:

$$\left(\frac{S_2}{S_1}\right) = \left(\frac{H_2}{H_1}\right)^{\beta_{wt}} \tag{4.3}$$

Where, S_1 and S_2 are wind speed at the reference point H_1 and at the turbine hub with height H_2, respectively; β_{wt} is the WT friction coefficient. According to the International Electrotechnical Committee (IEC) [162], [163], the value of the coefficient of friction in the case of normal wind conditions is 0.20 and in the case of intensive wind conditions is 0.11. The generated power from WT (P_{wt}) can be expressed as follows [28], [164]:

$$P_{wt}(t) = \begin{cases} 0, & S(t) < S_{cut}^{in} \text{ or } S(t) > S_{cut}^{off} \\ N_{wt}\, p_{rated}^{wt}\, \eta_{wt}\left(\dfrac{S^2(t) - S_{cut}^2}{S_{rated}^2 - S_{cut}^2}\right), & S_{cut}^{in} < S(t) < S_{rated} \\ N_{wt}\, p_{rated}^{wt}\, \eta_{wt}, & S_{rated} < S(t) < S_{cut}^{off} \end{cases} \tag{4.4}$$

Where $S(t)$, S_{cut}^{in} and S_{cut}^{off} are wind speed at time t, cut-in wind speed, and cut-off wind speed, respectively. N_{wt} is the number of WTs in the wind farm, η_{wt} is the WT efficiency and p_{rated}^{wt} is the rated power of the WT at rated wind speed.

4.2.3. Biomass System

This work uses a small-scale downdraft gasification technology that converts solid biomass into a gaseous fuel (syngas) used in turbines to generate electricity. The reason for choosing downdraft gasification technology is that the fixed bed gasifiers are often simple and low-cost, and it has a high total carbon conversion rate and high solids residence time and low gas velocity. A downdraft gasifier is a co-current reactor in which the gasification agent is supplied from the top or sides of the reactor, causing the feedstock and gasification agent to flow in the same direction. Downdraft gasifiers are commonly utilized in engine applications because of their simplicity, low investment costs, good product gas quality, and ability to install in small spaces.

In this study, two biomass feedstock are used which are CS and sugarcane bagasse. CS is one of the misused agricultural wastes in Egypt. In this study, CS is used as the biomass feedstock to the gasifier where the biomass particles are broken at a relatively high temperature (more than 700 degrees Celsius) and the cracking process takes place in four stages. After that, with the presence of the gasification agent, which is air, these particles are recombined to form a synthetic gas which is used in turn as fuel for turbines to produce electricity [12], [13]. Sugarcane bagasse is used as a raw material for biomass to feed a small-scale downdraft gasifier, as the cane crop is one of the agricultural crops available in the New Valley city.

The efficiency of the syngas produced by the gasification process η_g, generator output power $P_{BG}(t)$, and average fuel consumption per hour $F_{Cons_{BG}}(t)$ are calculated according to the following equations [13], [85];

$$\eta_g = \frac{LHV_{pg}\ m_{pg}}{LHV_B\ m_B} \tag{4.5}$$

$$P_{BG}(t) = \frac{N_{BG}}{F_m}\left(\frac{\eta_g\ LHV_B\ B_{rated}(t)}{LHV_{pg}} - F_0\ PG_{rated}\right) \tag{4.6}$$

$$F_{Cons\_BG}(t) = \frac{LHV_{pg}}{\eta_g\ LHV_B}\left(N_{BG}F_0PG_{rated} + F_m\ P_{BG}(t)\right) \tag{4.7}$$

Where N_{BG} is the number of biomass generators, B_{rated} is biomass consumption rate per hour (kg/h), F_m denotes Marginal fuel consumption, F_0 presents no-load fuel consumption, and PG_{rated} is the rated power of biomass generators.

The GHG emissions from the feedstock residues are calculated as [85]:

$$BE_T = LHV_B * Sum\ (B_{rated}), \quad (4.8)$$

$$E_{Con} = BE_T * 0.0002778, \quad (4.9)$$

$$GHG = E_{Con} * GWP * 0.43, \quad (4.10)$$

Where BE_T and E_{Con} are the total biomass consumption and the energy consumption (kWh), respectively. GWP is equal 1 [28], and 0.43 is the electricity emission factor ($kgCO_2$/kWh) [165].

4.2.4. Bi-directional Converter Model

A bidirectional transducer is adopted to maintain power flow between DC and AC components. There are two kinds of power conversion devices in a power system, the inverter that converts DC current to AC current and the rectifier, which converts AC current to DC current. The technical characteristics of the inverter model are presented in Table 5. The hourly input power of the inverter $P_{inv}(t)$ can be expressed as below [166];

$$P_{inv}(t) = P_L(t)/\eta_{inv} \quad (4.11)$$

- ✓ For PV/WT/Biomass/Batteries Module

$$P_{ren} = P_{pv} + P_{wt} + \frac{P_{BG}}{\eta_{inv}} \quad (4.12)$$

- ✓ For PV/Biomass/Batteries Module
- ✓ PV/Biomass/ELE/HT/FC Module

$$P_{ren} = P_{pv} + \frac{P_{BG}}{\eta_{inv}} \quad (4.13)$$

In which, η_{inv} represents the inverter efficiency, $P_L(t)$ is the hourly load demand, and P_{ren} is the generated power from renewable sources.

4.2.5. Battery Bank

The battery is the device that stores electrical energy in a chemical form and then supplies this energy as electrical energy when needed. In this study, the batteries are used to store the surplus energy when the power produced by the PV units, WTs, and biomass system is greater than the load demand. Batteries start discharging when the energy generated from sustainable sources is unable to meet the load demand or in the case of system maintenance. There are different types of batteries, but the type used in this study is the lead-acid battery [78]. The SOC_{Bat} expresses a measure of the capacity of the battery storage system. The operation of the battery storage system is controlled by the maximum (SOC_{max}) and minimum (SOC_{min}) charge boundaries. The SOC_{Bat}, the charging energy (B_{CH}), and discharging energy (B_{DIS}) can be expressed during charging and discharging stages according to the following equations [7], [85], [43]:

In the charging period,

$$B_{CH}(t) = (P_{ren}(t) - (P_L(t)/\eta_{inv})) * \Delta t * \eta_{CH} \tag{4.14}$$

$$SOC_{Bat}(t) = SOC_{Bat}(t-1) * (1-\sigma) + B_{CH}(t) \tag{4.15}$$

In discharging period,

$$B_{DIS}(t) = \left((P_L(t)/\eta_{inv}) - P_{ren}(t)\right) * \Delta t * \eta_{DIS} \tag{4.16}$$

$$SOC_{Bat}(t) = SOC_{Bat}(t-1) * (1-\sigma) - B_{DIS}(t) \tag{4.17}$$

Where η_{CH} and η_{DIS} are the battery charging and discharging efficiencies, respectively; and σ is self-discharge rate.

4.2.6. Electrolyzer (ELE)

ELE consists of an anode and a cathode separated by an electrolyte in which an electric current passes through, creating a chemical reaction, which decompose water into its two elements (hydrogen and oxygen). The generated hydrogen is collected around the surface of the anode. Based on [167], most of the ELEs, produce hydrogen at 30 bar but this hydrogen is transferred directly to the FC at a low pressure of 1.2 bar. In most research, the produced hydrogen is directly delivered to the hydrogen tank, however in other studies, the pressure is raised to 200 bar with the use of a compressor in order to increase the stored energy in the tank [167]. Other works employ two tanks with low and high pressure. If this tank is fully charged, a compressor is used to transport the hydrogen to the high-pressure tank in order to waste as little energy as possible because the compressor will not be running all the time [168]. In this study, Proton-conducting polymeric membrane electrolyzer (PEM) is used, where the produced hydrogen of the ELE is immediately transported to the hydrogen tank at a pressure of 30 bar. The energy is transferred to the hydrogen tank from the ELE ($P_{ELE/HT}$) is expressed as [28], [167];

$$P_{ELE/HT} = \eta_{ELE} * P_{ren/ELE}, \quad (4.18)$$

Where η_{ELE} denotes the efficiency of an electrolyzer and $P_{ren/ELE}$ represents the electrical energy feeding the ELE from renewable sources.

4.2.7. Hydrogen Tank Storage (HT)

After the hydrogen and oxygen separation process, the hydrogen gas is transported and stored in HT to be used in the FC for power generation. To ensure the process balance, the HT upper pressure is adjusted to the same as that of the water ELE pressure, while the HT lowest pressure is adjusted to the same fuel cell pressure [103]. During the operation, the stored hydrogen mass in the HT (HT_m) is constrained by the minimum and maximum values [28] according to this formulation:

$$HT_m^{min} \leq HT_m(t) \leq HT_m^{max}, \quad (4.19)$$

The stored hydrogen energy in the HT ($HT_E(t)$) and the stored hydrogen mass ($HT_m(t)$) at time step (t) are expressed as follows [28], [169], [170]:

$$HT_E(t) = HT_E(t-1) + \left(P_{ELE/HT}(t) - \frac{P_{HT/FC}(t)}{\eta_{HT}}\right) \times \Delta t, \quad (4.20)$$

$$HT_m(t) = HT_E(t)/HHV_H, \quad (4.21)$$

Where $P_{HT/FC}(t)$ indicates the power supplied towards the FC from the HT, η_{HT} is the HT efficiency, Δt is the time durations during simulation, and HHV_H denotes the higher heat value of the stored hydrogen gas (kWh/kg).

4.2.8. Fuel Cell (FC)

Fuel cells are electrochemical cells used to produce electrical energy through an electrochemical reaction by continuously supplying oxygen and hydrogen gases to the cell. At the anode, hydrogen is oxidized into protons (which rotate by the electrolyte to the anode) and electrons (which rotate from outside the cell to the anode), and after oxygen is collected, it is reduced to form water. Fuel cells produce electricity while having as byproducts not only water, but also thermal energy (heat) [171], [172].There are many types of fuel cells, the common types of fuel cells are Proton exchange membrane fuel cell, Alkaline fuel cells, Direct alcohol fuel cell, Molten carbonate fuel cell and SOFC [173]. In this study, a PEMFC is used. This PEMFC is characterized by its small size, long lifespan, and operation under relatively low temperatures [174]. The generated electrical power from PEMFC (FC_P) depends on its overall efficiency (η_{FC}) and can be expressed by [169], [170]:

$$FC_P = \eta_{FC} * P_{HT/FC} \quad , \tag{4.22}$$

4.3. Case Study Areas

4.3.1. Abu-Monqar Village

Abu-Monqar is a remote Egyptian settlement in the Western Desert of Egypt. It is a remote oasis located 100 km south of Frafra Oasis, 250 km from the El- Dakhla Oasis, and 650 km southwest of Cairo. The selected area's latitude and longitude are 26°30.3' North and 27°39.8' East, respectively[78] , as indicated in the map in Figure 4.3. The system average load value used for simulation is 260 kW, and the peak value is 420 kW[78]. Figure 4.4, shows the hourly load power over one summer day and one year [78]. The monthly average global solar radiation and temperature for one year are taken from the SOLAR RADIATION AND METEOROLOGICAL DATA SERVICES [175], which is based on the average long-term values over 20 years from the NASA Surface Meteorology and Solar Energy website for the proposed case study area. The hourly average solar radiation on the horizontal plane and temperature during one year and a summer day are shown in Figures 4.5 and 4.6, respectively.

Figure 4. 3: Map location of Abu-Monqar region, Egypt.

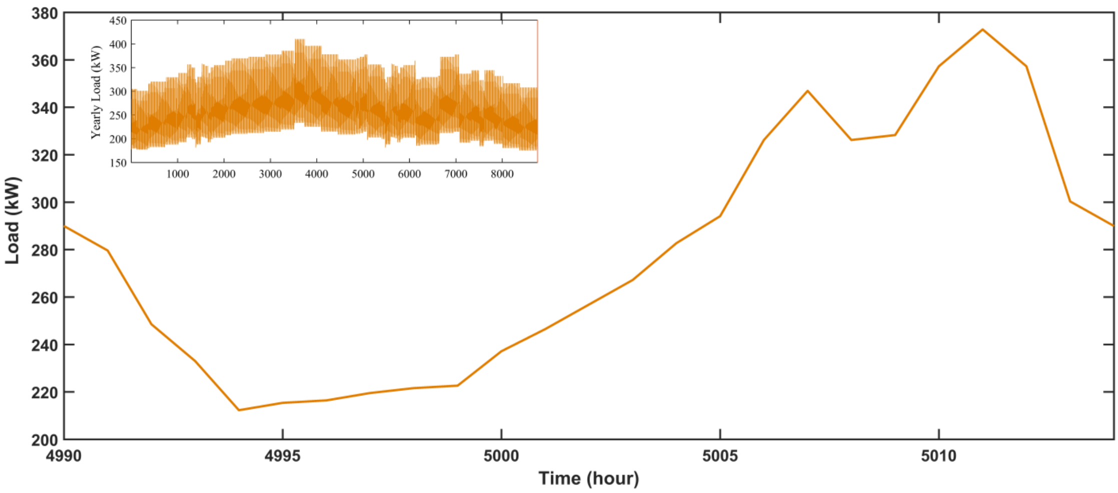

Figure 4. 4: Daily and yearly load profile in Abu-Monqar región

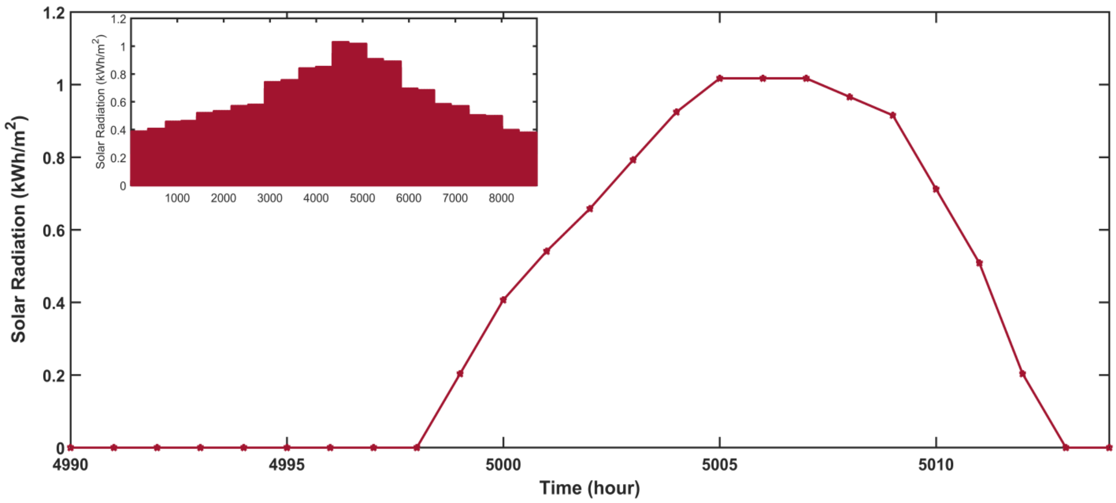

Figure 4. 5: Hourly PV average radiation during one year and a summer day in Abu-Monqar region

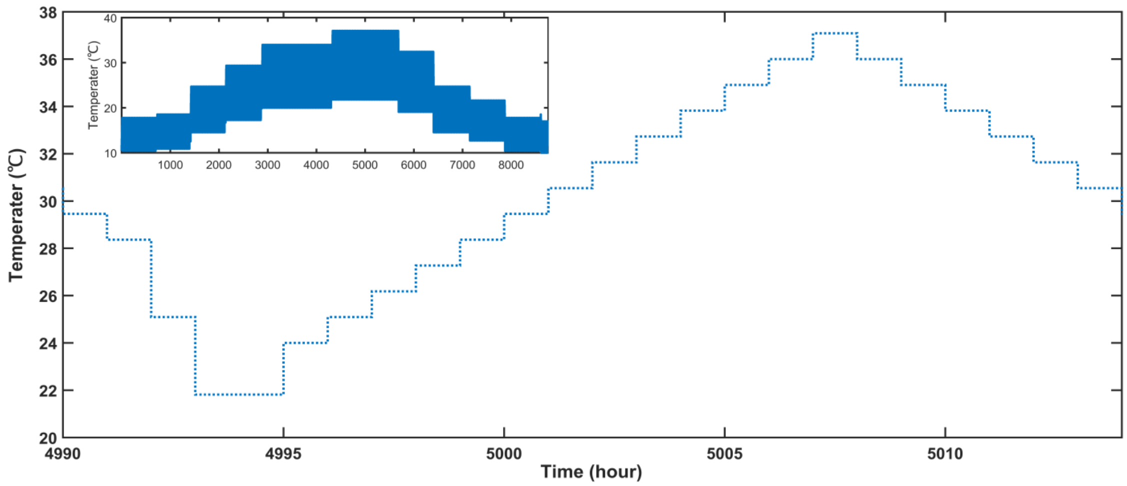

Figure 4. 6: Hourly PV average temperature during one year and a summer day in Abu-Monqar region

4.3.2. Alrashda Village

Alrashda village is located 10 km northwest of Mut town, the administrative center of the Dakhla Oasis in the New Valley Governorate in Egypt at 28.938º east longitude, 25.576º north latitude and an altitude of 243 m. The reason of choosing this village because of its comparatively high solar, wind, and biomass energy potential. The proposed mathematical model is used for designing a small-scale stand-alone hybrid system to feed a range of loads, which are represented in residential loads, where the peak loads are occurred during the summer and in the evening period from 19:00 to 23:00 pm. In Figure 4.7, the profile of the proposed loads during a year is depicted, which shows that the average residential load of the village has reached about 260 kW, with a maximum load of 410 kW. Figures. 4.8 – 4.10

illustrate the plot of hourly data of the solar radiation, temperature, and wind speed, which obtained from NASA Surface Meteorology and Solar Energy website for 20 years for the selected area. Figure 4.8, presents the short-wave solar irradiance of the studied area during a year, where the yearly radiation rate is between 2.45 kWh/m^2/day to 10.94 kWh/m^2/day, with the average yearly radiation on this site's horizontal surface is around 6.89 kWh/m^2/day. While, the yearly ambient temperature of the selected site is indicated in Figure 4.9, which showed that the maximum ambient temperature could be reached, is 40 º. Figure 4.10, illustrates the annual wind speed for the selected location with a maximum wind speed of about 13.9 m/s in addition, an average in the range from 8.71 m/s to 9.89 m/s.

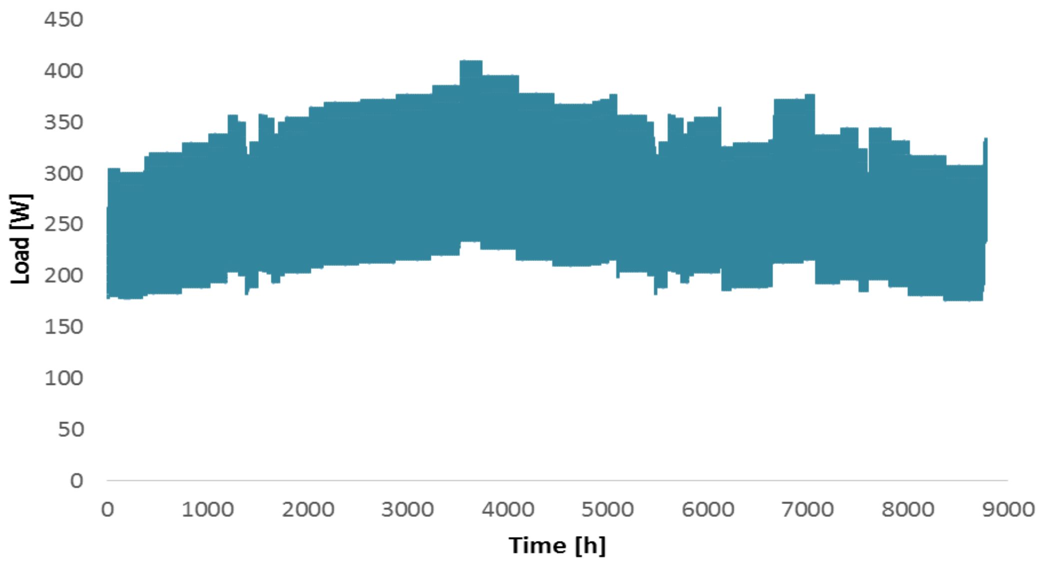

Figure 4. 7: Load profile of the studied area

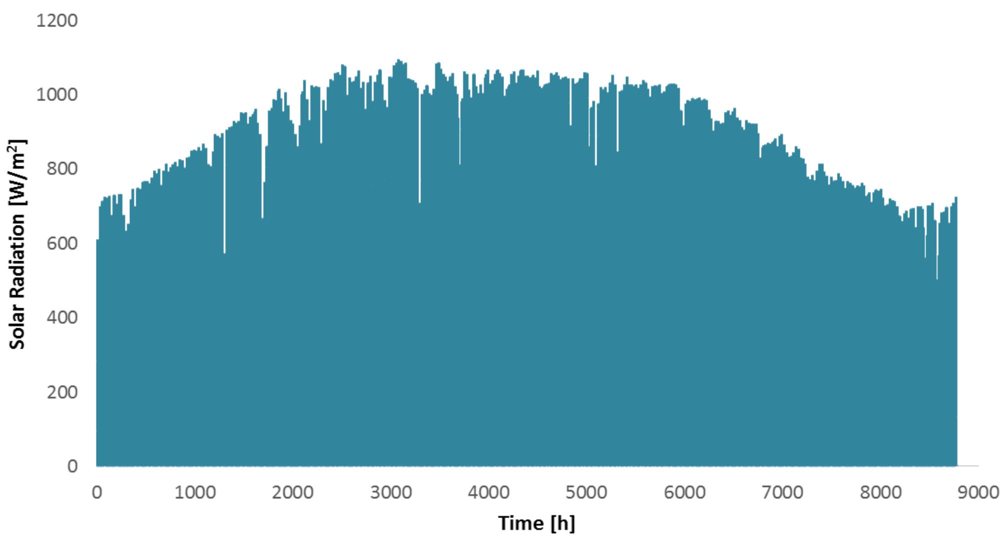

Figure 4. 8: The annual short-wave solar irradiance of the studied area

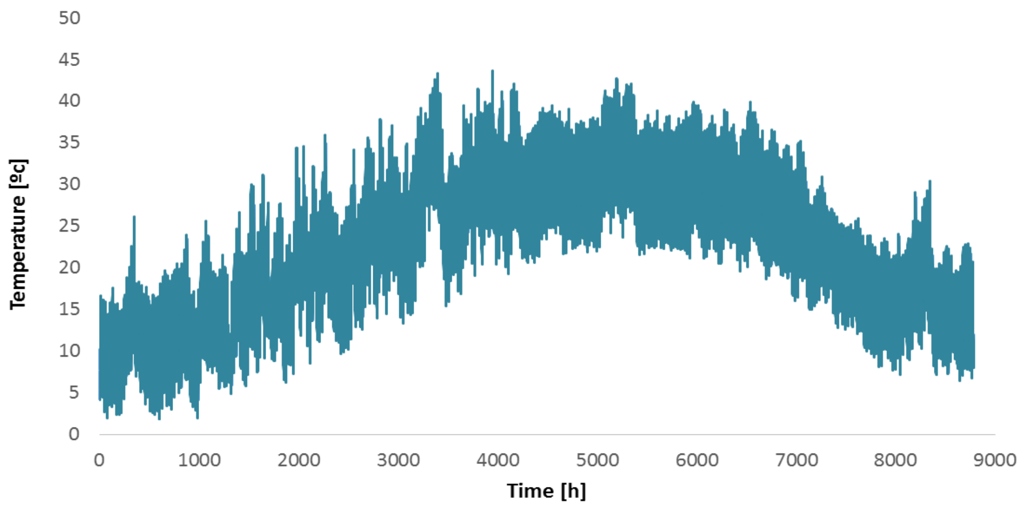

Figure 4. 9: The yearly ambient temperature of the studied area

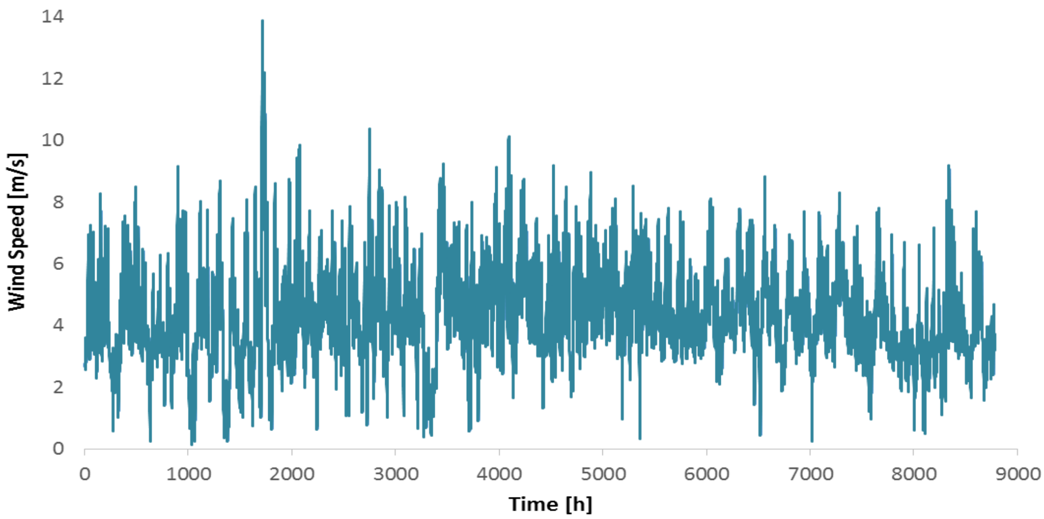

Figure 4. 10: The yearly wind speed of the studied area

4.3.3. New Tiba City

The new Tiba city is located 14 km northeast of Luxor and 10 km from Luxor International Airport (latitude of 25.733 and longitude of 32.771) as shown in the map in Figure 4.11. The proposed system is dedicated to supplying domestic loads. Figure 4.12 shows the hourly load demand profile during a year, with a maximum load of 410 kW, which is enough for most residential and commercial load demands. For the suggested case study area, the monthly average worldwide solar radiation and temperature are taken from the NASA / Modern-Era Retrospective Analysis for Research and Applications (MERRA) based on the studied area's latitude and longitude, which is based on the long-term average values over 20 years from the NASA Surface Meteorology and Solar Energy website [176]. The hourly average solar radiation on the horizontal plane and temperature during one year (from

1st of December 2020 to 30th of November 2021) are illustrated in Figures 4.13 and 4.14, respectively. Figure 4.15, indicates the typical hourly wind speed in the selected area over one year (from 1st of December 2020 to 30th of November 2021) with wind direction at 10 m above ground [176].

Figure 4. 11: Location of the case study area

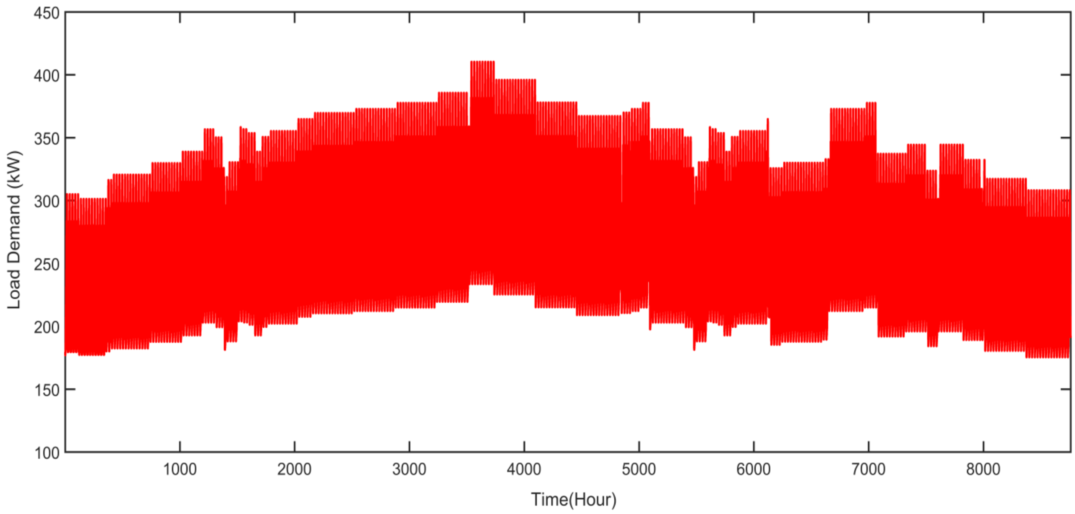

Figure 4. 12: Typical hourly load power requirement in the selected area

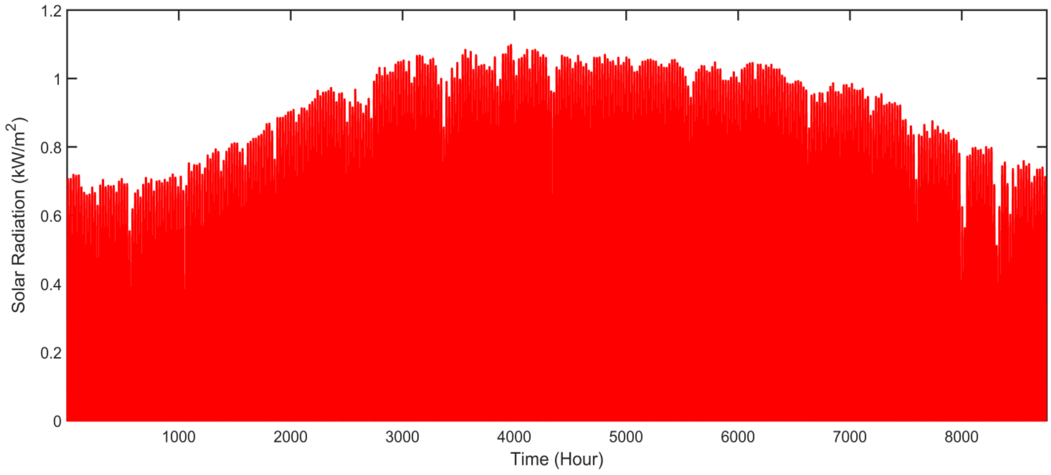

Figure 4. 13: Typical hourly solar radiation in the selected area over a year

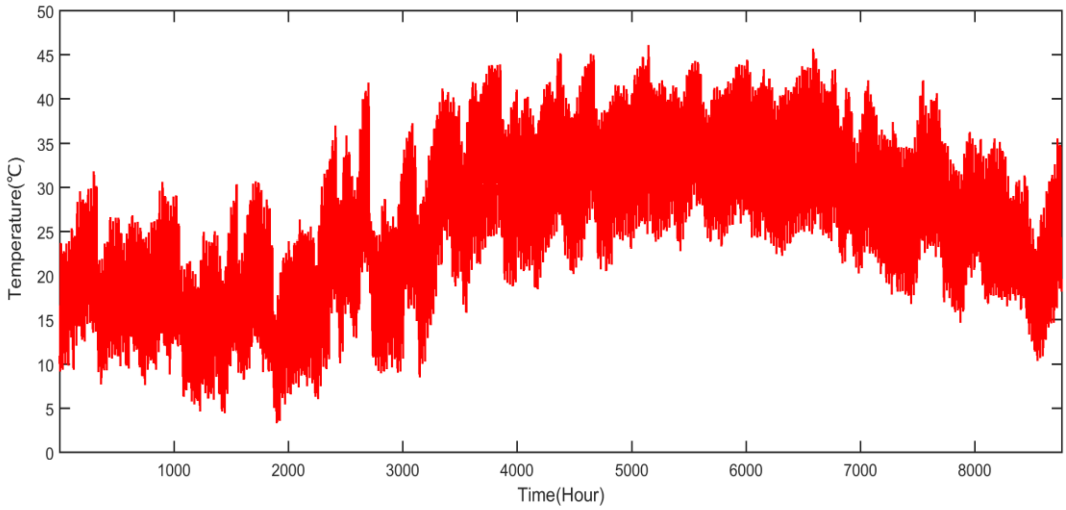

Figure 4. 14: Typical hourly solar temperature in the selected area over a year

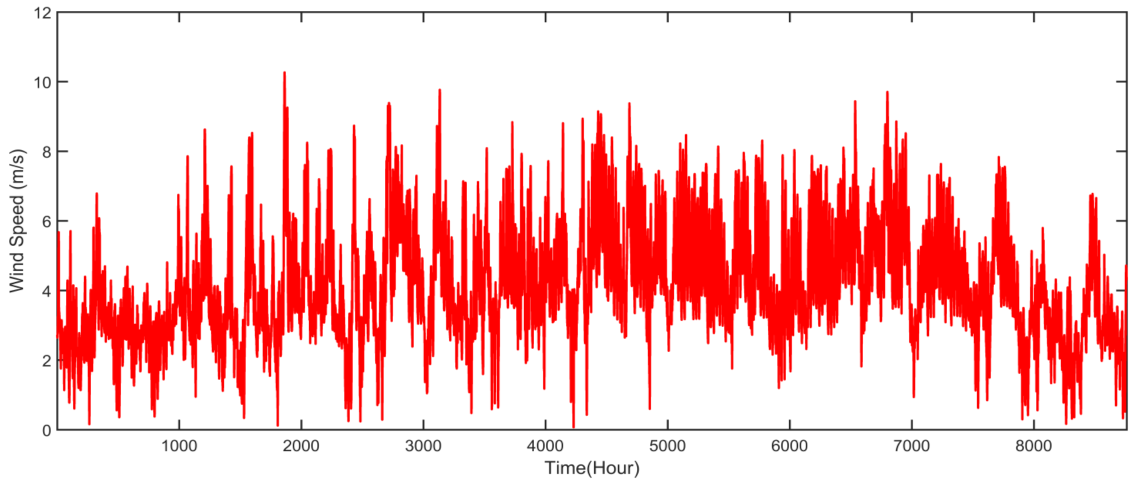

Figure 4. 15: Typical hourly wind speed in the selected area over a year

4.4. Formulation of the Optimization Problem

4.4.1. Objective Function

The main objective function of the proposed hybrid systems is to find the best unit combination for a hybrid renewable energy system so that it can provide the most energy. To accomplish this, the value of EC is decreased; the LPSP of the system is maintained, and the excess power (P_{ex}) absorption is reduced. At the same time, the power delivered to the dummy load (P_{dum}) has to be minimized in order to reduce the size of the generating units. A multi-objective optimization problem is expressed by the following objective function formula.

$$\text{Min } F(X) = \text{Min } (\lambda_1 \text{ EC} + \lambda_2 \text{ LSPS} + \lambda_3 P_{ex}), \tag{4.22}$$

$$P_{ex} = \sum_1^{8760} \frac{P_{dum}(t)}{P_L(t)}, \tag{4.23}$$

- ✓ For PV/WT/Biomass/Batteries Module

$$X = [N_{pv}\ N_{wt}\ N_{BG}\ N_B], \tag{4.24}$$

- ✓ For PV/Biomass/Batteries Module

$$X = [N_{pv}\ N_{BG}\ N_B], \tag{4.25}$$

$$LPSP = \sum_1^{8760} \frac{P_L(t) - (P_{ren}(t) + SOC_{Bat}(t-1) - SOC_{min}) * \eta_{inv}}{P_L(t)}, \tag{4.26}$$

- ✓ For PV/Biomass/ELE/HT/FC Module

$$X = [N_{pv}\ N_{BG}\ \ HT_m\ P_{ELE/HT}\ FC_P]\ , \tag{4.27}$$

$$LPSP = \sum_1^{8760} \frac{P_L(t) - P_{ren}(t) - FC_P(t)}{P_L(t)}, \tag{4.28}$$

Where λ_1, λ_2, and λ_3 represent the weighting factors for the multi-objective optimization problem (MOOP). The weighting factors usually depend on the studied problem and they are selected using a trial-and-error method [177]. The effect of the choice of these penalty factors in the case of solving the optimal reactive power dispatch problem has been studied in [177]. A similar study has been made and it is found that the best weight factor values for λ_1, λ_2, and λ_3 of EC, LPSP and P_{ex} are 0.3, 0.5 and 0.2, respectively. P_{ex} is the percentage of the excess energy consumed by the P_{dum} throughout the year (T = 8760 hours) and the sum of the load power for all time intervals. X represents the control variables of the optimization problem that must be optimized using the studied optimization algorithms.

4.4.2. Constraints

The optimization procedure operates within the confines listed below and is dependent on the upper and lower bounds of the choice parameters;

$$P_{ex} \leq P_{ex}^{max}, \tag{4.29}$$

$$LSPS \leq LPSP^{max}, \tag{4.30}$$

- ✓ For PV/WT/Biomass/Batteries Module

$$1 \leq \begin{bmatrix} N_{pv} \\ N_{wt} \\ N_{BG} \\ N_{B} \end{bmatrix} \leq \begin{bmatrix} N_{pv}^{max} \\ N_{wt}^{max} \\ N_{BG}^{max} \\ N_{B}^{max} \end{bmatrix}, \tag{4.31}$$

- ✓ For PV/BS/Batteries Module

$$1 \leq \begin{bmatrix} N_{pv} \\ N_{BG} \\ N_{B} \end{bmatrix} \leq \begin{bmatrix} N_{pv}^{max} \\ N_{BG}^{max} \\ N_{B}^{max} \end{bmatrix}, \tag{4.32}$$

- ✓ For PV/Biomass/ELE/HT/FC Module

$$1 \leq \begin{bmatrix} N_{pv} \\ N_{BG} \\ HT_{m} \\ P_{ELE/HT} \\ FC_{P} \end{bmatrix} \leq \begin{bmatrix} N_{pv}^{max} \\ N_{BG}^{max} \\ HT_{m}^{max} \\ P_{ELE/HT}^{max} \\ FC_{P}^{max} \end{bmatrix}, \tag{4.33}$$

4.4.3. Economic and Cost Analysis

The annual total cost (ATC) of the system is taken into account based on the capital cost annual interest (C_A^{cap}), the components replacement cost ($C_{rep,r}$), the feedstock's annual fuel cost (C_A^{fuel}), the components operation and maintenance cost ($C_{O\&M,r}$), this can expressed according to the following formula;

$$ATC = C_A^{cap} + C_A^{fuel} + \sum_{r=1}^{S} C_{rep,r} + \sum_{r=1}^{S} C_{O\&M,r}, \tag{4.34}$$

The NPC indicates the current value of the major investment and operating costs throughout the project's spin, while the EC ($/kWh) is the price of one kWh that the system generates. The NPC and EC can be represented as follows [28]:

$$NPC = ATC / CRP, \tag{4.35}$$

$$\mathrm{CRP} = \frac{\mathrm{r\,(I+1)^S}}{\mathrm{(r+1)^S-1}} \tag{4.36}$$

$$\mathrm{EC} = \frac{\mathrm{ATC}}{\sum_1^{8760} \mathrm{P_L}}, \tag{4.37}$$

Where CRP is the capital retrieval parameter, r denotes the interest rate factor, and S is the project lifetime.

4.5. Operation Strategy

Based on the previous literature review revealed that only a few studies have presented the optimal sizing performance of integrated a biomass unit with other renewable energy systems with using HOMER software. Thus, in this thesis, an operation management strategy for two combinations of stand-alone hybrid systems using real-time meteorological data of different remote areas located in the Egypt are suggested with using different optimization algorithms.

- The first system includes PV, WT, biomass, and battery units;
- The second one is PV, biomass, ELE, HT and FC units;

4.5.1. Hybrid PV/WT/Biomass/Battery System

The PV panels, and/or WT, and biomass gasification are the main sources for generating power in this system, while the batteries work to maintain the continuity of the power supply to the loads and enhancing the power supply. In this study, the power management strategy of the hybrid renewable energy system to meet the load demand is based on P_{ren} and the power of the (P_{inv}) [85].

The general operation strategy can be summarized in the following points:

- First, when P_{ren} meets the load demand ($P_{ren}(t) = P_{inv}(t)$), the SOC of the battery bank remains unchanged, and the LPS during this time interval is zero.
- Second, when P_{ren} generated from the system is greater than the load demand ($P_{ren}(t) > P_{inv}(t)$), and the SOC of the battery system during this time interval is below the maximum allowable charging limit, the battery will be charged by the surplus power ($P_S(t)$) until the maximum limit is reached.

$$P_S(t) = P_{ren}(t) - P_{inv}(t) \tag{4.38}$$

- If the battery reaches its maximum charging limit, the SOC of the storage system still unchanged and equal the SOC in the previous time interval ($SOC_{Bat}(t) = SOC_{Bat}(t-1)$), at the same time the power provided by the hybrid system will be dissipated in the P_{dum}.

- When the P_{re} generated from the proposed system cannot satisfy the load demand and the SOC of the battery storage system is higher than the minimum allowable limit ($P_{ren}(t) < P_{inv}(t)$ and $SOC_{Bat}(t-1) * (1-\sigma) > SOC_{min}$), then the energy stored in the battery bank will be used to cover the load demand.

4.5.2. Hybrid PV/Biomass/ ELE/HT/FC System

The operation strategy used in the proposed hybrid system is simplified in a flowchart shown in Figure 4.17. The operating strategy can be summarized in three main cases as follows:

1. When the energy produced from the renewable sources satisfies the load demand ($P_{ren}\ (t) = \frac{P_L\ (t)}{\eta_{inv}}$), in this case, the generated power is supplied to cover the required load demand, and no power is needed from the FC, and no power is supplied to the electrolyzer;
2. When the energy produced from renewable sources exceeds the load demand ($P_{ren}\ (t) > \frac{P_L\ (t)}{\eta_{inv}}$, in this case, this excess energy $P_{EXC}(t)$ will feed the electrolyzer, and the produced hydrogen is used to charge the HT units;
3. When the energy produced from renewable sources is insufficient to meet the load demand ($P_{ren}\ (t) < \frac{P_L\ (t)}{\eta_{inv}}$), in this case, the FC will use hydrogen stored in the HT units to make up for the deficiency in power generation. When the HT capacity reaches its minimum, this leads to load loss.

Chapter 5

Recent and Developed Optimization Techniques for Optimal Techno Economic Design

Chapter 5

Recent and Developed Optimization Techniques for Optimal Techno Economic Design

5.1. Introduction

The optimization procedure is known as mathematical programming in mathematics and computer science since it is connected to computer programming. Numerous industries, particularly engineering systems, utilize the optimization method. When required restrictions are present, it is used to find the optimal solution (upper/lower) for a single objective function or a multi-objective function between a numbers of variables [178]. The optimal sizing of various isolated hybrid systems based on employing the biomass system is addressed in this thesis using a number of optimization algorithms. Additionally, two modifications and enhancements are suggested to enhance the functionality of the traditional method. The novel algorithms suggested in this thesis to obtain the optimal techno-economic results are as follows:

1. Recent Optimization Algorithms
    - SMA method,
    - SOA method,
    - HBO algorithm,
    - CFA method,
    - STOA method,
    - MOA method,
2. Modified Optimization Algorithms
    - QRUN algorithm
    - GAHA optimizer

5.2. Recent Optimization Algorithms

A brief explanation of the mathematical presentation of the proposed algorithms is derived in the following subsections.

5.2.1. SMA and SOA

These novel algorithms have been used to obtain the optimum solution of the hybrid system PV/Wind/Biomass/Battery. The control parameters used in the optimization process for each algorithm are listed as follows:

- Number of search agents = 10.
- Maximum number of iterations = 50.
- Dimension size = 4.

Figure 5.1, illustrates the flowchart describing the operating strategy for the proposed hybrid system. Each optimization algorithm operates according to the following steps:

A. Run the program of designing the proposed hybrid energy system based on the energy balance, which has three main steps:

1. Generation of the initial population.
2. Run the program of designing the hybrid system described in equations in the components description section and in the economic and cost analysis section, as illustrated in the flowchart presented in Figure 5.1.
3. The evaluation process of the fitness functions for all agents/positions given in Eq. (4.22).

B. Run the optimization algorithm with the hybrid system, which involves the following processes:

1. Updating the sizing of the system elements, according to the nature of each optimization algorithm.
2. Run the program of designing the proposed system described in equations in the components description section and in the economic and cost analysis section, as illustrated in the flowchart of Figure 5.1.
3. The evaluation process of the fitness function for all agents/positions presented in Eq. (4.22)
4. Check whether the proposed system meets the end criterion or not. If so, (i.e., “Yes”), the program will be stopped and will go to the next step, otherwise (i.e., “No”), the three previous processes, namely from “1” to “3”, will be repeated.

Show the results such as sizing of RES and the best optimum values of EC, NPC, LPSP, and Dummy load.

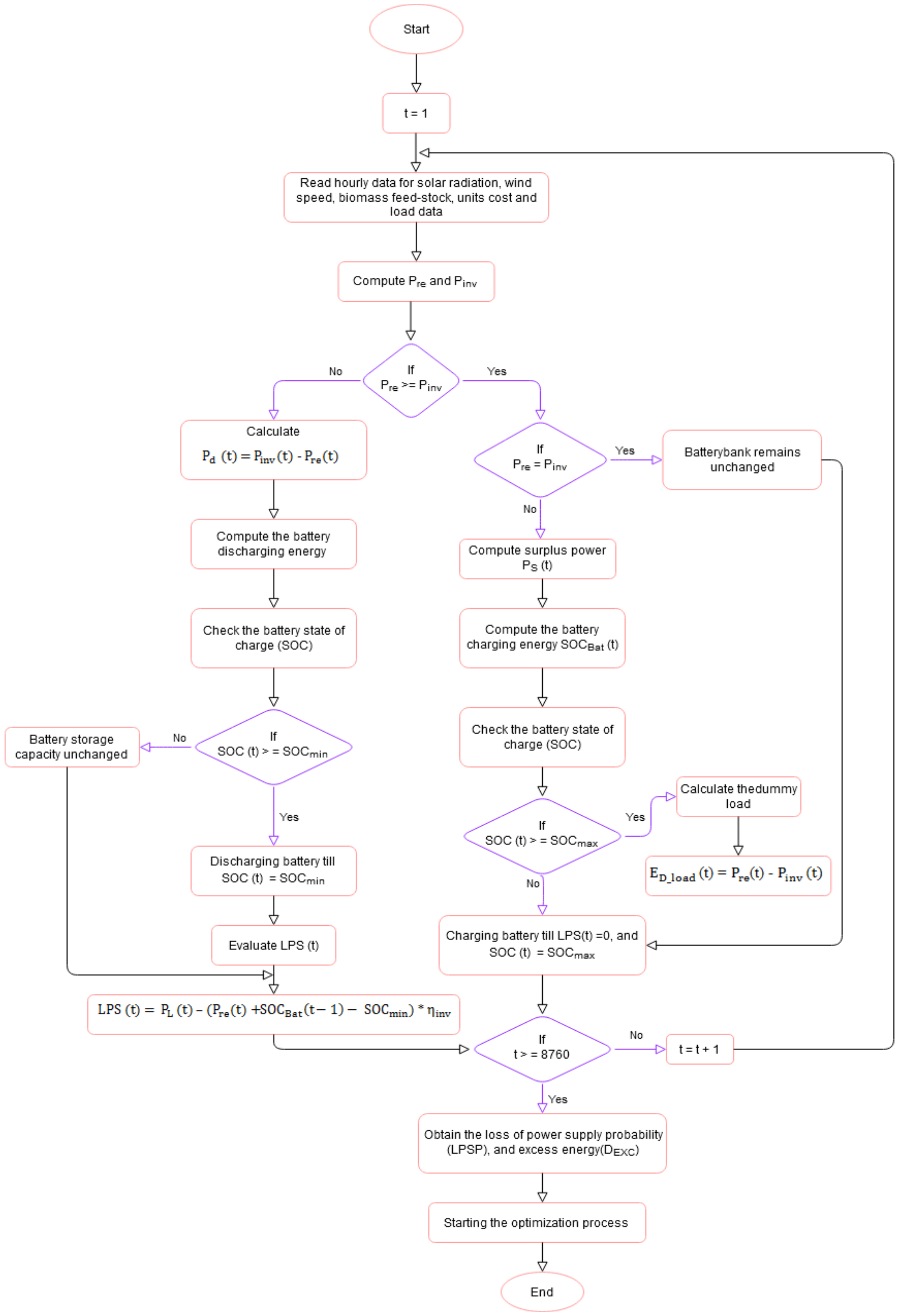

Figure 5. 1: Flowchart of the hybrid system operating strategy.

5.2.2. HBO, CFA and STOA

These optimization algorithms with the highest efficiency have been utilized, to find the solution to the optimal sizing problem of the hybrid PV/WT/Biomass/battery. The control parameters used in the optimization process for each algorithm are listed as follows:

- Number of search agents = 20,
- Maximum number of iterations = 100,
- Dimension size = 4.
- A linearly decreased from 2 to 0.

Each optimization algorithm works according to the previous steps mentioned in the SMA algorithm and is based on the operating strategy mentioned in Figure 5.1.

5.2.3. MOA and STOA

These optimization algorithms have been used to obtain the optimum solution of the hybrid system PV/Biomass/FC. The control parameters used in the each optimization process are given as:

- MOA: Population Size (males and females) =20, Maximum number of iterations = 100, and dimension size = 5. Personal Learning Coefficient =1. Global Learning Coefficient =1.5. Distance sight Coefficient = 2. Damping Ratio = 0.8. Random flight = 1. The block diagram of MOA used for optimizing the proposed hybrid renewable system is illustrated in Figure 5.2.
- STOA: Number of search agents = 20, Maximum number of iterations =100, and dimension size = 5, a linearly decreased from 2 to 0. The block diagram of STOA used for optimizing the proposed hybrid renewable system is illustrated in Figure 5.3.

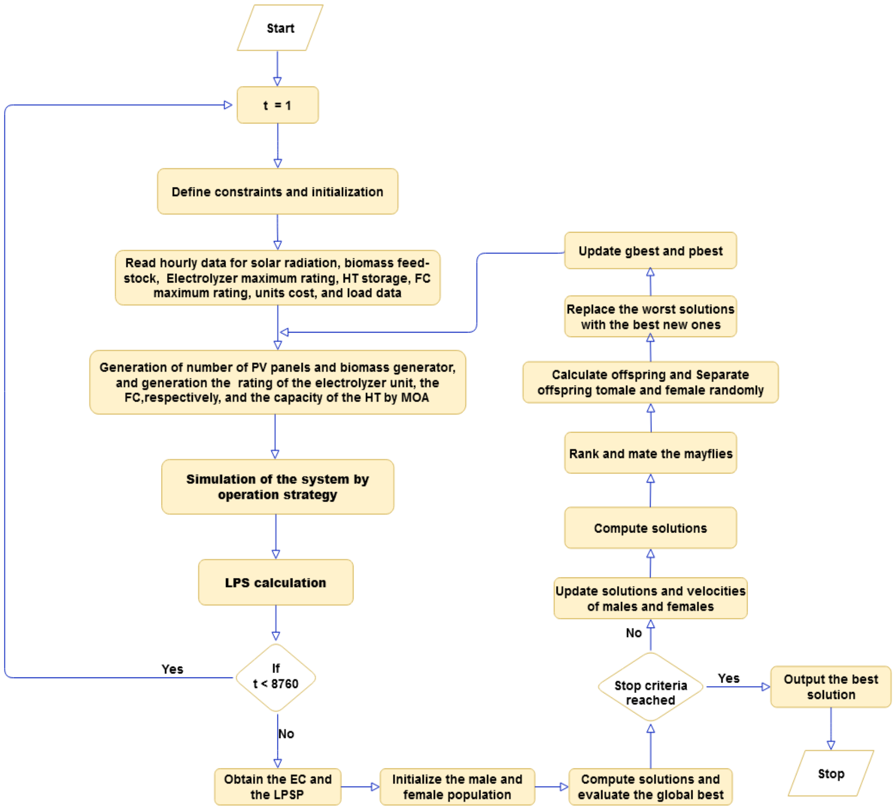

Figure 5. 2: Block diagram of MOA used for optimizing the proposed hybrid systems.

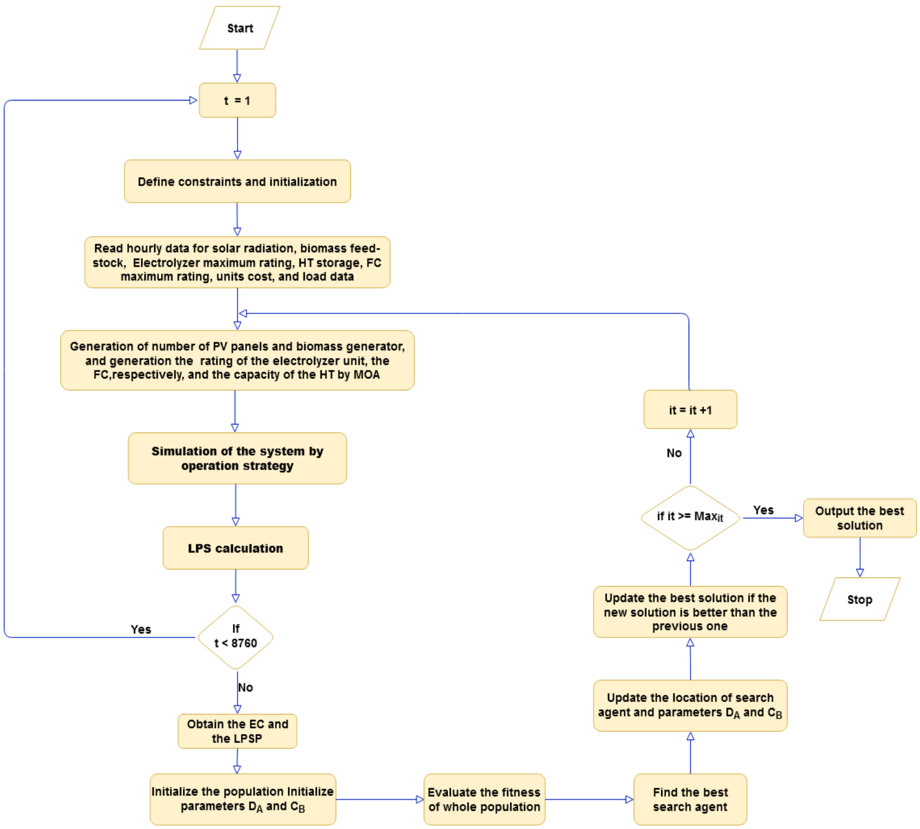

Figure 5. 3: Block diagram of STOA used for optimizing the proposed hybrid system.

Figure 5.4, illustrates the flowchart describing the operating strategy for the proposed hybrid system. Each optimization technique used in this study works by following the steps below:

1) Run the software of creating the proposed hybrid power system, and this step contains the following stages:
   a) Generation of the initial population.
   b) Run the code for creating the hybrid system, which is shown in the flowchart in Figure 5.4, and stated in equations in the components description section and in the economic and cost analysis section.
   c) The fitness functions are evaluated for all agents/positions according to equation (4.22).
2) Run the optimization technique with the proposed hybrid system, which includes the following stages:
   a) Depending on the nature of each optimization technique used, the size of the system parts is updated.
   b) Run the code for creating the hybrid system, which is shown in the flowchart in Figure 5.4, and stated in equations in the components description section and in the economic and cost analysis section.
   c) The fitness functions are evaluated for all agents/positions according to equation (4.22).
   d) Examine whether the proposed system satisfies the end criterion or not. If so, (Yes), the code will be paused and will move to the following step; otherwise (No), the three previous stages from “a” to “c”, will be repeated.

Display the required results, including hybrid system sizing and EC, NPC, LPSP, and dummy load optimal values.

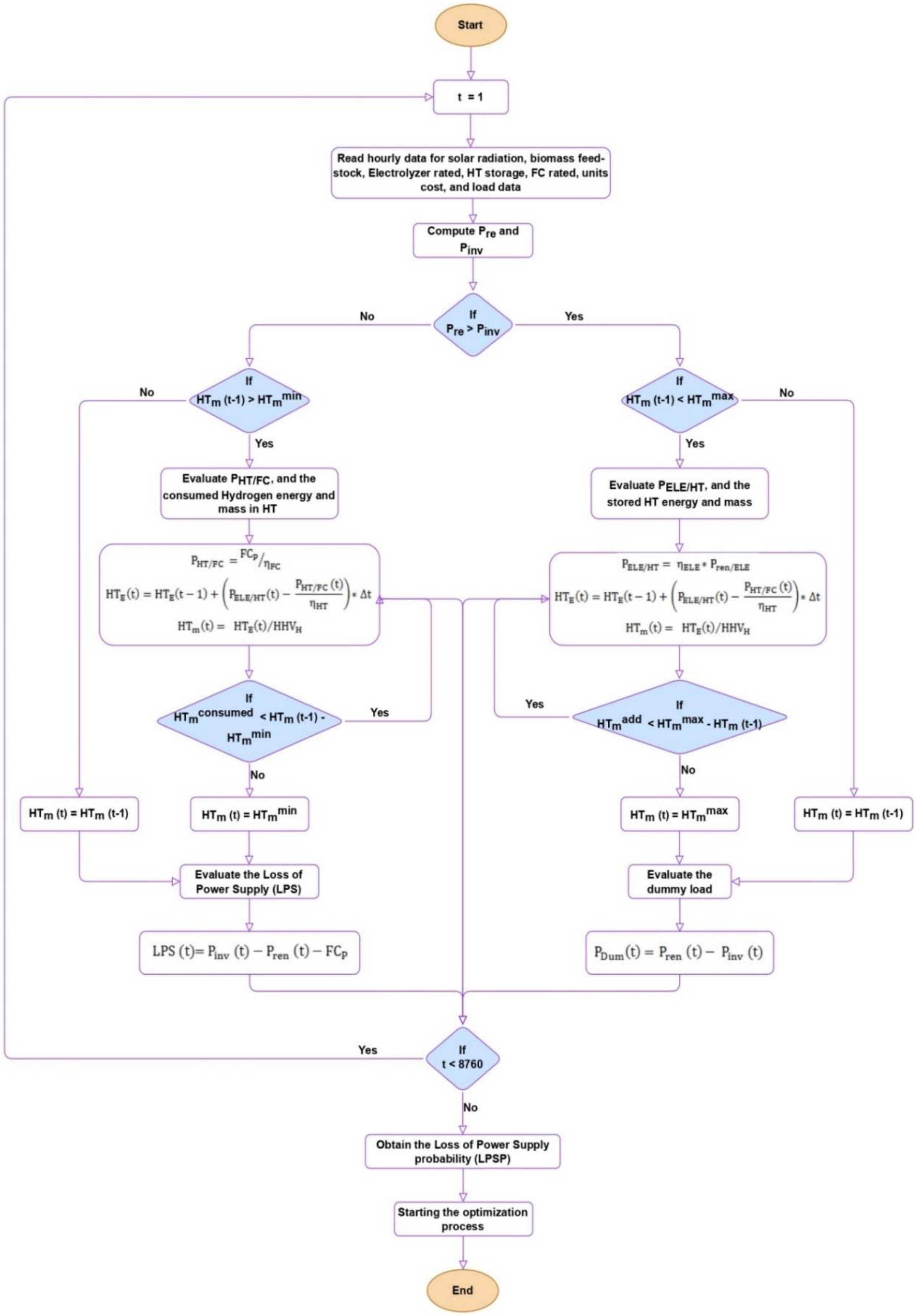

Figure 5. 4: The flowchart of the operation strategy of the proposed hybrid system.

5.3. Modified and Hybrid Optimization Algorithms

In this section, the process of the developed QRUN technique is presented which is based on the quantum model of the original RUN method. In addition, the procedure of the developed GAHA are carefully described which is based on the hybrid combination between a bio-inspired AHA and GBO methods.

5.3.1. QRUN and Original RUN Algorithms

This modified algorithm QRUN and original RUN algorithms are utilized for solving an optimal sizing problem of an off-grid hybrid system consisting of PV/Biomass/battery. The operation strategy schematic for the suggested HRPS based on the proposed algorithms is depicted in Figure 5.5. The control parameters used in the optimization process for each algorithm are listed as follows:

- Number of search agents = 20,
- Maximum number of iterations = 100,
- Dimension size = 3.
- RUN: initialization parameters a = 20 and b = 12.
- QRUN: improved parameters w_1 = 0.75 and w_2 = 1.

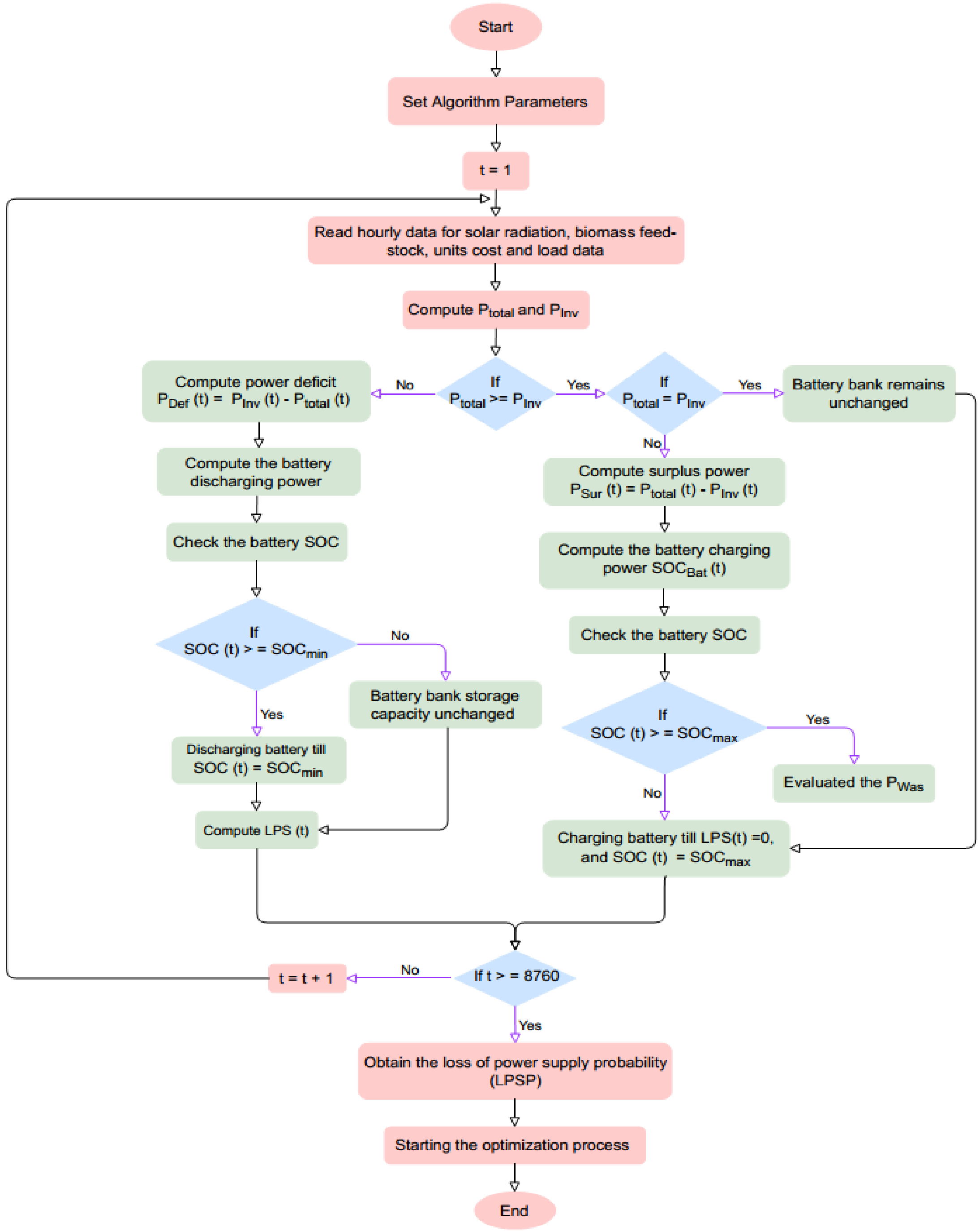

Figure 5. 5: The hybrid system operation strategy schematic.

5.3.1.1. RUN Optimization Algorithm

This algorithm is based on the theory of the Runge–Kutta method [179]. Figure 5.6, shows the three optimization process in the RUN method to reach the best solution. The first is the Runge Kutta (RK) search mechanism to create location x_{n+1} then uses the enhanced solution quality (ESQ) mechanism to enhance the quality of the solutions and try to avoid the local optima in the search space. Finally, the RUN algorithm selects the best solution. A brief description of the RUN algorithm is presented in this subsection.

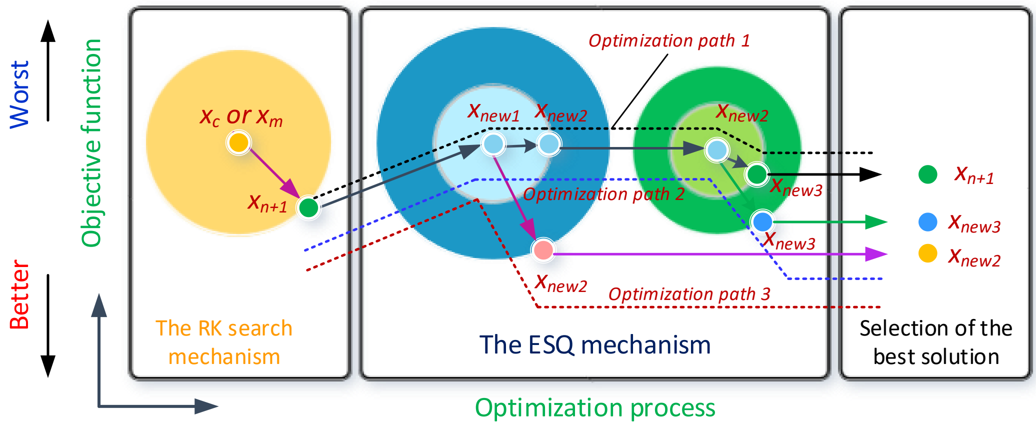

Figure 5. 6: Optimization process in the RUN algorithm.

A. Update solution:

The RK search mechanism generates the position x_{n+1} as follows:

$$\begin{aligned}
&\text{if rand} < 0.5\\
&\quad x_{n+1} = (x_c + r.SF.g.x_c) + SF.SM + \mu.randn.(x_m - x_c)\\
&\text{else} \qquad\qquad\qquad (5.1)\\
&\quad x_{n+1} = (x_m + r.SF.g.x_m) + SF.SM + \mu.randn.(x_{r1} - x_{r2})\\
&\text{end}
\end{aligned}$$

Where rand denotes to a random number in the range [0,1]. r refers to an integer number and it is either 1 or -1. g denotes to a random number in the range [0, 2]. SF refers to an adaptive factor. μ is a random number. SM is the leading search mechanism.

B. ESQ

This mechanism is responsible for exploring the required and best regions in the search space. The ESQ is used to create the solution x_{new2} as the following equation:

$$\begin{aligned}
&\text{if rand} < 0.5\\
&\text{if } w < 1\\
&\quad x_{new2} = x_{new1} + r.w.|(x_{new1} - x_{avg}) + randn|\\
&\text{else} \qquad\qquad\qquad (5.2)\\
&\quad x_{new2} = (x_{new1} - x_{avg}) + r.w.|(u.x_{new1} - x_{avg}) + randn|\\
&\text{end}\\
&\text{end}
\end{aligned}$$

Where w is a random number which can be defined as follows:

$$w = \mathrm{rand}(0,2).\exp\left(-c\left(\frac{i}{\mathrm{Maxi}}\right)\right) \quad (5.3)$$

Where, c is a random number and x_{new1} is calculated as follows:

$$x_{new1} = \beta \times x_{avg} + (1-\beta) \times x_{best} \quad (5.4)$$

$$x_{avg} = \frac{x_{r1} + x_{r2} + x_{r3}}{3} \quad (5.5)$$

The x_{new2} does not always have the optimal solution, so the RUN algorithm presents another solution using the x_{new3} which is defined as follows:

if rand$<$ w

$$x_{new3} = (x_{new2} - \mathrm{rand}.x_{new2}) + SF.(\mathrm{rand}.x_{RK} + (v.x_b - x_{new2})) \quad (5.6)$$

end

5.3.1.2. QRUN Optimization Algorithm

In this subsection, the quantum mechanics is used to develop the original RUN algorithm. This quantum model of a RUN algorithm called here QRUN algorithm. The quantum mechanics was employed to develop the PSO approach in ref. [180]. In the quantum model, by employing the Monte Carlo method, the solution x_{new4} can be calculated from this equation:

if $h \geq 0.5$

$$x_{new4} = p + \alpha.|Mbest_i - x_{n+1}|.\ln(1/u)$$

else (5.7)

$$x_{new4} = p - \alpha.|Mbest_i - x_{n+1}|.\ln(1/u)$$

end

Where α is a design parameter, u and h are uniform probability distribution in range [0,1], Mbest is the mean best of the population and it can be defined as the mean of the x_{best} positions. It is calculated as follows:

$$Mbest = \frac{1}{N}\sum_{l=1}^{N} p_{g,l}(i) \quad (5.8)$$

Where, g is the index of the best solution among all solutions. The flow chart of the proposed QRUN algorithm is illustrated in Figure 5.7.

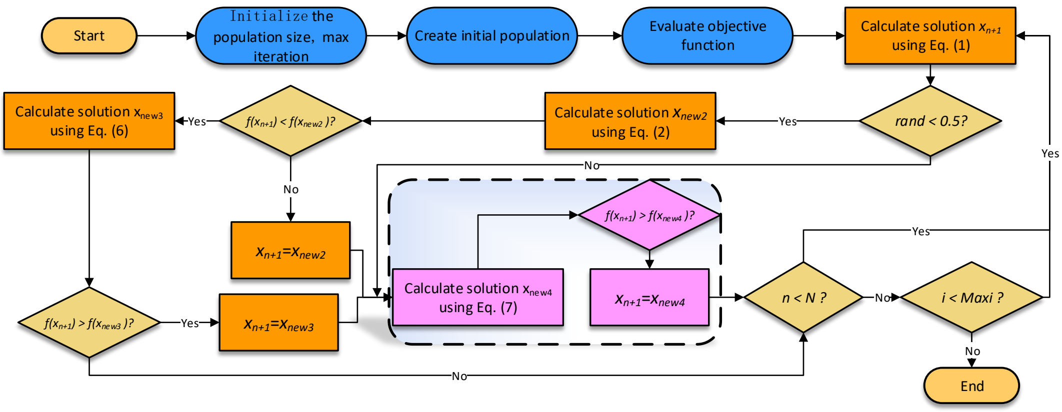

Figure 5. 7: The flow chart of the proposed QRUN technique.

5.3.2. GAHA and Original AHA Algorithms

The GAHA and AHA algorithms are applied for optimal design for different configurations of a hybrid PV/WT/biomass/battery system for supplying a load in the new Tiba city in Luxor, Egypt. The operation strategy schematic for the suggested HRPS based on the proposed algorithms is depicted in Figure 5.1. The control parameters used in the optimization process for each algorithm are listed as follows:

- Number of search agents = 20.
- Maximum number of iterations = 100.
- Dimension size = 4.
- AHA: migration coefficient = 2n.

The AHA method and the procedure of the developed GAHA are carefully described in this part. Although the AHA algorithm is a recent optimization algorithm that was proposed in 2022, it has been used in many applications such as optimal planning of multiple renewable energy-integrated distribution system with uncertainties [181] and Optimal allocation of renewable distributed generators (DGs) [182]. In order to increase the performance of AHA, hybrid AHA with SA algorithm has been used to solve three constrained engineering design problems in [183]. In this paper, the LEO is used to improve the local search capability in the AHA.

5.3.2.1. AHA Optimizer

AHA is an optimization algorithm inspired by the foraging and flights of hummingbirds, which is described in [184]. The following are explanations of three core forms for the AHA method:

A. Guided foraging

In guided foraging, three flight skills are named omnidirectional, diagonal and axial flights as shown in Figure 5.8. These skills have been employed for foraging in 3-D space. The following is the formula that represents this guided foraging and a potential source of food:

$$v_i(t+1) = x_{i,ta}(t) + h.b.\left(x_i(t) - X_{i,ta}(t)\right) \quad h \sim N(0,1) \tag{5.9}$$

Where, $x_{i,ta}(t)$ is the location of the source of the target of food, h represents the guided factor, $x_i(t)$ denotes the location of the ith food source at time t.

The following formula is to update the location for the ith food source:

$$x_{Ai}(t) = \begin{cases} x_i(t) & f(x_i(t)) \leq f(v_i(t+1)) \\ v_i(t+1) & f(x_i(t)) > f(v_i(t+1)) \end{cases} \tag{5.10}$$

Where, $f(x_i(t))$ and $f(v_i(t+1))$ represent the value of function fitness for $x_i(t)$ and $v_i(t+1)$, respectively.

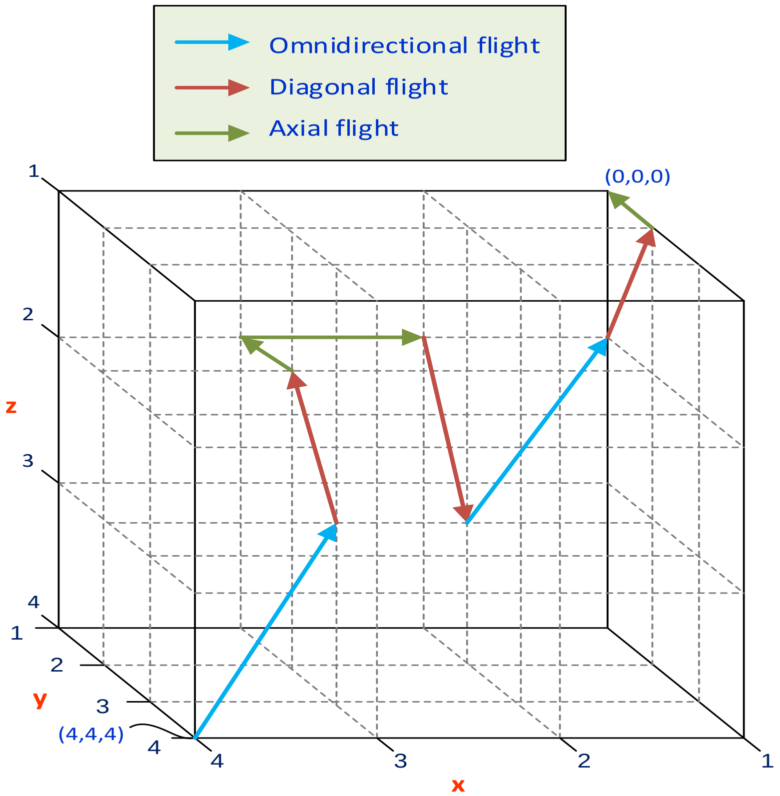

Figure 5. 8: Three flight behaviors in 3-D space

B. Territorial foraging

The local search of hummingbirds in the territorial foraging strategy is given from the following formula:

$$v_i(t+1) = x_i(t) + g.b.(x_i(t))$$
$$g \sim N(0,1) \tag{5.11}$$

Where, g is the territorial parameter

C. Migrating foraging

The hummingbird's migration foraging can be computed based on the following formula:

$$x_{wor}(t+1) = lb + r.(ub - lb) \tag{5.12}$$

Where x_{wor} denotes the dietary source with worst population rate of nectar-refilling. r represents a random parameter. ub and lb denote upper and lower limit range.

5.3.2.2. GAHA Optimizer

The local escaping operator (LEO) component is added in the local search stage to improve the local search capability in the AHA. The LEO is proposed to enhance the ability of the GBO algorithm [185]. The LEO aims to discover new regions that are needed to solve complicated real-world challenges. It enhances the performance of solutions by updating their locations according to certain criteria. Specially, it avoids the method from becoming stuck in the local optima and improves the method's convergence characteristics [186]. The LEO produces an appropriate solution (X_{LEO}^m) by using various solutions that include x_{best}, the solutions $X1_n^m$, and $X2_n^m$, two random solutions x_{r1}^m andx_{r2}^m, and a new randomly generated solution (x_k^m). The solution X_{LEO}^m is formulated as:

if rand < pr

if rand < 0.5

$$X_{LEO}^m = X_n^{m+1} + f_1 \times (u_1 \times x_{best} - u_2 \times x_k^m) + f_2 \times \rho_1 \times (u_3 \times (X2_n^m - X1_n^m) + u_2 \times (x_{r1}^m - x_{r2}^m))/2$$

$$X_n^{m+1} = X_{LEO}^m \tag{5.13}$$

Else

$$X_{LEO}^m = x_{\text{best}} + f_1 \times (u_1 \times x_{\text{best}} - u_2 \times x_k^m) + f_2 \times \rho_1 \times (u_3 \times (X2_n^m - X1_n^m) + u_2 \times (x_{r1}^m - x_{r2}^m))/2$$

$$X_n^{m+1} = X_{LEO}^m$$

End

End

where f_1 denotes a uniform distributed random number in the range of [-1,1], f_2 is a random number from a normal distribution with a mean of 0 and a standard deviation of 1, pr is the probability, and u_1, u_2, and u_3 are random values generated as follows:

$$u_1 = \begin{cases} 2 \times rand & if\ \mu_1 < 0.5 \\ 1 & otherwise \end{cases} \tag{5.14}$$

$$u_2 = \begin{cases} rand & if\ \mu_1 < 0.5 \\ 1 & otherwise \end{cases} \tag{5.15}$$

$$u_3 = \begin{cases} rand & if\ \mu_1 < 0.5 \\ 1 & otherwise \end{cases} \tag{5.16}$$

Where rand represents a random number in the range of [0, 1], and μ_1 refers to a number in the range of [0, 1]. The above equations are simply explained as follows:

$$u_1 = L_1 \times 2 \times rand + (1 - L_1) \tag{5.17}$$

$$u_2 = L_1 \times rand + (1 - L_1) \tag{5.18}$$

$$u_3 = L_1 \times rand + (1 - L_1) \tag{5.19}$$

Where L_1 denotes a binary factor with a value of 0 or 1. If factor μ_1<0.5, the value of L_1 = 1, otherwise, L_1= 0. The solution x_k^m is generated as follows:

$$x_k^m = \begin{cases} x_{rand} & if\ \mu_2 < 0.5 \\ x_p^m & otherwise \end{cases} \tag{5.20}$$

$$x_{rand} = X_{min} + rand(0,1) \times (X_{max} - X_{min}) \tag{5.21}$$

Where x_{rand} is a random generated solution, x_p^m is a randomly chosen solution of the population ($p \in [1, 2, \dots, N]$), and μ_2 represents a random number in the range of [0, 1], which is simplified as:

$$x_k^m = L_2 \times x_p^m + (1 - L_2) \times x_{rand} \tag{5.22}$$

Where L_2 denotes a binary factor with a value of 0 or 1. If μ_2<0.5, the value of L_2=1, otherwise, L_2=0. Figure 5.9, presents the flowchart of the proposed GAHA algorithm.

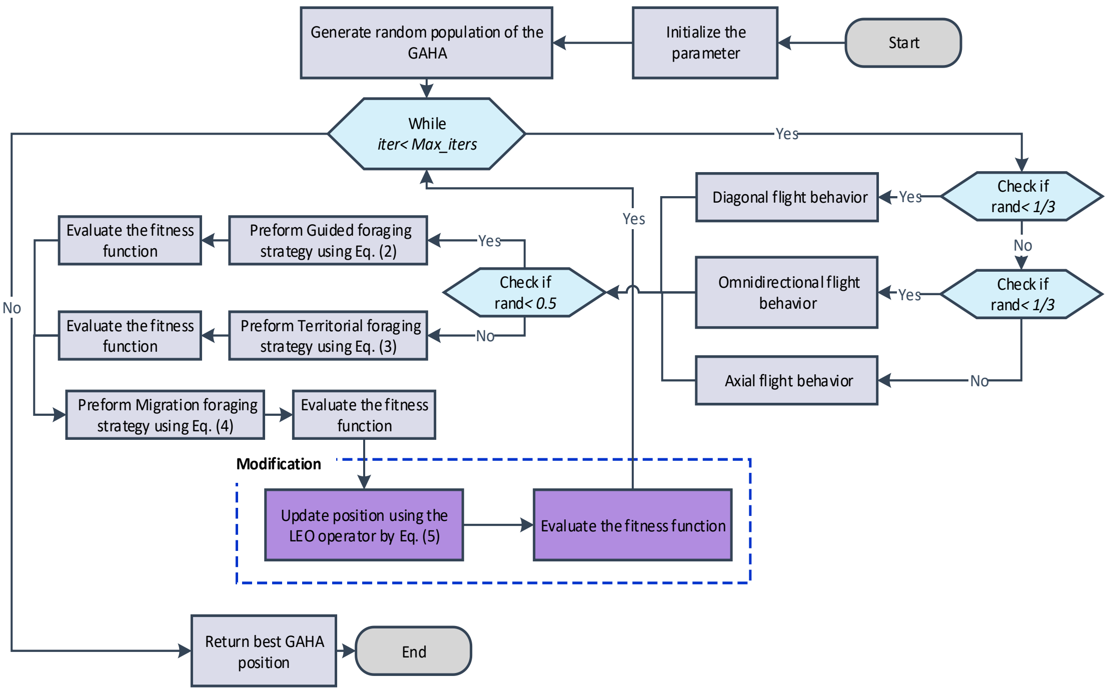

Figure 5. 9: Flow chart of GAHA algorithm.

Chapter 6

Results and Discussion

Chapter 6

Results and Discussion

6.1. Introduction

This chapter discusses the outcomes and discussions that resulted from implementing the proposed techniques in various suggested systems. The hybrid systems suggested in this thesis are outlined below:

1. Modeling the performance of a small-scale CCHP plant fueled with CS pieces using the professional Cycle-Tempo® software. This power plant is divided into three stages; the gasification unit (downdraft fixed bed gasifier), the EFGT as an electrical generation unit and heat recovery device with the absorption cooling cycle.

2. Study the optimal performance parameters including the operating conditions (maximum pressure, maximum temperature) and the system configuration for a theoretical model CCHP. The developed system is based on a direct burning biomass combustor, an EFGT and an ORC as bottoming unit for the maximizing the electrical efficiency. The tri-generation system presents an absorption refrigeration unit for cooling power production. The used biomass type is sugarcane bagasse

3. This system proposes an optimization model for minimizing the EC and enhancing the power supply for rural areas by designing and analyzing three different hybrid system configurations based on integrating a biomass system with PV, WT and battery system for a remote area located in the western desert of Egypt called Abu-Monqar village. Four recent optimization algorithms, namely SMA, SOA, GWO, WOA, and SCA are utilized and compared with each other to ensure that all load demand is met at the lowest EC for the proposed hybrid system.

4. The proposed hybrid system is designed to integrate a biomass system with PV, WT and battery storage system. This study presents an analysis and optimization of an isolated HRPS to operate Alrashda village in Dakhla Oasis in the New Valley Governorate in Egypt. Four different cases are proposed and compared for analyzing and optimizing. The optimization is designed to reduce component oversizing and ensure dependable control of power supplies, with the objective function of reducing

the levelized cost of energy and LPSP. Four optimization algorithms, namely HBO, CFA, the STOA, and GWO are utilized and compared with each other to ensure that all load demand is met at the lowest EC for the proposed hybrid system.

5. This isolated hybrid power system is simulated and analyzed to obtain the optimal sizing and meet the electricity demand with cost improvement for servicing Alrashda village, which is a small village of the Dakhla Oasis villages in the New Valley, Egypt. The major configuration of this system is PV, BG, and Batteries units. A modified approach based on the Quantum model of a RUNge Kutta optimization algorithm called QRUN algorithm is applied to guarantee that all load needs are covered with high reliability with the minimum EC of the proposed system. To ensure the superiority of the QRUN technique, its results are compared with those obtained by the original RUN optimizer, and well-known optimization algorithms, AO and GWO.

6. Novel hybrid algorithm called the GAHA is developed for reducing the EC of microgrid system; this hybrid approach is based on the combination between GBO and AHA. The developed GAHA algorithm is applied to obtain the optimal configuration of an isolated hybrid system, which is consists of PV modules, WT, biomass system, and battery storage system. The proposed standalone hybrid system is implemented for feeding loads in the new Tiba city, in northeast of Luxor in southern Egypt. The GAHA optimization findings are compared with the findings from other optimization algorithms namely the original AHA, SCA, and WOA methods.

7. A new isolated hybrid system is simulated and analyzed to obtain the optimal sizing and meet the electricity demand with cost improvement for servicing a small remote area with a peak load of 420 kW. The major configuration of this hybrid system is PV modules, BG, ELE units, HT units, and FC system. A recent optimization algorithm, namely MOA is utilized to ensure that all load demand is met at the lowest EC and minimize the GHG emissions of the proposed system. The MOA is selected as it collects the main merits of swarm intelligence and evolutionary algorithms; hence, it has good convergence characteristics. To ensure the superiority of the selected MOA, the obtained results are compared with other well-known optimization algorithms, namely STOA, WOA, and SCA.

6.2. CCHP System of Downdraft Gasifier, EFGT, and Absorption Cooling Cycle

The main objective of this system is to provide a new model of CCHP system based on the integration of downdraft fixed bed gasifier with EFGT (power generation system), heat recovery device and the absorption cooling cycle. Moreover, the possibility of improving the performance of this system to get better efficiency is studied. Also, the factors such as mass flow rate, TIT, CPR that effect on the performance of system is comprehensively studied. The proposed heating, power and cooling plant has been simulated using the professional Cycle-Tempo® [187] Software. This software determines the gasifier behavior and syngas characteristics in steady state conditions. However, the topic discussed and contribution of the work could be summarized as follows:

- Modeling the performance of a small-scale CCHP plant fueled with CS pieces using the professional Cycle-Tempo® software.
- The power plant is divided into three stages; the gasification unit (downdraft fixed bed gasifier), EFGT as an electrical generation unit and heat recovery device with the absorption cooling cycle.
- Technical parameters of the power plant have been specified, such as electrical power, thermal power, CHPC efficiency and optimum pressure ratio. The importance of TIT and CPR in affect the efficiency of the system.
- 100 Kg/h of the CS with 481.22 of energy input is converted into syngas at gasification temperature reaches to 995 °C and 1.65 of oxidant–fuel ratio. The hot gas efficiency is 94 % with 4.766 MJ/kg of calorific value and 243.18 Kg/h of mass flow.
- Syngas is converted into electrical power. The optimal performance parameters showed that the EFGT is capable of producing 70.57 kW of electrical power with hot side temperature difference of 110 ºC.
- The cooling power ($\mathbb{Q}_{\mathrm{eva}}$) of absorption cooling system is 130.92 kW with system PC is 0.6. The refrigerating heat flow is 48.83 $\mathrm{kW_{ref}}$.
- The general performance for the CHPC plant is 1.88 of the CPR with 21.78 % of the gross electrical efficiency ($\eta_{\mathrm{net_{EL}}}$) and 47.43% of net thermal efficiency (η_{th}).

Table 6.1, summarizes the gas compositions at the outlet of the gasifier. The thermodynamics performance of developed system is analyzed using the Tempo-Cycle software. The input energy of syngas produced from CS with flowing of 100 Kg/h is 481.22 kW at gasification temperature equals to 995 °C and $X_{of} = 1.65$. From Table 5, it can be observed that, the quality of hot gas is good for the reactor because its efficiency (94%) is better than cold gas efficiency (78.18%).

Table 6. 1: The performance of gasification reactor

Parameter	Value	Unit
Cold gas efficiency	78.18	%
Hot gas efficiency	94	%
m_{pg}	243.18	kg/h
X_{of}	1.65	Kg air/Kg biomass
Pyrolysis temperature	593.23	ºC
Reduction temperature	995.19	ºC
LHV_{pg}	4.766	MJ/kg
Volume flow	867	m^3/h
Energy input	481.22	kW
Product gas composition (% mole fraction)		
H_2	17.67	%
N_2	40	%
CH_4	1.12	%
CO_2	8.08	%
CO	20.82	%
H_2O	11.5	%
Impurities content	0.51	%

Figure 6.1, shows the composition mole fraction of the syngas with the variation of moisture content from 4 to 16 % at 995.19 ºC of gasification temperature. It can be observed that with increasing moisture content, both N_2 and CO are decreasing, while CH_4 and CO_2 are increasing slightly from 1.12 to 1.17 % and from 6.98 to 8.08 %, respectively. For H_2, its percentage is clearly increased from 12.65 to 17.67 %, which means the higher moisture content of the biomass. The concentration ofH_2, CH_4 and CO_2 produced by the gasification process is increased while the concentration of other gases is reduced. Part of the H_2, and CH_4 gases are produced at high temperatures due to the thermal crushing of the tar [188]. According to water gas shift reaction (Table 6.1), the concentration of H_2 and $CO_2$is

increased as a result of the conversion of CO at heat-absorbing reaction while the concentration of CO is reduced [189].

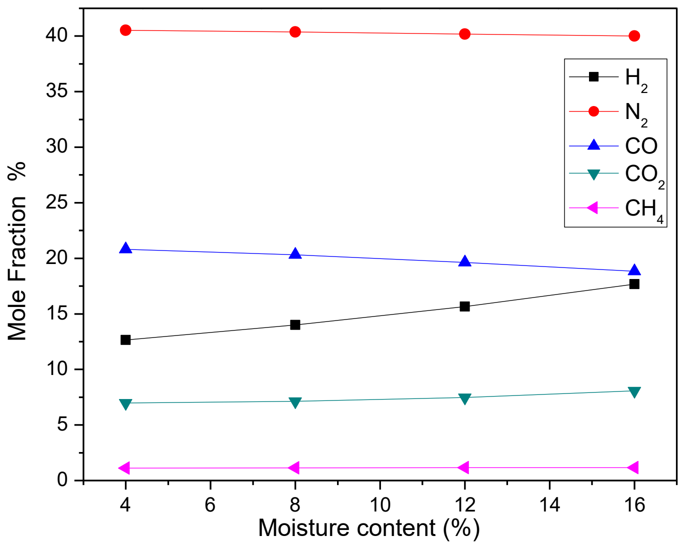

Figure 6. 1: The variation of moisture content with syngas mole fraction.

Figure 6.2, shows the effect of variation of the oxidant–fuel ratio (X_{of}) on syngas volume and gasification temperature. With rising the percentage of X_{of} from 1.35 to 2.2 Kg /Kg, both gasification temperature and volume are increased from 797.65 to 1285.95 ºC and 0.18 to 0.35 m^3/s, respectively. Overall, the volume flow of syngas is closely related to the change in the gasification temperature, and both are increasing linearly.

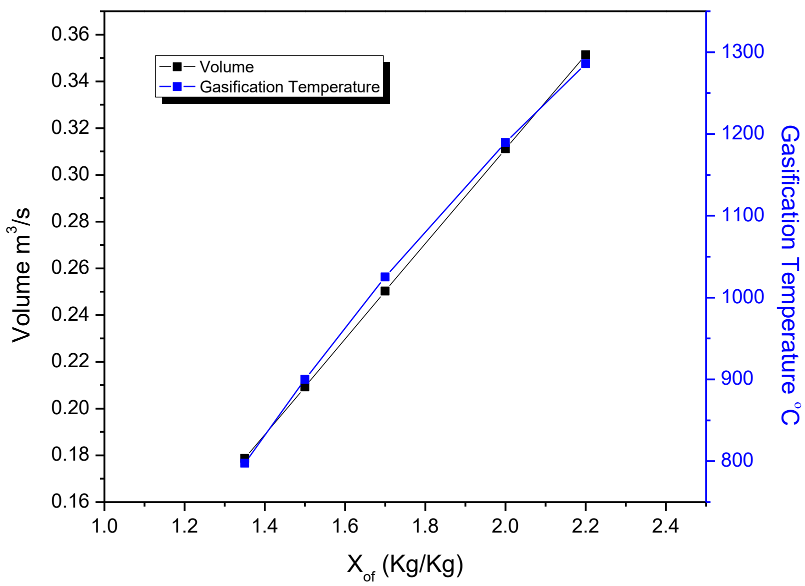

Figure 6. 2: The effect of variation of oxidant–fuel ratio on gasification temperature and syngas volume.

The syngas composition in a function of oxidant-fuel ratio (X_{of}) is depicted in Figure 6.3. The increasing in the amount of air supplied to the gasifier (X_{of}) from 1.35 to 2.2 Kg /Kg leads to significant change in the mole fraction of syngas. From this figure, it can be observed that the concentration of H_2 and CO are decreased from 23.24 to 10.41 and 22.48 to 17.19 %, respectively. On the opposite, the concentration of N_2 is significantly increased from 35.39 to 46.89 %. Hence, more power from this syngas can be produced. While CO_2 and CH_4 are reduced by a small amount from 8.72 to 8.24 and 1.23 to 0.98 %, respectively.

The effect of hot side temperature variation on EFGT electrical power (P_{EL}) and system electrical efficiency $\eta_{net_{EL}}$ is shown in Figure 6.4. $\eta_{net_{EL}}$ and P_{EL} decrease with further increase in hot side temperature due to the reduction in the heat transmitted between compressed air and the flue gas in the HTHE. Hot side temperature is one of the factors that determine the efficiency of the system. It is shown that $\eta_{net_{EL}}$ and P_{EL} decrease from 22.28 to 15.62 % and from 72.18 to 50.98 kW, respectively, when the hot side temperature difference increases from 50 to 200 °C. Although the best electrical efficiency and generated power are obtained when the hot side temperature difference becomes 50 °C, this means the system temperature increases, causing damage to the turbine body and increase in cost. Therefore, it is preferable to work at the hot side temperature between 100 and 200 °C.

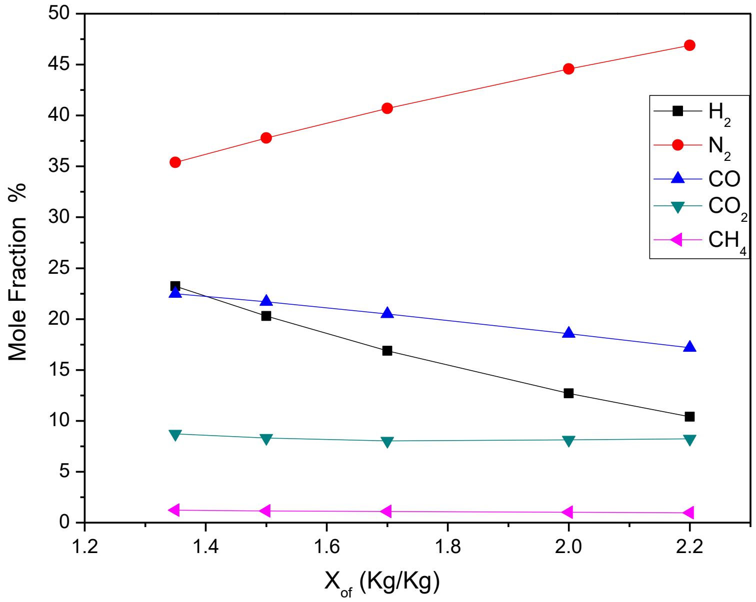

Figure 6. 3: The effect of variation of oxidant–fuel amount on syngas mole fraction.

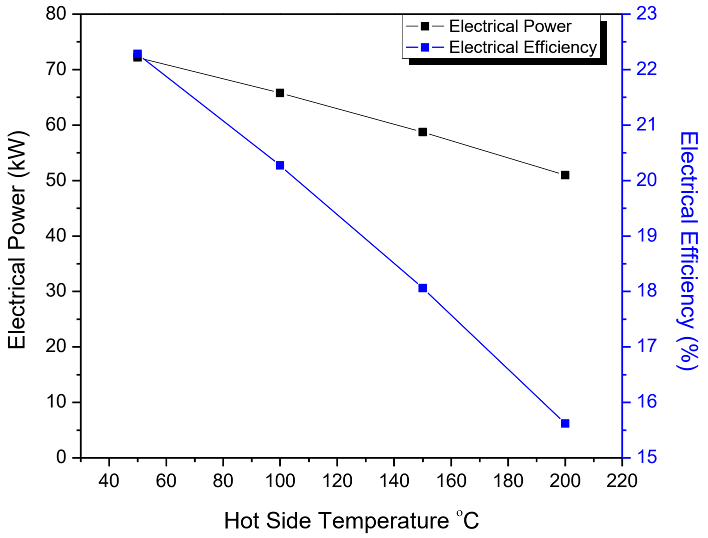

Figure 6. 4: Effect of hot side temperature variation on EFGT electrical power and system electrical efficiency.

TIT is one of factors that affect the overall performance of turbines. Reducing the temperature of the exhaust gas allows to improve efficiency of EFGT [190]. High TIT leads to increase the output of the turbine; hence, the overall efficiency and output of the system are increased. To increase the TIT, there are some difficulties; including some turbine components cannot stand the high temperature. However, recent studies have been overcome this issue by enhancing the technology of materials, where special materials like high performance alloys are used. In [133], another method has been used to increase TIT by adding combustor before the turbine. There is a limit to improve the efficiency depending on TIT [191]. By increasing the pressure ratio to such an extent that the increased work is never recovered because expansion through turbines is inadequate to recover the work [39].

Figure 6.5, shows the effect of increasing EFGT compressor pressure ratio on $\eta_{net_{EL}}$at three values of TIT. From this figure, it can be observed that the $\eta_{net_{EL}}$is increased to a certain value and then decreased. At TIT of 800, 850 and 925 °C with rising the pressure ratio from 2 to 4, the $\eta_{net_{EL}}$ is increased from 14.99 to 18.89 %, 16.82 to 21.72 % and 17.28 to 23.43 %, respectively. When the pressure ratio is decreased from 4 to 10 at the same TIT, the $\eta_{net_{EL}}$ is decreased from 18.89 to 12.49 %, 21.72 to 17.53 % and 23.43 to 20.40 %, respectively. Overall, it can be concluded that the maximum $\eta_{net_{EL}}$ is obtained when the pressure ratio ranges from 4 to 5 and TIT equals to 925 °C.

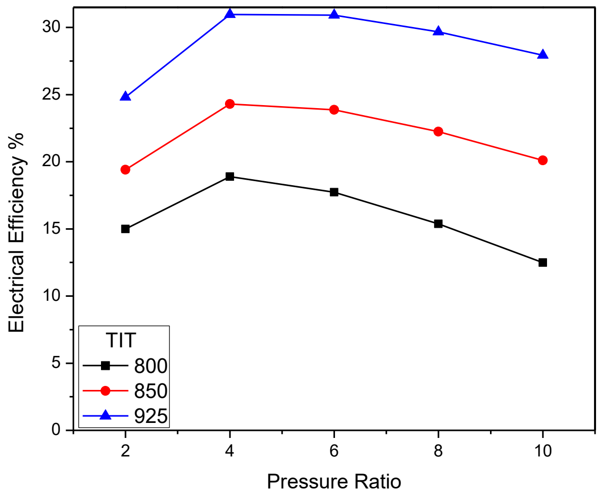

Figure 6. 5: Effect of compressor pressure ratio and TIT on electrical efficiency.

Figure 6.6, shows the relation between the CPR with different values of compressor pressure ratio at three different values of TIT. From this figure, it can be observed that by increasing the TIT from 800 to 925°C, the CPR decreases and its highest value is achieved when the TIT is 800°C. CPR declines with increasing the pressure ratio from 2 to 4 at a certain value (from 3.24 to 2.31 at TIT 800 °C, from 2.94 to 2.03 at TIT 850 °C and from 2.58 to 1.72 at TIT 925 °C) and after this certain value, the CPR dramatically increases again. The lowest CPR is achieved at 925 °C TIT and pressure ratio of 6. CPR is the ratio of the cooling capacity to the total power output of the system. With fixed output power of the system, the maximum efficiency occurs at the minimum cooling capacity. The efficiency of absorption chiller energy is based on the fuel consumption per tonne of cooling, the higher the electric efficiency value means the lower of the biomass consumption.

The effect of ammonia concentration variation (strong solution) in generator unit on circulation ratio (CR) in VAC subsystem and PC is plotted in Figure 6.7. From this figure, it can be observed that the PC rises from 0.55 to 0.66 with increasing the concentration of ammonia from 40 to 65 %, which means that the system is improved by increasing the rate of ammonia concentration getting into the generator. The CR dramatically decreases from 7.66 to 2.28 until ammonia concentration reaches 55% and then it decreases at low rate.

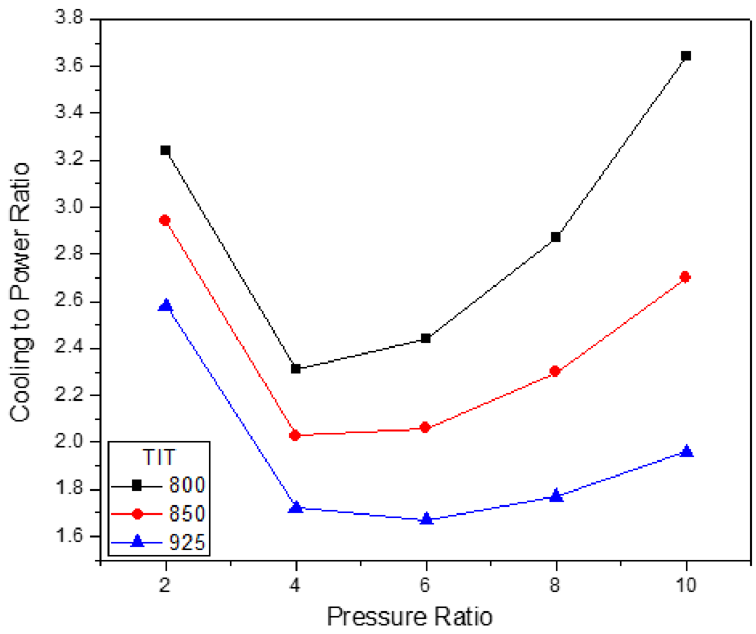

Figure 6. 6: Effect of the variation of compressor pressure ratio and TIT on cooling to power ratio.

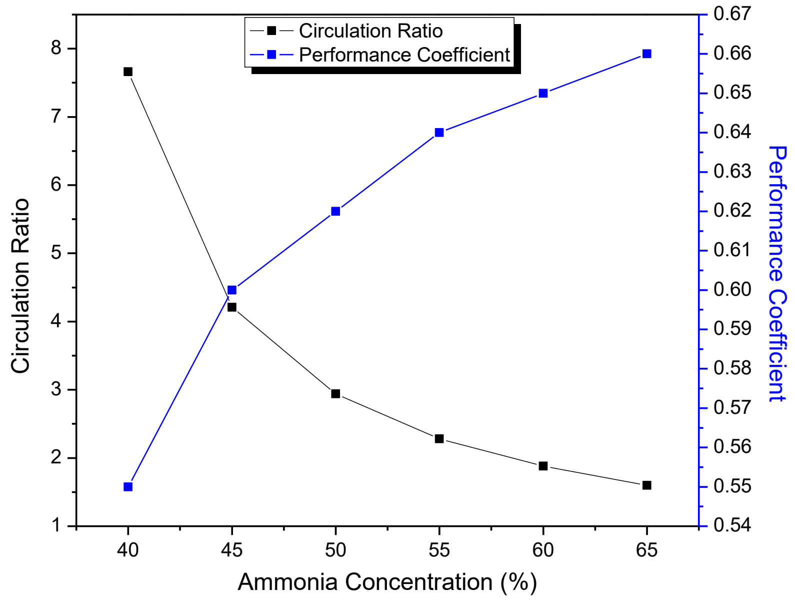

Figure 6. 7: Effect of the variation of ammonia concentration on circulation ratio and performance coefficient.

The external temperature of generator is a fundamental factor affecting the amount of the PC [145], and this is illustrated in Figure 6.8. The PC rises from 0.31 to 0.6 with increasing in the generator temperature from 90 to 120 ºC. The PC values remain fixed (0.6) with a temperature rise up to 140 ºC and then the PC value start to decrease. It is concluded that the optimal PC is 8 when the generator temperature is 120 ºC.

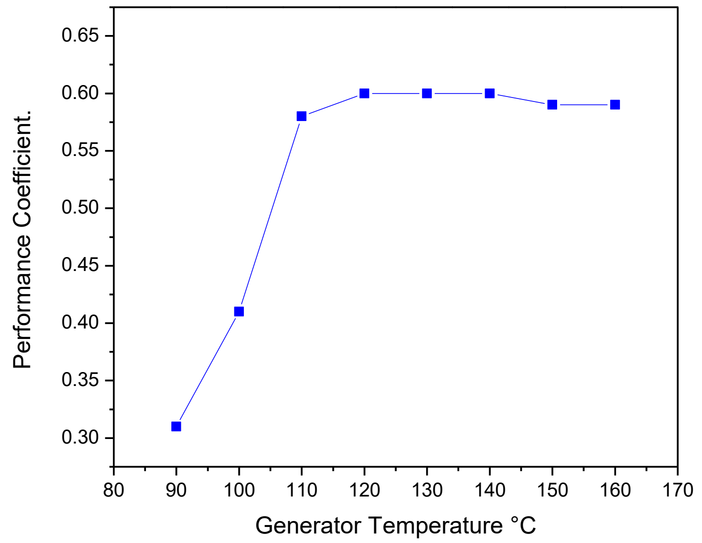

Figure 6. 8: Effect of changing the outside temperature of the generator on the performance coefficient.

Figure 6.9, shows the percentage of transmitted heat flow for the major units in absorption cooling system at 875 °C of TIT and 4.07 of CR. It is observed that the generator is the component with highest heat flow of 82.62 kW (20 %), followed by HR evaporator with 79.51 kW (19.34 %) and Absorber with 74.95 kW (18.23 %). The low heat flow is occurred in precooler unit with 9.9 kW (2.41 %).

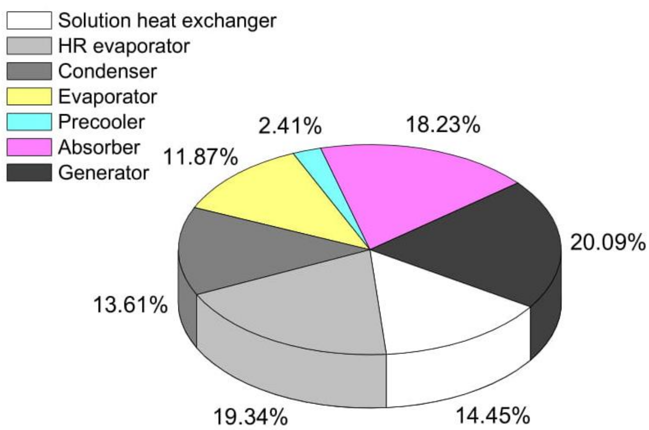

Figure 6. 9: Transmitted heat flow in main units in absorption cooling system.

Table 6.2, presents the important parameters of EFGT with absorption cooling system. It is estimated that the EFGT is capable of producing 70.57 kW of P_{EL} with HTHE efficiency of 75% and 4.84 pressure ratio. The cooling power ($\mathbb{Q}_{eva}$) of absorption cooling system is

130.92 kW with 15 ºC of cooling tower and system PC of 0.6. The supplied heat to generator ($\mathbb{Q}_{\mathrm{gen}}$) is 82.62 kW with 4.07 of CR. For whole system (gasifier, EFGT and absorption cooling), the gross electrical efficiency ($\eta_{\mathrm{net}_{\mathrm{EL}}}$) is 21.78 % and the net thermal efficiency (η_{th}) is 47.43% with 1.88 of CPR.

Table 6. 2: The performance of EFGT with absorption cooling system

Parameter	Value	Unit
HTHE efficiency	75	%
Compressor pressure ratio of EFGT	4.84	-
Combustor air factor of EFGT	7.31	-
P_{EL} of EFGT	70.57	kW
EFGT energy input	320.02	kW
Ammonia concentration in generator unit	45	%
$\mathbb{Q}_{eva}$	130.92	kW
$\mathbb{Q}_{gen}$	82.62	$\mathrm{kW_{th}}$
Refrigerating heat flow	48.83	$\mathrm{kW_{ref}}$
Temperature of cooling tower	15	ºC
CPR	1.88	-
PC	0.6	-
CR in generator unit	4.07	-
$\eta_{\mathrm{net}_{\mathrm{EL}}}$	21.78	%
η_{th} of the plant	47.43	%

The main features of developed system can be summarized as follows:

-Developing a simulation model to design a small-scale CHPC system fueled with 100 Kg/h CS.

- The obtained results indicate the importance of TIT and CPR on the efficiency of the system

-High TIT leads to increase the output of the turbine; hence the overall efficiency and output of the system are increased.

- The optimal performance parameters shown that the EFGT is capable of producing 70.57 kW of electrical power at TIT 875 ºC.

- The cooling power ($\mathbb{Q}_{\mathrm{eva}}$) of absorption cooling system is 130.92 kW with 45 % of Ammonia concentration in generator unit.

-The system CPR is 1.88 with 21.78 % of the gross electrical efficiency ($\eta_{net_{EL}}$) and 47.43% of net thermal efficiency (η_{th}).

6.3. CCHP System of EFGT, ORC, and Absorption Cooling Cycle

This system focuses on the modeling of a tri-generation system for converting biomass into electrical, cooling and heat power. This target is achieved by direct burning of biomass using a combustor chamber, at atmospheric pressure, connected with an EFGT, an ORC and absorption cooling system. The used feedstock is sugarcane bagasse which is available in various areas of Upper Egypt, especially in Qena and Aswan. For ORC system, several working fluids (cyclohexane, benzene, toluene, and R113) have been studied to analyze the optimum fluid that corresponds to the entire system. The selection of more suitable ORC working fluid is mainly depends on the temperature difference between the heat source and its boiling point. Based on the simulation results, toluene is the most appropriate working fluid for CCHP applications. The net electric power is 177.56 kW (142.92 kW from EFGT and 34.64 kW from ORC), net electrical efficiency is 24.2%, cooling capacity is 38.50 kW and CCHP efficiency is 43.50%. The biomass consumption at the optimal operating conditions is 144 kg/h. The developed CCHP system based on direct biomass combustion integrated with EFGT, ORC and absorption cooling unit are discussed and analyzed in this section.

Figure 6.10, shows the relation between the system electrical efficiency with different values of compressor pressure (from 2 to 12 bar) at four different values of TIT of EFGT. It can be observed as the $\eta_{EFGT_{el}}$ increases by increasing the value of TIT from 800 to 925 ℃ and the highest efficiency is achieved when the TIT reaches to 900 ℃. The efficiency rises when the pressure is increased until specific rate, then it is dramatically decreased. The optimal pressure value for getting the highest η_{el} is between 4 and 5 bar for the three TITs. According to Perna et al. (2017), the TIT of EFGT should not exceed 900 ℃, because this will need the availability of maintenance and cooling units, which increases the investment cost of the system.

Hot side temperature difference (the value of subtracting the temperature of flue gas produced from the combustion process and TIT) and the exchanger heat losses are the most important factors, which define the efficiency of HTHE. Efficiency of HTHE is settled at 87% for the developed system. Figure 6.11, shows the change of EFGT electrical efficiency with the hot side temperature difference. It can be observed the inverse relation between hot side temperature difference and electrical power. When hot side temperature difference leaps from 50 °C to 200 °C, the electrical power reduces from 157.0 to 109.4 kW, which means decreasing in the system efficiency. The highest electrical power and efficiency are reached when the hot side temperature difference become between 50 to 100 °C degrees. This can be done by increasing the combustion chamber temperature or TIT. In fact, this increment will lead to raise the capital costs of system due to appropriate equipment should be available to withstand high temperatures.

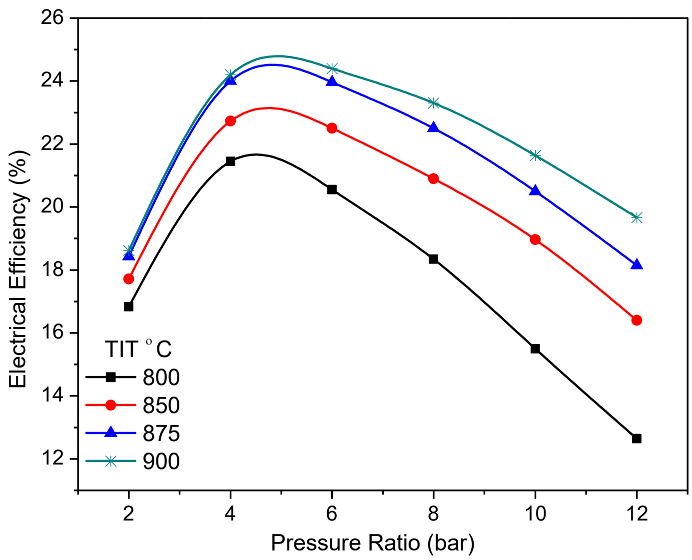

Figure 6. 10: Relation between system electrical efficiency with different values of compressor pressure and TIT.

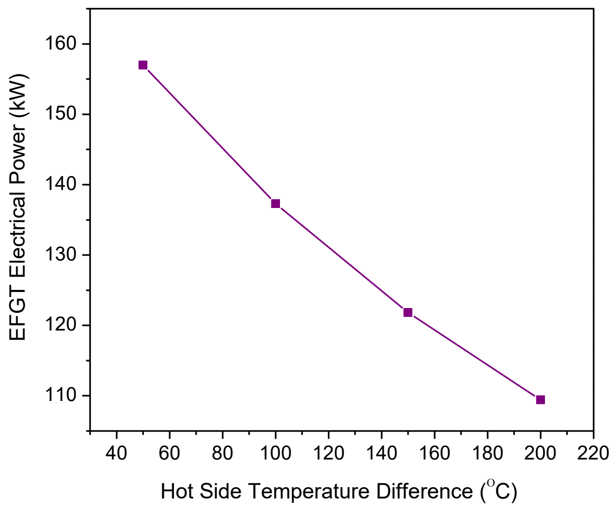

Figure 6. 11: The electrical power of EFGT at different hot side temperature difference.

The relation between the generated electrical power ($P_{ORC_{el}}$) from ORC and the pump pressure, ρ_{Pump} (15, 20 and 25 bar) at different values of TIT (ranging from 200 to 310 °C) in case of using different working fluids are shown in Figure 6.12. It can be observed that the $P_{ORC_{el}}$ rises with increasing both of P_{Pump} and TIT. For all working fluids, the maximum value of $P_{ORC_{el}}$ can be obtained when the ρ_{Pump} is 25 bar. $P_{ORC_{el}}$ also varies with TIT from a fluid to another due to its physical properties. The maximum values of $P_{ORC_{el}}$ are 34.56 kW at TIT 309 °C, 33.46 kW at TIT 260 °C, 32.53 kW at TIT 250 °C and 28.39 kW at TIT 208 °C, for toluene, cyclohexane, benzene and R113. One of the reasons for the low generated power in case of using some fluids is due to high PPTD, decreasing at the same time the amount of heat entering the evaporator [150].

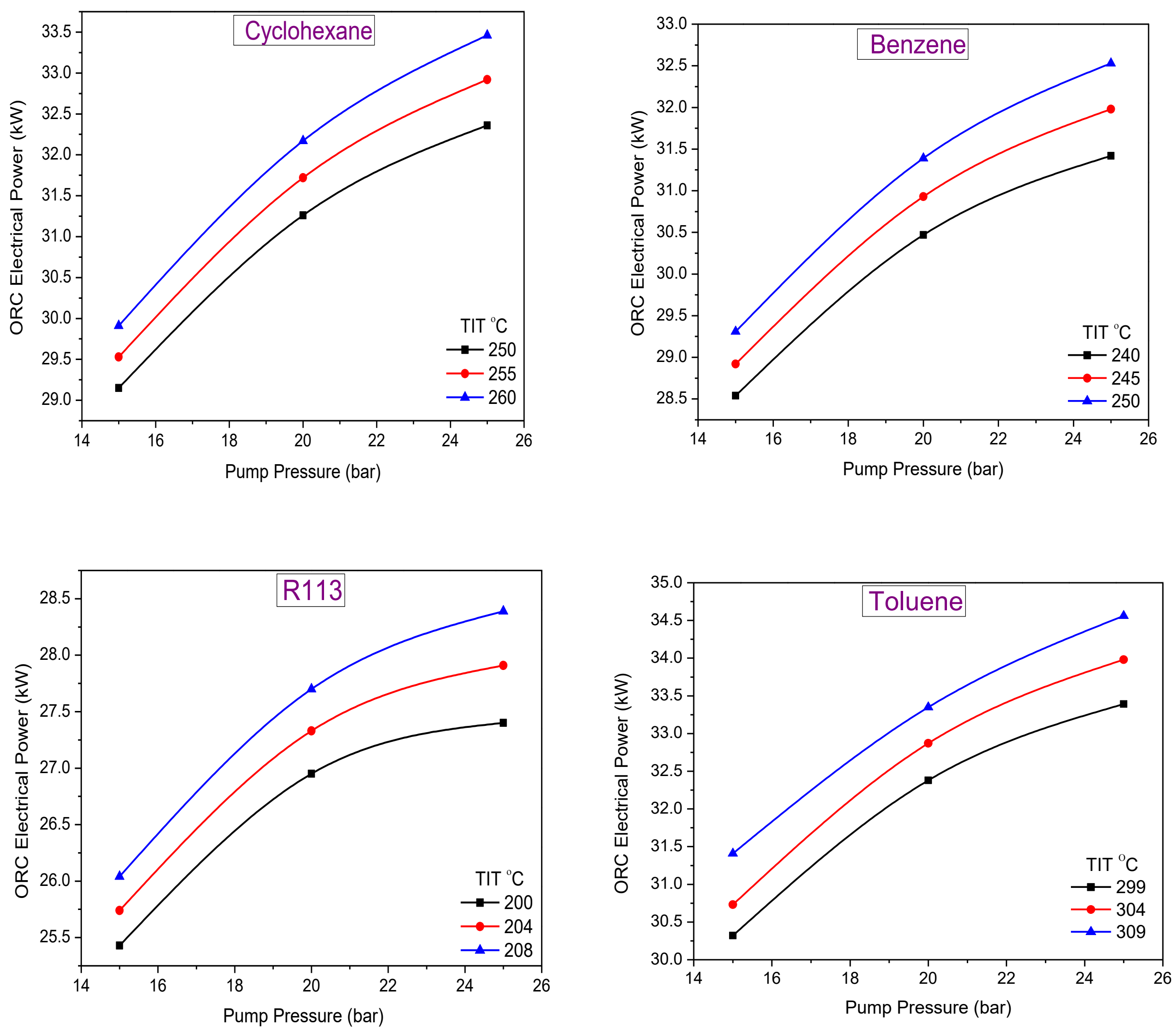

Figure 6. 12: The relation between $\mathbf{P_{ORC_{el}}}$ and $\boldsymbol{\rho_{Pump}}$ at different values of TIT for different working fluids.

Figure 6.13, shows the variations of ORC thermal efficiency (η_{th}) at different values of TIT (below critical temperature by 10 °C) for different working fluids and fixed pressure value (25 bar). It can be observed η_{th} of the ORC subsystem raises with TIT increasing. Toluene gives the highest η_{th} compared with other working fluids, where η_{th} has values from 19.8 to 20.5 % at TIT from 294 to 309 °C. For benzene and cyclohexane, both are closed values, the ORC η_{th} ranging from 18.5 to 19.35 % at TIT from 240 to 255 °C and 18.79 to 19.5 % at TIIT from 250 to 265 °C. R113 has the lowest ORC η_{th} which changes between 16.6 to 17.3 % at TIT from 200 to 212 °C.

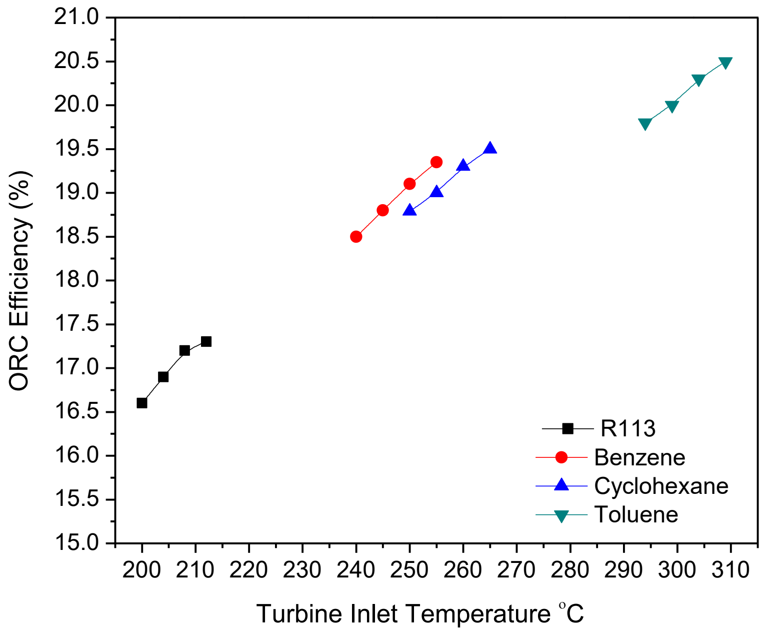

Figure 6. 13: Variation of ORC efficiency with TIT for different working fluids

Table 6.3, presents a comparison of possible ORC working fluids, including $P_{ORC_{el}}$, η_{th}, TIT, P_{Pump}, PPTD and fluid mass flow (m_{orc}). Toluene is the best fluid for maximizing the electrical power and efficiency, followed by cyclohexane, benzene and R113. The four working fluids are considered suitable for CHP applications, where the maximum thermal power produced for toluene is 110.85 kW, followed by benzene (110.32 kW), R113 (110.29 kW) and cyclohexane (104.95 kW). R113 gives the best performance in terms of CHP applications due to the lowest PPTD (10 °C) and its safety, cost, stability, corrosion, pressure and environmental hazards.

Table 6. 3: Optimal performance of suggested ORC fluids.

Fluid Type	$P_{ORC_{el}}$ (kW)	P_{pump} (kW)	η_{th}(%)	TIT (°C)	ρ_{pump} (bar)	m_{orc} (kg/s)	PPTD (°C)	$P_{ORC_{th}}$ (kW)
Cyclohexane	33.46	1.42	19.3	260	25	0.337	16	104.95
Benzene	32.53	1.42	`19.1	250	25	0.32	20	110.32
Toluene	34.64	1.65	20.5	309	25	0.35	23	110.85
R113	28.39	1.66	17.2	208	25	0.75	10	110.29

Figure 6.14, depicts the effect of ammonia concentration in the generator unit, drum CR and PC. It can be seen a positive correlation between ammonia concentration and PC. PC rises from 0.5 to 0.63 with increasing ammonia concentration from 40 to 60 %. In contrast, there is a negative correlation between ammonia concentration and CR, CR decreases from 7.66 to 1.88 with increasing ammonia concentration from 40 to 60 %.

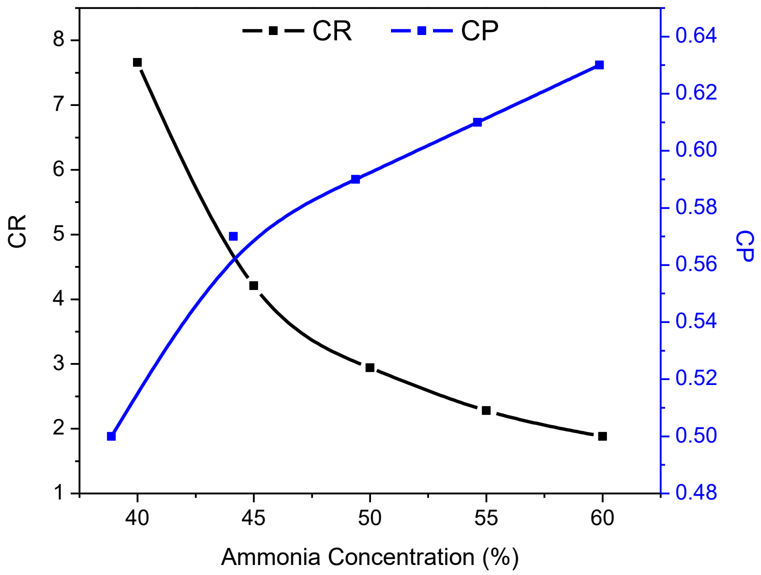

Figure 6. 14: The variation of ammonia concentration on circulation ratio and performance coefficient.

Figure 6.15, depicts the effect of generator unit temperature on CR, PC and cooling capacity. A positive correlation between the generator temperature and both PC and cooling power is observed. PC and cooling power rise from 0.25 to 0.58 and from 32.49 to 34.61 with increasing generator temperature from 100 to 130 °C. While there is a negative correlation between the generator temperature and CR, CR decreases from 7.66 to 1.88 with increasing generator temperature from 100 to 130 °C.

Figure 6.16, shows the effect of variation of reflux ratio on drum CR and PC. There is a negative correlation between reflux ratio and both of PC and CR. CR and PC decrease from 4.21 to 3.29 and from 0.63 to 0.16, respectively, with increasing reflux ratio from 0 to 0.8 %.

Figure 6.17, shows the effect of EFGT pressure ratio variation from 2 to 10 bar at three different TITs (800, 850 and 900 ºC) on CPR. It is observed a negative correlation between TIT and CPR. With increasing the TIT from 800 to 900 ℃, CPR decreased, and the highest value of CPR is achieved when the TIT is 800℃. CPR dramatically declines with increasing the pressure ratio from 2 to 6 at certain value (from 1.45 to 0.64 at TIT of 800 ℃, 1.3 to 0.45 at 850 ℃ and 1.19 to 0.31 at 900 ℃) which means decreasing in cooling capacity, and after this certain value the CPR increases slightly again. The lowest CPR is 0.38 achieved at TIT of 900 ℃ and pressure ratio of 6.

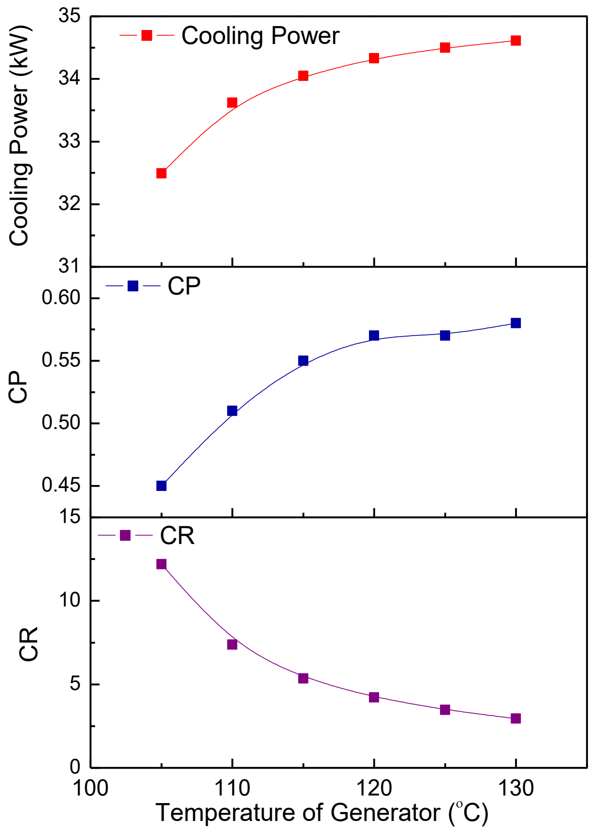

Figure 6. 15: The variation of generator temperature on circulation ratio, performance coefficient and cooling power.

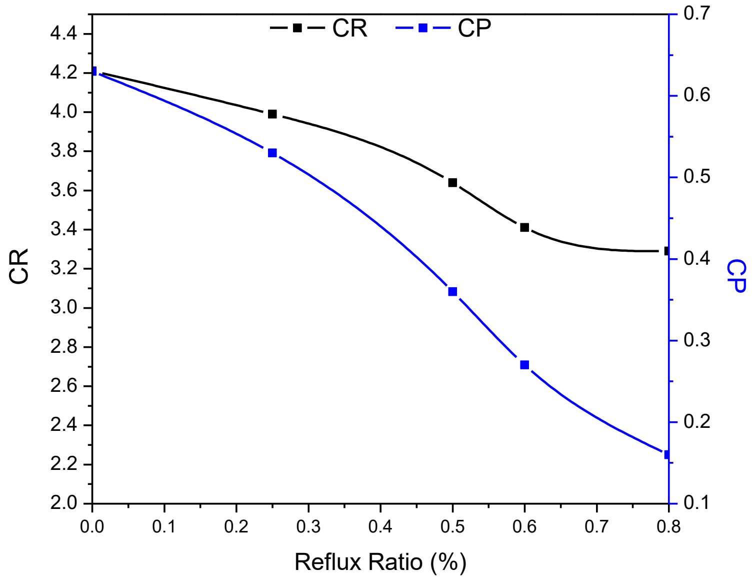

Figure 6. 16: The variation of reflux ratio on circulation ratio and performance coefficient.

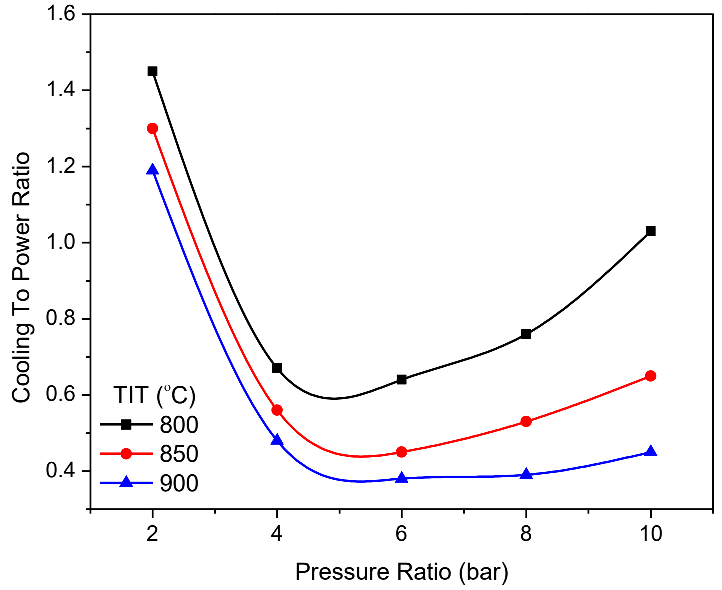

Figure 6. 17: The Effect of EFGT pressure ratio on cooling to power ratio at different TIT.

Figure 6.18, shows the variation of ORC ρ_{Pump} from 10 to 35 bar on CPR for toluene, benzene, cyclohexane and R113. The highest values of CPR are achieved with R113 fluid and the lowest values are achieved using cyclohexane. CPR dramatically declines with increasing the ρ_{Pump} from 10 to 30 bar at certain value: from 2.44 to 1.66 for R113, 2.25 to 1.4 for benzene, 1.9 to 1.07 for toluene and 1.8 to 1 for cyclohexane). Decreasing the cooling capacity, CPR increases dramatically after this certain value.

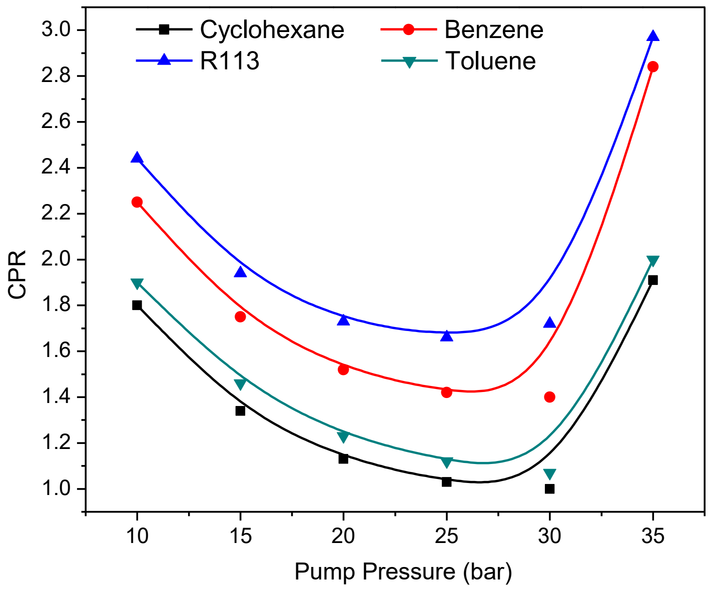

Figure 6. 18: The Effect of ORC pressure ratio variation on cooling to power ratio for different working fluids.

Table 6.4, presents the optimal performance of the present study compared with the CHP system presented in [59] (downdraft gasification with EFGT and ORC). The main purpose of both systems is to maximize the generated electrical and thermal powers. The present study is more suitable electricity, heating and cooling necessities, such as buildings, while the study of Vera et al. (2018) is more suitable for heating and power applications. These studies use different types of biomass conversion technologies.

A downdraft gasifier is used to convert 217 kg h-1of olive tree pruning to syngas in [59], the efficiency of this gasifier reached to 89%. While in the current work, the direct combustion is used to convert 121.68 kg h-1 of bagasse. The efficiency of direct combustion reached to 96%. It is not necessary that the working fluid which gives the highest electrical power is the best suited to be used in ORC technology. The main criteria for selecting the appropriate ORC working fluid are the temperature difference between the heat source and boiling point of the working fluid. The secondary considerations are safety, cost, stability, corrosion, pressure and environmental hazards of working fluid. Vera et al. (2018) considered both of Iso-pentane and R113 the most appropriate working fluids. Iso-pentane presented the largest electric power (57.1 kW) with an ORC efficiency of 20.45% and a net electric efficiency of 20.7% (without producing thermal energy). For R113, the thermal power produced was 200 kW and the electric power 49.1 kW which was suitable for a hybrid system with ORC efficiency (17.60 %) and net electric efficiency (20%).

It can be observed in the present study the electrical power from EFGT is 142.92 kW. When the ORC used as bottoming subsystem, the generated electrical power is increased depending on the type of working fluid used. Toluene is considered the optimal working fluid for maximizing electricity generation (177.56 kW) with the highest η_{CCHP} (43.9 %), while R113 is the best working fluid for cooling generation (46.51 kW). These results indicate higher improvement in the electrical efficiency system and the overall system efficiency.

Table 6. 4: Optimum performance of proposed tri-generation system.

Parameter	**Present study CCHP**	**CHP (Gasifier + EFGT +ORC)** [59]
Combustion chamber efficiency (%)	90	80
HTHE efficiency (%)	87	85
Compressor pressure ratio of EFGT	4.84	4.94
Hot side temperature difference (ºC)	85	100
Combustor air factor of EFGT	6.27	6.40
EFGT energy input (kW)	708.40	714.14
EFGT electric power (kW)	142.92	150.2
Refrigerating heat flow (kW)	48.83	-
Temperature of generator unit (ºC)	120	-
CP	0.57	-
CR in generator unit	4.07	-
Ammonia concentration in generator unit (%)	45.5	-
Net electric power (kW)	Toluene (177.56) Cyclohexane (176.38) Benzene (175.22) R113 (171.21)	Iso-pentane (207.3) R113 (199.3)
$Q_{cooling}$ (kW)	Toluene (38.50) Cyclohexane (34.33) Benzene (45.68) R113 (46.51)	-
$\eta_{net_{el}}$ (%)	Toluene (24.8) Cyclohexane (24.6) Benzene (24.5) R113 (23.8)	Iso-pentane (20.7) R113 (20)
Overall efficiency of the system (%)	Toluene (43.9) Cyclohexane (42.5) Benzene (43.7) R113 (43.5)	R113 (40.62)

In the study [62], have revealed that Toluene is the most appropriate working fluid and this study showed that the electrical efficiency using toluene ranges from 20.5% to 24.5% while in this work the electrical efficiency reaches 24.8%.

6.4. Hybrid PV/WT/Biomass/Battery using SMA and SOA Algorithms

The main contributions of this system can be summarized in the following significant points:

- Based on the previous literature review revealed that only a few studies have presented the optimal sizing performance of integrated a biomass unit with other renewable energy systems with using HOMER software. Thus, in this section three different combinations of stand-alone hybrid systems using real-time meteorological data of a remote area located in the Western Desert of Egypt called Abu-Monqar village are suggested with using different optimization algorithms. The first system includes PV, WT, biomass, and battery; the second one is PV, biomass, and battery unit; and the last one is WT, biomass, and battery unit.

- A new flexible optimization approaches namely, SMA and SOA for determining the optimal sizing of a stand-alone system is proposed. A comprehensive comparison of the proposed two techniques with other optimization methods namely GWO, WOA and SCA has been presented for the different configurations of the proposed system and comprehensive discussion and analysis are provided.

- The proposed design algorithms are implemented with the aim of reducing the system energy cost while achieving significant improvement in the power supply and determining the best optimal size of the components, i.e., number of PV modules, number of WTs, number of biomass generators, and number of battery banks.

Matlab software has been used to run the optimization programs. The results obtained by the SMA and SOA algorithms are compared with those obtained from recent optimization methods such as GWO [192], SCA [193], and WOA [194], for the three proposed cases of the proposed renewable energy system.

In this system, three configurations of sustainable systems have been studied and evaluated regarding the cost of energy produced from the hybrid system, the main parameters of the this hybrid system are illustrated in Table 6.5:

- Case (1): PV, WT, Biomass, and Battery
- Case (2): PV, Biomass, and Battery
- Case (3): WT, Biomass, and Battery

In this study, during the simulation and analysis, the time interval for all input parameters is adjusted at one hour, in which the hourly load curve is taken over the day. In order to avoid the randomness of the proposed algorithms and validate their stability and robustness, the optimization programs based on both SMA and SOA techniques have been implemented 50 individual times and the lower value of the objective function has been recorded. Each algorithm has been operated in the same manner for the three case studies. The Convergence curves for the proposed cases of the hybrid system using the SOA and SMA methods over the 50 runs are shown in Figure 6.19. It is observed that the final values of the objective function for the proposed SMA algorithm are arranged in a narrow range, which proves the stability of SMA for solving the optimization problem.

Table 6. 5: Main parameters of the hybrid system

Parameter	Value	Unit
PV System [78]		
Model		PV-MLT260HC
PV panel cost (PV_{cost})	14854	$/m^2$
γ_T	0.0037	-
η_{pv}	15	%
T_r	25	ºC
R_{nom}	1000	W/m^2
Rated power	1	kW
Length	1625	mm
Width	1019	mm
Thickness	46	mm
lifetime of the PV system (S_{PV})	20	year
PV replacement cost (C_{rep}^{PV})	13885	$
WT System [78]		
Model		Fuhrländer FL 30
p_{rated}^{wt}	30	kw
WT height	50	m
η_{wt}	80	%
S_{cut}^{in}	2.5	m/s
S_{rated}	12	m/s
S_{cut}^{off}	25	m/s
lifetime of wind system	20	year

WT cost	3200	$/kw
Inverter device [78]		
η_{inv}	95	%
inverter lifetime (S_{inv})	10	year
Inverter cost	711	$/kw
Inverter replacement cost (C_{rep}^{inv})	650	$/kw
Battery unit		
Model		RS lead acid battery
Nominal battery voltage [195]	5	V
Nominal battery capacity [195]	360	Ah
Storage capacity of battery [7]	4.8	kWh
η_{CH} [78]	90	%
η_{DIS} [78]	85	%
σ [78]	0.005	-
Battery cost (Bat_{cost}) [78]	3880	$
Battery lifetime (S_{Bat}) [78]	25	year
Biomass System		
LHV_B [12]	14,824	kJ/kg
LHV_{pg} [12]	4.766	MJ/kg
η_g	80	%
PG_{rated}	40	KW
F_0 [85]	0.0644	kg/h/50kW
F_m [85]	0.2998	kg/h/50kW
Capital cost of Biomass system (BG_{cost}) [87]	4000	$/kw
lifetime of Biomass plant (S_{BG}) [87]	25	years

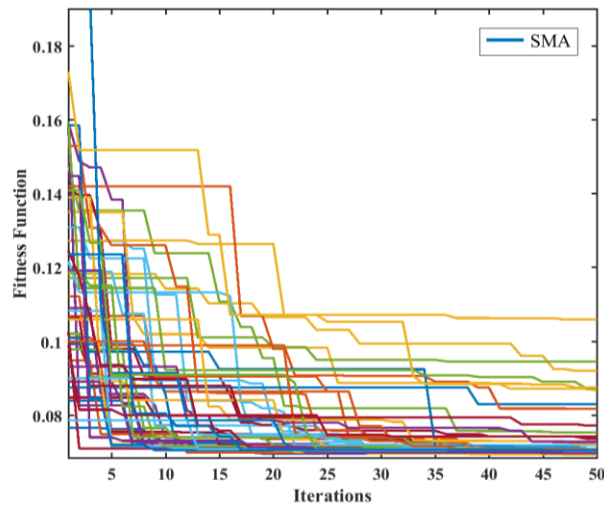

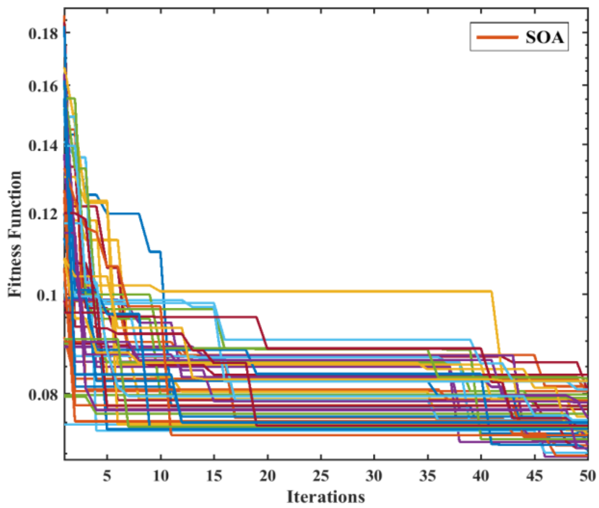

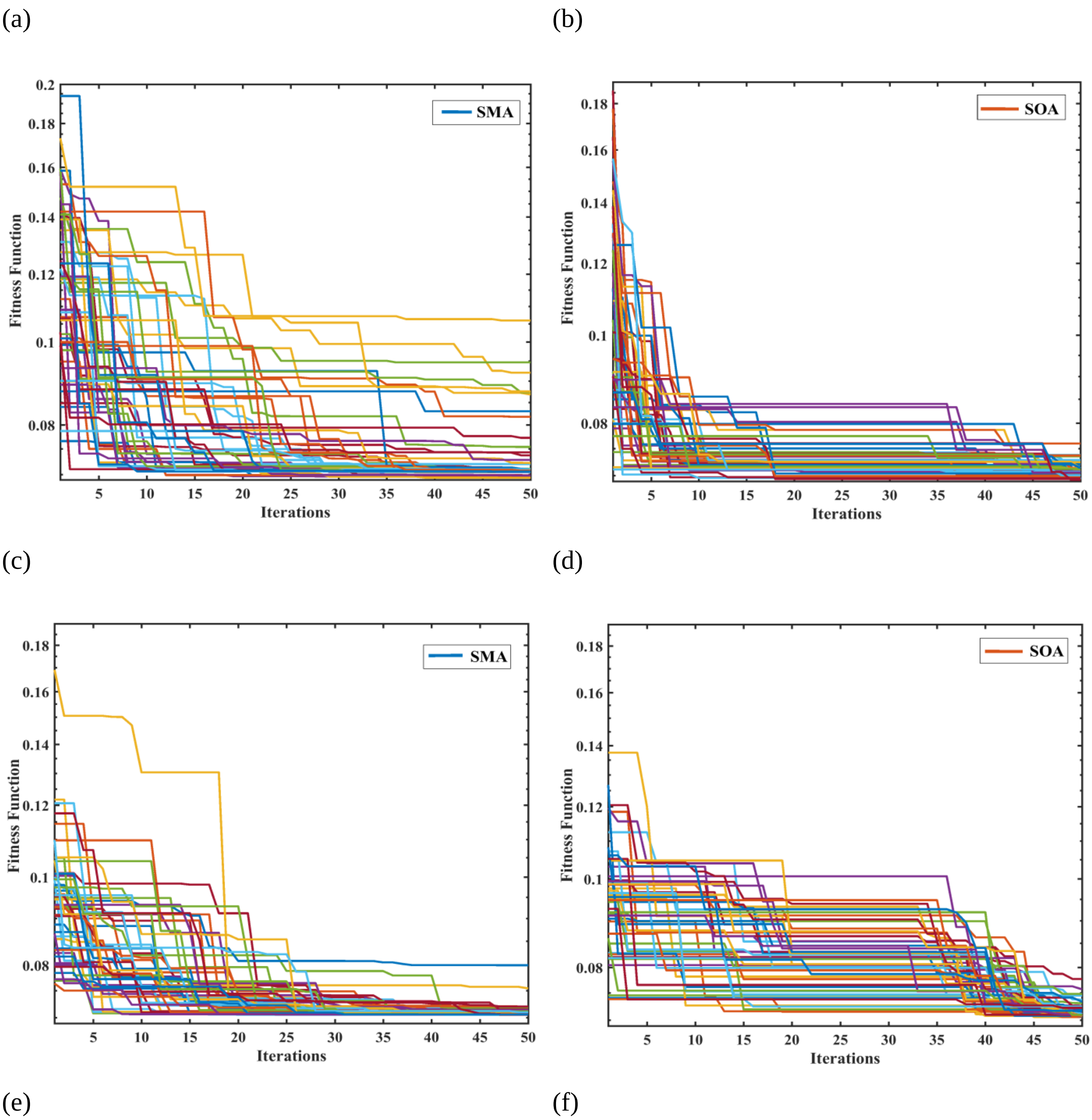

Figure 6. 19: Convergence curves of the optimization techniques for 50 runs: (a) SMA for Case 1, (b) SOA for Case 1, (c) SMA for Case 2, (d) SOA for Case 2, (e) SMA for Case 3, (f) SOA for Case 3.

To provide a more precise comparison between both methods, parametric and nonparametric statistical measurements have been conducted based on the obtained values of the objective function over the 50 individual runs for all studied cases. The parametric measures include the lower value of the objective function, its maximum value, and the mean value, while the nonparametric measures include the median, RE, the MAE, SD, the RMSE, and efficiency. The efficiency here referred to the ratio between the lower value of the objective function and its mean value. The results of the statistical measurements for both

SMA and SOA algorithms for the three case studies are listed in Table 6.6. Based on the obtained results, it can be concluded that the proposed SMA presents better performance than the SOA method in all cases.

Table 6. 6: Estimation of the statistical performance of the studied optimization algorithms

	Case (1)		**Case (2)**		**Case (3)**	
	SOA	SMA	SOA	SMA	SOA	SMA
Max.	0.0835666	0.1059949	0.0759832	0.1006895	0.0777398	0.0800107
Min.	0.0695232	0.0694226	0.069305	0.0692953	0.0705996	0.0705902
Mean	0.0751	0.0740	0.0736	0.0710	0.0717	0.0711
Median	0.0746	0.0706	0.0704	0.0708	0.0710	0.0706
SD	0.3375	0.7727	0.8006	0.1340	0.1453	0.1492
RE	3.8794	3.3321	3.1023	1.1969	0.7733	0.3644
MAE	0.0054	0.0046	0.0043	0.0017	0.0011	0.000515
RMSE	0.0064	0.0089	0.0090	0.0021	0.0018	0.0016
Efficiency	92.9824	94.57	95.0359	97.6955	98.5148	99.3153

Figure 6.20, shows the convergence curve of the best optimal solution for each case using the SMA, SOA. In this figure, the convergence curves of the proposed algorithms are compared with the corresponding ones obtained from well-known optimization algorithms, namely GWO, SCA, and WOA. From the figure, the reader clearly notices that SMA and SOA techniques provide the best minimum value of the objective function for the three cases compared with those obtained by other optimization algorithms. For Case (1), the best solution using SMA is 0.0694226 which is achieved after 24 iterations while the best solution using SOA is 0.0695232 which is achieved after 11 iterations. For Case (2), the best solution using SMA is 0.0692953 which is achieved after 3 iterations while the best solution using SOA is 0.069305 and obtained after 49 iterations. For Case (3), the best solution using SMA is 0.0705909 and achieved after 35 iterations while the best solution using SOA is 0.0705996 after 30 iterations. As the problem under study is an off-line optimization problem, the computation time or the number of iterations taken to reach the optimal solution is not a matter. The value of the objective function is the only factor considered for comparison purposes. Finally, the reader can notice that the SMA provides a good convergence characteristic over the SOA algorithm and the conventional GWO, SCA, and WOA methods in all cases.

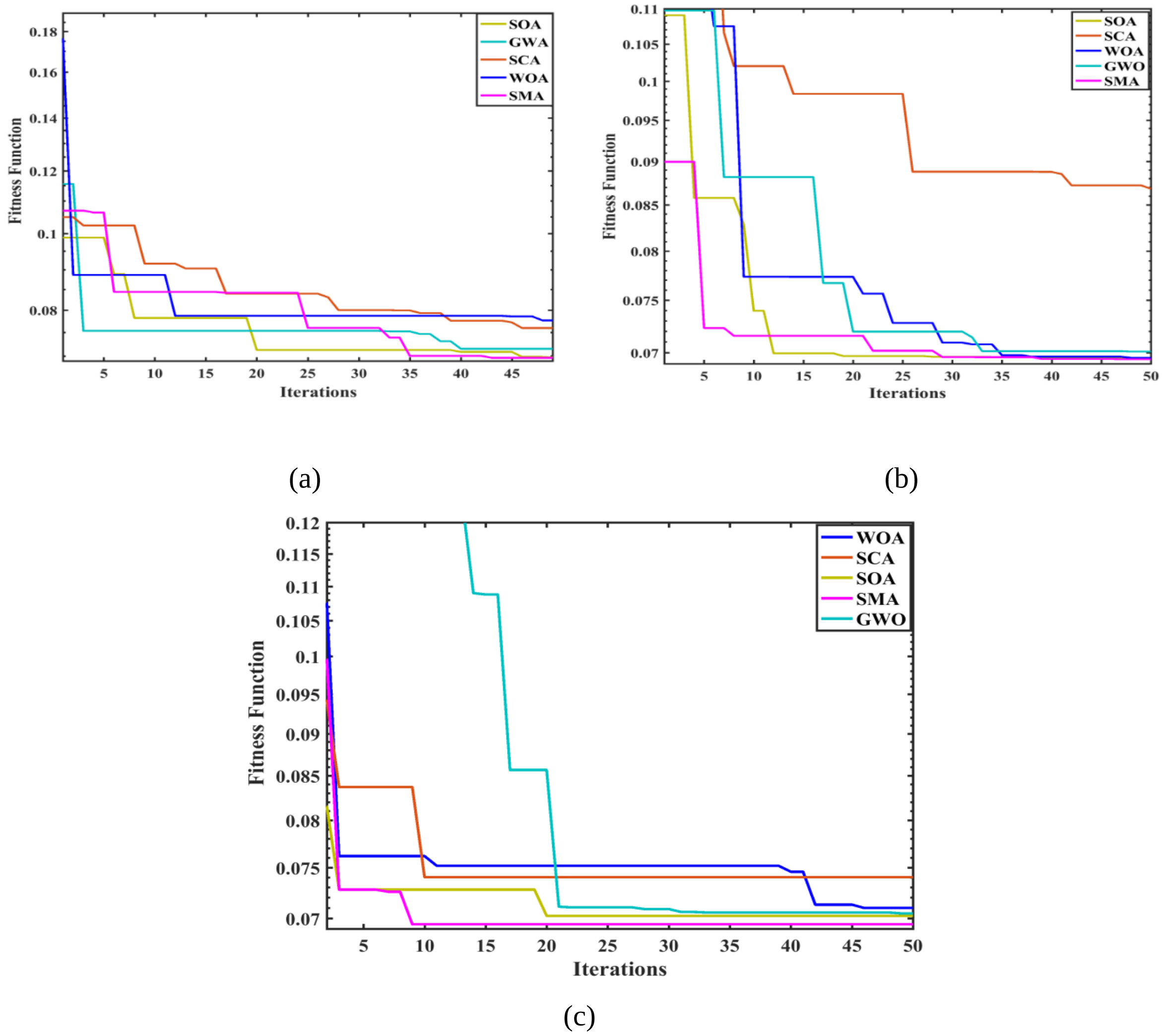

Figure 6. 20: Convergence curves of the best optimal solution for SMA, SOA, GWO, SCA and WOA for (a) case 1, (b) case 2, (c) case 3.

Table 6.7, Table 6.8, and Table 6.9, provide the results of the optimization problem for the three suggested cases. The comparison is based on many factors including the best value of the objective function, the decision variables (N_{pv}, N_{wt}, N_{BG} and N_B), the EC, LPSP, NPC, C_{ann}^{fuel}, the number of iterations, and the computation time of the optimization algorithms. It can be noted that for Case (2) in Table 6.7, both algorithms took a shorter computation time compared with the other cases. In all cases, SMA was faster than SOA in reaching the optimal solution. For the three cases, the SMA provides the best results compared with those obtained by SOA and the conventional GWO, SCA, and WOA. It can be concluded that for all studied cases the SMA algorithm provides fast convergence characteristics, the best minimum values of the objective function, and minimum energy production cost.

Table 6. 7: Optimization characteristics based on SMA and other algorithms for PV/WT/Biomass hybrid system.

Case (1)					
Algorithm	**SMA**	**SOA**	**GWO**	**SCA**	**WOA**
Best obj. fun.	0.0694226	0.0695232	0.0695501	0.0696859	0.0697121
$\mathbf{N_{pv}}$ **(units)**	20	16	21	27	22
$\mathbf{N_{wt}}$**(units)**	1	1	1	1	1
$\mathbf{N_{BG}}$**(units)**	2	2	2	2	2
$\mathbf{N_{B}}$**(units)**	438	464	463	443	480
EC ($/kWh)	0.1330443	0.133588	0.137488	0.138342	0.139902
LPSP	0.0279623	0.027016	0.021711	0.020839	0.0203683
$\mathbf{C_{ann}^{fuel}}$ **($/year)**	39438.196	40400.304	39943.53	37836.25	39529.17
NPC($)	3896930.397	3912841.92	4027083.99	4052103.48	4097807.11
No. of iterations	24	11	34	17	18
Computation time (sec)	445	600	965	1096	2465

Table 6. 8: Optimization characteristics based on SMA and other algorithms for PV/Biomass hybrid system.

Case (2)					
Algorithm	**SMA**	**SOA**	**GWO**	**SCA**	**WOA**
Best obj. fun.	0.0692953	0.069305	0.0693185	0.069757	0.0693142
$\mathbf{N_{pv}}$**(units)**	18	15	19	14	17
$\mathbf{N_{BG}}$**(units)**	2	2	2	2	2
$\mathbf{N_{B}}$**(units)**	425	446	457	496	448
EC($/kWh)	0.12941073	0.1299702	0.134553	0.136057	0.131711
LPSP	0.0285965	0.0260045	0.0244631	0.024189	0.0239458
$\mathbf{C_{ann}^{fuel}}$**($/year)**	40755.41	41003.529	40151.053	41266.83	40837.48
NPC($)	3790500.895	3806888.284	3941116.479	3985169.12	3857880.9
No. of iterations	3	49	37	10	13
Computation time (sec)	330	408	965	960	1260

Table 6. 9: Optimization characteristics based on SMA and other algorithms for WT/Biomass hybrid system.

Case (3)					
Algorithm	**SMA**	**SOA**	**GWO**	**SCA**	**WOA**

Best obj. fun.	0.0705909	0.0705996	0.0706139	0.0707111	0.0706287
N_{wt}(units)	1	1	1	2	1
N_{BG}(units)	2	2	2	2	2
N_{B}(units)	441	456	462	470	465
EC ($/kWh)	0.1186861	0.1190885	0.1215502	0.1228269	0.1217932
LPSP	0.032493	0.0313134	0.030717	0.0303097	0.0307507
C_{ann}^{fuel}($/year)	44016.516	43767.04	43971.59	43828.35	43819.64
NPC ($)	3476371.76	3522224.83	3560263.25	3597656.27	3567380.91
No. of iterations	35	30	10	40	31
Computation time (sec)	422	530	1440	1080	1980

Figure 6.21, presents a comparison of the main optimization factors such as EC, LPSP, and NPC for the three cases based on the application of SOA and SMA. The simulation results for the three cases showed that the SMA algorithm gives the lowest value of EC and NPC compared with SOA while an insignificant increase in the value of LPSP is observed. The value of LPSP for all cases using both algorithms is within its constraints (i.e., LPSP < 0.05). Case (3) ensures the lowest value of EC supplied by the proposed hybrid system as compared with Case (1) and Case (2) with a value of 0.1186861 $/kWh. As a result, Case (3) ensures the lowest value of the NPC of the system as compared to Case (1) and Case (2) with a value of $3,476,371.76.

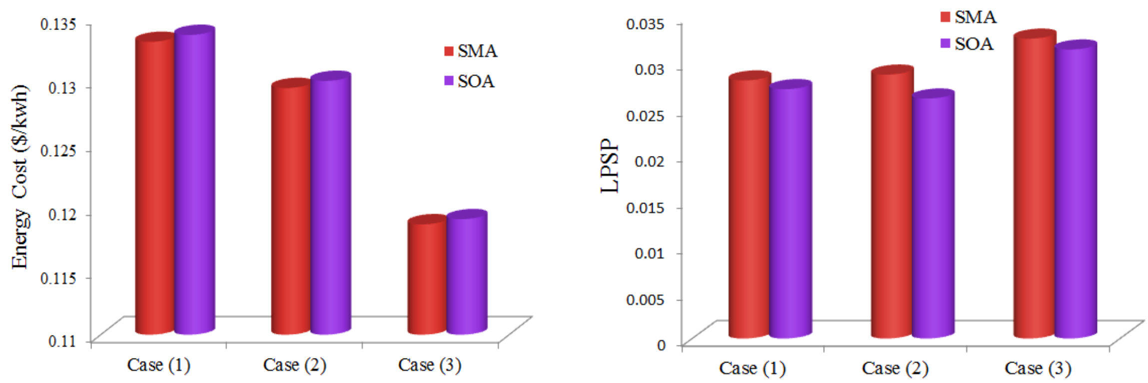

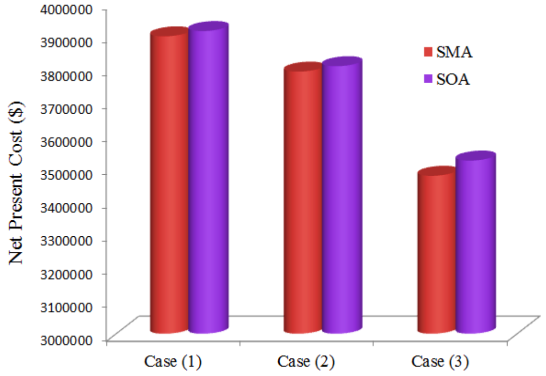

Figure 6. 21: A comparison of the main optimization factors for SOA and SMA

Figure 6.22, reveals the contribution of each unit in the proposed hybrid renewable energy system in the total NPC for the three cases based on the results of the SMA. The annual costs of the main generating components in the system for all cases, based on the application of the optimal solution obtained from the SMA, are shown in Figure 6.23. For Case (1), the batteries represent the highest annual cost compared with the other units with \$135,187.244, followed by the inverter, biomass system, PV panels, fuel consumption cost, and finally, WTs, with \$66,321.51, \$61,965.97, \$40,726.54, \$39,438.2, and \$642.81, respectively. For Case (2), the batteries also represent the highest annual cost compared with the other units with \$131,158.43, followed by the inverter, biomass system, fuel, and PV panels with \$66,321.51, \$64,035.6, \$40,755.41, and \$35,002.9, respectively. For Case (3), again the batteries represent the highest annual cost with \$135,821.33, followed by the biomass system with \$69,159.5, then the inverter, fuel, and WTs with \$66,321.51, \$44,016.52, and \$642.81, respectively.

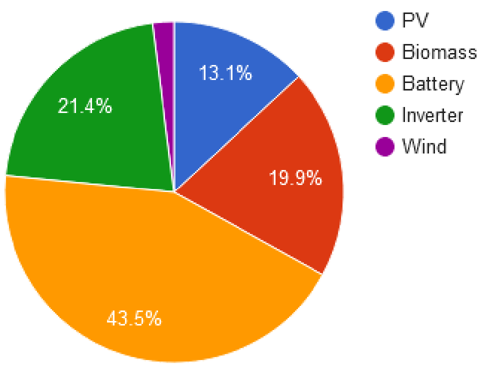

Case (1)

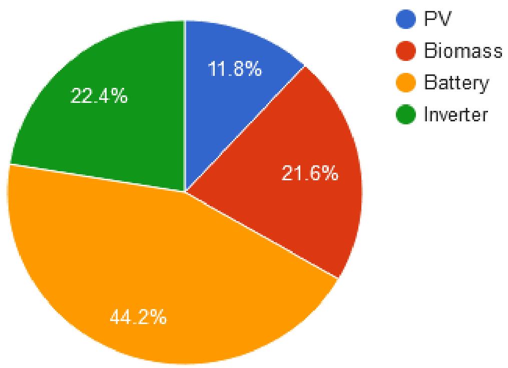

Case (2)

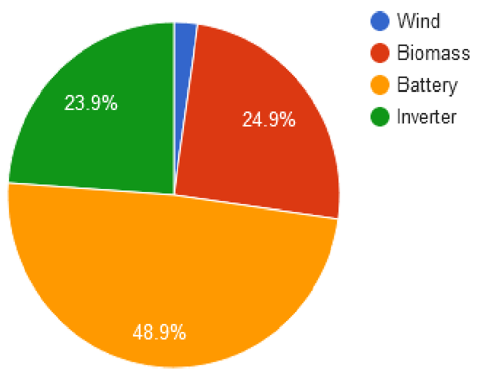

Case (3)

Figure 6. 22: The net present cost divided between the main units of the hybrid system.

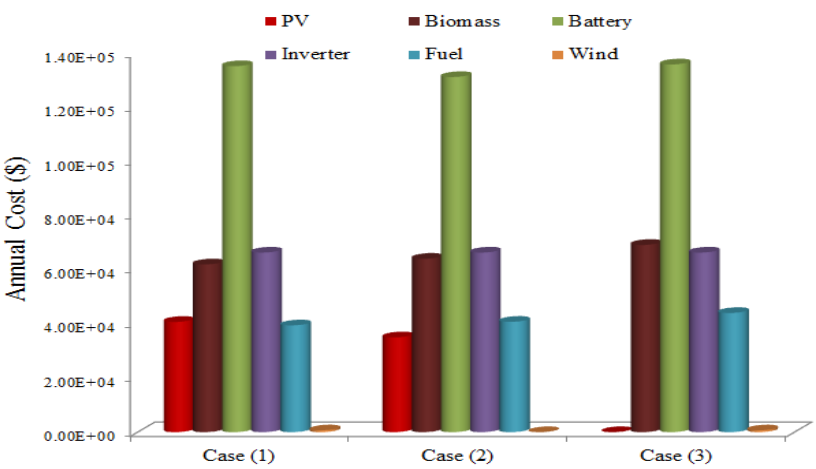

Figure 6. 23: The yearly cost of the main hybrid system components for the three cases using SMA.

The percentage of the yearly cost which includes yearly capital cost, yearly replacement cost, operating and the yearly fuel cost, and maintenance cost for each unit of the hybrid system for Case (1) are shown in Figure 6.24. The reader can notice that, for the battery storage system, the inverter, the PV system, and the WT, the annual sharing of the capital cost is the highest compared to other types of cost. While for the BG the fuel consumption cost is the highest part. Also, the BG has the highest operating and maintenance cost compared with other generating units included in the proposed hybrid system.

Figure 6.25, illustrates the operation of the proposed hybrid system during four different days throughout the year based on the results of the SMA technique. It is shown that during the daytime, when the energy generated by the renewable sources and the biomass generator is higher than the load demand, the battery storage system starts to charge the excess of energy (i.e., increase in the SOC_{Bat}). When the battery system is fully charged, SOC_{Bat} is 100%, the excess power is dissipated in the dummy load. When the load power is greater than the generation, the load is covered by discharging the stored energy in the battery system thus leading to a decrease in the SOC_{Bat}.

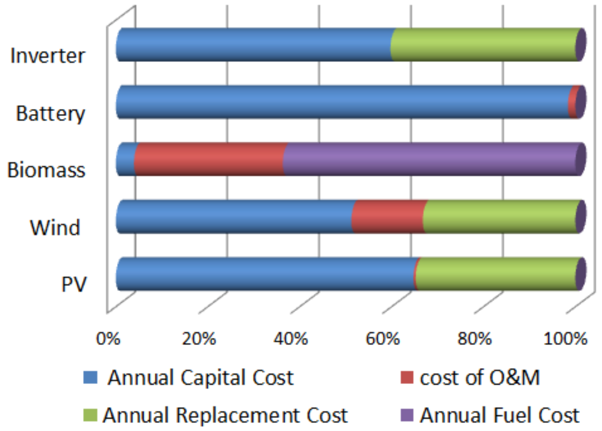

Figure 6. 24: The percentage of the yearly cost of the main hybrid system components for Case (1).

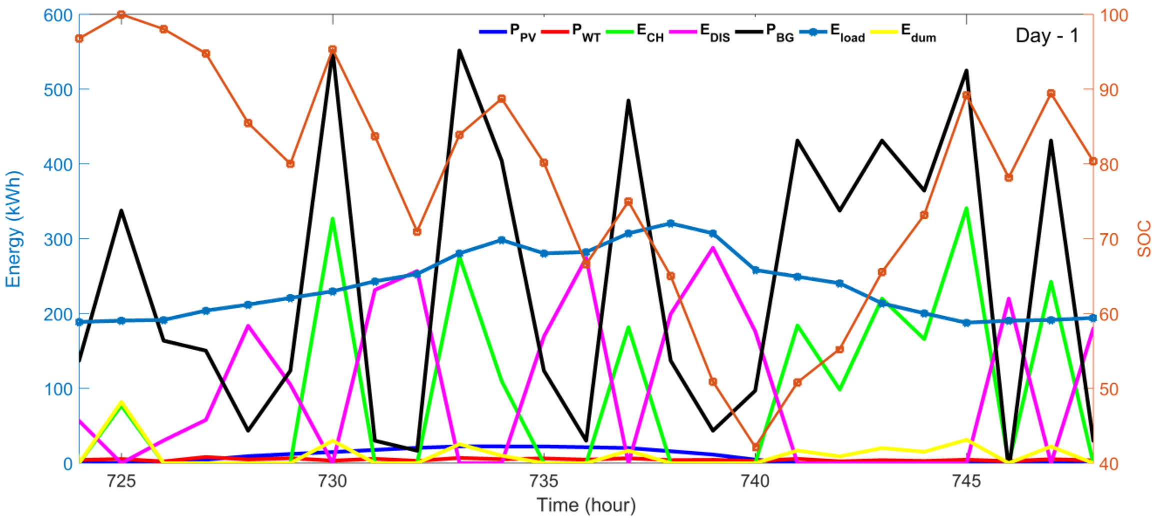

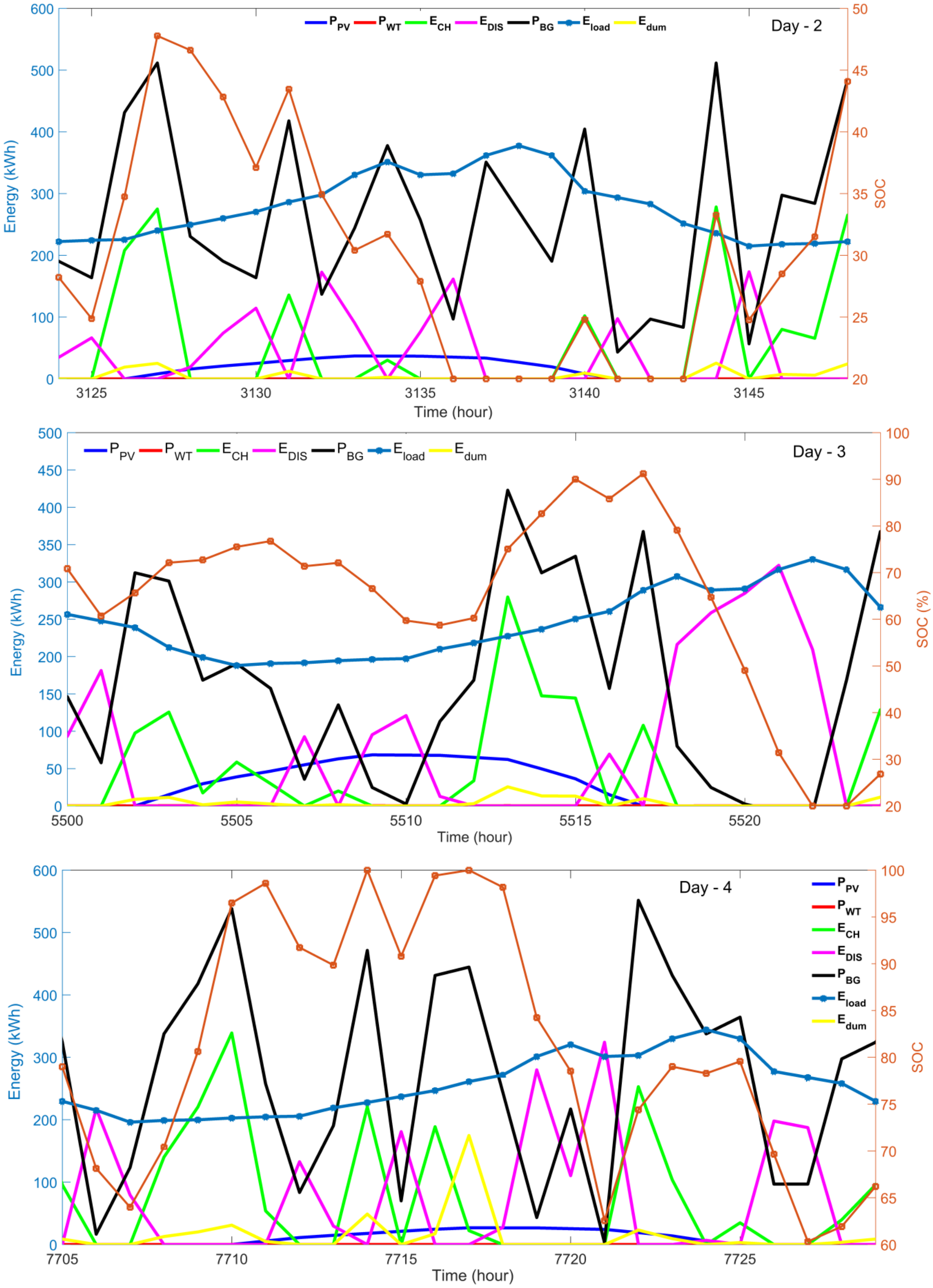

Figure 6. 25: Operation of the hybrid system during four different days using the results of SMA

6.5. Hybrid PV/WT/Biomass/Battery using HBO, CFA and STOA Algorithms

This system contains the study of four scenarios of a stand-alone hybrid system utilizing real-time meteorological data for a remote area located in the New Valley Governorate of Egypt called Alrashda village in Dakhla Oasis. These four scenarios of the hybrid system are namely:

- The first system scenario is PV/WT/Biomass/Battery
- The second is PV/Biomass/Battery
- The third is WT/Biomass/Battery
- The fourth one is PV/WT/Battery.

The system includes studying a new optimization algorithm which is HBO technique and make a comparison with a three recent types of optimization methods namely, CFA, the STOA, and GWO. The study includes exploiting the capabilities of the proposed algorithms to optimize and minimize EC with increasing the reliability and efficiency of the suggested hybrid systems, and performs different sensitivity analyses on an optimal design to predict the upcoming system implementation.

Figure 6.26, presents the graphic form of the final values of the target function over the 50 executes for the four analyzed configurations scenarios utilizing the optimization techniques namely, HBO, CFA, GWO, and STOA. It can be noted that, the fitness values for the suggested HBO method in the four system cases were within a limited range, which demonstrated the stability of the suggested technique over the other techniques. Therefore, parametric and nonparametric metric values are superior for the HBO.

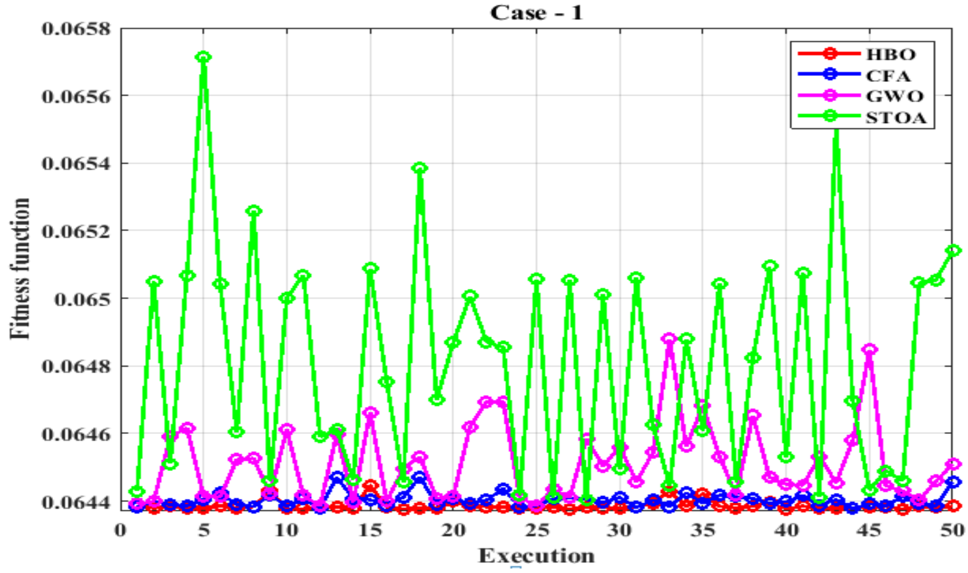
Case - 1
Fitness function
Execution
HBO
CFA
GWO
STOA
0.0658
0.0656
0.0654
0.0652
0.065
0.0648
0.0646
0.0644
0
5
10
15
20
25
30
35
40
45
50

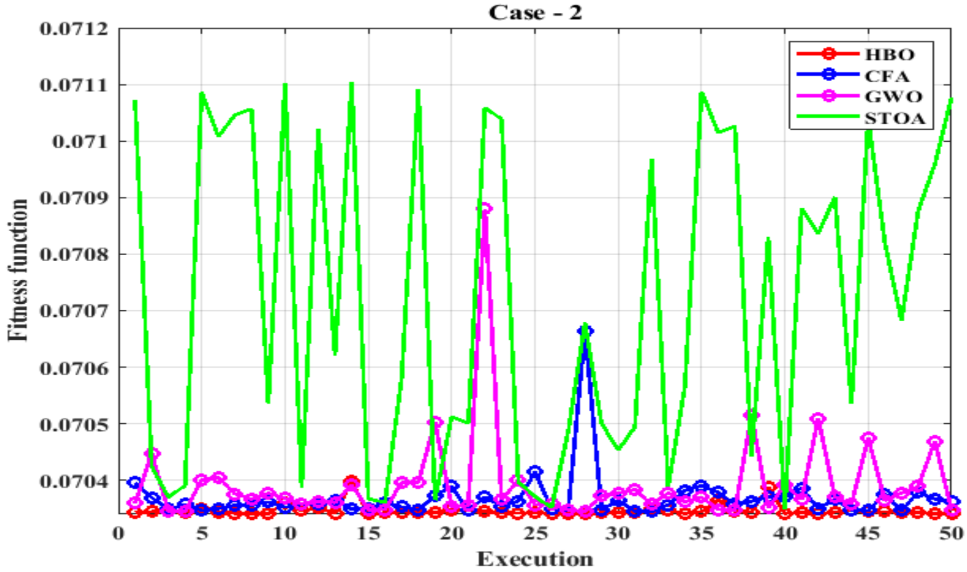
Case - 2
Fitness function
Execution
HBO
CFA
GWO
STOA
0.0712
0.0711
0.071
0.0709
0.0708
0.0707
0.0706
0.0705
0.0704
0
5
10
15
20
25
30
35
40
45
50

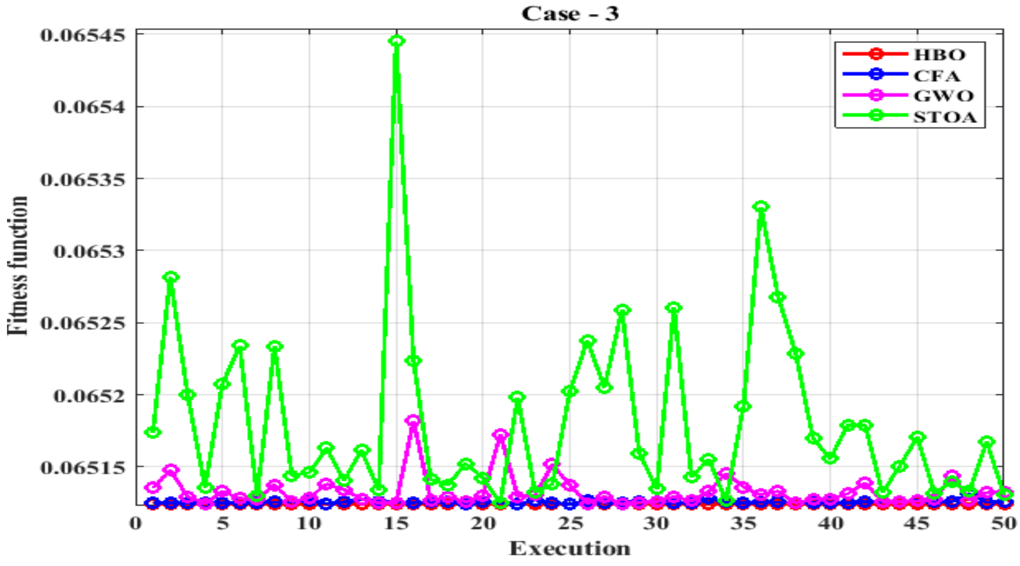
Case - 3
Fitness function
Execution
HBO
CFA
GWO
STOA
0.06545
0.0654
0.06535
0.0653
0.06525
0.0652
0.06515
0
5
10
15
20
25
30
35
40
45
50

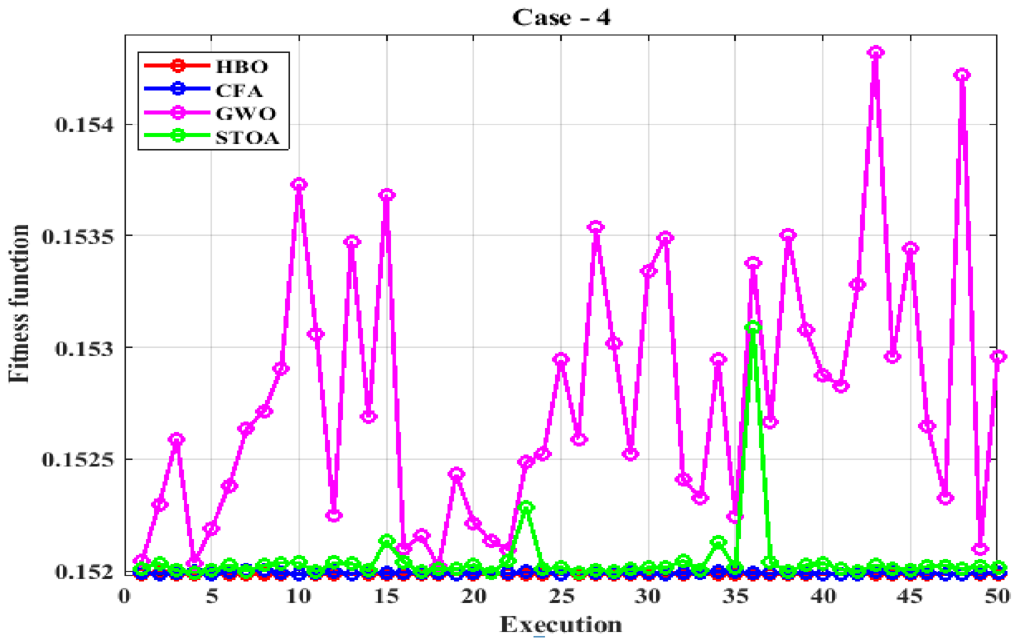

Figure 6. 26: End values of the fitness function for 50 executions using HBO, CFA, GWO, and STOA methods: case-1: PV/WT/Biomass/ Battery system, case-2: PV/Biomass/ Battery system, case-3: WT/Biomass/ Battery system, case-4: PV/WT/ Battery system.

Figure 6.27, displays the best optimal solution convergence curve for each scenario utilizing HBO, CFA, GWO, and STOA. For Case (1), the best solution achieved by using HBO technique which is 0.0643767 after 27 iterations, followed by CFA technique with 0.06437783 after 44 iterations. For Case (2), the best solution achieved by using HBO technique which is 0.0703404 after 49 iterations, followed by best solution achieved by CFA technique with 0.07034462 after 32 iterations. For Case (3), the best solution achieved by using HBO technique with 0.0705909 after 41 iterations, followed by best solution achieved by CFA technique with 0.0651240320 after 39 iterations. Finally for Case (4), the best solution achieved by using HBO technique with 0.151991724 after 41 iterations, followed by best solution achieved by CFA technique with 0.152001799 after 58 iterations. It can be noticed that the HBO method provides a good convergence characteristic over the other optimization algorithms CFA, GWO, and STOA in all suggested cases.

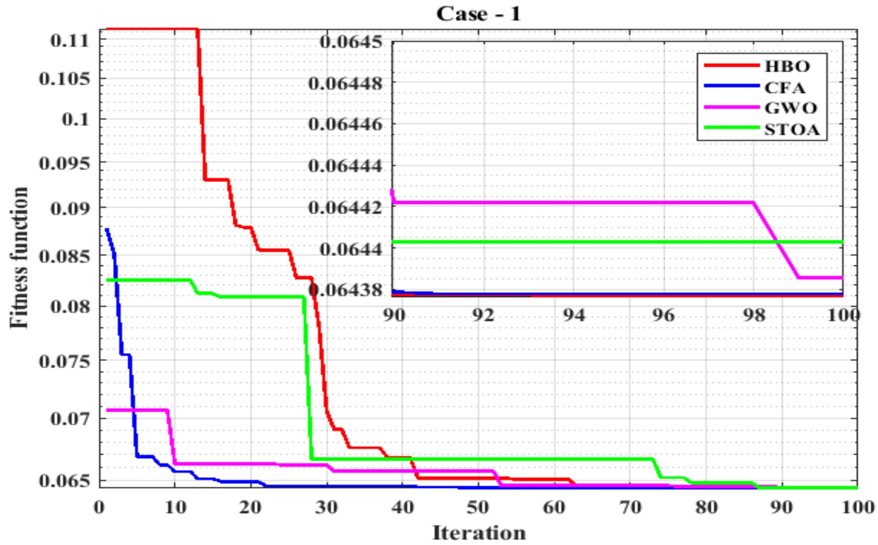
Case - 1
HBO
CFA
GWO
STOA
Fitness function
Iteration
0.11
0.105
0.1
0.095
0.09
0.085
0.08
0.075
0.07
0.065
0
10
20
30
40
50
60
70
80
90
100
0.0645
0.06448
0.06446
0.06444
0.06442
0.0644
0.06438
90
92
94
96
98
100

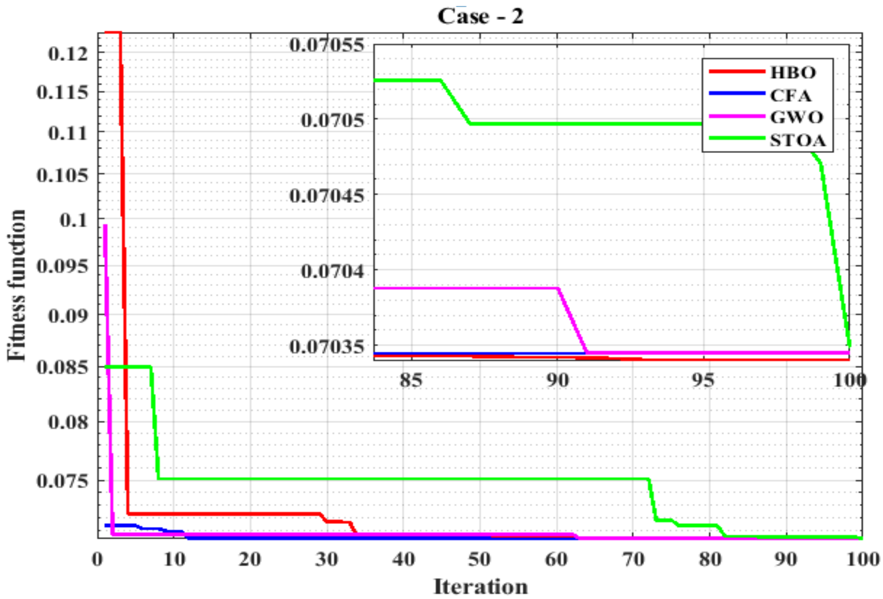
Case - 2
HBO
CFA
GWO
STOA
Fitness function
Iteration
0.12
0.115
0.11
0.105
0.1
0.095
0.09
0.085
0.08
0.075
0
10
20
30
40
50
60
70
80
90
100
0.07055
0.0705
0.07045
0.0704
0.07035
85
90
95
100

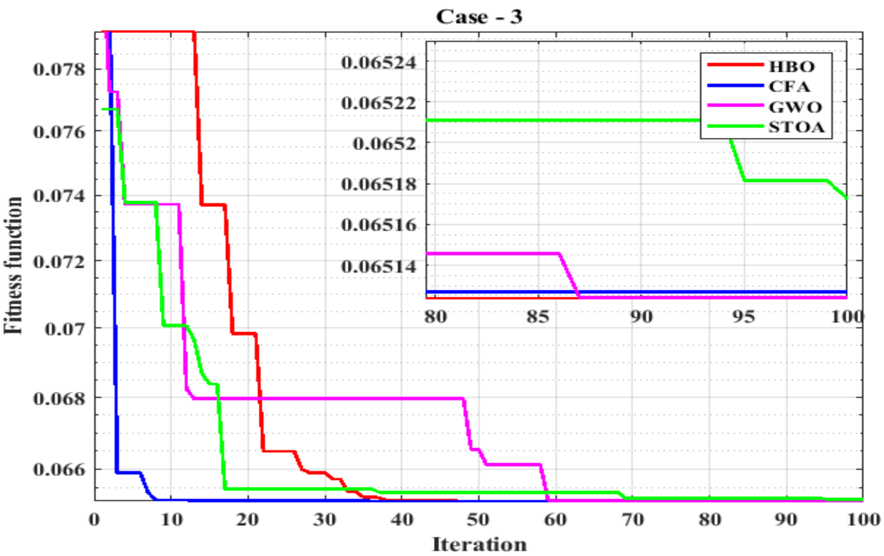
Case - 3
HBO
CFA
GWO
STOA
Fitness function
Iteration
0.078
0.076
0.074
0.072
0.07
0.068
0.066
0
10
20
30
40
50
60
70
80
90
100
0.06524
0.06522
0.0652
0.06518
0.06516
0.06514
80
85
90
95
100

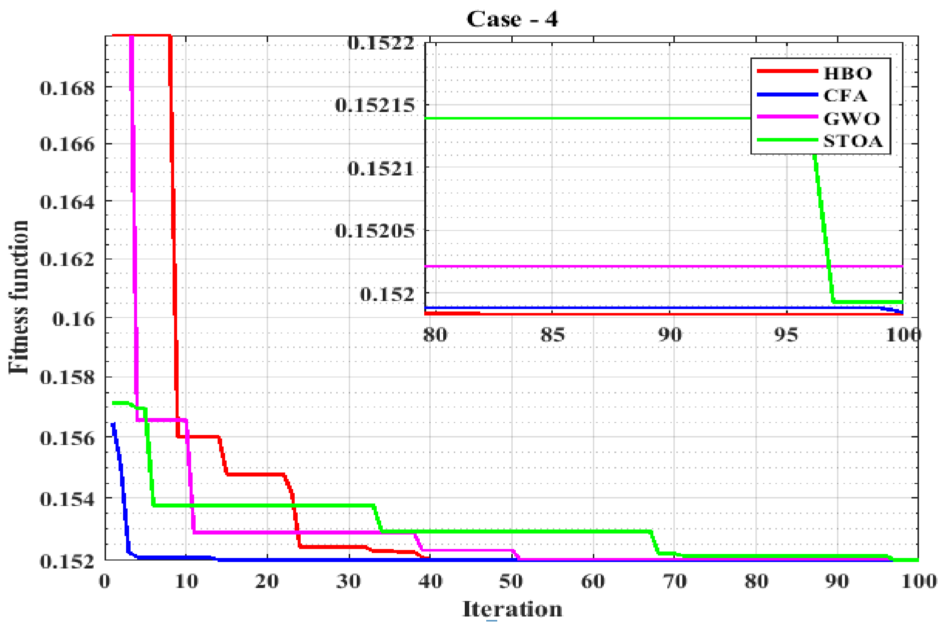

Figure 6. 27: The Convergence curves for 100 iterations using HBO, CFA, GWO, and STOA methods: case-1: PV/WT/Biomass/Battery system, case-2: PV/Biomass/Battery system, case-3: WT/Biomass/Battery system, case-4: PV/WT/Battery system.

Table 6.10, Table 6.11, Table 6.12, and Table 6.13, illustrate the results of the optimization properties for the four system scenarios proposed, which is based on many factors including the best value of the objective function, the decision variables (N_{PV}, N_{WT}, N_{BG} and N_{Bat}), the COE, LPSP, and NPC of the suggested optimization algorithms (HBO, CFA, GWO and STOA).

In Table 6.10, for the PV, WT, Biomass, and Bat system, the results indicate that the HBO has the best configuration by using 15 PV panels, 1 WTs, 2 biomass generators, and 400 batteries, achieving the least COE, and NPC with 0.121171$ /kWh and $ 3,559,143, respectively. In Table 6.11, for the second system case based on PV, Biomass, and Bat, the results prove that the HBO has the best configuration by using 17 PV panels, 2 biomass generators, and 447 batteries, achieving the least COE, and NPC with 0.1311804$ /kWh and $ 3,853,160, respectively.

While Table 6.12, for the WT, Biomass, and Bat system, the results prove that the STOA has the best configuration by using 1 WT, 2 biomass generators, and 375 batteries, achieving the least COE, and NPC with 0.1056732 $ /kWh and $ 3,103,938, respectively. In Table 6.13, for the fourth system case based on PV, WT, and Bat, the results illustrate that the STOA has the best configuration by using 170 PV panels, 88 WTs, and 983 batteries, achieving the least COE, and NPC with 0.3324975$ /kWh and $ 9,766,441, respectively.

Table 6. 10: The optimization properties for the proposed hybrid system based on using HBO, CFA, GWO and STOA for an isolated PV/WT/Biomass/Bat

	Best	It. Num.	N_{PV}	N_{WT}	N_{BG}	N_{Bat}	COE	LPSP	NPC
HBO	0.0643767	27	15	1	2	400	0.121171	0.026789	3,559,143
CFA	0.06437783	44	15	1	2	401	0.1213225	0.0267184	3,563,603
GWO	0.0643857	12	17	1	2	406	0.1236759	0.0262159	3,632,730
STOA	0.0644027	28	15	1	2	441	0.1291354	0.0096015	3,793,092

Table 6. 11: The optimization properties for the proposed hybrid system based on using HBO, CFA, GWO and STOA for an isolated PV/Biomass/Bat

	Best	It. Num.	N_{PV}	N_{BG}	N_B	COE	LPSP	NPC
HBO	0.0703404	49	17	2	447	0.1311804	0.0298557	3,853,160
CFA	0.07034462	32	17	2	447	0.1315446	0.0291707	3,863,857
GWO	0.07034495	28	16	2	450	0.1316478	0.0287446	3,866,887
STOA	0.0703484	40	21	2	468	0.1384959	0.0163783	4,068,036

Table 6. 12: The optimization properties for the proposed hybrid system based on using HBO, CFA, GWO and STOA for an isolated WT/Biomass/Bat

	Best	It. Num.	N_{WT}	N_{BG}	N_B	COE	LPSP	NPC
HBO	0.0651238467	41	1	2	413	0.11216872966	0.0300781042	3,294,729.69
CFA	0.0651240320	39	1	2	403	0.11097771588	0.0306442748	3,259,746.07
GWO	0.0651241750	87	1	2	412	0.11213661772	0.0301290735	3,293,786.47
STOA	0.0651252636	99	1	2	375	0.10567322935	0.0504315519	3,103,937.501

Table 6. 13: The optimization properties for the proposed hybrid system based on using HBO, CFA, GWO and STOA for an isolated PV/WT/Bat

	Best	It. Num.	N_{PV}	N_{WT}	N_B	COE	LPSP	NPC
HBO	0.1519917239	41	182	94	999	0.3471381051	0.05921588	10,196,480.121
CFA	0.1520017987	58	182	94	1000	0.3470716848	0.059466541	10,194,529.161
GWO	0.1543193268	51	181	98	996	0.3469565942	0.05992429	10,191,148.605
STOA	0.1530886015	97	170	88	983	0.3324974563	0.089288773	9,766,440.657

Parametric and non-parametric statistical measurements were performed for a more accurate comparison between the four optimization methods (HBO, CFA, GWO and STOA) on the basis of the acquired values of the objective function across a hundred individual runs for all analyzed cases. Parametric measurements comprise the lower value (Min.), maximum value (Max.) and mean of the target function, whereas the non-parametric measurements contain the median, RE, MAE, SD, and efficiency. The efficiency here referred to the ratio of the lower value to the mean value of the goal function. For all four system scenarios, the results for statistical metrics for HBO, CFA, GWO, and STOA are shown in Table 6.14. On the basis of the results obtained, the proposed HBO in each case showed the best results compared to other optimization methods.

Table 6. 14: The statistical performance of the studied optimization algorithms for the four system cases

	HBO	CFA	GWO	STOA
Case 1				
Max.	0.0644471	0.0644714	0.0648796	0.0657149
Min.	0.0643767	0.0643778	0.0643857	0.0644027
Mean	0.064386	0.064403	0.064513	0.064812
Median	0.064382	0.064401	0.064484	0.064838
SD	0.001476	0.002092	0.011667	0.032557
RE	0.007403	0.019536	0.099052	0.317511
MAE	0.0000095	0.000025	0.000128	0.000409
RMSE	0.000017	0.000033	0.000172	0.000521
Efficiency	99.9852	99.9609	99.8026	99.3714
Case 2				
Max.	0.0703979	0.0706643	0.0708796	0.0711048
Min.	0.0703404	0.0703446	0.07034495	0.0703484
Mean	0.070347	0.070368	0.070392	0.070722
Median	0.070344	0.070358	0.070368	0.070681
SD	0.001061	0.004539	0.008255	0.028633
RE	0.004321	0.016689	0.033444	0.265769
MAE	0.000006	0.000023	0.000047	0.000374
RMSE	0.000012	0.000051	0.000094	0.000469
Efficiency	99.9914	99.9667	99.9333	99.4729
Case 3				
Max.	0.0651243	0.06513126	0.0651819	0.06544516
Min.	0.065123847	0.065124032	0.06512418	0.06512526
Mean	0.065123988	0.065125588	0.06513273	0.06518123
Median	0.065123916	0.065125436	0.06512924	0.06516043
SD	0.000014838	0.000112835	0.00111241	0.00612358
RE	0.0001089	0.001194718	0.00657080	0.04296589
MAE	0.000000142	0.000001556	0.00000856	0.00005596
RMSE	0.000000204	0.000001915	0.00001395	0.00008250
Efficiency	99.9998	99.9976	99.9869	99.91423
Case 4				
Max.	0.151983478	0.15198479	0.1520216	0.151993102
Min.	0.151991724	0.152001799	0.154319327	0.153088601
Mean	0.151985107	0.151991986	0.152775666	0.152047201
Median	0.151984263	0.151991439	0.152656294	0.152014582
SD	0.000194530	0.000389174	0.057991385	0.015732186
RE	0.000535826	0.002367153	0.248002849	0.01779644
MAE	0.000001629	0.000007195	0.000754036	0.000054099
RMSE	0.000002522	0.000008162	0.000947705	0.000164869
Efficiency	99.99893	99.99527	99.50784	99.96452

Figure 6.28, illustrate the sensitivity analysis of studying the impact of the variation of the decision parameters on the stand-alone system objective functions, a) COE, b) NPC, c) LPSP, d) EXP. Where ``0" on the x-axis refers to the nominal values of the sensitivity factors.

Figure A) and B), illustrate the effect on the EC and the NPC. As it can be noted that, at lower values of the specified parameters, both EC and NPC drop when the number of each PV panels, biomass generators, and batteries decreased. While, at a higher parameter values, the EC and NPC raise with increasing the number of each PV panels, biomass generators, and batteries. For the number of WTs, it can be noted that both the EC and NPC are nearly constant with the variation of the WTs number. Figure C) and D), indicates that the chosen parameters has an effect on the system parameters, especially the number of the biomass generators.

Table 6.15, illustrate the yearly expenses breakdown of the hybrid system units and in turns show the system's NPC. The reader can notice that, for all suggested system cases the battery storage system has the highest yearly sharing of the capital cost compared to other system units. While the Biomass system has the highest operating and maintenance cost compared with other generating units in the suggested hybrid power system.

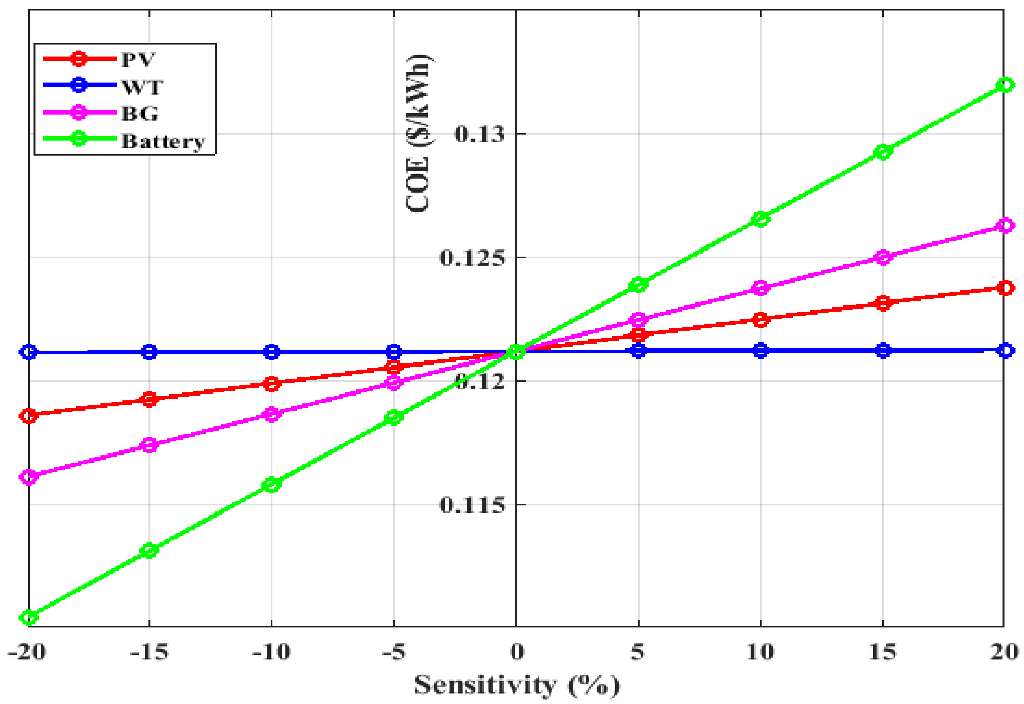

A) The influence of sizing change on the energy cost

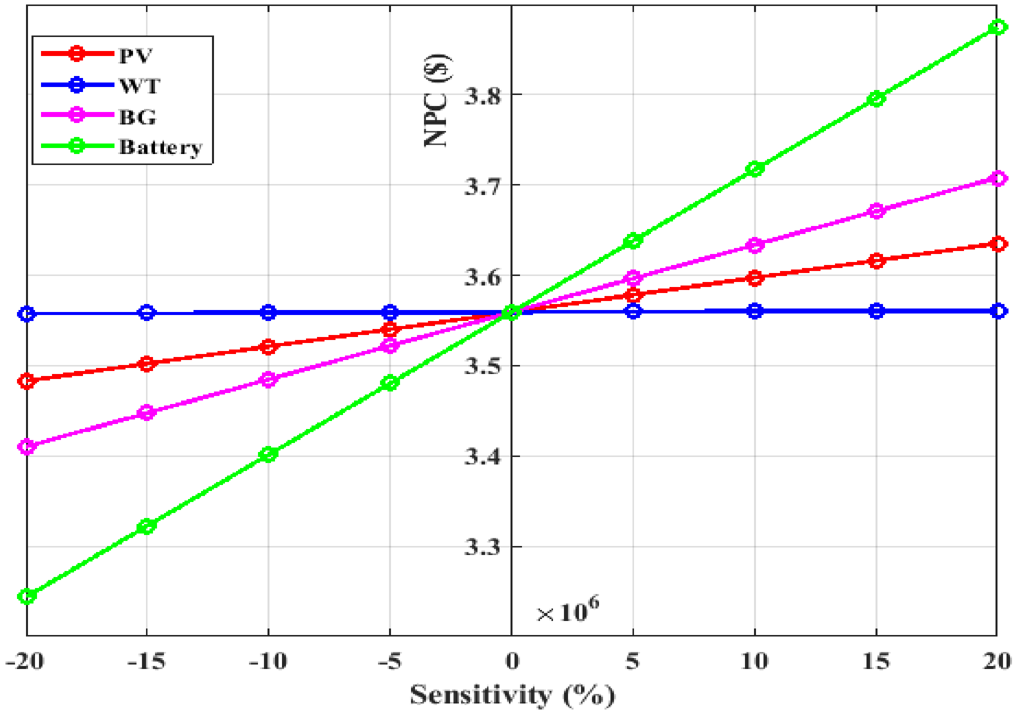

B) The influence of sizing change on the NPC

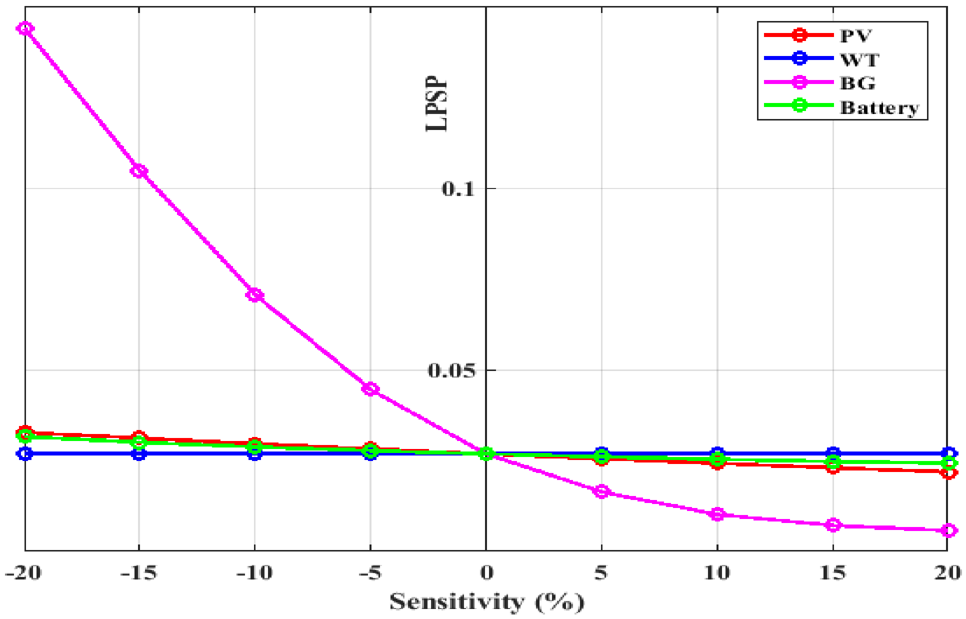

C) The influence of sizing variation on the LPSP

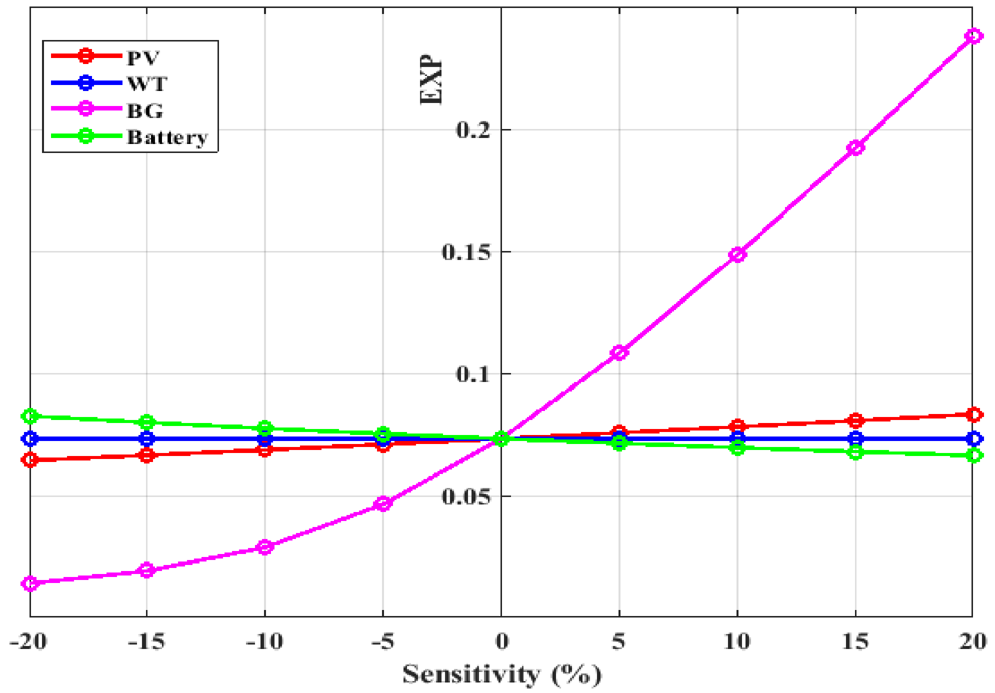

D) The influence of sizing variation on the an excess of energy

Figure 6. 28: Sensitivity analysis of studying the influence of sizing parameters variation on the stand-alone system variables, a) EC, b) NPC, c) LPSP, d) EXP

Table 6. 15: The contribution of the yearly cost of the system regarding the type of cost which includes the yearly interest of capital cost, operating and maintenance costs, and annual replacement cost

	PV			WT			Biomass			Battery			Inverter
	Cap ($)	**O&M ($)**	**Rep ($)**	**Cap ($)**	**O&M ($)**	**Rep ($)**	**Cap ($)**	**O&M ($)**	**Fuel ($)**	**Cap ($)**	**O&M ($)**	**Rep ($)**	**Cap ($)**
Case 1													
HBO	21881.639	168.965	11730.398	329.481	100	213.333	2359.588	19385.299	36345.833	122392.681	2016.223	39645.509	26676
CFA	21335.236	164.74584	11437.480	329.480	100	213.333	2333.178	19168.3297	35939.033	121501.132	2001.536	39645.510	26676
GWO	14779.440	114.123	7923.022	512.442	155.530	331.797	2432.913	19987.708	37475.301	135376.241	2230.106	39645.510	26676
STOA	17705.137	136.7150	9491.442	1011.176	306.899	654.719	2348.039	19290.416	36167.936	125554.249	2068.305	39645.510	26676
Case 2													
HBO	21436.	165.530	11491.98				2621.525	21537.259	40380.580	135236.988	2227.812	39645.510	26676
CF	21786.	168.23	11679.				2622.	21548.	40401.	135494	2232.	39645.	2667

A	985	4	655				910	632	905	.976	062	510	6
GW	21159.	163.39	11343.				2633.	21633.	40561.	136429	2247.	39645.	2667
O	690	0	373				295	953	875	.340	454	510	6
ST	26555.	205.05	14235.				2700.	22187.	41600.	142081	2340.	39645.	2667
OA	090	2	760				724	919	514	.934	572	510	6
Case 3													
HB				329.48	100	213.33	2579.	21189.	39729.	125210	2062.	39645.	2667
O				1		3	229	775	077		647	510	6
CF				329.48	100	213.33	2577.	21175.	39701.	122561	2019.	39645.	2667
A				0		3	439	068	502	.892	010	510	6
GW				329.48	100	213.33	2578.	21186.	39723.	125147	2061.	39645.	2667
O				0		3	854	690	293	.341	601	510	6
ST				341.76	103.7	221.28	2448.	20113.	37711.	113676	1872.	39645.	2667
OA				1	27	4	266	842	79	.027	630	510	6
Case 4													
HB	235285	1816.8	126132	30769.	9338.	19922.				303057	4992.	39645.	2667
O	.415	20	.763	429	761	690				.402	384	510	6
CF	235117	1815.5	126042	30739.	9329.	19903.				303219	4995.	39645.	2667
A	.876	26	.948	268	607	162				.603	056	510	6
GW	233972	1806.6	125428	32047.	9726.	20750.				302188	4978.	39645.	2667
O	.041	78	.684	435	645	177				.858	077	510	6
ST	219195	1692.5	117507	28791.	8738.	18641.				298195	4912.	39645.	2667
OA	.935	81	.449	202	353	821				.455	292	510	6

6.6. Hybrid PV/Biomass/Battery using Modified QRUN Algorithm

6.6.1. Performance of the proposed QRUN algorithm

The effectiveness and performance of the proposed QRUN algorithm are evaluated on several benchmark functions in this subsection, including the minimum values, mean values, maximum values, and SD for the solutions achieved by the QRUN algorithm, the conventional RUN technique and the three well-known optimization techniques, including the AO algorithm [196], HBA [197], and TSO algorithm [198]. The results of the suggested QRUN technique is compared with these recent optimization techniques. These algorithms have been performed for the maximum number of iterations is 500 and the population size is 50 for 20 independent runs using Matlab R2016a. All simulations have been executed on a laptop including Core i5-4210U CPU@ 2.40 GHz of speed, and 8 GB of RAM. The Qualitative metrics using the proposed QRUN technique for nine benchmark functions including 2D views of the functions, search history, average fitness history, and convergence curve are illustrated in Figure 6.29.

6. RESULTS AND DISCUSSION

F1

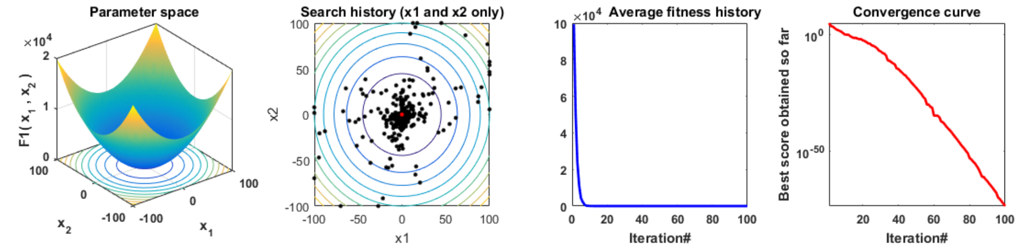

F3

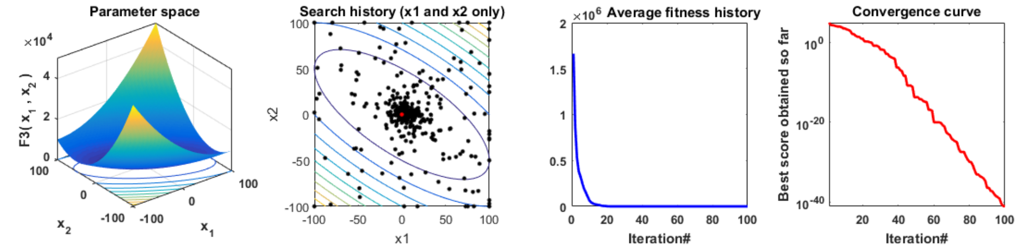

F4

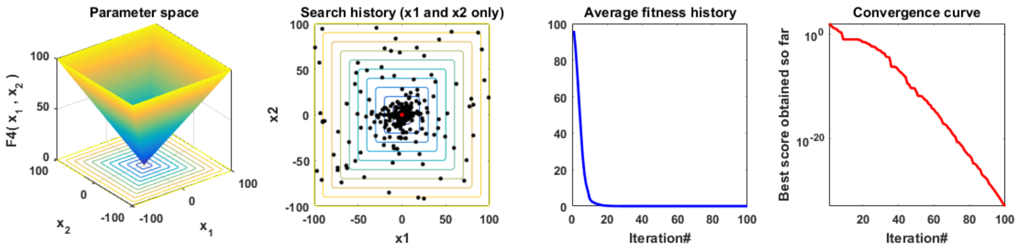

F5

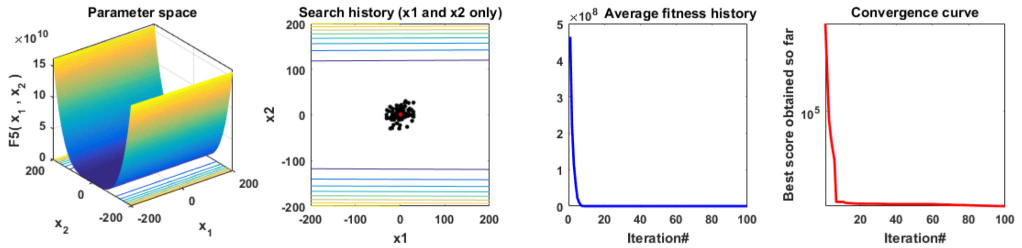

F8

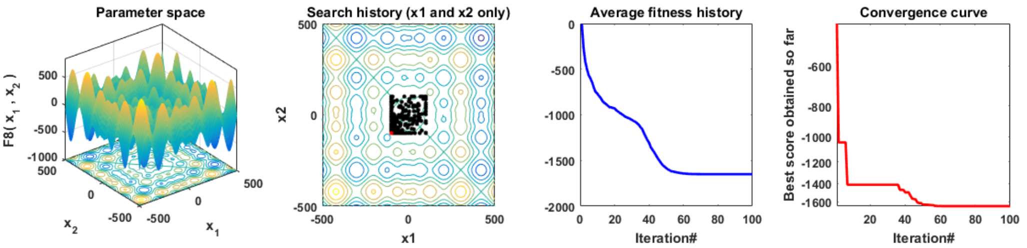

F12

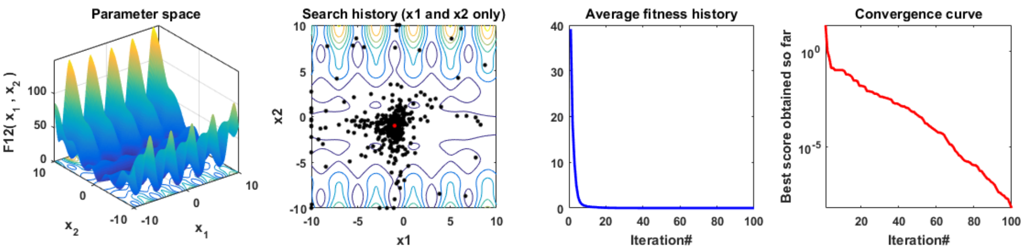

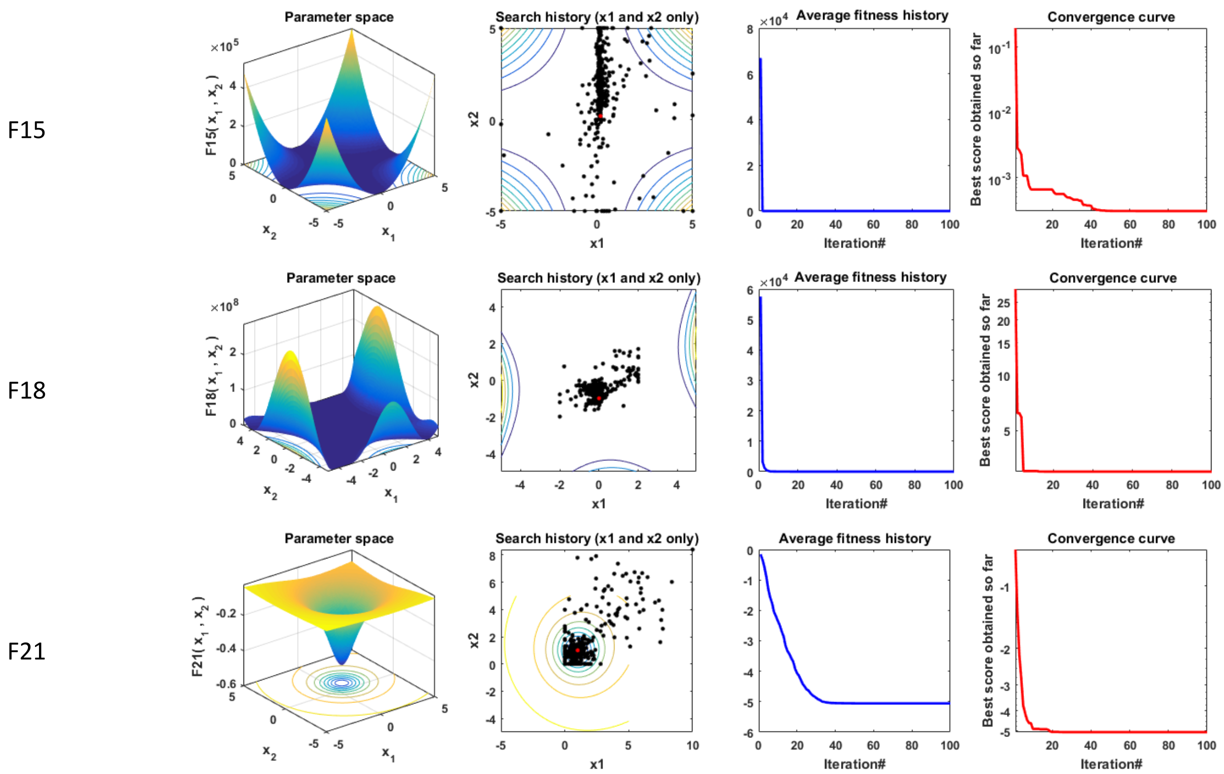

Figure 6. 29: Qualitative metrics of nine benchmark functions: 2D views of the functions, search history, average fitness history, and convergence curve using QRUN technique.

The statistical results of the proposed QRUN technique and other recent algorithms when applied for unimodal benchmark functions, multimodal benchmark functions, and composite benchmark functions are tabulated in Tables 6.16, 6.17, and 6.18, respectively. The best values were obtained with the proposed QRUN, RUN, AO, HBA, and TSO techniques shown in bold. It is clearly seen that the proposed QRUN technique reaches to the optimal solution for several benchmark functions. Figure 6.30, presents the convergence curves of all algorithms for the first type of these function (unimodal benchmark) while Figure 6.31, displays the Boxplots for these algorithms for this type of functions. Also, the convergence curves of these approaches for the multimodal benchmark functions are illustrated in Figure 6.32, while the Boxplots for each technique for these functions are presented in Figure 6.33. Finally, Figure 6.34 shows all of the techniques' convergence curves for the composite benchmark functions while Figure 6.35, presents the Boxplots for all algorithms for this type of benchmark functions. From those figures, it can be noted that the recommended QRUN algorithm achieves a constant location for all functions and the boxplots of the suggested algorithm are relatively limited for most functions compared to the other recent algorithms.

Table 6. 16: The statistical Results of unimodal benchmark functions using the proposed QRUN technique and other recent techniques.

Function		QRUN	RUN	AO	HBA	TSO
F1	Best	**2.1E-147**	9.07E-86	7.15E-76	1.78E-61	6.12E-63
	Worst	**1.1E-141**	1E-75	4.17E-57	7.11E-57	4.97E-39
	Mean	**6.8E-143**	5.02E-77	2.09E-58	4.31E-58	2.5E-40
	std	**2.5E-142**	2.24E-76	9.33E-58	1.58E-57	1.11E-39
F2	Best	**7.07E-79**	1.04E-47	1.3E-36	4.11E-33	5.22E-35
	Worst	**3.13E-76**	2.3E-42	9.5E-32	1.23E-30	1.03E-19
	Mean	**4.62E-77**	1.87E-43	1.37E-32	1.9E-31	6.11E-21
	std	**8.13E-77**	5.35E-43	3.28E-32	3.19E-31	2.32E-20
F3	Best	**1.57E-78**	5.75E-77	3.39E-71	6.41E-48	6.55E-51
	Worst	**4.58E-67**	4.54E-61	1.58E-62	2.94E-39	2.78E-18
	Mean	**2.48E-68**	2.33E-62	1.28E-63	2.6E-40	1.4E-19
	std	**1.02E-67**	1.01E-61	3.7E-63	7.23E-40	6.22E-19
F4	Best	**3.92E-66**	1.35E-42	8.91E-40	1.01E-26	8.91E-36
	Worst	**2.93E-63**	4.16E-34	1.67E-31	2.59E-23	1.18E-23
	Mean	**3.43E-64**	2.09E-35	1.26E-32	1.84E-24	6.88E-25
	std	**6.72E-64**	9.3E-35	4.05E-32	5.79E-24	2.63E-24
F5	Best	**23.12299**	23.34961	24.13219	24.45441	23.78264
	Worst	**26.04562**	26.52757	29.26575	28.73684	29.26575
	Mean	**24.4467**	24.73586	26.85075	26.34739	28.01758
	std	**0.782291**	0.832917	1.924605	1.35166	1.797863
F6	Best	**4.5E-09**	7.23E-09	1.61E-08	0.00285	3.29E-06
	Worst	**1.71E-08**	2.24E-08	0.000556	0.997439	0.0215
	Mean	**1.11E-08**	1.19E-08	0.000145	0.315209	0.002346
	std	**2.92E-09**	3.7E-09	0.000182	0.289771	0.004807
F7	Best	1.9E-05	3.74E-05	6.04E-06	3.52E-05	**9.22E-06**
	Worst	**0.000396**	0.000865	0.000818	0.001023	0.000665
	Mean	**0.000153**	0.00042	0.00021	0.000436	0.000265
	std	**0.000117**	0.000268	0.000197	0.000261	0.000234

The best values obtained are in bold.

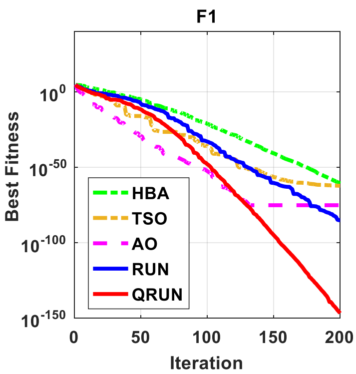

(a) F1

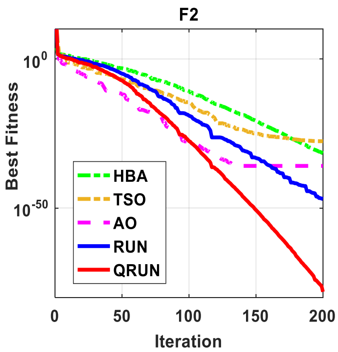

(b) F2

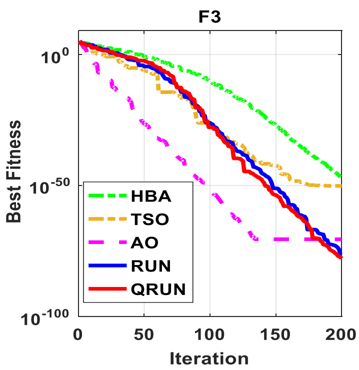

(c) F3

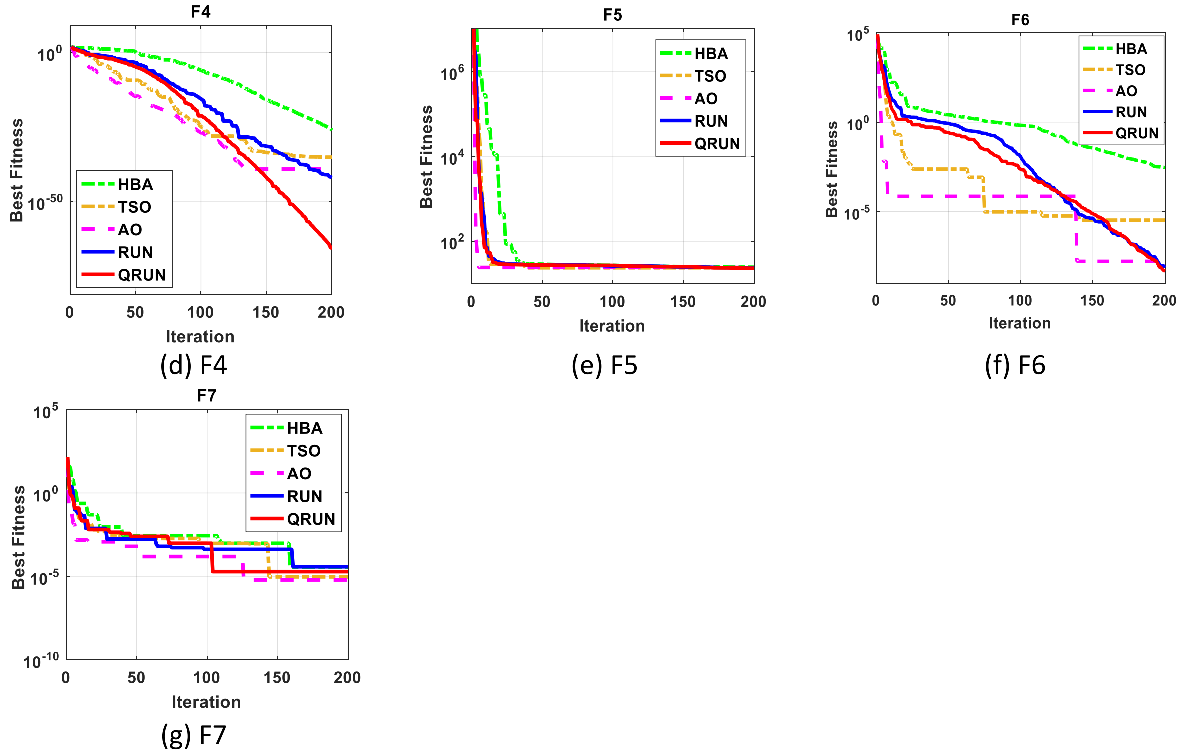

Figure 6. 30: The convergence curves of all algorithms for seven unimodal benchmark functions.

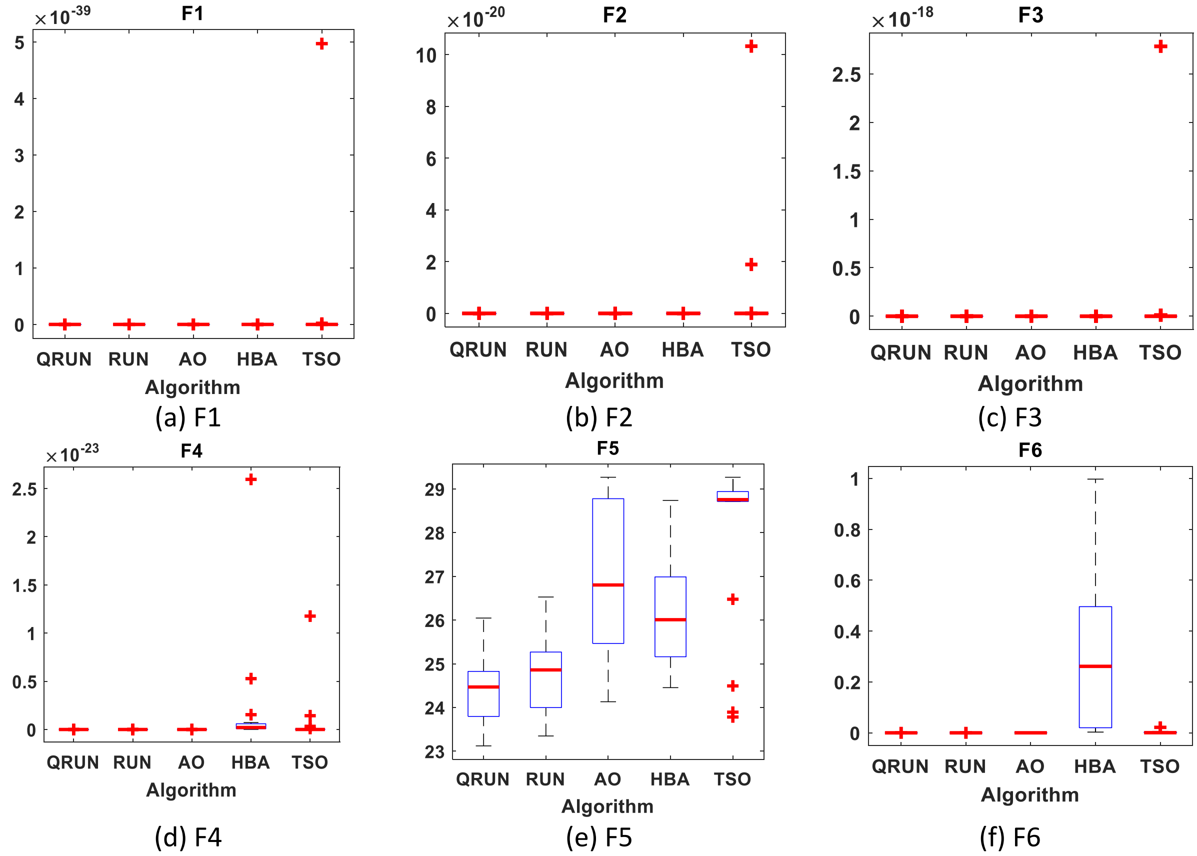

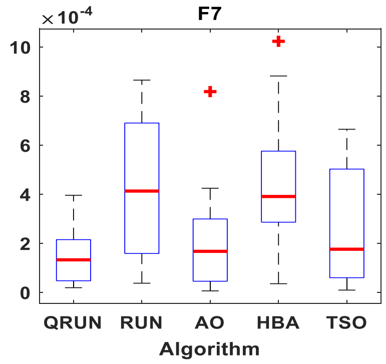

(g) F7

Figure 6. 31: Boxplots for all methods for seven unimodal benchmark functions.

Table 6. 17: The statistical Results of multimodal benchmark functions using the proposed technique and other recent algorithms.

Function		QRUN	RUN	AO	HBA	TSO
F8	Best	-1696.47	-1660.17	-1901.64	-1785.77	**-1909.05**
	Worst	-1418.48	-1397.78	-718.461	-870.434	**-1909.04**
	Mean	-1585.11	-1580.75	-1061.31	-1463.33	**-1909.05**
	std	78.70104	78.84949	353.9877	257.6176	**0.002483**
F9	Best	**0**	**0**	**0**	**0**	**0**
	Worst	**0**	**0**	**0**	**0**	**0**
	Mean	**0**	**0**	**0**	**0**	**0**
	std	**0**	**0**	**0**	**0**	**0**
F10	Best	**8.88E-16**	**8.88E-16**	**8.88E-16**	3.88E-13	**8.88E-16**
	Worst	**8.88E-16**	**8.88E-16**	**8.88E-16**	20	**8.88E-16**
	Mean	**8.88E-16**	**8.88E-16**	**8.88E-16**	17.99989	**8.88E-16**
	std	**0**	**0**	**0**	6.155818	**0**
F11	Best	**0**	**0**	**0**	**0**	**0**
	Worst	**0**	**0**	**0**	**0**	**0**
	Mean	**0**	**0**	**0**	**0**	**0**
	std	**0**	**0**	**0**	**0**	**0**
F12	Best	3.57E-09	2.99E-09	**1.05E-10**	3.74E-05	5.33E-08
	Worst	**1.45E-08**	1.57E-08	5.46E-06	0.012809	0.000181
	Mean	7.71E-09	**6.93E-09**	6.23E-07	0.004038	2.84E-05
	std	**2.49E-09**	3.43E-09	1.2E-06	0.004263	4.6E-05
F13	Best	**3.04E-08**	4.07E-08	1.82E-07	0.388465	1.72E-05
	Worst	0.043949	0.021025	**0.000479**	1.37095	0.013883
	Mean	0.004944	0.00805	**7.63E-05**	0.84146	0.001934
	std	0.010378	0.008325	**0.000126**	0.298394	0.003327

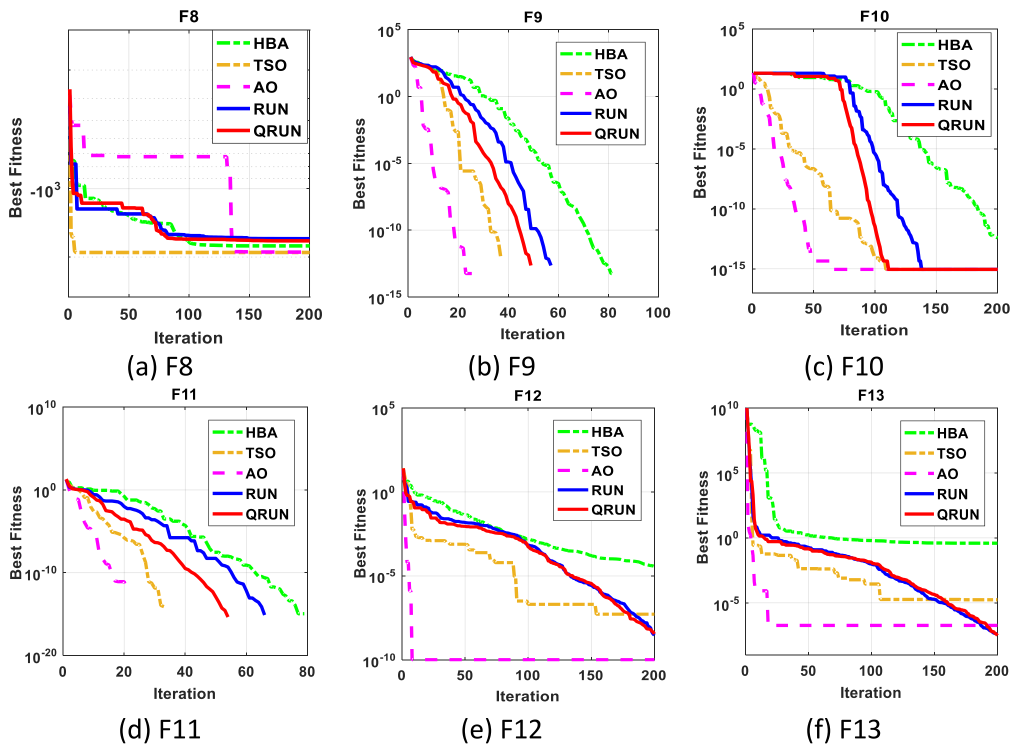

Figure 6. 32: The convergence curves of all algorithms for six multi-modal benchmark functions.

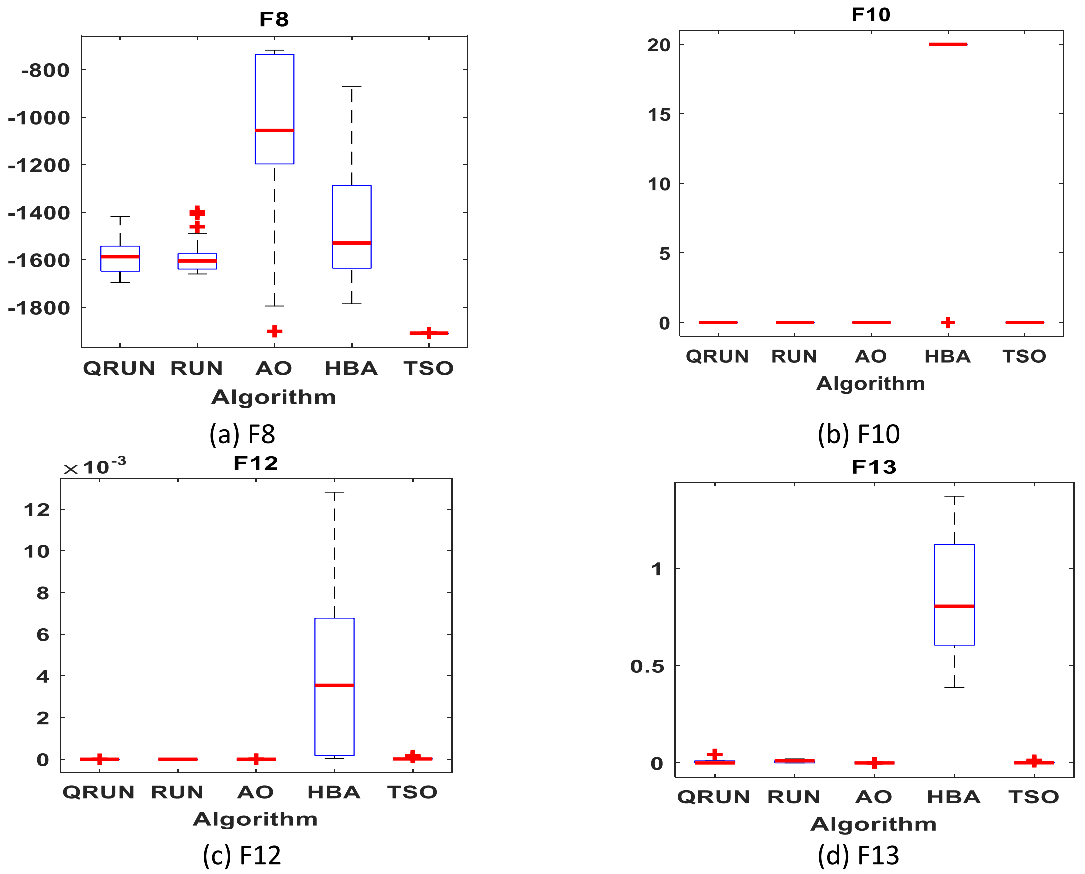

Figure 6. 33: Boxplots for all algorithms for some of multi-modal benchmark functions (a) F8, (b) F10, (c) F12 and (d) F13.

Table 6. 18: The statistical Results of composite benchmark functions using the proposed technique and other well-known algorithms.

Function		QRUN	RUN	AO	HBA	TSO
F14	Best	**0.998004**	**0.998004**	**0.998004**	**0.998004**	**0.998004**
	Worst	10.76318	10.76318	12.67051	10.76318	**2.982105**
	Mean	2.230795	2.081493	2.573682	1.585468	**1.196414**
	std	2.171429	2.241941	2.574285	2.205174	**0.610693**
F15	Best	**0.000307**	**0.000307**	0.000325	**0.000307**	0.000336
	Worst	**0.000307**	0.001223	0.001155	0.022553	0.002252
	Mean	**0.000307**	0.00072	0.00053	0.002592	0.00051
	std	**4.05E-11**	0.000467	0.00018	0.006475	0.00043
F16	Best	**-1.03163**	**-1.03163**	**-1.03163**	**-1.03163**	**-1.03163**
	Worst	**-1.03163**	**-1.03163**	-1.02995	**-1.03163**	-1.0315
	Mean	**-1.03163**	**-1.03163**	-1.03104	**-1.03163**	-1.03161
	std	6.67E-13	8.13E-12	0.000547	**1.61E-16**	3.37E-05
F17	Best	**0.397887**	**0.397887**	**0.397893**	**0.397887**	0.39789
	Worst	**0.397887**	**0.397887**	0.399082	**0.397887**	0.398203
	Mean	**0.397887**	**0.397887**	0.398149	**0.397887**	0.397935
	std	1.13E-11	4.27E-12	0.000274	**0**	7.37E-05
F18	Best	**3**	**3**	3.00648	**3**	3.000001
	Worst	**3**	**3**	3.100674	**3**	32.39249
	Mean	**3**	**3**	3.042457	**3**	4.469787
	std	1.36E-12	5.41E-13	0.02737	**1.72E-14**	6.572323
F19	Best	**-0.30048**	**-0.30048**	**-0.30048**	**-0.30048**	**-0.30048**
	Worst	**-0.30048**	**-0.30048**	**-0.30048**	**-0.30048**	**-0.30048**
	Mean	**-0.30048**	**-0.30048**	**-0.30048**	**-0.30048**	**-0.30048**
	std	**1.14E-16**	**1.14E-16**	**1.14E-16**	**1.14E-16**	**1.14E-16**
F20	Best	**-3.322**	**-3.322**	-3.2947	**-3.322**	-3.06193
	Worst	**-3.2031**	-3.20309	-2.67041	-0.11825	-1.14308
	Mean	**-3.30416**	-3.28038	-3.1067	-2.49398	-2.25316
	std	**0.043556**	0.058183	0.143442	1.00449	0.567183
F21	Best	**-10.1532**	**-10.1532**	-10.1527	**-10.1532**	**-10.1532**
	Worst	-5.0552	-5.0552	-10.1019	**-10.1532**	-10.0957
	Mean	-8.114	-8.3689	-10.1365	**-10.1532**	-10.1451
	std	2.562382	2.494761	0.016429	**9.01E-14**	0.013884
F22	Best	**-10.4029**	**-10.4029**	-10.4028	**-10.4029**	**-10.4029**
	Worst	-5.08767	-5.08767	-10.3216	-2.7659	**-10.3892**
	Mean	-8.5426	-9.07412	-10.3889	-8.97137	**-10.3996**
	std	2.601082	2.36137	0.019955	2.945733	**0.004207**
F23	Best	**-10.5364**	**-10.5364**	-10.5362	-10.5364	-10.5363
	Worst	-5.12848	-5.12848	**-10.4701**	-1.85948	-10.4096
	Mean	-8.37324	-9.18443	**-10.5212**	-8.21554	-10.519
	std	2.718159	2.402536	**0.019921**	3.662183	0.030992

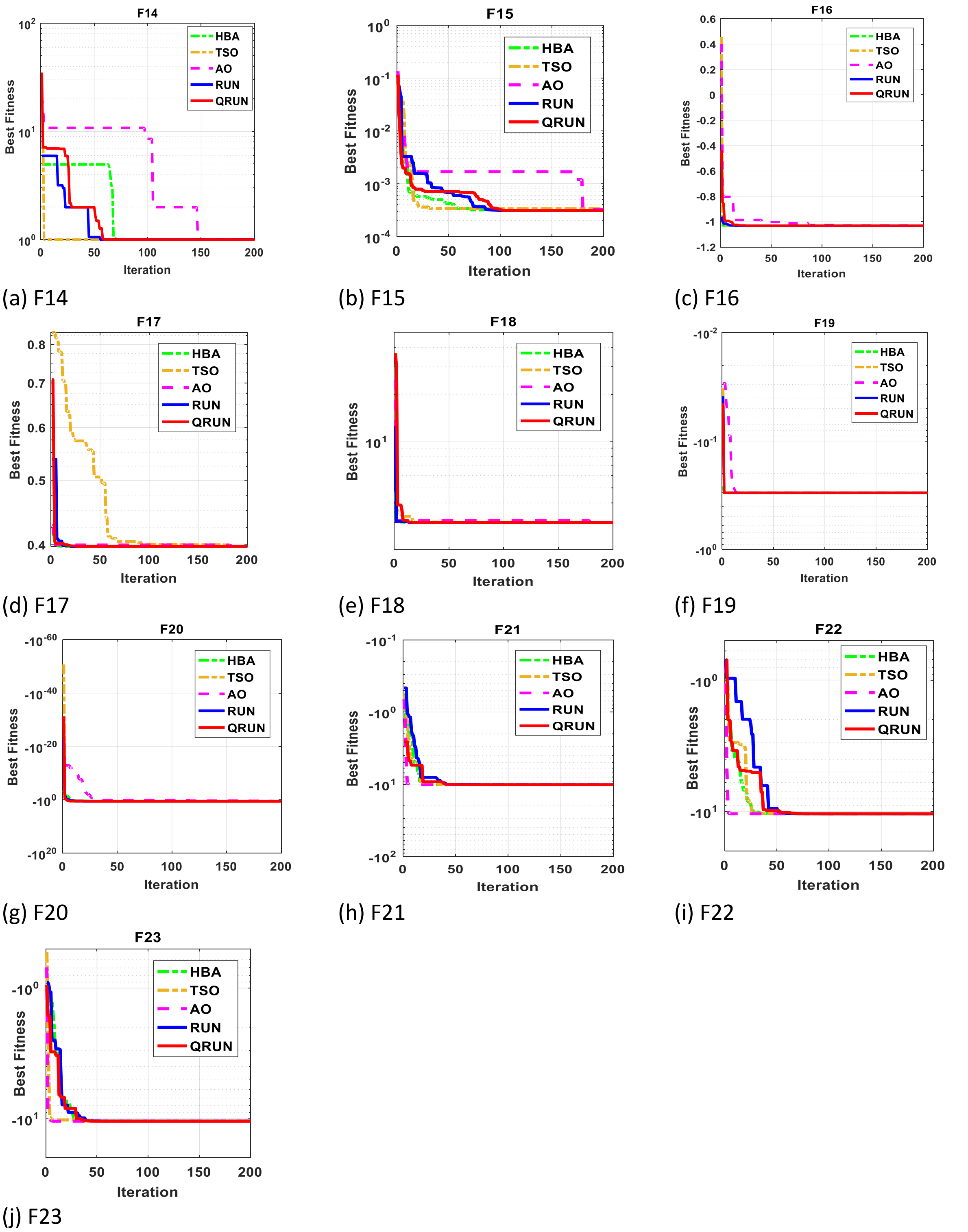

Figure 6. 34: The convergence curves of all algorithms for composite benchmark functions (a) F14, (b) F15, (c) F16, (d) F17, (e) F18, (f) F19, (g) F20, (h) F21, (i) F22, and (j)F23.

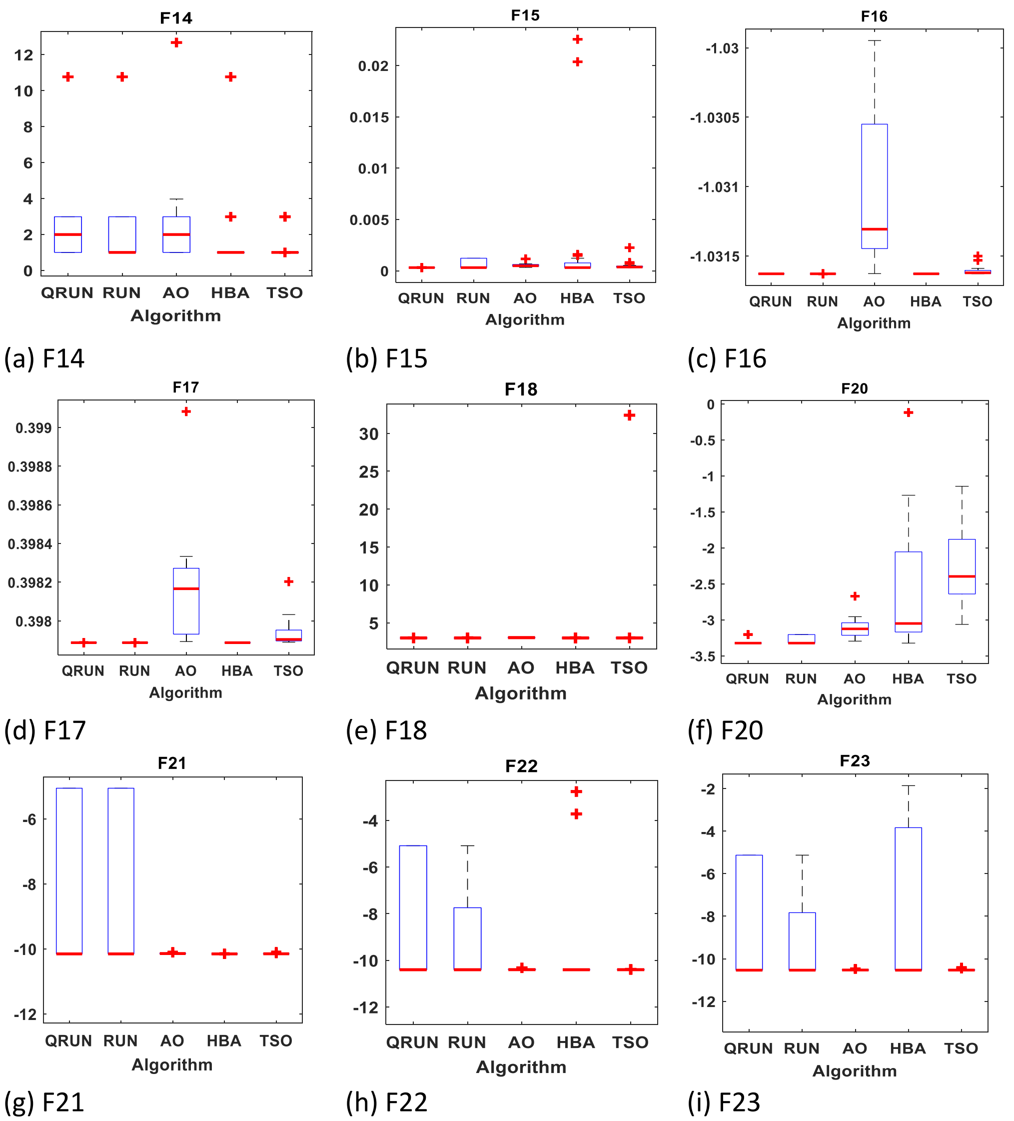

Figure 6. 35: Boxplots for all algorithms for some of composite benchmark functions (a) F14, (b) F15, (c) F16, (d) F17, (e) F18, (f) F20, (g) F21, (h) F22, and (i)F23.

6.6.2. Real-world application

A Quantum model of a RUNge Kutta optimization algorithm called QRUN algorithm is applied for modeling the optimal sizing of the suggested isolated hybrid system which consists of PV panels, BG, and Batteries units. The results of the suggested modification QRUN technique are compared to the original RUN algorithm and a well-known AO and GWO methods to confirm the proposed developed QRUN's superiority in obtaining the maximum reliability and minimum cost. The suggested optimization methods were ran using the Matlab software, with a total of 100 iteration with 50 times run to determine the appropriate fitness function value in order to control the suggested algorithms' randomness and ensure their stability and robustness.

Table 6.19, summarizes the results of the HRPS's optimal sizing characteristics for the case study concerning the PV, BG, and battery bank. The table contained the established constraints ($\mathbf{N_{PV}}$, $\mathbf{N_G}$, $\mathbf{N_B}$), the best fitness function, the best iteration number, EC, NPC and LPSP for all suggested algorithms QRUN, RUN, AO, and GWO. As may be observed from this table, the modified QRUN algorithm has the best objective function with 0.070339764 followed by RUN, GWO and AO methods with 0.070339794, 0.070345472 and 0.070354906 respectively. When analyzing the obtained results in the table, it can be seen that the QRUN technique has the lowest EC with 0.080076 \$/kWh, the lowest NPC with \$ 3,352,062, and the maximum LPSP value with 0.490866, compared to the other algorithms used, followed by the RUN, GWO and AO techniques.

Table 6. 19: The Optimization Parameters for the Proposed HRPS Based on Using QRUN, RUN, AO and GWO Algorithms

	QRUN	RUN	GWO	AO
Best Fitness Function	0.070339764	0.070339794	0.070345472	0.070354906
EC	0.080076	0.122828	0.131071	0.1321219
Iteration Number	13	25	32	11
$\mathbf{N_{PV}}$	16	17	16	17
$\mathbf{N_G}$	2	2	2	2
$\mathbf{N_B}$	446	446	447	450
NPC	3,352,062	3,607,838	3,849,937	3,880,817
LPSP	0.490866	0.032773	0.029405	0.0282405

Based on the results from Table 6.18, the outcomes of using the QRUN and RUN techniques for the proposed HRPS problem are the more optimal compared to the GWO and AO approaches. The convergence curves of QRUN and original RUN optimization methods are shown in Figure 6.36. Where, all proposed optimization approaches were used with the same modes to apply them to the proposed isolated system. The modification QRUN algorithm's numerical results of the fitness function are determined to be within a limited set, proving QRUN's reliability in finding the optimal sizing to the optimization problem compared with the original RUN method.

Figure 6.37, reveals the convergence curve for the best function using QRUN and RUN algorithms for 100 iterations, where QRUN demonstrated its superiority over the original RUN algorithm in achieving the optimal solution.

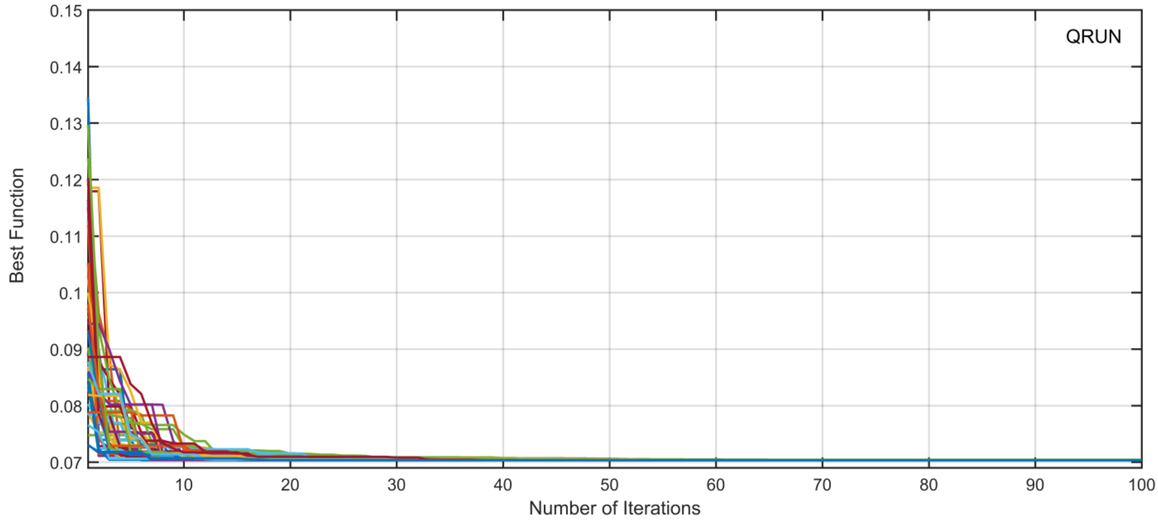

QRUN

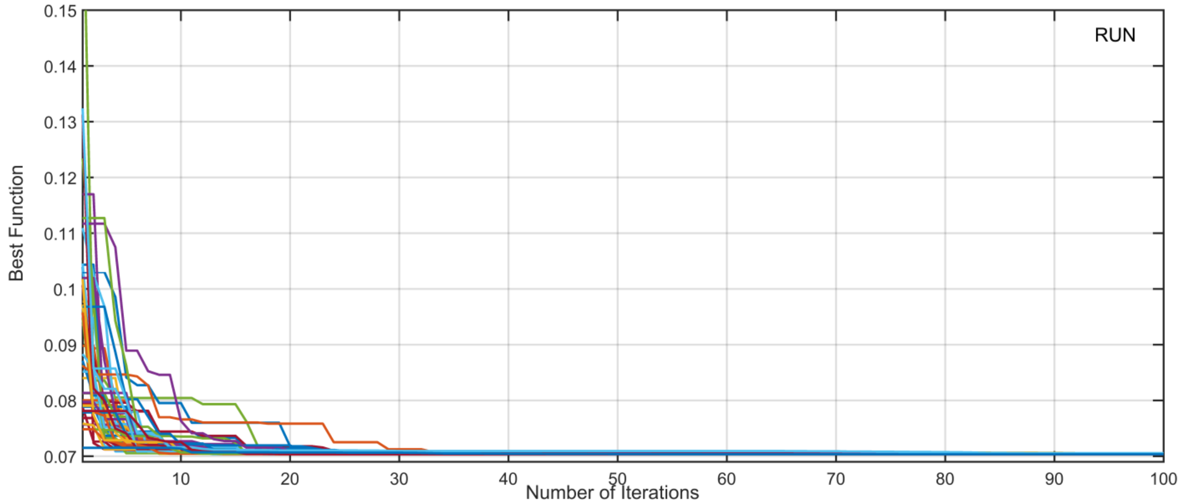

RUN

Figure 6. 36: The Convergence Curve of QRUN and RUN for 100 iteration 50 time run

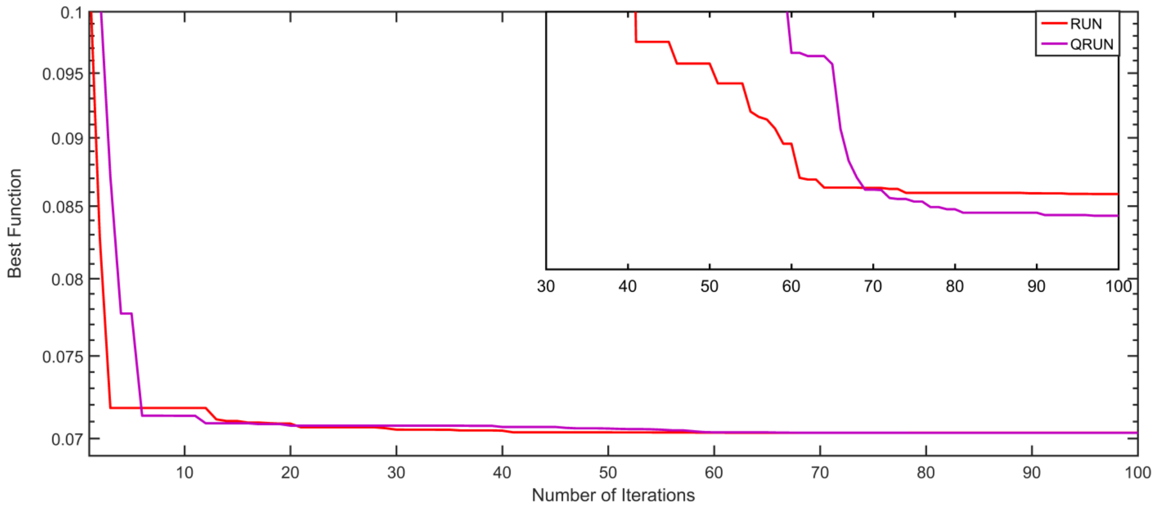

Figure 6. 37: The Convergence Curve for the Best Function Using QRUN and RUN for 100 Iterations

Figure 6.38, depicts the impact of each component used in the suggested isolated system on the yearly cost by using the QRUN and RUN algorithms. As shown, the battery bank units represent the greatest yearly percentage cost for the QRUN approach, accounting for 34% of the overall cost of the proposed system, followed by inverter units with 32%, BG with 16%, the fuel with 10%, and lastly the PV panels with 8%. For the RUN algorithm, the battery units represent also the highest annual percentage of the system cost with 37%, followed by the inverter units with 21%, BG with 20%, the fuel with 12%, and lastly the PV panels with 10%. From this obtained results, it can be indicated that the annual percentage cost of battery units shows the highest cost among all units.

Figure 6.39, indicates the power variation of the renewable sources units for 8760 hours using QRUN algorithm, where the power generated over the year from the PV and BG are indicated. During the night and early hours of the morning, the energy produced by the solar panels is minimal, which requires the operation of the BG and batteries at a high capacity. As the sun rises, the energy generated from the PV is gradually increasing, but all renewable energy sources are still working in tandem to meet the energy demand. When the energy generated from the hybrid sources is greater than the load demand, this additional energy is used to charge the batteries as the battery begins to charge until it reaches its maximum allowable capacity. Furthermore, when the battery is fully charged, as shown by the battery's SOC, the surplus power is consumed in the dummy load. After sunset, the biomass system continues to operate while the battery begins to discharge its energy until it reaches SOC_{min}.

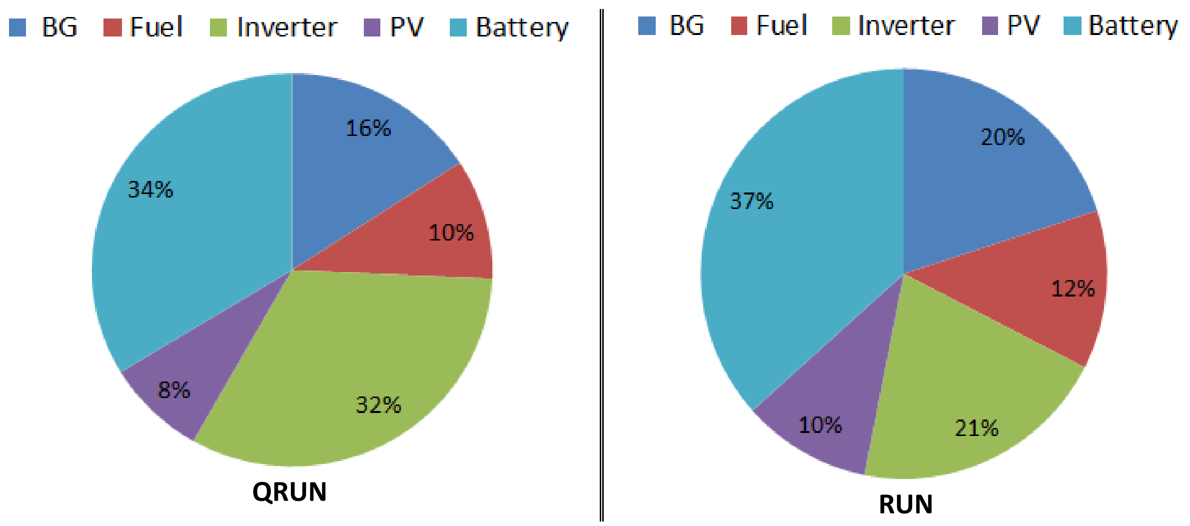

Figure 6. 38: The Breakdown of the Yearly Cost of the Hybrid System Components

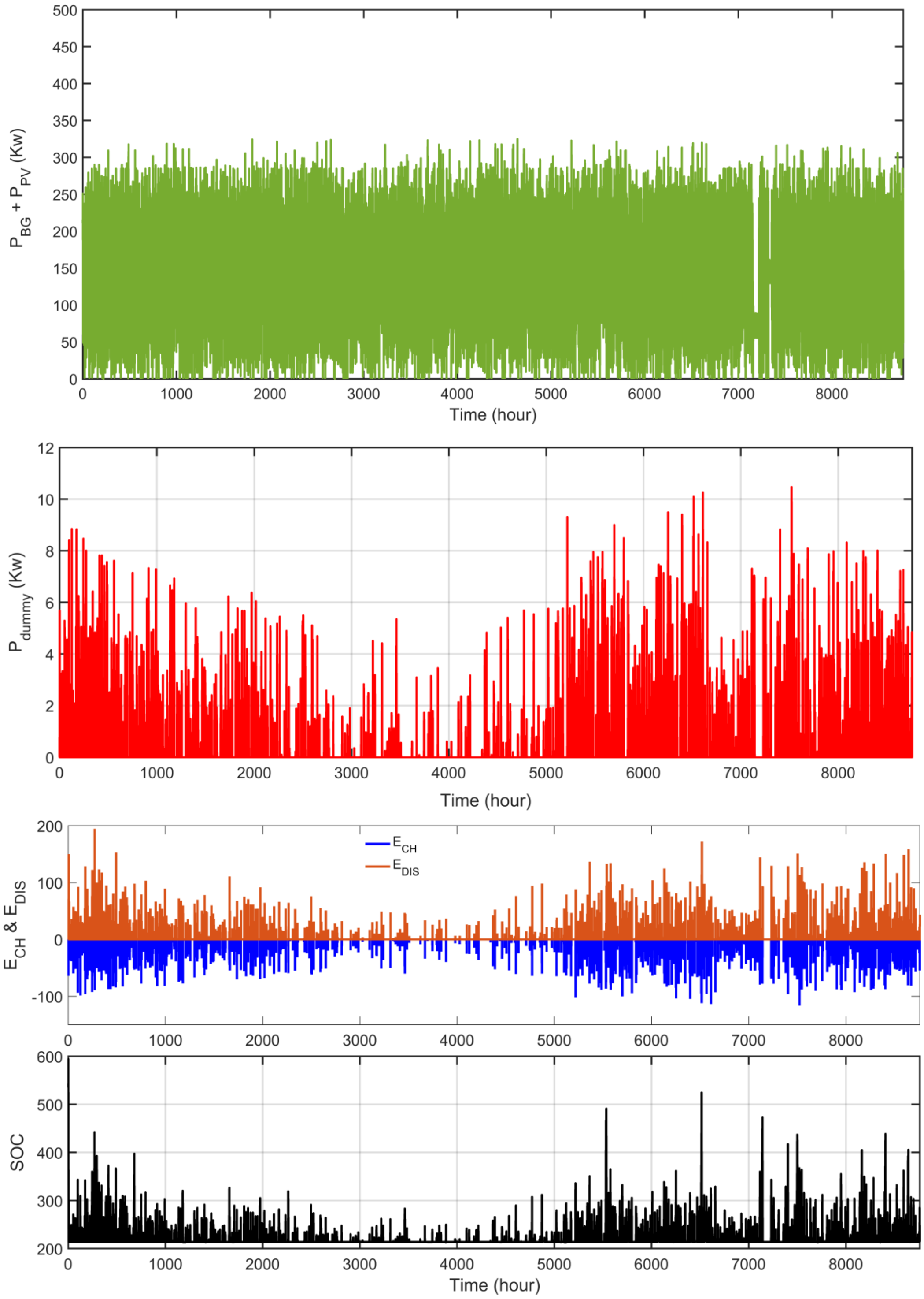

Figure 6. 39: The power variation of the renewable sources for 8760 hours using QRUN algorithm

Table 6.20, provides the statistical performance metrics for each optimization algorithm used. On the basis of the acquired values of the objective function throughout 100 iterations with 50 individual runs for the proposed HRPS, parametric and non-parametric statistical measurements were done for a more accurate comparison of the three optimization techniques, namely QRUN, RUN, GWO, and AO. The lower value (Min.), maximum value (Max.), and mean of the target function (Mean) are parametric measurements, whereas the median, SD, RE, MAE, and efficiency are non-parametric metrics. Based on the results obtained, the proposed QRUN achieved the best values when compared to other optimization approaches.

Table 6. 20: The Statistical Performance of the Studied Optimization Algorithms

	QRUN	RUN	GWO	AO
Max.	0.070475737	0.070565957	0.070767194	0.077441507
Min.	0.070339764	0.0703397936	0.0703454722	0.070354906
Mean	0.0703525	0.0703736	0.0703910	0.071349834
Median	0.0703439	0.0703579	0.0703652	0.070718303
SD	0.0021210	0.0045269	0.0070266	0.15488957
RE	0.0088083	0.0239945	0.0323742	0.70707809
MAE	0.0000124	0.0000338	0.0000456	0.00099493
RMSE	0.0000244	0.0000561	0.0000831	0.00182783
Efficiency	99.982395	99.952075	99.935391	98.6490

6.7. Hybrid PV/WT/Biomass/Battery using Novel Hybrid GAHA Algorithm

The novelty of this system is characterized by presenting an enhanced gradient algorithm based on a bio-inspired optimization approach called AHA. The suggested method is known as GAHA. The GBO is one of the most recent algorithms, which was developed to solve several problems such as cost-effective emission dispatch [199], effective coordination settings for directional overcurrent relay[200], predicting the COVID-19 pandemic [201], parameter estimation of photovoltaic models [202], [203], PEMFC parameter identification [186], multi-reservoir hydropower systems optimization [204]. The LEO is the most effective part in the GBO algorithm which enhancing the ability of algorithm to find a new region and achieve the optimal solution [185]. In [205], the LEO was used to enhances the balance between exploration and exploitation capabilities of the Marine Predators Algorithm (MPA), handles premature convergence, and leads to the significant improvement of the optimization performance. In this study, the LEO is used to improve the local search capability in the AHA. To verify the effectiveness of the proposed improved algorithm GAHA, it was used to find the optimal solution for different configurations of an isolated hybrid system of PV/WT/biomass/batteries modules. Well-known algorithms are utilized in the comparison of the findings to validate the efficacy of the suggested GAHA technique, namely the original AHA, SCA, and WOA methods, these optimization methods are chosen because of their impressive effectiveness in solving various mathematics and engineering design issues. GAHA demonstrated its potential for handling the proposed problems compared to the results of other known techniques. The aim and contribution of this work are to theoretically describe a novel modified algorithm GAHA for the optimization of hybrid renewable energy systems. The algorithm is tested in several problem instances and its efficiency is compared with existing algorithms. It is also applied to a real-life isolated hybrid system-sizing problem; the major contributions of the proposed work can be summarized as follows:

- An enhanced hybrid algorithm called GAHA based on the combination between a bio-inspired AHA and GBO methods;
- Test the performance of the suggested GAHA on several benchmark functions;
- The GAHA algorithm is applied for optimal design for different configurations of a hybrid PV/WT/biomass/battery system for supplying a load in the new Tiba city, north-east of Luxor city in Egypt;
- The proposed GAHA algorithm is applied for resolving the multi-objective optimization issue of minimizing the EC, the LPSP, and excess energy under the constraints.
- Results of the gradient algorithm are compared to the original AHA, SCA, and WOA methods.

6.7.1. The Performance of GAHA

The proposed GAHA algorithm ability and efficiency are checked on the numerous benchmark functions, using the statistical measurement including the best values, mean values, median values, worst values, and SD for optimal solutions achieved using the GAHA technique and the other recent optimization methods. The findings obtained with the developed GAHA algorithm are compared with five recent techniques such as, SDO algorithm [206], WHO [207], GWO [192], TSA [208], and the conventional AHA approach. The Qualitative metrics on F1, F2, F3, F5, F6, F8, F10, F12, F15, F18, and F22: 2D views of the functions, convergence curve, average fitness history, and search history are presented in Figure 6.40.

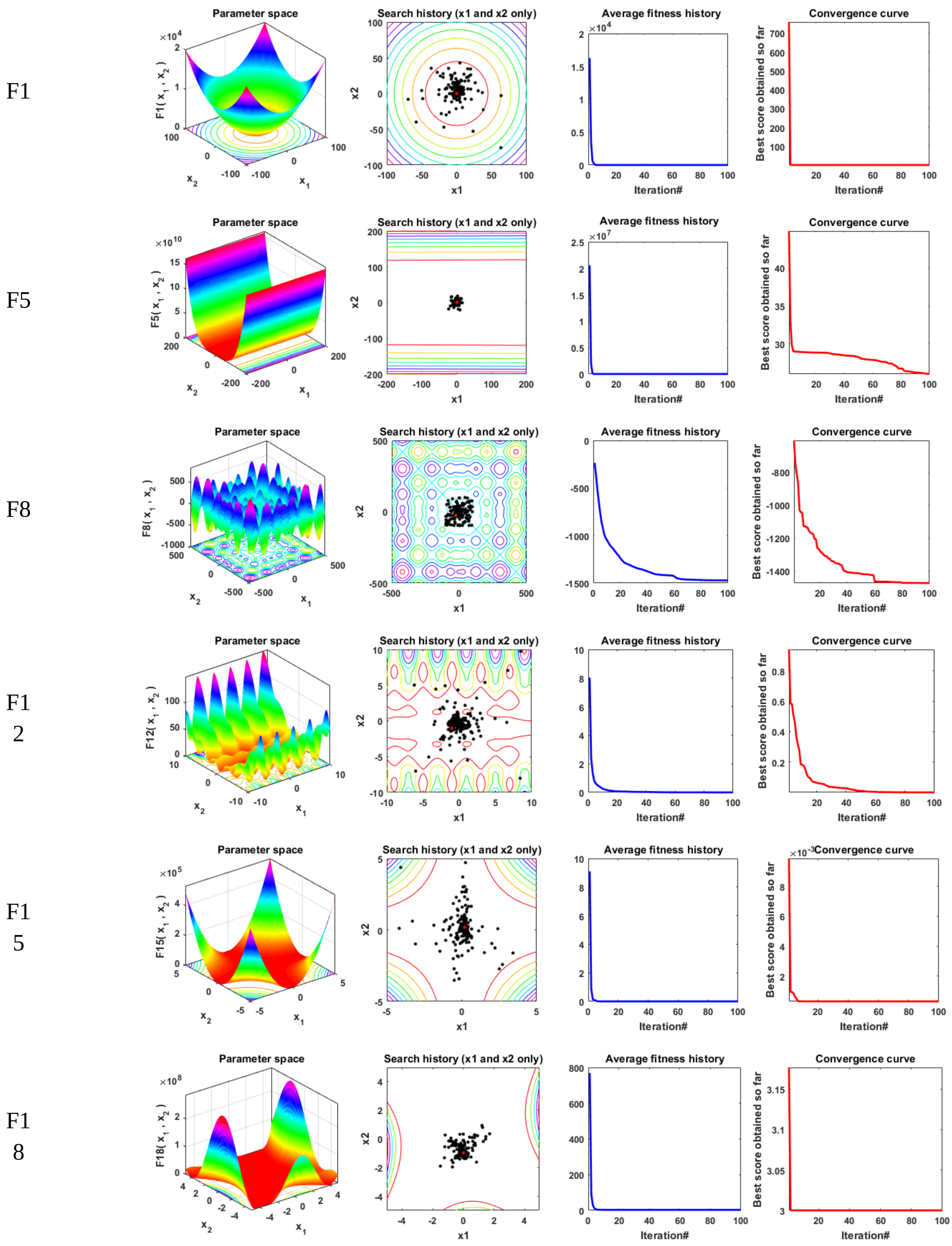

Figure 6. 40: Qualitative metrics of six benchmark functions: 2D views of the functions, search history, average fitness history, and convergence curve using GAHA technique.

Tables 6.21, 6.22, and 6.23 display the statistical results of the GAHA technique and other well-known techniques when performed for three types of benchmark functions (unimodal, multimodal, and composite, respectively). The optimum values were obtained with the GAHA, AHA, SDO, WHO, GWO and TSA methods presented in bold. As can be observed that the proposed GAHA algorithm achieves the optimal solution for most of those benchmark functions. The convergence characteristic curves of all techniques for these functions are shown in Figure 6.41, while the Boxplots for these algorithms for these types of functions are displayed in Figure 6.42. From Figures 6.41 and 6.42, the suggested GAHA method clearly reached a steady position for all processes, and the GAHA algorithm's boxplots are highly narrow and steady for most processes when compared to other techniques.

Table 6. 21: Results of unimodal benchmark functions.

Function		GAHA	AHA	SDO	WHO	GWO	TSA
	Best	**4.2E-244**	3.01E-66	1.39E-55	5.08E-21	4.47E-12	3.79E-08
	Mean	**7.7E-224**	3.87E-53	1.37E-51	2.85E-18	3.12E-11	3.92E-07
F1	Median	**2E-232**	3.32E-59	3.74E-54	1.14E-18	2.46E-11	1E-07
	Worst	**1.5E-222**	7.66E-52	8.43E-51	1.11E-17	8.73E-11	4.09E-06
	std	**0.00**	1.71E-52	2.74E-51	3.57E-18	2.31E-11	9.2E-07
	Best	**4.7E-126**	4.74E-34	1.83E-29	4.13E-13	1.42E-07	2.44E-06
	Mean	**3.3E-113**	1.07E-29	3.76E-25	1.3E-10	2.77E-07	1.9E-05
F2	Median	**5.1E-118**	3.11E-31	1.13E-26	5.29E-11	2.66E-07	1.86E-05
	Worst	**3.6E-112**	9.48E-29	3.98E-24	6.34E-10	4.78E-07	3.68E-05
	std	**8.4E-113**	2.51E-29	9.1E-25	1.77E-10	9.9E-08	9.44E-06
	Best	**1.9E-245**	3.15E-61	6.27E-46	5.13E-13	0.008462	0.027608
	Mean	**1.4E-214**	4.36E-48	6.91E-34	1.2E-08	0.610441	1.122677
F3	Median	**1.4E-228**	1.01E-54	1.4E-39	6.29E-11	0.185412	0.772195
	Worst	**2.9E-213**	6.68E-47	1.38E-32	2.3E-07	3.567009	3.914695
	std	**0.00**	1.53E-47	3.09E-33	5.14E-08	0.827115	1.096313
	Best	**5.8E-124**	5.07E-29	1.11E-26	5.11E-09	0.002608	0.67531
F4	Mean	**1.2E-109**	4.63E-26	4.52E-23	3.5E-07	0.008	3.616654
	Median	**6.4E-116**	1.05E-27	1.14E-23	1E-07	0.007092	3.022253

	Worst	**2.3E-108**	4.23E-25	1.94E-22	2.14E-06	0.016667	9.361516
	std	**5.2E-109**	1.02E-25	6.34E-23	6.09E-07	0.003845	2.343658
F5	Best	**25.12518**	26.40974	27.90967	26.68451	25.92515	27.18973
	Mean	**25.85314**	27.5024	28.65096	37.10656	27.18903	39.01094
	Median	**25.5468**	27.47815	28.74726	27.67985	27.09814	28.66203
	Worst	**28.39616**	28.53304	28.98699	208.5133	28.79035	239.7785
	std	0.745457	0.472237	**0.295026**	40.37046	0.72182	47.26339
F6	Best	**0.000816**	0.058638	0.039957	0.013248	0.252254	2.886997
	Mean	**0.015046**	0.442296	2.568541	0.064784	0.647554	3.800719
	Median	**0.00269**	0.393054	2.038779	0.058665	0.611378	3.736935
	Worst	0.221049	1.029767	7.250251	**0.16971**	1.172757	4.850371
	std	0.048696	0.249876	1.852701	**0.043941**	0.280888	0.527851
F7	Best	2.27E-05	**1.47E-05**	8.66E-05	0.000605	0.001477	0.007604
	Mean	**0.000205**	0.000346	0.002356	0.001779	0.004433	0.019206
	Median	**0.000175**	0.000219	0.001136	0.001387	0.003685	0.018479
	Worst	**0.000529**	0.001202	0.013813	0.004938	0.01033	0.04436
	std	**0.000149**	0.000292	0.003331	0.001255	0.002554	0.007628

The best values obtained are in bold.

Table 6. 22: Results of multimodal benchmark functions.

Function		**GAHA**	**AHA**	**SDO**	**WHO**	**GWO**	**TSA**
F8	Best	-1749.82	-1724.06	-1655	**-1807.46**	-1495.31	-1394.45
	Mean	-1490.22	-1551.13	-1312.83	**-1721.44**	-1245.57	-1212.82
	Median	-1522.2	-1562.44	-1385.86	**-1729.69**	-1224.18	-1232.52
	Worst	-1153.67	-1364.15	-598.802	**-1630.81**	-1123.85	-976.635
	std	159.3218	93.45685	294.008	**54.13894**	104.0153	122.0762
F9	Best	**0.00**	**0.00**	4.33E-30	**0.00**	1.062467	156.667
	Mean	**0.00**	**0.00**	1.75E-22	1.11E-05	9.801018	228.0177
	Median	**0.00**	**0.00**	4.17E-25	1E-09	9.824713	228.634
	Worst	**0.00**	**0.00**	3.02E-21	0.000177	24.96968	331.7581

	std	**0.00**	**0.00**	6.75E-22	3.96E-05	5.565812	46.40919
	Best	**8.88E-16**	**8.88E-16**	**8.88E-16**	**8.88E-16**	20.76487	20.81133
	Mean	**8.88E-16**	**8.88E-16**	**8.88E-16**	1.003597	20.92344	20.9608
F10	Median	**8.88E-16**	**8.88E-16**	**8.88E-16**	7.99E-06	20.94465	20.99356
	Worst	**8.88E-16**	**8.88E-16**	**8.88E-16**	20.01369	21.06309	21.0961
	std	**0.00**	**0.00**	**0.00**	4.474524	0.083433	0.091505
	Best	**0.00**	**0.00**	**0.00**	**0.00**	6.56E-13	1.3E-09
	Mean	**0.00**	**0.00**	**0.00**	1.83E-16	0.009891	0.007018
F11	Median	**0.00**	**0.00**	**0.00**	**0.00**	4.55E-12	1.44E-08
	Worst	**0.00**	**0.00**	**0.00**	3.66E-15	0.055407	0.029126
	std	**0.00**	**0.00**	**0.00**	8.19E-16	0.015766	0.010243
	Best	**1.44E-05**	0.001029	0.001152	4.64E-05	0.006066	0.374956
	Mean	**6.66E-05**	0.008654	0.23467	0.026544	0.026151	2.805889
F12	Median	**4.84E-05**	0.006918	0.067805	0.000309	0.023474	2.009833
	Worst	**0.000172**	0.031416	1.492821	0.207386	0.047176	7.656863
	std	**4.37E-05**	0.007552	0.352063	0.056802	0.013414	2.128936
	Best	0.245955	1.456302	0.046216	**0.011802**	0.09955	2.372295
	Mean	2.447208	2.339115	1.867552	**0.173897**	0.613832	3.298085
F13	Median	2.583917	2.436057	1.934246	**0.136817**	0.609981	3.22876
	Worst	2.967355	2.969591	2.999924	**0.700833**	1.044	4.16073
	std	0.760658	0.361111	0.961284	**0.157716**	0.280029	0.565835

The best values obtained are in bold.

Table 6. 23: Results of composite benchmark functions.

Function		**GAHA**	**AHA**	**SDO**	**WHO**	**GWO**	**TSA**
	Best	**0.998004**	**0.998004**	**0.998004**	**0.998004**	**0.998004**	**0.998004**
	Mean	**0.998004**	**0.998004**	3.494696	1.097209	3.892106	8.298683
F14	Median	**0.998004**	**0.998004**	1.495017	**0.998004**	2.982105	10.76318
	Worst	**0.998004**	**0.998004**	12.67051	2.982105	12.67051	18.30431
	std	**1.25E-16**	1.03E-09	3.953203	0.443659	3.727681	5.533952

	Best	**0.000307**	**0.000307**	**0.000307**	**0.000307**	0.00031	0.000308
	Mean	**0.000313**	0.000318	0.00067	0.000602	0.003547	0.007136
F15	Median	**0.000307**	0.000308	0.000527	0.000593	0.000546	0.000505
	Worst	**0.000424**	0.000485	0.002121	0.001223	0.020363	0.031699
	std	**2.61E-05**	3.95E-05	0.000473	0.000286	0.007255	0.010606
	Best	**-1.03163**	**-1.03163**	**-1.03163**	**-1.03163**	**-1.03163**	**-1.03163**
	Mean	**-1.03163**	**-1.03163**	-1.03005	**-1.03163**	-1.03158	-1.0253
F16	Median	**-1.03163**	**-1.03163**	-1.03163	**-1.03163**	**-1.03163**	**-1.03163**
	Worst	**-1.03163**	**-1.03163**	-1.00046	**-1.03163**	-1.03063	-0.99999
	std	2.1E-16	1.18E-12	0.006966	**5.09E-17**	0.000223	0.012981
	Best	**0.397887**	**0.397887**	**0.397887**	**0.397887**	0.397888	0.39789
	Mean	**0.397887**	**0.397887**	**0.397987**	**0.397887**	0.397891	0.397927
F17	Median	**0.397887**	**0.397887**	**0.397887**	**0.397887**	0.397891	0.397907
	Worst	**0.397887**	**0.397887**	0.399795	**0.397887**	0.397897	0.398082
	std	**0.00**	**0.00**	0.000426	**0.00**	3.01E-06	4.53E-05
	Best	**3.00**	**3.00**	**3.00**	**3.00**	**3.00**	3.000009
	Mean	**3.00**	**3.00**	4.371758	**3.00**	3.000068	8.400078
F18	Median	**3.00**	**3.00**	**3.00**	**3.00**	3.000036	3.000084
	Worst	**3.00**	**3.00**	30.41145	**3.00**	3.000238	84.00001
	std	1.17E-15	1.6E-15	6.129111	**1.13E-15**	6.53E-05	18.78799
	Best	**-0.30048**	**-0.30048**	**-0.30048**	**-0.30048**	**-0.30048**	**-0.30048**
	Mean	**-0.30048**	-0.30047	-0.2893	**-0.30048**	**-0.30048**	**-0.30048**
F19	Median	**-0.30048**	-0.30047	-0.30038	**-0.30048**	**-0.30048**	**-0.30048**
	Worst	**-0.30048**	-0.30044	-0.19165	**-0.30048**	**-0.30048**	**-0.30048**
	std	5.99E-13	1.04E-05	0.026531	**1.14E-16**	**1.14E-16**	**1.14E-16**
	Best	**-3.322**	**-3.322**	**-3.322**	**-3.322**	-3.32198	-3.32148
	Mean	-3.29227	**-3.30415**	-3.09697	-3.21756	-3.22876	-3.07223
F20	Median	**-3.322**	**-3.322**	-3.2031	**-3.322**	-3.26239	-3.20118
	Worst	**-3.2031**	**-3.2031**	-0.89904	-2.43178	-2.84039	-0.20816

	std	0.05282	**0.043552**	0.550986	0.239908	0.125558	0.679321
	Best	**-10.1532**	**-10.1532**	**-10.1532**	**-10.1532**	-10.1502	-10.0895
	Mean	-9.6434	**-10.1059**	-8.703	-9.77706	-8.51218	-5.89545
F21	Median	**-10.1532**	-10.153	**-10.1532**	**-10.1532**	-10.1413	-4.90994
	Worst	-5.0552	**-9.2237**	-4.99677	-2.63047	-2.62918	-2.58642
	std	1.569132	**0.207648**	2.23952	1.682133	2.963153	2.775111
	Best	**-10.4029**	**-10.4029**	**-10.4029**	**-10.4029**	-10.4024	-10.3637
	Mean	-9.87141	**-10.0864**	-8.45822	-9.75463	-10.0134	-7.02119
F22	Median	**-10.4029**	**-10.4029**	**-10.4029**	**-10.4029**	-10.3959	-9.8942
	Worst	**-5.08767**	**-5.08767**	-1.0677	-2.75193	-2.76526	-1.82478
	std	1.636005	**1.19136**	3.128689	2.031123	1.706042	3.57071
	Best	**-10.5364**	**-10.5364**	**-10.5364**	**-10.5364**	-10.5348	-10.4599
	Mean	-9.99561	-10.2621	-7.90449	**-10.5364**	-9.74305	-5.50502
F23	Median	**-10.5364**	**-10.5364**	-10.5357	**-10.5364**	-10.5274	-2.83596
	Worst	-5.12848	-5.12848	-3.79083	**-10.5364**	-2.42135	-1.66783
	std	1.664522	1.208388	3.015319	**1.58E-15**	2.418464	3.728197

The best values obtained are in bold.

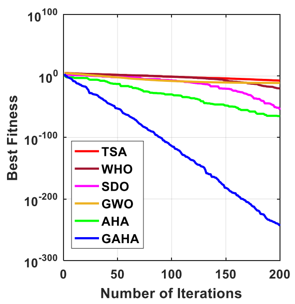

F1

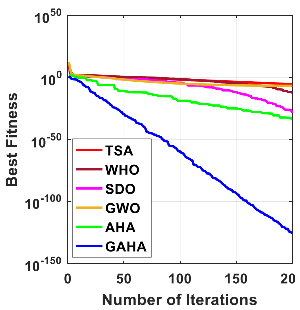

F2

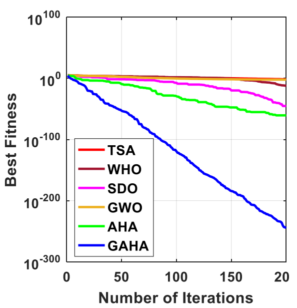

F3

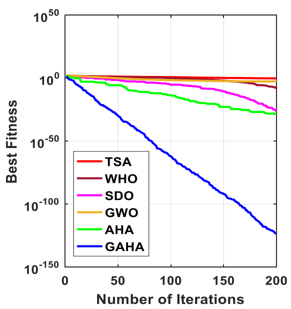

F4

6. RESULTS AND DISCUSSION

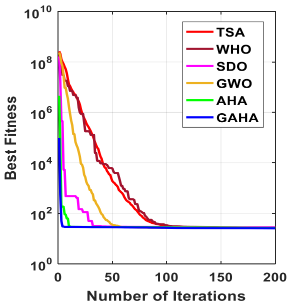

F5

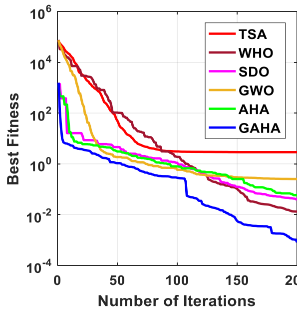

F6

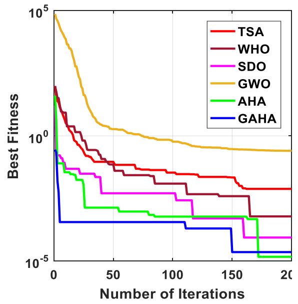

F7

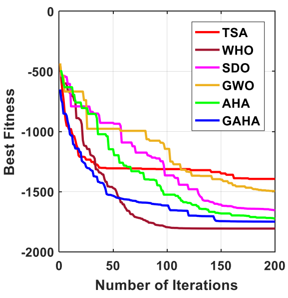

F8

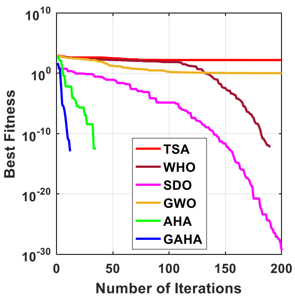

F9

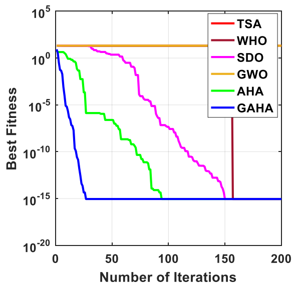

F10

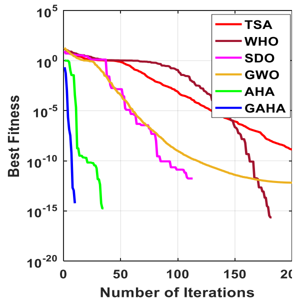

F11

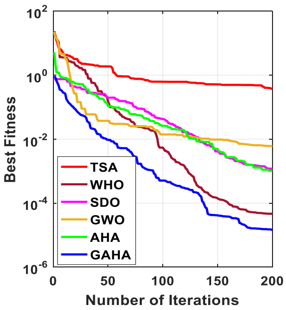

F12

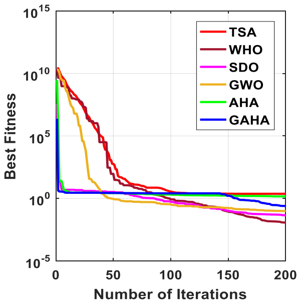

F13

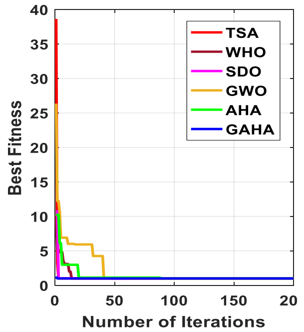

F14

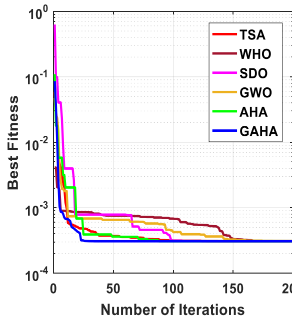

F15

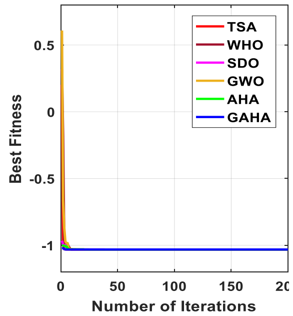

F16

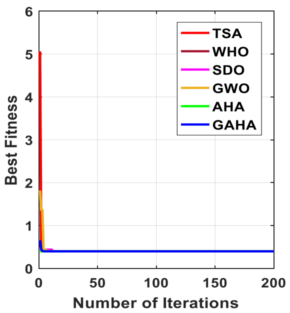

F17

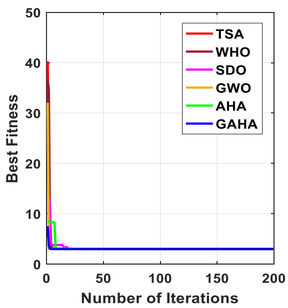

F18

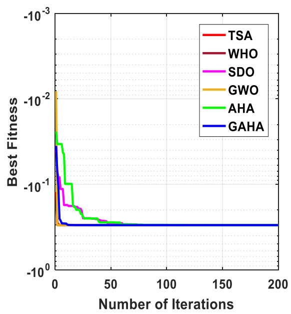

F19

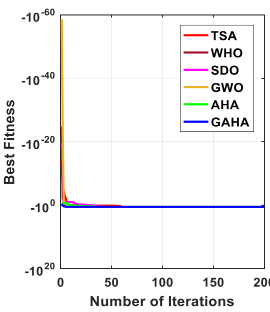

F20

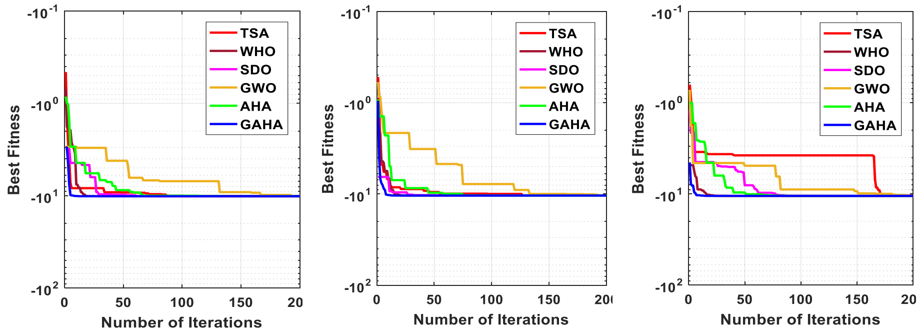

F21 F22 F23

Figure 6. 41: The convergence curves of all algorithms for 23 benchmark functions.

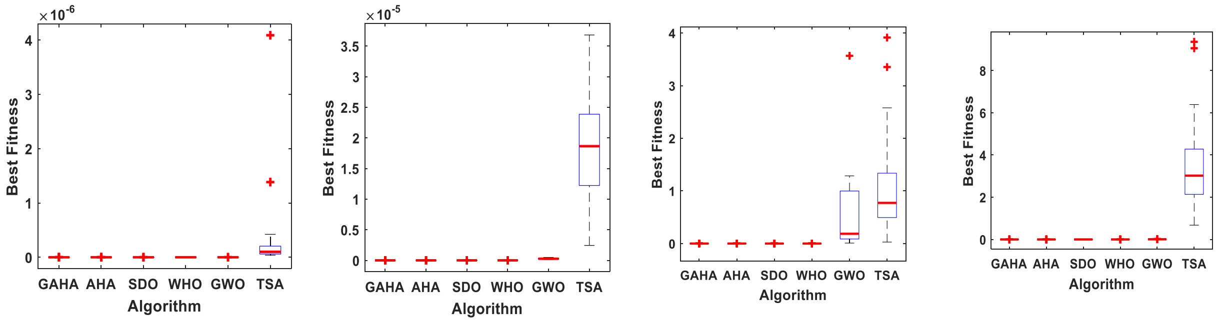

F1 F2 F3 F4

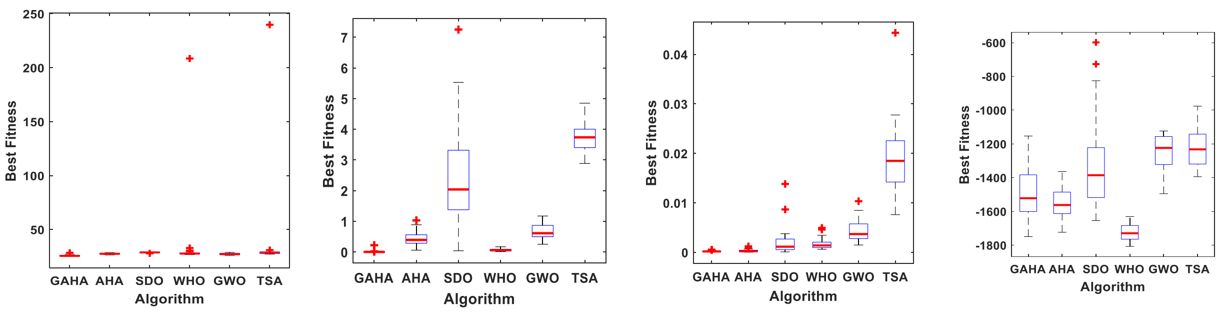

F5 F6 F7 F8

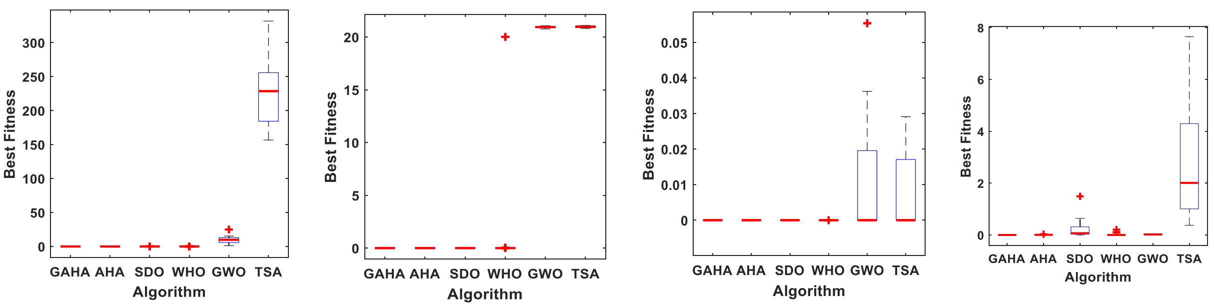

F9 F10 F11 F12

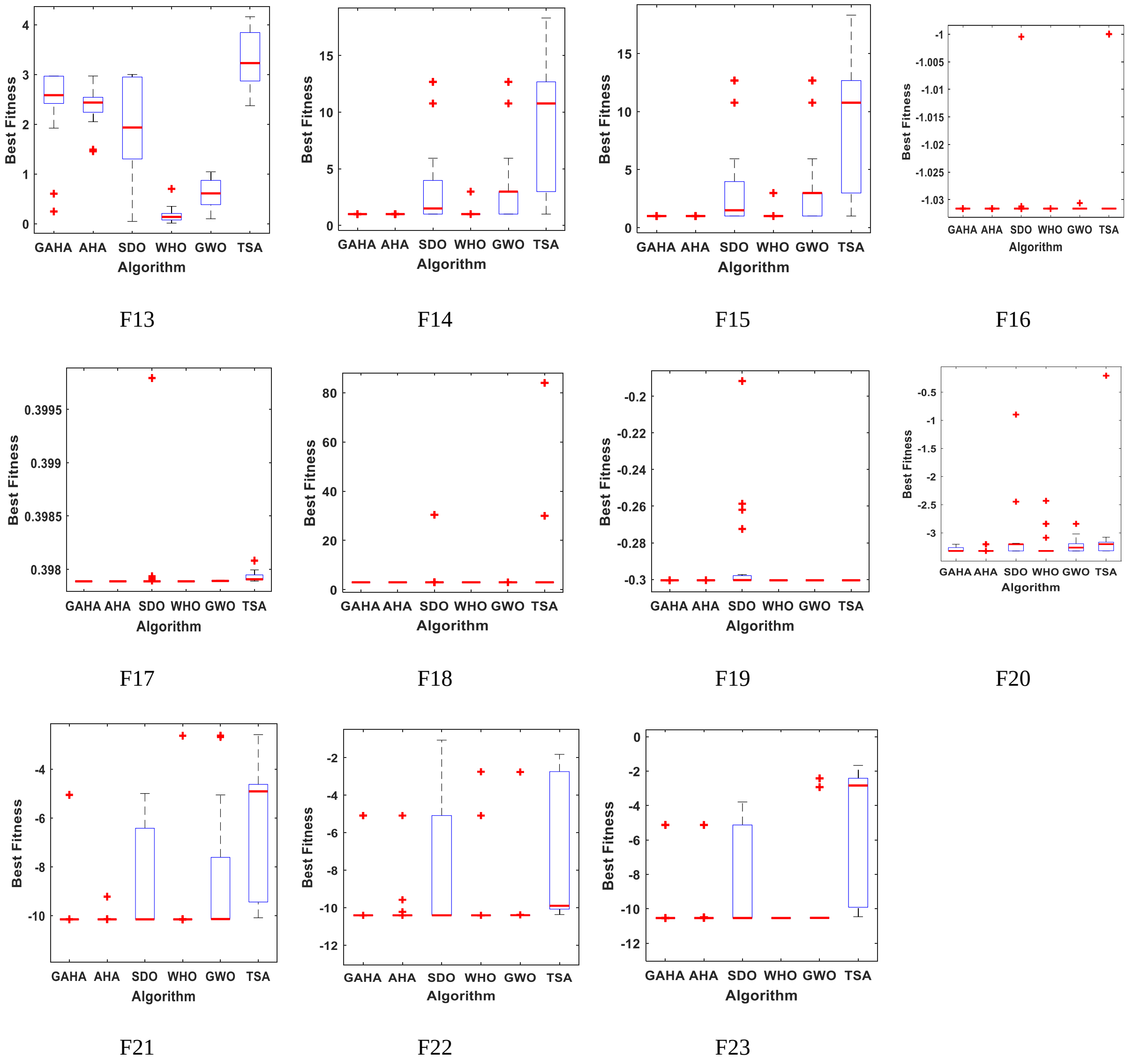

Figure 6. 42: Boxplots for all algorithms for 23 benchmark functions.

6.7.2. Real-world application

In this system, a developed optimization GAHA algorithm is applied to design the optimal sizing of four alternative standalone hybrid system configurations. The first configuration is based on the PV/WT/biomass/battery bank, the second configuration is based on the PV/biomass/battery bank, while the third configuration is based on the WT/biomass/battery bank, and finally, the fourth configuration is consisted of the PV/WT/battery bank. In order to show the features of the proposed GAHA, the findings obtained are compared with the optimization results from the AHA, WOA, and SCA algorithms. The control factors used in the optimization for each algorithm are set to be 20 for the search agent number and 100 for the maximum iterations number. Figure 6.43, indicates the convergence properties of the

GAHA, AHA, WOA, and SCA methods for each proposed configuration. As noted, for all the proposed configuration cases, the GAHA method has the best performance to reach the optimal function compared to other used optimization algorithms.

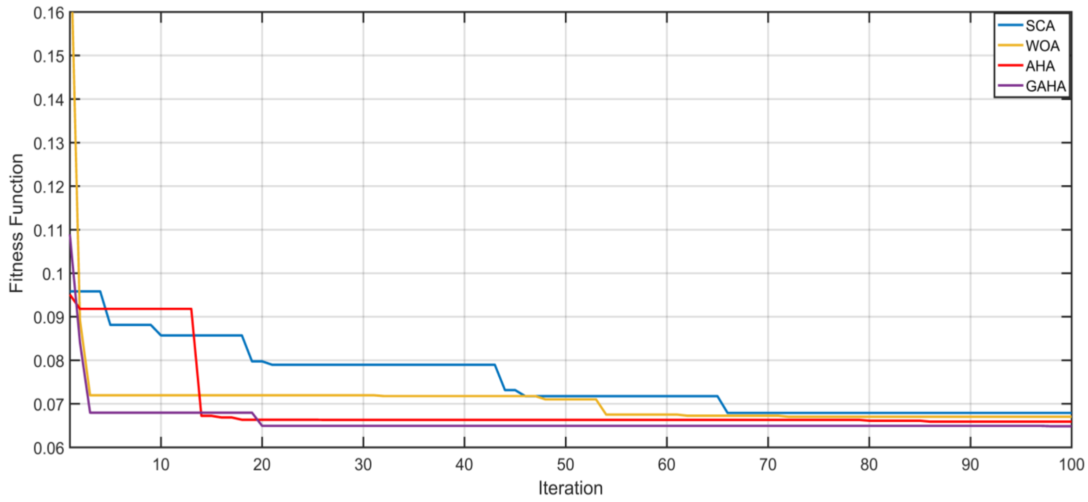

(a) PV/WT/Biomass/Battery

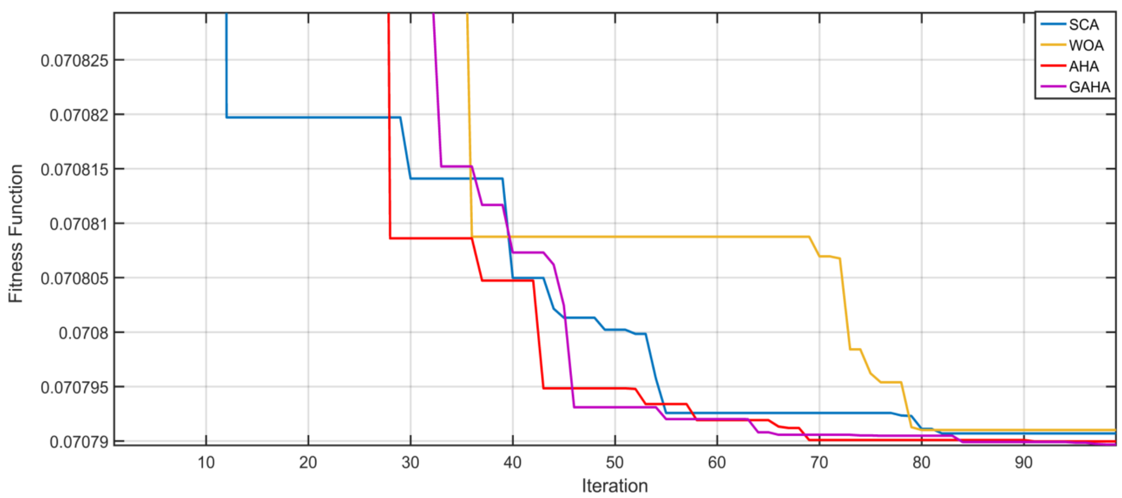

(b) PV/Biomass/Battery

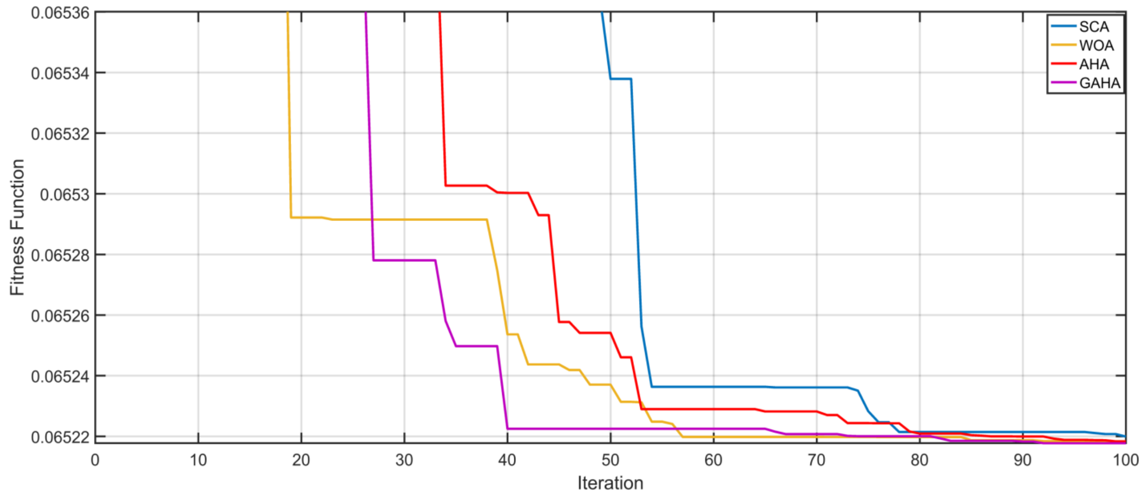

(c) WT/Biomass/Battery

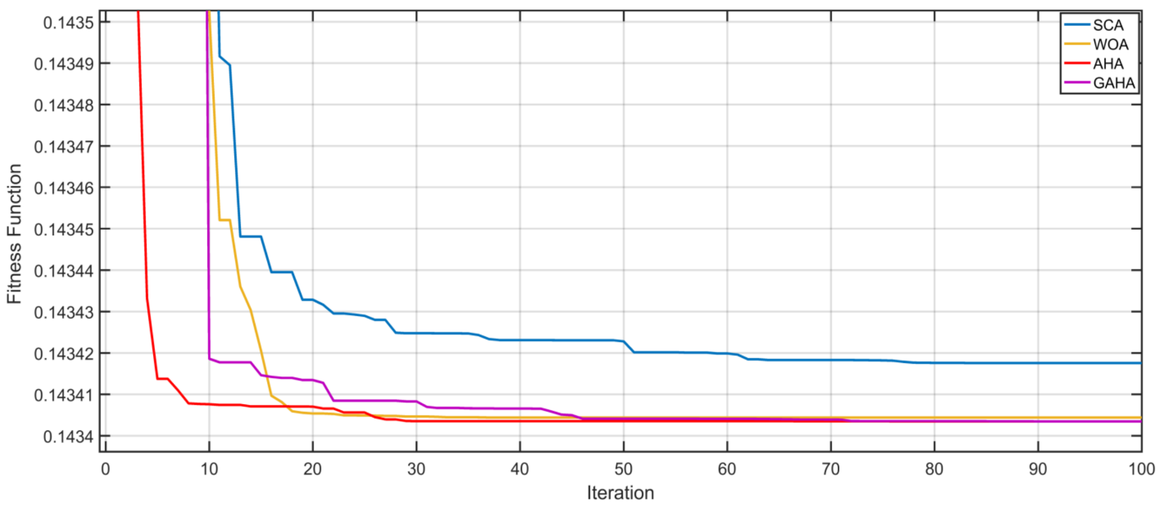

(d) PV/WT/Battery

Figure 6. 43: The Convergence process for 100 iterations using GAHA, AHA, WOA, and SCA techniques

Table 6.24, highlights the optimal sizing results for the four proposed configuration scenarios for all algorithms used GAHA, GAHA, WPA, and SCA. This table contains the optimal fitness function, the proposed constraints (N_{PV}, N_{WT}, N_{BG}, N_B), and the objective function factors (EC, LPSP, NPC). For the first configuration (PV/WT/Biomass/Battery), the GAHA method achieved the best results with the lowest EC by 0.11064139$/kWh, NPC by 3,240,738$, and LPSP by 0.28445995. For the second configuration (PV/Biomass/Battery), also the GAHA method achieved the best results with the lowest EC by 0.10573885$/kWh, NPC by 3,097,141$, and LPSP by 0.03147283. For the third configuration (WT/Biomass/Battery), the GAHA achieved the best findings with the minimum EC by

0.10772087$/kWh, NPC by 3,155,195$, and LPSP by 0.03553988. For the fourth configuration (PV/WT/Battery), the GAHA method achieved the best results with the minimum EC by 0.18145176$/kWh, NPC by 5,314,807$, and LPSP by 0.44678373. By comparing the results of the four proposed configuration scenarios, we find that the second configuration scenario achieved a significant reduction in EC and NPC, which makes it the best proposed hybrid system for the selected region for our study.

Table 6. 24: The optimization features for the suggested system based on using GAHA, AHA, WOA and SCA for a stand-alone hybrid system

PV/WT/Biomass/ Battery		Fitness Function	N_{PV}	N_{WT}	N_{BG}	N_{B}	EC	LPSP	NPC
	GAHA	**0.06479444**	**12**	**1**	**2**	**404**	**0.11064139**	**0.28445995**	**3,240,738**
	AHA	0.06479641	12	1	2	411	0.11516616	0.05809951	3,373,271
	WOA	0.06487514	17	1	2	408	0.12399406	0.0264469	3,631,844
	SCA	0.06492708	18	1	2	429	0.12753017	0.0233937	3,735,419
PV/Biomass/Battery	**GAHA**	**0.07078957**	**12**	**0**	**2**	**458**	**0.10573885**	**0.03147283**	**3,097,141**
	AHA	0.07078971	13	0	2	458	0.12068813	0.03185672	3,535,012
	WOA	0.07082439	16	0	2	438	0.12951598	0.03188575	3,793,584
	SCA	0.07082164	12	0	3	442	0.12717794	0.03252885	3,725,102
WT/Biomass/ Battery	**GAHA**	**0.06521712**	**0**	**1**	**2**	**411**	**0.10772087**	**0.03553988**	**3,155,195**
	AHA	0.06521776	0	1	2	412	0.11191188	0.03358965	3,277,952
	WOA	0.06522905	0	1	2	412	0.11223473	0.03123139	3,287,408
	SCA	0.06522948	0	1	2	413	0.11251091	0.02937543	3,295,498
PV/WT/Battery	**GAHA**	**0.143403480**	**175**	**131**	**0**	**974**	**0.18145176**	**0.44678373**	**5,314,807**
	AHA	0.143403521	175	132	0	974	0.22923413	0.36632164	6,714,375
	WOA	0.143458339	177	129	0	977	0.35062814	0.04167453	10,270,063
	SCA	0.143669286	175	132	0	977	0.35255437	0.04037409	10,326,483

The annual components cost of the proposed hybrid system for the four suggested configuration using the GAHA method is indicated in Figure 6.44. As can be seen, for the first configuration scenario the WT represents the highest yearly percentage cost with 27%, followed by battery with 25%, inverter with 24%, biomass system with 19%, and finally the PV modules with 5%. For the second configuration scenario the biomass system is the highest yearly percentage cost with 44%, followed by inverter with 23%, the PV modules with 17%, and finally the batteries unit with 5%. In the third scenario the biomass system and the battery present the highest yearly percentage cost with 35%, followed by inverter with 23%, and finally the WT with 7%. For the last configuration, the WT is the highest yearly percentage cost with 37%, followed by the PV with 25%, the battery with 22%, and finally the inverter unit with 16%.

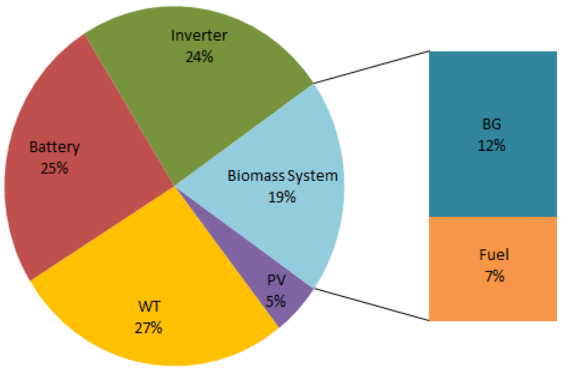

(a) PV/WT/Biomass/Battery

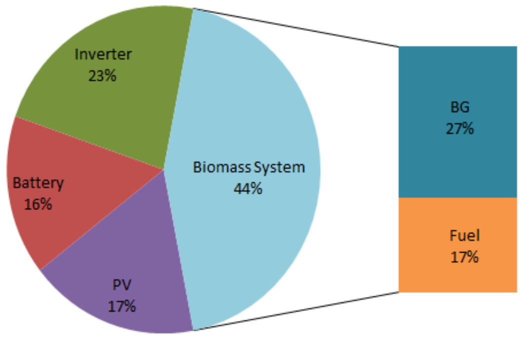

(b) PV/Biomass/Battery

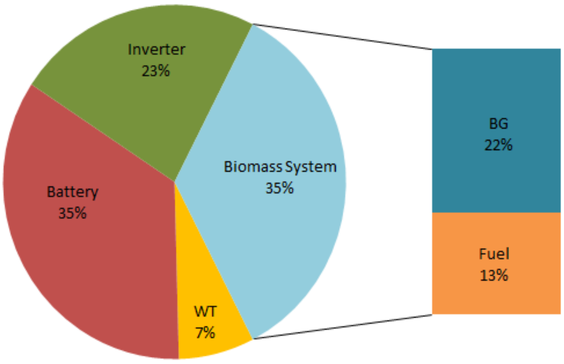

(c) WT/Biomass/Battery

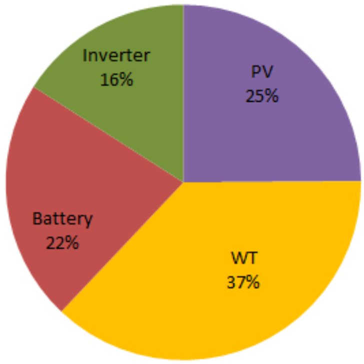

(d) PV/WT/Battery

Figure 6. 44: The Breakdown of the Annual Cost of the Hybrid System Components using the GAHA technique

6.8. Hybrid PV/Biomass/ELE/HT/FC System

The major contributions of this study can be summarized as follows and the main parameters of this stand-alone hybrid system PV/Biomass/FC are illustrated in Table 6.25;

- A new hybrid energy system, consisting of PV, BG, FC, Electrolyzer units, and HT units, has been developed for a small village located in the Western Desert of Egypt;
- The optimal size of the proposed stand-alone hybrid system is determined using a novel MOA approach;
- To prove the optimal effective and performance of the MOA methodology, the results of MOA are compared with a three optimization algorithms; STOA [42], WOA [43], and SCA [44];

- The optimal function of this hybrid system is to minimize the EC, and reduce the CO_2 emissions;
- Evaluate the optimal decision variables of the components, which include the PV_N, G_N, FC_P, $P_{ELE/HT}$, and HT_m.

Table 6. 25: Main parameters of the stand-alone hybrid system PV/Biomass/FC.

Component	Parameter	Value	Unit
PV System [28], [78]	PV module capital cost	7000	$
	δ_T	0.0037	-
	PV_η	15	%
	T_r	25	ºC
	Rated power	1	kW
	Length	1625	Mm
	Width	1019	Mm
	Thickness	46	Mm
	lifetime of PV system	20	year
	PV replacement cost	13885	$
	O&M cost	20	$/ unit-year
Inverter Unit [28]	η_{inv}	95	%
	inverter lifespan	15	year
	Inverter Capital Cost	800	$/unit
	Replacement cost	750	$/kw
	O&M cost	8	$/ unit-year
Gasification System	LHV_B [122]	14.8	MJ/kg
	LHV_{sy} [122]	4.766	MJ/kg
	η_{sy}	80	%
	GP_{rat}	40	KW
	No-load fuel consumption (F_0) [85]	0.0644	kg/h/50kW
	Marginal fuel consumption (F_m) [85]	0.2998	kg/h/50kW
	Capital Cost [99]	23,700	$/kw
	Lifespan [99]	15,000	h
	Replacement cost [99]	15000	$/unit
	Yearly O&M cost [99]	0.05	$/ h
Electrolyzer Unit [28]	Rated Power	1	kW
	Lifespan	20	year
	Efficiency	75	%
	Capital cost	2000	$/unit
	Replacement cost	1500	$/unit
	Yearly O&M cost	25	$/ unit
Hydrogen Tank Unit [28]	Power	1	kW
	Efficiency	95	%
	Capital cost	1300	$/unit
	O&M cost	15	$/unit-year
	Replacement cost	1200	$/unit
	Lifespan	20	year
FC System [28]	Power	1	kW
	Efficiency	50	%
	Capital cost	3000	$/unit
	O&M cost	175	$/unit-year

	Replacement cost	2500	$/ unit
	Lifespan	5	year

Figure 6.45, displays the convergence curves of the optimization process based on MOA, STOA, WOA, and SCA techniques. These optimization algorithms have been applied 50 runs for 100 iterations to assess the best fitness function value to subjugate the proposed algorithms' randomness and verify their stability and robustness. For the proposed case study, each optimizer is used in the same way. The final values of the proposed MOA's objective function are within a small range, demonstrating MOA's consistency in finding the best solution for the optimization problem.

Figure 6.46, shows a comparison between the convergence curves for the best implementation within the 50 runs of the optimization programs for the different algorithms. According to the convergence characteristics, MOA has the best results in achieving the minimum fitness value after 44 iterations, outperforming STOA, WOA and SCA.

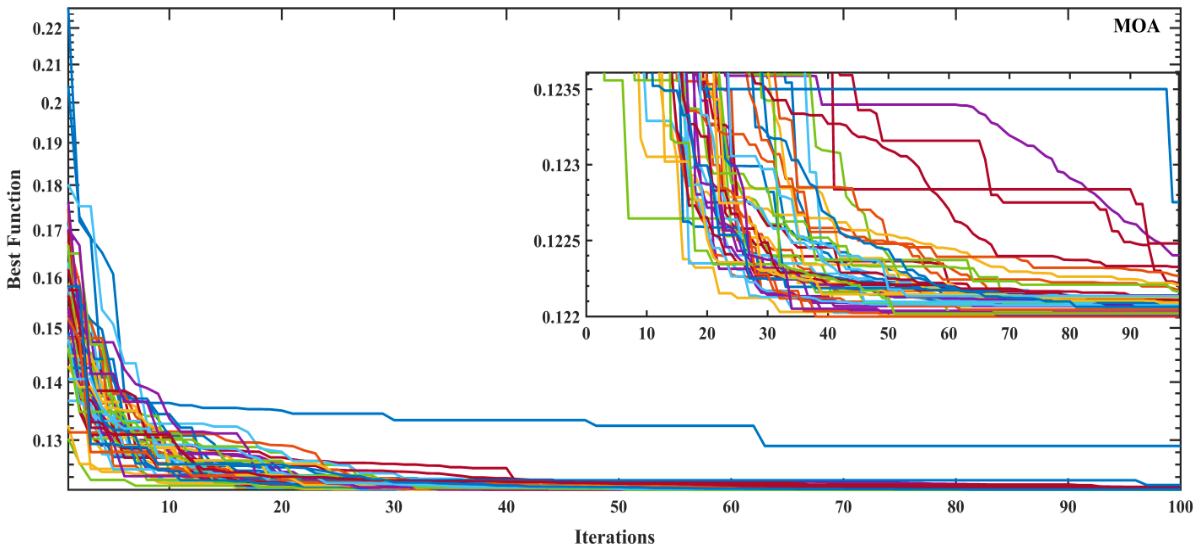

(a)

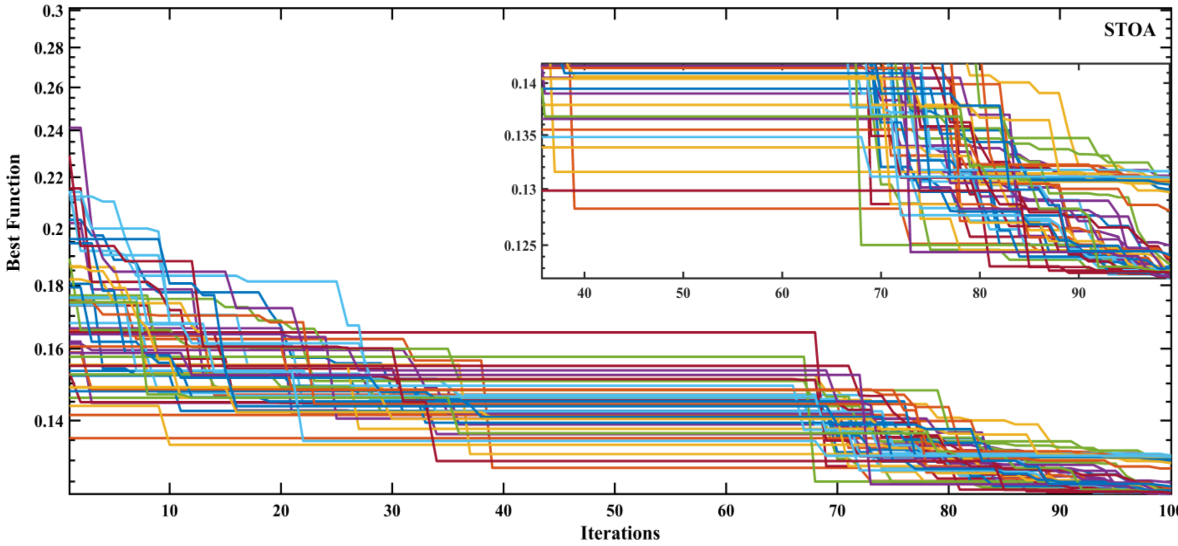
STOA
Best Function
Iterations

(b)

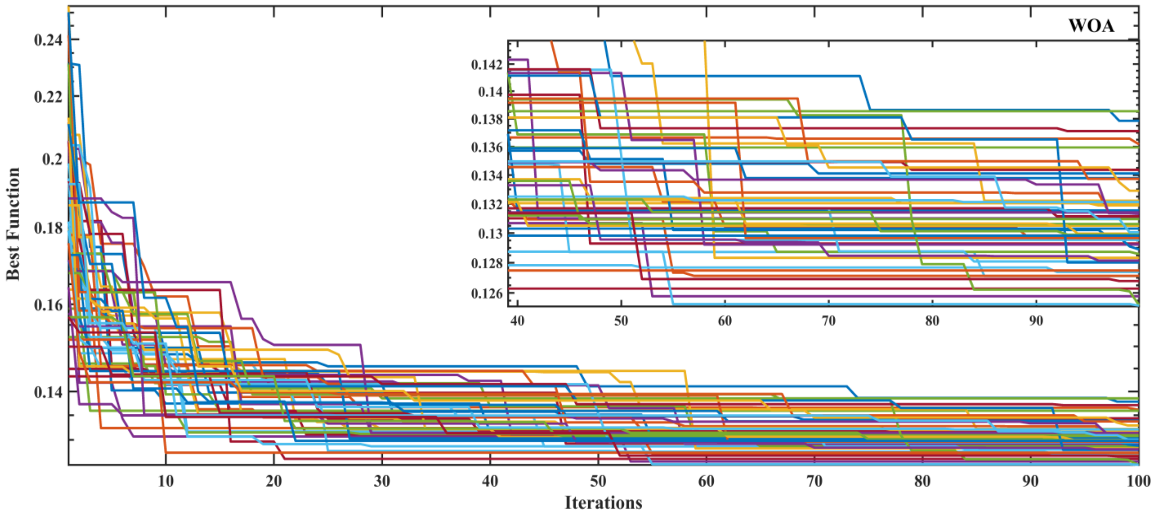
WOA
Best Function
Iterations

(c)

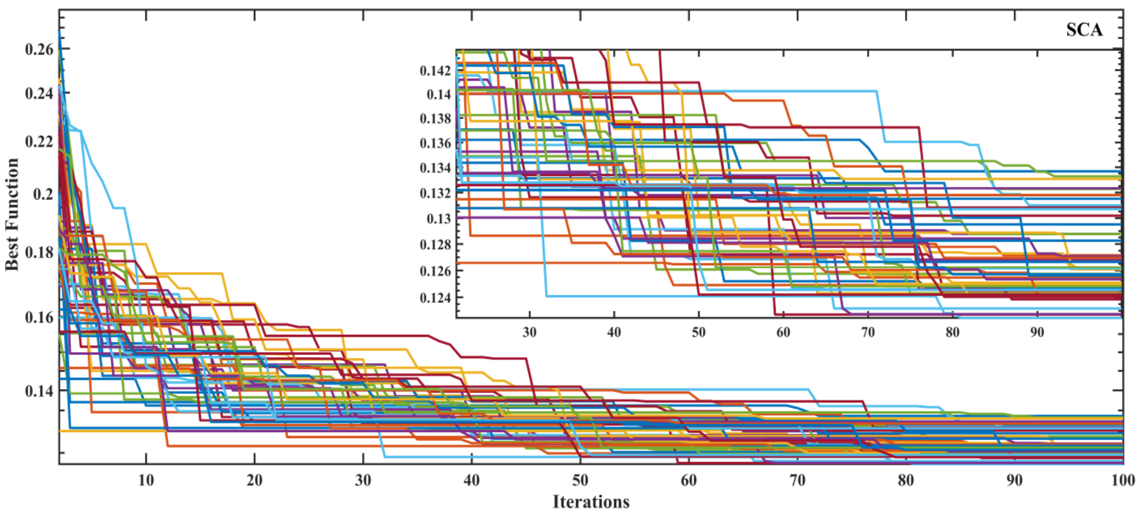
SCA
Best Function
Iterations

(d)

Figure 6. 45: The convergence curves of the studied algorithms for 100 iterations, (a) MAO, (b) STOA, (c) WOA, (d) SCA.

Table 6.26, indicates the results of the optimal sizing characteristics of the hybrid microgrid for the four optimization algorithms used in this study. These results include the best fitness function, the number of iterations to reach the optimal solution, the optimal values of the decision variables, EC ($/kWh), NPC ($), LPSP (%), and GHG (ton/y). This table shows that the MOA has the best fitness function with 0.1219998, followed by STOA, SCA, and WOA with 0.1221296, 0.1224865, and 0.1251143, respectively. By comparing the results provided in the table, it can be noticed that the MOA is characterized by the minimum EC, the minimum NPC, and the lowest GHG, compared with the rest of the used algorithms, followed by the STOA, SCA, and WOA. The values of the LPSP obtained from all algorithms are within constraints.

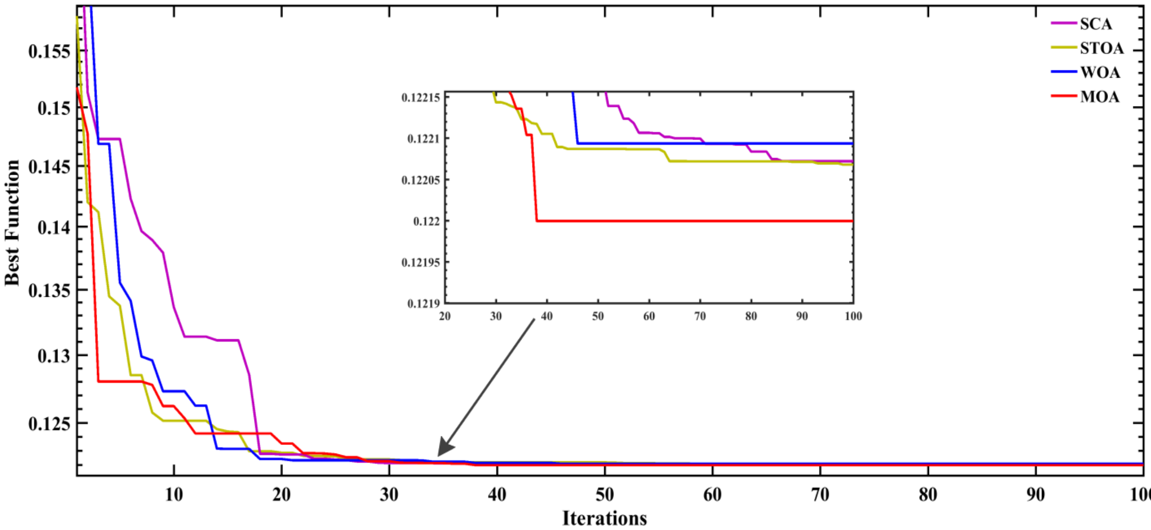

Figure 6. 46: The convergence curves for the best implements using MOA, STOA, WOA and SCA for 100 iterations.

Table 6. 26: The Optimization Features Parameters for the Proposed Hybrid System Based On Using MOA, STOA, WOA, and SCA

	MOA	STOA	SCA	WOA
Best Fitness Function	**0.1219998**	0.1221296	0.1224865	0.1251143
Iteration Number	**44**	41	27	33
PV (units)	**47**	42	41	51
Nominal PV power (kW)	46.7	41.92	40.1	50.79
Generators (units)	**2**	3	3	3

Nominal generator power (kW)	**72**	84.9	86	89.6
Electrolyzer rated (kW)	**319.87**	326.35	323.419	336.78
Hydrogen tank (kg)	**62.48**	61.28	66.15	67.41
Fuel cell (kW)	**124.71**	130.09	134.927	155.03
EC ($/kWh)	**0.2106533**	0.210961	0.2123484	0.2367564
NPC ($)	**6,170,134**	6,179,148	6,219,783	6,934,705
LPSP(%)	**0.05993**	0.059411	0.059187	0.0365246
GHG (ton/y)	**792.534**	806.654	808.559	849.626

Figure 6.47, shows the contribution of the annual cost of each unit (representing the operating and maintenance costs, which are costs spent each year) of the proposed hybrid system for the MOA algorithm. As is evident, the FC represents the highest annual percentage cost with 36% of the total cost of the proposed system, followed by PV modules with 19%, then the Electrolyzer units with 18%, inverter with 14%, biomass system with 11%, and finally the HT with 2%. The results from the MOA indicated that the annual percentage cost of the FC represents the largest portion of all units.

Figure 6.48, reveals the contribution of each unit to the NPC percentage of the proposed hybrid system using the MOA. The results revealed that the NPC of the PV modules accounts for the largest portion with 27% (1,066,906 $), followed by the Electrolyzer unit with 25% (1,006,631$), the FC with 18% (728,728 $), the biomass system with 15% (614,001$), the inverter with 12% (488,132$), and the HT represents the lowest NPC value with 3% (134,966$).

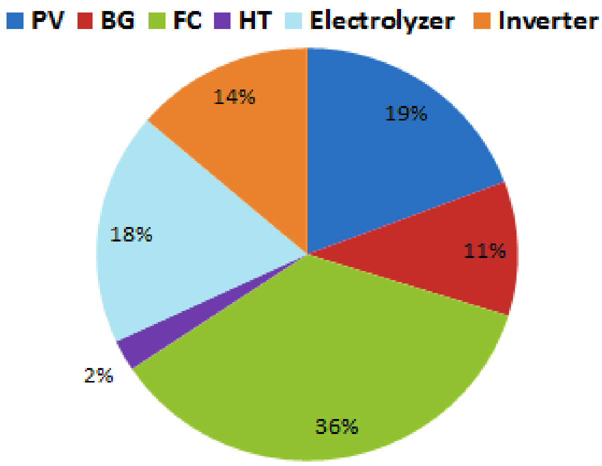

Figure 6. 47: Break down of the annual costs of the hybrid system's units.

Figure 6.49, indicates the hybrid PV, BG, and FC power system's power output performance over a 24-hour cycle for four different days with high energy consumption over the year. According to the obtained results, the excess power from PV and BG units (P_{ren}) is used to power the electrolyzer for hydrogen production. When the power generated by the P_{ren} is not able to meet the load power needs, then the FC will use the hydrogen stored in the HT unit to make up for the shortage in power generation. Figure 6.50, shows the variation in the stored mass amounts of hydrogen in each hour in the HT during one year (8760 hours) in case of using the MOA method. It can be noticed that the maximum amount of hydrogen mass stored is 63 kg.

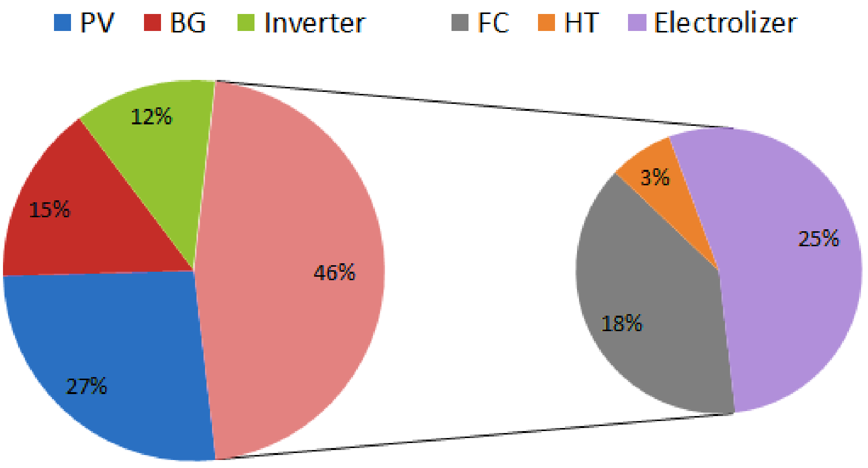

Figure 6. 48: Break down of the NPC of the hybrid system units using MOA.

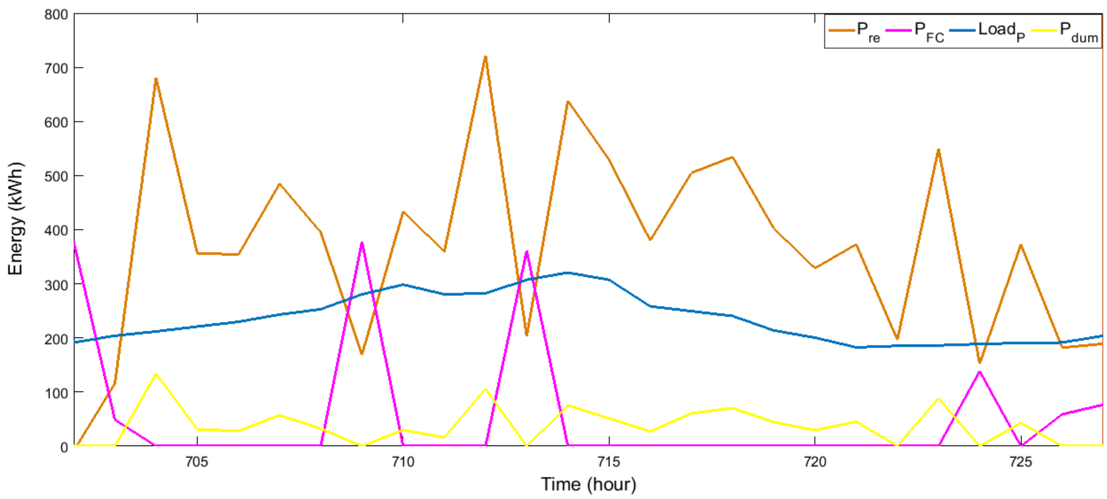

(a) a day of Winter season

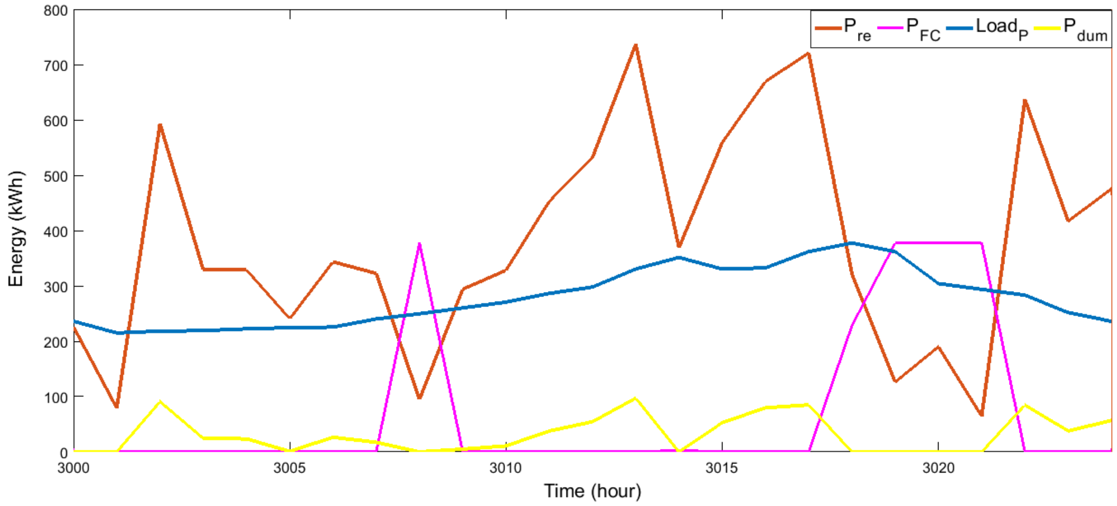

(b) a day of Spring season

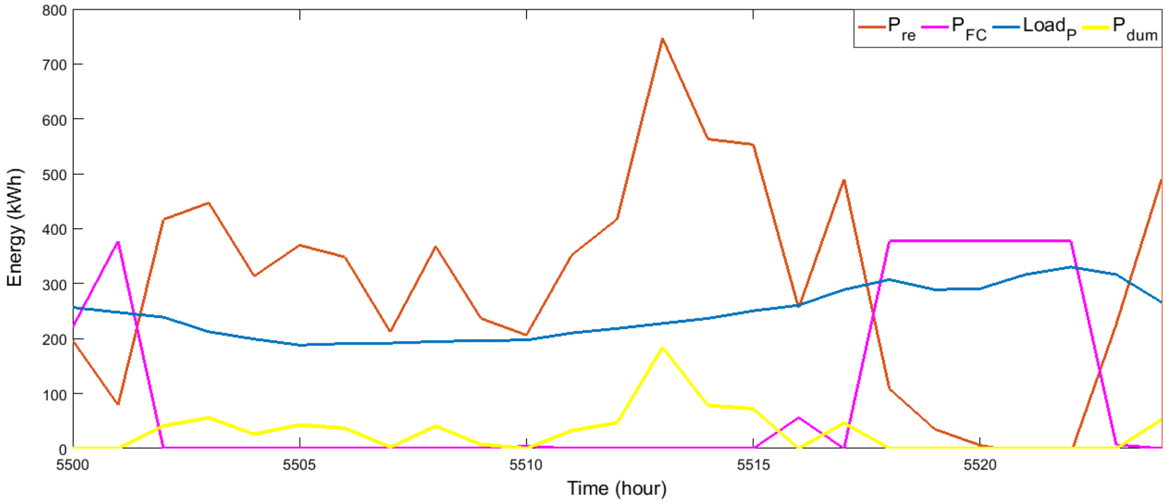

(c) a day of Summer season

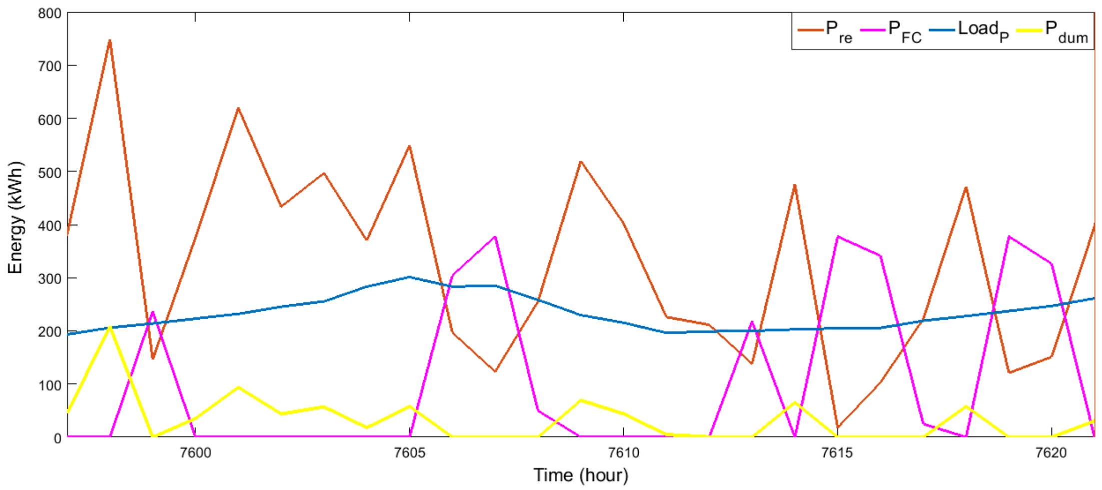

(d) a day of Autumn season

Figure 6. 49: The operation capacity of the proposed hybrid system for 4 different days using MOA.

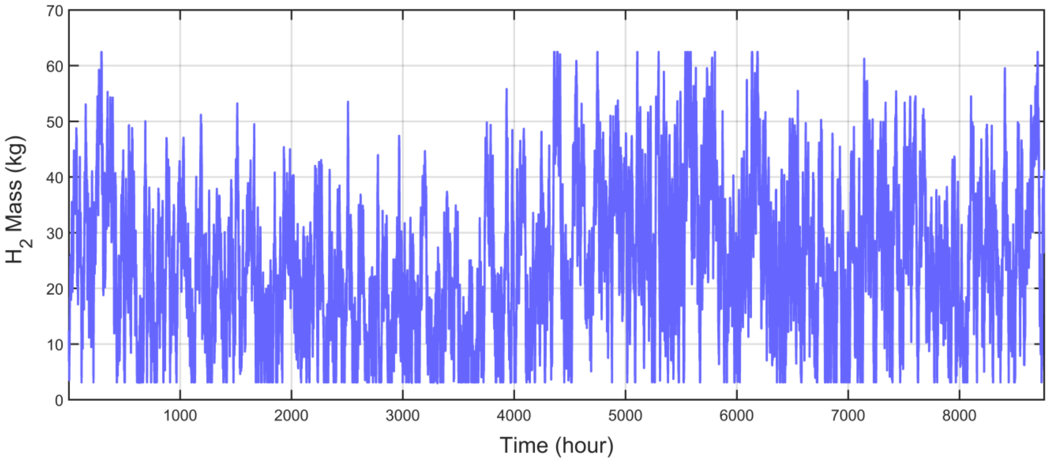

Figure 6. 50: The hourly change in the mass of hydrogen stored during a year.

Chapter 7

Conclusions and Future Perspectives

Chapter 7

Conclusions and Future Works

7.1. Conclusions and Contributions of the Thesis

The optimal usage of agricultural waste in an attempt to spread the concept of bioenergy in Egypt due to its economic, environmental and social benefits has been studied. This thesis has focused on the optimal performance and modeling of a tri-generation system for converting biomass into electrical, cooling and heat power. This target has achieved by developed two CCHP systems. In addition, this thesis has proposed different hybrid renewable systems based on the integration of the BG with other renewable sources and has proposed different optimization techniques to solve the techno-economic and sizing problem of the suggested hybrid sources. The proposed techniques have been compared with recent and other well-known optimization techniques.

The major goal of the optimization process in renewable energy systems is to give deep analysis and develop general models of these energy systems. Using such optimization programs allows finding the optimal combination of different energy components for a typical rural community to reduce the total NPC of the system (Techno-economic Analysis) through the lifetime of the project. Such research studies drive investors to participate in such projects because of their economic return.

The optimal configurations that are obtained and presented in this thesis can be utilized as guidelines for designing electrification systems with a minimized cost for the considered rural communities and other small villages with similar characteristics and conditions.

7.1.1. CCHP System of Downdraft Gasifier, EFGT, and Absorption Cooling Cycle

In this system, biomass small-scale tri-generation system based on generating cooling, heat and power energy has been developed. The simulated plant has been carried out using Cycle-Tempo software. The developed system consists of the following three phases:

1. The first phase is the gasification process that based on using the down draft gasifier, where 100 Kg/h of the CS with 481.22 of energy input and lower heat value of 14.824 MJ/kg is converted into syngas at gasification temperature reaches to 995 °C and 1.65 of

oxidant–fuel ratio. The hot gas efficiency is 94% with 4.766 MJ/kg of calorific value and 243.18 Kg/h of mass flow.

2. The second phase is the EFGT, where the syngas is converted into electrical power. The optimal performance parameters shown that the EFGT is capable of producing 70.57 kW of electrical power with HTHE of 75% and 4.84 pressure ratio at TIT of 875 ºC and hot side temperature difference of 110 ºC.

3. The third phase is the absorption refrigeration system. This process is divided into two subsystems, heat recovery steam generator and VAC. Ammonia/water is the more suitable working fluid during this cycle. Based on the EFGT performance, the cooling power ($\mathbb{Q}_{\text{eva}}$) of absorption cooling system is 130.92 kW with 15 ºC of cooling tower and 0.6 of system CP. The supplied heat to generator ($\mathbb{Q}_{\text{gen}}$) is 82.62 kW_{th} at generator temperature 120 ºC with 4.07 of CR and 5 % of ammonia concentration. The refrigerating heat flow is 48.83 kW_{ref}.

The general performance for the developed plant is 1.88 of system CPR with 21.78 % of the gross electrical efficiency ($\eta_{\text{net}_{\text{EL}}}$) and 47.43% of net thermal efficiency (η_{th}).

7.1.2. CCHP System of EFGT, ORC, and Absorption Cooling Cycle

A theoretical modeling for small-scale tri-generation system has been proposed. The developed system has been simulated using Cycle-Tempo software tool including several units.

The EFGT includes the combustion chamber and the HTHE. In direct combustion, a sugarcane bagasse (with ash content 2.4%) is converted into flue gases under atmospheric pressure at reaction temperature of 985.63°C. The efficiency of the chamber in this stage was 96 %. The electric power generated from the EFGT reached 142.92 kW at TIT of 875 °C, compressor pressure of 4.9 bar, hot side temperature difference of 85 °C, HTHE efficiency of 87% and exhaust gases temperature of 271.9 °C.

An ORC generator has been used to maximize the electrical energy produced of the CCHP system based on a working fluid and the heat source temperature. Four working fluids (toluene, benzene, cyclohexane and R113) have been proposed to determine the more suitable fluid. The parametric study showed toluene is the best working fluid for maximizing the electrical power (34.64 kW) and efficiency (20.5%), followed by cyclohexane, benzene and

R113. The four working fluids are considered suitable for CHP applications, where the maximum thermal power produced using toluene is 110.85 kW followed by benzene (110.32 kW), R113 (110.29 kW) and cyclohexane (104.95 kW). R113 gives the best performance in terms of CHP applications due to its lowest PPTD (10 ºC) together with safety, cost, stability, corrosion, pressure and environmental hazards features. The cooling power generated by the absorption chiller has been 46.51 kW using R113 in ORC, followed by benzene (45.68 kW), toluene (38.50 kW) and cyclohexane (34.33 kW).

The optimum conditions of the chiller have been reached at 15 ºC of cooling tower temperature, 0.57 of CP, 4.07 of CR and 45.5 % of ammonia concentration. Toluene is considered the most appropriate working fluid; the net electrical power is 177.56 kW with the highest η_{CCHP} (43.9 %) and heating capacity (110.85 kW), followed by benzene (43.7%), R113 (43.5 %) and cyclohexane (42.5 %).

7.1.3. Hybrid PV/WT/Biomass/Battery using SMA and SOA Algorithms

In this system, two new optimization algorithms, namely SMA and SOA algorithms have been developed and utilized for solving the optimization problem of optimal design of a standalone hybrid system consisting of PV, WTs, biomass, and battery bank units. Three configurations have been studied, namely, Case (1): PV, WT, biomass, and battery; Case (2) PV, biomass, and battery; and Case (3): WT, biomass, and battery. The obtained results from SMA and SOA have been compared with the results of GWO, SCA, and WOA. The control parameters are kept constant for all algorithms over all cases. Real-time meteorological data of a remote area located in the western desert of Egypt called Abu-Monqar village has been used. The obtained results are summarized below:

- The convergence curves for the three cases showed that the SMA achieved the best objective function compared with the other optimization methods used.
- Case (2) presented the fastest iteration time (running in 330 sec), compared with the other two cases; followed by case (3) and then case (1). In all cases, the SMA algorithm was faster than SOA in reaching the optimal solution.
- Case (3) showed the lowest value of the system EC with 0.1186861 $/kWh, the lowest NPC with $3,476,371.76, and the highest LPSP with 0.032493.

- Comparing the percentage of the NPC of all units in the three cases, the percentage of the NPC of the batteries was always the largest portion. The batteries represented the highest annual cost compared with the other units.

The suggested configurations of the hybrid system have been compared considering several economic indicators, NPC, total annual operating cost, energy cost, and the number of generating units. The obtained results have revealed that the hybrid PV, wind, and Biomass system using the SMA is the most economically viable scenario. The obtained optimal configuration leads to an NPC of $3,896,930.397 with EC 0.1330443 $ /kWh.

7.1.4. Hybrid PV/WT/Biomass/Battery using HBO, CFA and STOA Algorithms

This study offered a new meta-heuristic optimization method, called the HBO technique, for design four different scenarios of a stand-alone hybrid power model based on PV, WT, Biomass system, and battery storage unit. The major objective function is minimizing the EC with increasing the reliability LPSP, which fulfills the required load of an isolated society in Alrashda village, Dakhla Oasis in the New Valley Governorate, Egypt. The operation of the suggested off-grid system relies on the meteorological data of wind speed, radiation and temperature per hour which obtained from NASA Surface Meteorology and Solar Energy website for 20 years for the selected region. The result obtained by the proposed methodology HBO which is based on utilizing MATLAB software was compared with other optimization methods CFA, GWO, STOA techniques.

The simulation results clearly showed that the suggested optimization method HBO is an effective method in identifying the optimal capacities of the generating and energy storage units and ensured good execution in the different scenarios of proposed the hybrid system. The results from the analyses presented in this study show the following:

- The obtained results indicated that the HBO technique showed the optimal convergence between the investigated algorithms in reaching the best solution.

- The HBO method has achieved the best optimal solution for Case-1 scenario. This case is a combination of PV/WT/biomass/Battery units, the best optimal solution has achieved after 27 iterations with the minimal EC of 0.121171 $/kWh, NPC of $ 3,559,143, and LPSP of 0.026789, followed by the results obtained from the CFA technique with the minimal COE of 0.1213225 $/kWh, NPC of $ 3,563,603, and LPSP of 0.0267184 after 44 iterations, followed by the results obtained from GWO, and STOA methods

- The HBO technique has achieved the best optimal solution for Case-2 scenario. This case is consisted of PV/biomass/Bat units, the best optimal solution has achieved after 49 iterations with the minimal EC of 0.1311804 $/kWh, NPC of $ 3,853,160, and LPSP of 0.0298557, followed by the results obtained from the CFA method with the minimal COE of 0.1315446 $/kWh, NPC of $ 3,863,857, and LPSP of 0.0291707 after 32 iterations, followed by the results obtained from GWO, and STOA techniques.
- Based on the results of parametric and non-parametric statistical measurements performed for a more accurate comparison of the four optimization methods, the proposed HBO in all studied cases showed the best results compared to other optimization methods.
- STOA has achieved the best optimal solution for Case-3, and Case-4 with EC of 0.105673 and 0.332497 $/kWh, and NPC of $ 3,103,938 and $ 9,766,441, respectively.
- By comparing the NPC of the four suggested cases, it finds that Case-3 achieved the lowest NPC, followed by the Case-1. Although the third scenario which based on WT/biomass/Battery units is the least NPC, but it is not the optimal and efficient system for use. As the design of this case is based on batteries and biomass generators only, which have the highest yearly sharing of the capital cost, operating and maintenance cost.
- The hybrid power system which is consists of PV/WT/biomass/Battery units would be an appropriate solution with minimal investment cost for rural communities, small industries, isolated wells and isolated farming areas where grid access is too costly or even impossible.

7.1.5. Hybrid PV/Biomass/Battery using Modified QRUN Algorithm

This system deals with the development of the original RUN algorithm, by applying a quantum mechanics to the RUN algorithm, and this new algorithm called the Quantum model of QRUN method. The performance of the proposed QRUN has been tested on several standard functions, and compared with the original RUN and with three well-known optimization techniques, including the AO algorithm, the HBA, and the TSO algorithm. The QRUN has proven its effective compared to other algorithms that have been used. This QRUN algorithm has been also applied to solve an optimization problem, which is represented in solving an optimal sizing of an isolated hybrid system based on the PV/Biomass/battery units. The major function of this isolated system is to reduce the system EC and the LPSP to meet the electricity requirements of a small remote village in the Dakhla Oasis, in Egypt.

The proposed QRUN results have been compared with other optimization techniques, namely RUN, GWO and AO methods in order to evaluate the accuracy of the QRUN technique. The simulation results demonstrated that the proposed optimization algorithm QRUN has achieved the best optimal solution for the proposed system after 13 iterations with the lowest EC of 0.080076 $/kWh, NPC of $3,352,062, and LPSP of 0.490866.

7.1.6. Hybrid PV/WT/Biomass/Battery using Novel Hybrid GAHA Algorithm

In this system, an enhanced method named the GAHA has been described. This improved algorithm GAHA is based on enhancing the local search capabilities of the AHA approach, the LEO component is incorporated in the local search stage. The GBO method is intended to have its capabilities improved by the LEO. In order to address challenging real-world problems, the LEO seeks to find new regions. Adjusting their locations in accordance with predetermined criteria improves the performance of solutions. It improves the method's convergence characteristics and prevents the approach from becoming trapped in the local optima. The effectiveness of the proposed GAHA algorithm has been tested on a set of 23 benchmark test functions, and the results are then compared to those of five well-known algorithms, the GAHA technique achieved better solutions compared to these algorithms.

In order to demonstrate the effectiveness of this modified algorithm GAHA, it has been applied to solve the optimum size of a suggested hybrid power system for the new Tiba city, located in the northeast of Luxor city south Egypt. The major aim is to reduce the EC, the NPC, and increase the LPSP. Four different configuration scenarios have been studied, the first one consists of the PV modules/WT/biomass/batteries, the second configuration is based on the PV modules/biomass/batteries, the third scenario is the WT/biomass/batteries, and finally, the fourth configuration consists of the PV modules/WT/batteries. In order to prove GAHA's superior performance, its obtained results have been compared to the optimization results from other algorithms, such as the original AHA, WOA, and SCA methods. The GAHA method has achieved the optimal results for the four system configurations, and the second configuration scenario proved its optimal design compared to the other configurations. The second configuration which consists of the PV/Biomass/Battery, achieved the best results with the lowest EC by 0.10573885$/kWh, NPC by 3,097,141$, and LPSP by 0.03147283. The proposed GAHA technique can be improved even more by carefully examining its performance and identifying other alternatives to modify it for future work. To confirm its capacity to address other issues, it can also be tested for more cases. Additionally, the suggested approach can resolve issues with high dimensional feature selection, industrial engineering, allocating cloud computing resources, and parameter estimation issues. Future work will focus on developing configurations considering the biomass rate, biomass price, and inflation rate parameters.

7.1.7. Hybrid PV/Biomass/ELE/HT/FC System

This work's main objective is to assist officials, decision-makers, and the private sector in identifying advantages, opportunities, and obstacles to the future of solar and biomass energy in Egypt and potential profit opportunities. Hence, this will attract investments by the private sector to expand the use of solar and biomass energy as an alternative to traditional energy.

In this system, a recent optimization technique called MOA has been utilized to design a small stand-alone microgrid with the aim of meeting the electricity requirements of a small remote area in the Western Desert of Egypt with a peak load of 420 kW. This hybrid power system is based on two renewable resources, the PV modules and biomass generating system integrated with the FC and an electrolyzer for hydrogen production. This work aims to reduce the energy production cost, NPC, and GHG while maintaining high values of power supply reliability. In order to assess the accuracy of the proposed algorithm, its results have been compared with those obtained by other well-known techniques; STOA, WOA, and SCA. The simulation results demonstrated the proposed algorithm's effectiveness in identifying the optimal capacities of the generating and energy storage units in the proposed grid-independent hybrid system. The MOA has achieved the best optimal solution for the proposed system after 44 iterations with the minimum EC of 0.2106533 $/kWh, NPC of 6,170,134 $, LPSP of 0.05993 %, and GHG of 792.534 t/y.

7.2. Future Works

This research work leads to various promising topics for future investigations. The following recommendations are made for future research:

- Applying the proposed optimization algorithms for solving other complex optimization problems in electrical field or other areas.
- Solving the problem of optimal techno - economic and sizing of the suggested hybrid systems connected to the national grids.
- Developing configurations considering the biomass rate, biomass price, and inflation rate parameters.
- Developing various modeling, operation, and control methods, algorithms, methodologies, and techniques for use in the future development of electric vehicles and micro/smart grid technologies.
- Determine and investigate the possible configurations of the hybrid renewable systems using different types of storage technologies and components, for effective energy management.

List of Publications

Some contents of this thesis have been published to international conferences and journals indexed in Journal Citation Reports (JCR)/Science Edition (Thomson Reuters) as follows:

Journal papers (JCR):

[1] Abd El-Sattar, Hoda, et al. "Fixed bed gasification of corn stover biomass fuel: Egypt as a case study." Biofuels, Bioproducts and Biorefining 14.1 (2020): 7-19.

[2] Abd El-Sattar, Hoda, et al. "Tri-generation biomass system based on externally fired gas turbine, organic rankine cycle and absorption chiller." Journal of Cleaner Production 260 (2020): 121068.

[3] Abd El-Sattar, Hoda, et al. "Optimal design of stand-alone hybrid PV/wind/biomass/battery energy storage system in Abu-Monqar, Egypt." Journal of Energy Storage 44 (2021): 103336.

[4] Abd El-Sattar, Hoda, et al. "Performance Analysis of a Stand-Alone PV/WT/Biomass/Bat System in Alrashda Village in Egypt." Applied Sciences 11.21 (2021): 10191.

[5] Abd El-Sattar, Hoda, et al. "Optimal sizing of an off-grid hybrid photovoltaic/biomass gasifier/battery system using a quantum model of Runge Kutta algorithm." Energy Conversion and Management 258 (2022): 115539.

[6] Abd El-Sattar, Hoda, et al. "Optimal design of Photovoltaic, Biomass, Fuel Cell, Hydrogen Tank units and Electrolyzer hybrid system for a remote area in Egypt." Energy Reports 8 (2022): 9506-9527.

[7] Abd El-Sattar, Hoda, et al. "An effective optimization strategy for design of standalone hybrid renewable energy systems." Energy 260 (2022): 124901.

IEEE international conferences:

[8] Abd El-Sattar, Hoda, et al. "Optimal Design of Hybrid Stand-alone Microgrids Using Tunicate Swarm Algorithm." 2021 IEEE International Conference on Automation/XXIV Congress of the Chilean Association of Automatic Control (ICA-ACCA). IEEE, 2021.

References

[1] R. Vakulchuk, I. Overland, and D. Scholten, “Renewable energy and geopolitics : A review,” *Renew. Sustain. Energy Rev.*, vol. 122, no. June 2019, p. 109547, 2020, doi: 10.1016/j.rser.2019.109547.

[2] G. Deep, M. Ibrahim, U. Shahzad, and M. Jain, “Exploring the nexus between agriculture and greenhouse gas emissions in BIMSTEC region : The role of renewable energy and human capital as moderators,” *J. Environ. Manage.*, vol. 297, no. July, p. 113316, 2021, doi: 10.1016/j.jenvman.2021.113316.

[3] H. A. El-Sattar, S. Kamel, D. Vera, and F. Jurado, “Tri-generation biomass system based on externally fired gas turbine, organic rankine cycle and absorption chiller,” *J. Clean. Prod.*, vol. 260, 2020, doi: 10.1016/j.jclepro.2020.121068.

[4] “Global Energy Review 2020 – Analysis - IEA.” https://www.iea.org/reports/global-energy-review-2020 (accessed Sep. 09, 2020).

[5] “World Energy Outlook 2020 – Analysis - IEA.” https://www.iea.org/reports/world-energy-outlook-2020 (accessed Feb. 06, 2021).

[6] H. A. El-Sattar, S. Kamel, M. A. Tawfik, and D. Vera, “Modeling of a Downdraft Gasifier Combined with Externally Fired Gas Turbine using rice straw for generating electricity in Egypt,” in *2016 Eighteenth International Middle East Power Systems Conference (MEPCON)*, Dec. 2016, pp. 747–752. doi: 10.1109/MEPCON.2016.7836977.

[7] “Renewables | Energy Egypt.” https://energyegypt.net/category/renewables/ (accessed Sep. 10, 2020).

[8] “IRENA – International Renewable Energy Agency.” https://www.irena.org/ (accessed Sep. 09, 2020).

[9] International Renewable Energy Agency, *Renewable Energy Outlook: Egypt*. 2018. [Online]. Available: https://www.irena.org/publications/2018/Oct/Renewable-Energy-Outlook-Egypt

[10] “The Ministry of Electricity and Renewable Energy.” http://www.moee.gov.eg/english_new/home.aspx (accessed Feb. 07, 2021).

[11] H. B. A. Hassan, M. R. el Gebaly, S. S. A. Ghani, and Y. M. M. Hussein, “An economic study of recycling agricultural wastes in Egypt,” *Middle East J Agric Res*, vol. 3, no. 3, pp. 592–608, 2014.

[12] H. A. El-Sattar, S. Kamel, and F. Jurado, “Fixed bed gasification of corn stover biomass fuel: Egypt as a case study,” *Biofuels, Bioprod. Biorefining*, vol. 14, no. 1, pp. 7–19, 2020, doi: 10.1002/bbb.2044.

[13] H. Abd El-Sattar, S. Kamel, M. A. Tawfik, D. Vera, and F. Jurado, “Modeling and Simulation of Corn Stover Gasifier and Micro-turbine for Power Generation,” *Waste and Biomass Valorization*, vol. 10, no. 10, 2019, doi: 10.1007/s12649-018-0284-z.

[14] M. D. A. Al-falahi, S. D. G. Jayasinghe, and H. Enshaei, “A review on recent size optimization methodologies for standalone solar and wind hybrid renewable energy system,” *Energy Convers. Manag.*, vol. 143, pp. 252–274, 2017, doi: 10.1016/j.enconman.2017.04.019.

[15] C. Ammari, D. Belatrache, B. Touhami, and S. Makhloufi, “Sizing, optimization, control and energy management of hybrid renewable energy system—A review,” *Energy Built Environ.*, vol. 3, no. 4, pp. 399–411, 2021, doi: 10.1016/j.enbenv.2021.04.002.

[16] K. Ramasamy and C. S. Ravichandran, “Optimal design of renewable sources of PV/wind/FC generation for power system reliability and cost using MA-RBFNN approach,” *Int. J. Energy Res.*, vol. 45, no. 7, pp. 10946–10962, Jun. 2021, doi: 10.1002/er.6578.

[17] “Egypt - Renewable Energy | Privacy Shield.” https://www.privacyshield.gov/article?id=Egypt-Renewable-Energy (accessed Feb. 07, 2021).

[18] “Egypt - Renewable Energy.” https://www.trade.gov/knowledge-product/egypt-renewable-energy (accessed Feb. 07, 2021).

[19] “Land area (sq. km) - Egypt, Arab Rep. | Data.” https://data.worldbank.org/indicator/AG.LND.TOTL.K2?locations=EG (accessed Jan. 27, 2022).

[20] “Agricultural land (sq. km) - Egypt, Arab Rep. | Data.” https://data.worldbank.org/indicator/AG.LND.AGRI.K2?end=2020&locations=EG&most_recent_value_desc=false&start=1990&type=shaded&view=chart (accessed Jan. 27, 2022).

[21] “Egypt Arable Land 1961-2022 | MacroTrends.” https://www.macrotrends.net/countries/EGY/egypt/arable-land (accessed Jan. 27, 2022).

[22] "Egy Agri App." http://www.agri-db.org/ (accessed Aug. 20, 2018).

[23] "Ministry of Environment - EEAA > Home." http://www.eeaa.gov.eg/ (accessed Jul. 30, 2018).

[24] "Egypt Agriculture Sheet - Egypt Data Portal." http://egypt.opendataforafrica.org/kddlloe/egypt-agriculture-sheet (accessed May 01, 2018).

[25] U. Arena, "Process and technological aspects of municipal solid waste gasification . A review," *Waste Manag.*, vol. 32, no. 4, pp. 625–639, 2012, doi: 10.1016/j.wasman.2011.09.025.

[26] D. Yemshanov and D. McKenney, "Fast-growing poplar plantations as a bioenergy supply source for Canada," *Biomass and Bioenergy*, vol. 32, no. 3, pp. 185–197, 2008, doi: 10.1016/j.biombioe.2007.09.010.

[27] O. Ellabban, H. Abu-Rub, and F. Blaabjerg, "Renewable energy resources: Current status, future prospects and their enabling technology," *Renew. Sustain. Energy Rev.*, vol. 39, pp. 748–764, 2014, doi: 10.1016/j.rser.2014.07.113.

[28] H. M. Sultan, A. S. Menesy, S. Kamel, A. Korashy, S. A. Almohaimeed, and M. Abdel-Akher, "An improved artificial ecosystem optimization algorithm for optimal configuration of a hybrid PV/WT/FC energy system," *Alexandria Eng. J.*, vol. 60, no. 1, pp. 1001–1025, 2021, doi: 10.1016/j.aej.2020.10.027.

[29] H. Zhao, Q. Wu, S. Hu, H. Xu, and C. N. Rasmussen, "Review of energy storage system for wind power integration support," *Appl. Energy*, vol. 137, pp. 545–553, 2015, doi: 10.1016/j.apenergy.2014.04.103.

[30] A. Khan and N. Javaid, "Optimal sizing of a stand-alone photovoltaic, wind turbine and fuel cell systems," *Comput. Electr. Eng.*, vol. 85, 2020, doi: 10.1016/j.compeleceng.2020.106682.

[31] F. A. Alturki, A. A. Al-Shamma'a, H. M. H. Farh, and K. AlSharabi, "Optimal sizing of autonomous hybrid energy system using supply-demand-based optimization algorithm," *Int. J. Energy Res.*, vol. 45, no. 1, pp. 605–625, Jan. 2021, doi: 10.1002/er.5766.

[32] T. Khatib, I. A. Ibrahim, and A. Mohamed, "A review on sizing methodologies of photovoltaic array and storage battery in a standalone photovoltaic system," *Energy Convers. Manag.*, vol. 120, pp. 430–448, Jul. 2016, doi: 10.1016/j.enconman.2016.05.011.

[33] R. Poli, J. Kennedy, and T. Blackwell, “Particle swarm optimization: An overview,” *Swarm Intell.*, vol. 1, no. 1, pp. 33–57, 2007, doi: 10.1007/s11721-007-0002-0.

[34] Lawrence Davis, *Handbook of genetic algorithms*, vol. 1st editio, no. 1st edition. 1991. doi: 10.1017/S0269888900006068.

[35] B. Bala and S. A. Siddique, “Optimal design of a PV-diesel hybrid system for electrification of an isolated island—Sandwip in Bangladesh using genetic algorithm,” *Energy Sustain. Dev.*, vol. 13, no. 3, pp. 137–142, Sep. 2009, doi: 10.1016/j.esd.2009.07.002.

[36] D. Karaboga and B. Basturk, “A powerful and efficient algorithm for numerical function optimization: artificial bee colony (ABC) algorithm,” *J. Glob. Optim.*, vol. 39, no. 3, pp. 459–471, Oct. 2007, doi: 10.1007/s10898-007-9149-x.

[37] Zong Woo Geem, Joong Hoon Kim, and G. V. Loganathan, “A New Heuristic Optimization Algorithm: Harmony Search,” *Simulation*, vol. 76, no. 2, pp. 60–68, Feb. 2001, doi: 10.1177/003754970107600201.

[38] S. Saremi, S. Mirjalili, and A. Lewis, “Grasshopper Optimisation Algorithm: Theory and application,” *Adv. Eng. Softw.*, vol. 105, pp. 30–47, Mar. 2017, doi: 10.1016/j.advengsoft.2017.01.004.

[39] A. Khan *et al.*, “Enhanced Evolutionary Sizing Algorithms for Optimal Sizing of a Stand-Alone PV-WT-Battery Hybrid System,” *Appl. Sci.*, vol. 9, no. 23, p. 5197, Nov. 2019, doi: 10.3390/app9235197.

[40] X. S. Yang, “Optimization and Metaheuristic Algorithms in Engineering,” in *Metaheuristics in Water, Geotechnical and Transport Engineering*, no. January 1970, 2013, pp. 1–23. doi: 10.1016/B978-0-12-398296-4.00001-5.

[41] F. L. Howard, “ the Life History of Physarum Polycephalum ,” *Am. J. Bot.*, vol. 18, no. 2, pp. 116–133, 1931, doi: 10.1002/j.1537-2197.1931.tb09577.x.

[42] S. Li, H. Chen, M. Wang, A. A. Heidari, and S. Mirjalili, “Slime mould algorithm: A new method for stochastic optimization,” *Futur. Gener. Comput. Syst.*, vol. 111, pp. 300–323, 2020, doi: 10.1016/j.future.2020.03.055.

[43] C. Kumar, T. D. Raj, M. Premkumar, and T. D. Raj, “A New Stochastic Slime Mould Optimization Algorithm for the Estimation of Solar Photovoltaic Cell Parameters,” *Optik (Stuttg).*, p. 165277, 2020, doi: 10.1016/j.ijleo.2020.165277.

[44] G. Dhiman and V. Kumar, “Seagull optimization algorithm: Theory and its applications for large-scale industrial engineering problems,” *Knowledge-Based Syst.*,

vol. 165, pp. 169–196, 2019, doi: 10.1016/j.knosys.2018.11.024.

[45] H. Jia, Z. Xing, and W. Song, "A New Hybrid Seagull Optimization Algorithm for Feature Selection," *IEEE Access*, vol. 7, pp. 49614–49631, 2019, doi: 10.1109/ACCESS.2019.2909945.

[46] G. Dhiman and V. Kumar, "Spotted hyena optimizer: A novel bio-inspired based metaheuristic technique for engineering applications," *Adv. Eng. Softw.*, vol. 114, pp. 48–70, 2017, doi: 10.1016/j.advengsoft.2017.05.014.

[47] Q. Chen, B. Liu, Q. Zhang, and J. Liang, "Evaluation Criteria for CEC 2015 Special Session and Competition on Bound Constrained Single-Objective Computationally Expensive Numerical Optimization," *Mysites.Ntu.Edu.Sg*, 2015, [Online]. Available: http://web.mysites.ntu.edu.sg/epnsugan/PublicSite/Shared Documents/CEC-2015/Expensive Problems/CEC15-single objective optimization competition - expensive.pdf

[48] Q. Askari, M. Saeed, and I. Younas, "Heap-based optimizer inspired by corporate rank hierarchy for global optimization," *Expert Syst. Appl.*, vol. 161, p. 113702, 2020, doi: 10.1016/j.eswa.2020.113702.

[49] M. Ghasemi, S. Ghavidel, J. Aghaei, E. Akbari, and L. Li, "CFA optimizer: A new and powerful algorithm inspired by Franklin's and Coulomb's laws theory for solving the economic load dispatch problems," *Int. Trans. Electr. Energy Syst.*, vol. 28, no. 5, pp. 1–30, 2018, doi: 10.1002/etep.2536.

[50] G. Dhiman and A. Kaur, "STOA: A bio-inspired based optimization algorithm for industrial engineering problems," *Eng. Appl. Artif. Intell.*, vol. 82, no. January, pp. 148–174, 2019, doi: 10.1016/j.engappai.2019.03.021.

[51] K. Zervoudakis and S. Tsafarakis, "A mayfly optimization algorithm," *Comput. Ind. Eng.*, vol. 145, no. May, 2020, doi: 10.1016/j.cie.2020.106559.

[52] Z. Gao, J. Zhao, S. Li, and Y. Hu, "The improved mayfly optimization algorithm The improved mayfly optimization algorithm," *J. Phys. Conf. Ser.*, vol. 1684, p. 012077, 2020, doi: 10.1088/1742-6596/1684/1/012077.

[53] X. Guo, X. Yan, and K. Jermsittiparsert, "Using the modified mayfly algorithm for optimizing the component size and operation strategy of a high temperature PEMFC-powered CCHP," *Energy Reports*, vol. 7, pp. 1234–1245, 2021, doi: 10.1016/j.egyr.2021.02.042.

[54] C. Diyoke, N. Gao, M. Aneke, M. Wang, and C. Wu, "Modelling of down-draft

gasification of biomass – An integrated pyrolysis, combustion and reduction process," *Appl. Therm. Eng.*, vol. 142, no. July, pp. 444–456, 2018, doi: 10.1016/j.applthermaleng.2018.06.079.

[55] W. Gao *et al.*, "Techno-economic evaluation of biomass-to-synthesis gas (BtS) based on gasification," *Energy Sources, Part B Econ. Plan. Policy*, vol. 13, no. 2, pp. 83–90, 2018, doi: 10.1080/15567249.2016.1241839.

[56] X. Zhang *et al.*, "Thermodynamic and economic analysis of biomass partial gasification process," *Appl. Therm. Eng.*, vol. 129, pp. 410–420, 2018, doi: 10.1016/j.applthermaleng.2017.10.069.

[57] A. Datta, R. Ganguly, and L. Sarkar, "Energy and exergy analyses of an externally fired gas turbine (EFGT) cycle integrated with biomass gasifier for distributed power generation," *Energy*, vol. 35, no. 1, pp. 341–350, 2009, doi: 10.1016/j.energy.2009.09.031.

[58] A. Perna, M. Minutillo, E. Jannelli, V. Cigolotti, S. W. Nam, and K. J. Yoon, "Performance assessment of a hybrid SOFC/MGT cogeneration power plant fed by syngas from a biomass down-draft gasifier," *Appl. Energy*, vol. 227, no. May 2017, pp. 80–91, 2017, doi: 10.1016/j.apenergy.2017.08.077.

[59] D. Vera, F. Jurado, J. Carpio, and S. Kamel, "Biomass gasification coupled to an EFGT-ORC combined system to maximize the electrical energy generation: A case applied to the olive oil industry," *Energy*, vol. 144, pp. 41–53, 2018, doi: 10.1016/j.energy.2017.11.152.

[60] Y. Cao, Y. Gao, Y. Zheng, and Y. Dai, "Optimum design and thermodynamic analysis of a gas turbine and ORC combined cycle with recuperators," *Energy Convers. Manag.*, vol. 116, pp. 32–41, 2016, doi: 10.1016/j.enconman.2016.02.073.

[61] S. M. Camporeale, A. M. Pantaleo, P. D. Ciliberti, and B. Fortunato, "Cycle configuration analysis and techno-economic sensitivity of biomass externally fired gas turbine with bottoming ORC," *Energy Convers. Manag.*, vol. 105, pp. 1239–1250, 2015, doi: 10.1016/j.enconman.2015.08.069.

[62] D. Maraver, S. Quoilin, and J. Royo, "Optimization of Biomass-Fuelled Combined Cooling, Heating and Power (CCHP) Systems Integrated with Subcritical or Transcritical Organic Rankine Cycles (ORCs)," *Entropy*, vol. 16, pp. 2433–2453, 2014, doi: 10.3390/e16052433.

[63] H. Ozcan and I. Dincer, "Performance evaluation of an SOFC based trigeneration

system using various gaseous fuels from biomass gasification," *Int. J. Hydrogen Energy*, vol. 40, no. 24, pp. 7798–7807, 2014, doi: 10.1016/j.ijhydene.2014.11.109.

[64] S. Chattopadhyay and S. Ghosh, "Combined energetic and exergetic assessment of a biomass-based integrated power and refrigeration plant," *J. Brazilian Soc. Mech. Sci. Eng.*, vol. 40, no. 3, pp. 1–13, 2018, doi: 10.1007/s40430-018-1060-5.

[65] J. Kalina, "Integrated biomass gasification combined cycle distributed generation plant with reciprocating gas engine and ORC," *Appl. Therm. Eng.*, vol. 31, no. 14–15, pp. 2829–2840, 2011, doi: 10.1016/j.applthermaleng.2011.05.008.

[66] J. Li, P. Liu, and Z. Li, "Optimal design and techno-economic analysis of a solar-wind-biomass off-grid hybrid power system for remote rural electrification: A case study of west China," *Energy*, vol. 208, p. 118387, 2020, doi: 10.1016/j.energy.2020.118387.

[67] H. Hassani, F. Zaouche, D. Rekioua, S. Belaid, T. Rekioua, and S. Bacha, "Feasibility of a standalone photovoltaic/battery system with hydrogen production," *J. Energy Storage*, vol. 31, no. February, p. 101644, 2020, doi: 10.1016/j.est.2020.101644.

[68] S. Mandal, B. K. Das, and N. Hoque, "Optimum sizing of a stand-alone hybrid energy system for rural electrification in Bangladesh," *J. Clean. Prod.*, vol. 200, pp. 12–27, 2018, doi: 10.1016/j.jclepro.2018.07.257.

[69] D. Tsuanyo, Y. Azoumah, D. Aussel, and P. Neveu, "Modeling and optimization of batteryless hybrid PV (photovoltaic)/Diesel systems for off-grid applications," *Energy*, vol. 86, pp. 152–163, 2015, doi: 10.1016/j.energy.2015.03.128.

[70] A. Maleki and F. Pourfayaz, "Sizing of stand-alone photovoltaic/wind/diesel system with battery and fuel cell storage devices by harmony search algorithm," *J. Energy Storage*, vol. 2, pp. 30–42, 2015, doi: 10.1016/j.est.2015.05.006.

[71] S. Singh and S. C. Kaushik, "Optimal sizing of grid integrated hybrid PV-biomass energy system using artificial bee colony algorithm," *IET Renew. Power Gener.*, vol. 10, no. 5, pp. 642–650, 2016, doi: 10.1049/iet-rpg.2015.0298.

[72] L. Al-Ghussain, H. Ahmed, and F. Haneef, "Optimization of hybrid PV-wind system: Case study Al-Tafilah cement factory, Jordan," *Sustain. Energy Technol. Assessments*, vol. 30, no. August, pp. 24–36, 2018, doi: 10.1016/j.seta.2018.08.008.

[73] D. Mazzeo, G. Oliveti, C. Baglivo, and P. M. Congedo, "Energy reliability-constrained method for the multi-objective optimization of a photovoltaic-wind hybrid system with battery storage," *Energy*, vol. 156, pp. 688–708, 2018, doi: 10.1016/j.energy.2018.04.062.

[74] K. Anoune, A. Laknizi, M. Bouya, A. Astito, and A. Ben Abdellah, "Sizing a PV-Wind based hybrid system using deterministic approach," *Energy Convers. Manag.*, vol. 169, no. January, pp. 137–148, 2018, doi: 10.1016/j.enconman.2018.05.034.

[75] D. Mazzeo, N. Matera, and G. Oliveti, "Interaction between a Wind-PV-Battery-Heat Pump Trigeneration System and Office Building Electric Energy Demand Including Vehicle Charging," *Proc. - 2018 IEEE Int. Conf. Environ. Electr. Eng. 2018 IEEE Ind. Commer. Power Syst. Eur. EEEIC/I CPS Eur. 2018*, pp. 0–6, 2018, doi: 10.1109/EEEIC.2018.8493710.

[76] D. Mazzeo, "Solar and wind assisted heat pump to meet the building air conditioning and electric energy demand in the presence of an electric vehicle charging station and battery storage," *J. Clean. Prod.*, vol. 213, pp. 1228–1250, 2019, doi: 10.1016/j.jclepro.2018.12.212.

[77] D. Mazzeo *et al.*, "Artificial intelligence application for the performance prediction of a clean energy community," *Energy*, vol. 232, p. 120999, 2021, doi: 10.1016/j.energy.2021.120999.

[78] A. A. Z. Diab, H. M. Sultan, I. S. Mohamed, O. N. Kuznetsov, and T. D. Do, "Application of Different Optimization Algorithms for Optimal Sizing of PV/Wind/Diesel/Battery Storage Stand-Alone Hybrid Microgrid," *IEEE Access*, vol. 7, pp. 119223–119245, 2019, doi: 10.1109/access.2019.2936656.

[79] M. A. M. Ramli, H. R. E. H. Bouchekara, and A. S. Alghamdi, "Optimal sizing of PV/wind/diesel hybrid microgrid system using multi-objective self-adaptive differential evolution algorithm," *Renew. Energy*, vol. 121, pp. 400–411, 2018, doi: 10.1016/j.renene.2018.01.058.

[80] A. L. Bukar, C. W. Tan, and K. Y. Lau, "Optimal sizing of an autonomous photovoltaic/wind/battery/diesel generator microgrid using grasshopper optimization algorithm," *Sol. Energy*, vol. 188, no. May, pp. 685–696, 2019, doi: 10.1016/j.solener.2019.06.050.

[81] A. Yahiaoui, F. Fodhil, K. Benmansour, M. Tadjine, and N. Cheggaga, "Grey wolf optimizer for optimal design of hybrid renewable energy system PV-Diesel Generator-Battery : Application to the case of Djanet city of Algeria," *Sol. Energy*, vol. 158, no. October, pp. 941–951, 2017, doi: 10.1016/j.solener.2017.10.040.

[82] D. K. Geleta, M. S. Manshahia, P. Vasant, and A. Banik, "Grey wolf optimizer for optimal sizing of hybrid wind and solar renewable energy system," *Comput. Intell.*, no.

April, pp. 1–30, 2020, doi: 10.1111/coin.12349.

[83] A. Maleki, M. A. Nazari, and F. Pourfayaz, "Harmony search optimization for optimum sizing of hybrid solar schemes based on battery storage unit," *Energy Reports*, 2020, doi: 10.1016/j.egyr.2020.03.014.

[84] A. Fathy, K. Kaaniche, and T. M. Alanazi, "Recent Approach Based Social Spider Optimizer for Optimal Sizing of Hybrid PV/Wind/Battery/Diesel Integrated Microgrid in Aljouf Region," *IEEE Access*, vol. 8, pp. 57630–57645, 2020, doi: 10.1109/ACCESS.2020.2982805.

[85] M. B. Eteiba, S. Barakat, M. M. Samy, and W. I. Wahba, "Optimization of an off-grid PV/Biomass hybrid system with different battery technologies," *Sustain. Cities Soc.*, vol. 40, pp. 713–727, 2018, doi: 10.1016/j.scs.2018.01.012.

[86] A. González, J. R. Riba, and A. Rius, "Optimal sizing of a hybrid grid-connected photovoltaic-wind-biomass power system," *Sustain.*, vol. 7, no. 9, pp. 12787–12806, 2015, doi: 10.3390/su70912787.

[87] A. Gonzalez, J. R. Riba, B. Esteban, and A. Rius, "Environmental and cost optimal design of a biomass–Wind–PV electricity generation system," *Renew. Energy*, vol. 126, pp. 420–430, 2018, doi: 10.1016/j.renene.2018.03.062.

[88] C. Serir, D. Rekioua, N. Mezzai, and S. Bacha, "ScienceDirect Supervisor control and optimization of multi-sources pumping system with battery storage," *Int. J. Hydrogen Energy*, pp. 1–13, 2016, doi: 10.1016/j.ijhydene.2016.05.096.

[89] W. Cai *et al.*, "Optimal sizing and location based on economic parameters for an off-grid application of a hybrid system with photovoltaic, battery and diesel technology," *Energy*, vol. 201, p. 117480, 2020, doi: 10.1016/j.energy.2020.117480.

[90] A. A. Zaki Diab, S. I. El-Ajmi, H. M. Sultan, and Y. B. Hassan, "Modified farmland fertility optimization algorithm for optimal design of a grid-connected hybrid renewable energy system with fuel cell storage: Case study of Ataka, Egypt," *Int. J. Adv. Comput. Sci. Appl.*, vol. 10, no. 8, pp. 119–132, 2019.

[91] M. Kharrich *et al.*, "Developed approach based on equilibrium optimizer for optimal design of hybrid PV/Wind/Diesel/Battery Microgrid in Dakhla, Morocco," *IEEE Access*, vol. 9, pp. 13655–13670, 2021, doi: 10.1109/ACCESS.2021.3051573.

[92] M. Suresh and R. Meenakumari, "An improved genetic algorithm-based optimal sizing of solar photovoltaic/wind turbine generator/diesel generator/battery connected hybrid energy systems for standalone applications," *Int. J. Ambient Energy*, vol. 0, no. 0, pp.

1–20, 2019, doi: 10.1080/01430750.2019.1587720.

[93] M. Kharrich, O. H. Mohammed, N. Alshammari, and M. Akherraz, “Multi-objective optimization and the effect of the economic factors on the design of the microgrid hybrid system,” *Sustain. Cities Soc.*, vol. 65, p. 102646, 2021, doi: 10.1016/j.scs.2020.102646.

[94] A. Naderipour, Z. Abdul-Malek, M. Zahedi Vahid, Z. Mirzaei Seifabad, M. Hajivand, and S. Arabi-Nowdeh, “Optimal, Reliable and Cost-Effective Framework of Photovoltaic-Wind-Battery Energy System Design Considering Outage Concept Using Grey Wolf Optimizer Algorithm - Case Study for Iran,” *IEEE Access*, vol. 7, pp. 182611–182623, 2019, doi: 10.1109/ACCESS.2019.2958964.

[95] S. Sanajaoba, “Optimal sizing of off-grid hybrid energy system based on minimum cost of energy and reliability criteria using firefly algorithm,” *Sol. Energy*, vol. 188, no. February, pp. 655–666, 2019, doi: 10.1016/j.solener.2019.06.049.

[96] A. Tabak, E. Kayabasi, M. T. Guneser, and M. Ozkaymak, “Grey wolf optimization for optimum sizing and controlling of a PV/WT/BM hybrid energy system considering TNPC, LPSP, and LCOE concepts,” *Energy Sources, Part A Recover. Util. Environ. Eff.*, vol. 00, no. 00, pp. 1–21, 2019, doi: 10.1080/15567036.2019.1668880.

[97] N. Alshammari and J. Asumadu, “Optimum unit sizing of hybrid renewable energy system utilizing harmony search, Jaya and particle swarm optimization algorithms,” *Sustain. Cities Soc.*, vol. 60, no. March, p. 102255, 2020, doi: 10.1016/j.scs.2020.102255.

[98] S. Ghosh and V. Karar, “Assimilation of optimal sized hybrid photovoltaic-biomass system by dragonfly algorithm with grid,” *Energies*, vol. 11, no. 7, 2018, doi: 10.3390/en11071892.

[99] F. A. Alturki and E. M. Awwad, “Sizing and Cost Minimization of Standalone Hybrid WT/PV/Biomass/Pump-Hydro Storage-Based Energy Systems,” *Energies*, vol. 14, no. 2, p. 489, 2021, doi: 10.3390/en14020489.

[100] M. Das, M. A. K. Singh, and A. Biswas, “Techno-economic optimization of an off-grid hybrid renewable energy system using metaheuristic optimization approaches – Case of a radio transmitter station in India,” *Energy Convers. Manag.*, vol. 185, no. August 2018, pp. 339–352, 2019, doi: 10.1016/j.enconman.2019.01.107.

[101] R. Shi, W. Wang, Z. Yuan, X. Fan, and E. Ramezani, “A novel optimum arrangement for a hybrid renewable energy system using developed student psychology based

optimizer: A case study," *Energy Reports*, vol. 7, pp. 70–80, 2021, doi: 10.1016/j.egyr.2020.11.168.

[102] W. Dong, Y. Li, and J. Xiang, "Optimal sizing of a stand-alone hybrid power system based on battery/hydrogen with an improved ant colony optimization," *Energies*, vol. 9, no. 10, 2016, doi: 10.3390/en9100785.

[103] N. S. Attemene, K. S. Agbli, S. Fofana, and D. Hissel, "Optimal sizing of a wind, fuel cell, electrolyzer, battery and supercapacitor system for off-grid applications," *Int. J. Hydrogen Energy*, vol. 45, no. 8, pp. 5512–5525, 2020, doi: 10.1016/j.ijhydene.2019.05.212.

[104] A. C. Duman and Ö. Güler, "Techno-economic analysis of off-grid PV/wind/fuel cell hybrid system combinations with a comparison of regularly and seasonally occupied households," *Sustain. Cities Soc.*, vol. 42, pp. 107–126, 2018, doi: 10.1016/j.scs.2018.06.029.

[105] M. Jamshidi and A. Askarzadeh, "Techno-economic analysis and size optimization of an off-grid hybrid photovoltaic, fuel cell and diesel generator system," *Sustain. Cities Soc.*, vol. 44, pp. 310–320, 2019, doi: 10.1016/j.scs.2018.10.021.

[106] M. Gharibi and A. Askarzadeh, "Technical and economical bi-objective design of a grid-connected photovoltaic/diesel generator/fuel cell energy system," *Sustain. Cities Soc.*, vol. 50, no. April, p. 101575, 2019, doi: 10.1016/j.scs.2019.101575.

[107] A. Fathy, "A reliable methodology based on mine blast optimization algorithm for optimal sizing of hybrid PV-wind-FC system for remote area in Egypt," *Renew. Energy*, vol. 95, pp. 367–380, 2016, doi: 10.1016/j.renene.2016.04.030.

[108] M. J. Hadidian Moghaddam, A. Kalam, S. A. Nowdeh, A. Ahmadi, M. Babanezhad, and S. Saha, "Optimal sizing and energy management of stand-alone hybrid photovoltaic/wind system based on hydrogen storage considering LOEE and LOLE reliability indices using flower pollination algorithm," *Renew. Energy*, vol. 135, pp. 1412–1434, 2019, doi: 10.1016/j.renene.2018.09.078.

[109] "Egypt Corn Production by Year (1000 MT)." https://www.indexmundi.com/agriculture/?country=eg&commodity=corn&graph=production (accessed Sep. 28, 2018).

[110] J. S. Tumuluru, "Comparison of Chemical Composition and Energy Property of Torrefied Switchgrass and Corn Stover," vol. 3, no. November, pp. 1–11, 2015, doi: 10.3389/fenrg.2015.00046.

[111] M. El Achaby *et al.*, “Processing and properties of eco-friendly bio-nanocomposite films filled with cellulose nanocrystals from sugarcane bagasse,” *Int. J. Biol. Macromol.*, vol. 96, pp. 340–352, 2017, doi: 10.1016/j.ijbiomac.2016.12.040.

[112] M. O. de Souza Dias *et al.*, “Sugarcane processing for ethanol and sugar in Brazil,” *Environ. Dev.*, vol. 15, pp. 35–51, 2015, doi: 10.1016/j.envdev.2015.03.004.

[113] S. M. Atnaw, S. A. Sulaiman, and S. Yusup, “Biomass gasification,” in *Waste Biomass Management - A Holistic Approach*, 2017. doi: 10.1007/978-3-319-49595-8_8.

[114] A. Bhavanam and R. C. Sastry, “Biomass Gasification Processes in Downdraft Fixed Bed Reactors : A Review,” *Int. J. Chem. Eng. Appl.*, vol. 2, no. 6, pp. 425–433, 2011, doi: 10.1016/S0140-6701(98)96589-4.

[115] J. Ahrenfeldt, T. P. Thomsen, U. Henriksen, and L. R. Clausen, “Biomass gasification cogeneration - A review of state of the art technology and near future perspectives,” *Appl. Therm. Eng.*, vol. 50, no. 2, pp. 1407–1417, 2013, doi: 10.1016/j.applthermaleng.2011.12.040.

[116] A. Melgar, J. F. Pérez, H. Laget, and A. Horillo, “Thermochemical equilibrium modelling of a gasifying process,” *Energy Convers. Manag.*, vol. 48, no. 1, pp. 59–67, 2007, doi: 10.1016/j.enconman.2006.05.004.

[117] Z. A. Zainal, R. Ali, C. H. Lean, and K. N. Seetharamu, “Prediction of performance of a downdraft gasifier using equilibrium modeling for different biomass materials,” *Energy Convers. Manag.*, vol. 42, no. 12, pp. 1499–1515, 2001, doi: 10.1016/S0196-8904(00)00078-9.

[118] J. George, P. Arun, and C. Muraleedharan, “Stoichiometric Equilibrium Model Based Assessment of Hydrogen Generation through Biomass Gasification,” *Procedia Technol.*, vol. 25, no. Raerest, pp. 982–989, 2016, doi: 10.1016/j.protcy.2016.08.194.

[119] A. Kumar, D. D. Jones, and M. A. Hanna, “Thermochemical biomass gasification: A review of the current status of the technology,” *Energies*, vol. 2, no. 3, pp. 556–581, 2009, doi: 10.3390/en20300556.

[120] B. Fortunato, G. Brunetti, S. M. Camporeale, M. Torresi, and F. Fornarelli, “Thermodynamic model of a downdraft gasifier,” *Energy Convers. Manag.*, vol. 140, pp. 281–294, 2017, doi: 10.1016/j.enconman.2017.02.061.

[121] N. Tippayawong, S. Pang, and J. Fournier, “Biomass gasification in a fixed downdraft reactor with oxygen enriched air : a modified equilibrium modeling study,” *Energy Procedia*, vol. 160, no. April 2019, pp. 317–323, 2019, doi:

10.1016/j.egypro.2019.02.163.

[122] H. A. El-Sattar, S. Kamel, M. A. Tawfik, D. Vera, and F. Jurado, “Modeling and Simulation of Corn Stover Gasifier and Micro-turbine for Power Generation,” *Waste and Biomass Valorization*, vol. 10, no. 10, pp. 1–14, 2018, doi: 10.1007/s12649-018-0284-z.

[123] C. Bang-Møller and M. Rokni, “Thermodynamic performance study of biomass gasification, solid oxide fuel cell and micro gas turbine hybrid systems,” *Energy Convers. Manag.*, vol. 51, no. 11, pp. 2330–2339, 2010, doi: 10.1016/j.enconman.2010.04.006.

[124] A. Gambarotta, M. Morini, and A. Zubani, “A non-stoichiometric equilibrium model for the simulation of the biomass gasification process,” *Appl. Energy*, no. July, pp. 1–9, 2017, doi: 10.1016/j.apenergy.2017.07.135.

[125] C. Dejtrakulwong and S. Patumsawad, “Four zones modeling of the downdraft biomass gasification process: Effects of moisture content and air to fuel ratio,” *Energy Procedia*, vol. 52, pp. 142–149, 2014, doi: 10.1016/j.egypro.2014.07.064.

[126] N. Gao and A. Li, “Modeling and simulation of combined pyrolysis and reduction zone for a downdraft biomass gasifier,” *Energy Convers. Manag.*, vol. 49, no. 12, pp. 3483–3490, 2008, doi: 10.1016/j.enconman.2008.08.002.

[127] T. K. Patra and P. N. Sheth, “Biomass gasification models for downdraft gasifier: A state-of-the-art review,” *Renew. Sustain. Energy Rev.*, vol. 50, pp. 583–593, 2015, doi: 10.1016/j.rser.2015.05.012.

[128] B. V. Babu and P. N. Sheth, “Modeling and simulation of reduction zone of downdraft biomass gasifier: Effect of char reactivity factor,” *Energy Convers. Manag.*, vol. 47, no. 15–16, pp. 2602–2611, 2006, doi: 10.1016/j.enconman.2005.10.032.

[129] A. Perna, M. Minutillo, S. P. Cicconardi, E. Jannelli, and S. Scarfogliero, “Conventional and advanced biomass gasification power plants designed for cogeneration purpose,” *Energy Procedia*, vol. 82, pp. 687–694, 2015, doi: 10.1016/j.egypro.2015.11.793.

[130] M. Kouhia, “Biomass Gasification,” 2011.

[131] A. Kumar, H. Noureddini, Y. Demirel, D. D. Jones, and M. A. Hanna, “Simulation of Corn Stover and Distillers Grains Gasification with Aspen Plus,” *Trans. ASABE*, vol. 52, no. 6, pp. 1989–1995, 2009.

[132] S. A. Channiwala and P. P. Parikh, “A unified correlation for estimating HHV of solid,

liquid and gaseous fuels," *Fuel*, vol. 81, no. 8, pp. 1051–1063, 2002, doi: 10.1016/S0016-2361(01)00131-4.

[133] K. A. Al-attab and Z. A. Zainal, "Externally fired gas turbine technology: A review," *Appl. Energy*, vol. 138, pp. 474–487, 2015, doi: 10.1016/j.apenergy.2014.10.049.

[134] S. Soltani, S. M. S. Mahmoudi, M. Yari, and M. A. Rosen, "Thermodynamic analyses of an externally fired gas turbine combined cycle integrated with a biomass gasification plant," *Energy Convers. Manag.*, vol. 70, pp. 107–115, 2013, doi: 10.1016/j.enconman.2013.03.002.

[135] K. A. Al-attab and Z. A. Zainal, "Externally fired gas turbine technology : A review," *Appl. Energy*, vol. 138, pp. 474–487, 2015, doi: 10.1016/j.apenergy.2014.10.049.

[136] D. Roy, S. Samanta, and S. Ghosh, "Techno-economic and environmental analyses of a biomass based system employing solid oxide fuel cell, externally fired gas turbine and organic Rankine cycle," *J. Clean. Prod.*, vol. 225, pp. 36–57, 2019, doi: 10.1016/j.jclepro.2019.03.261.

[137] M. Rahman and A. Malmquist, "Modeling and Simulation of an Externally Fired Micro-Gas Turbine for Standalone Polygeneration Application," *J. Eng. Gas Turbines Power*, vol. 138, no. 11, p. 112301, 2016, doi: 10.1115/1.4033510.

[138] D. Vera, F. Jurado, and J. Carpio, "Study of a downdraft gasifier and externally fired gas turbine for olive industry wastes," *Fuel Process. Technol.*, vol. 92, no. 10, pp. 1970–1979, 2011, doi: 10.1016/j.fuproc.2011.05.017.

[139] A. Uusitalo, J. Honkatukia, T. Turunen-Saaresti, and A. Grönman, "Thermodynamic evaluation on the effect of working fluid type and fluids critical properties on design and performance of Organic Rankine Cycles," *J. Clean. Prod.*, vol. 188, pp. 253–263, 2018, doi: 10.1016/j.jclepro.2018.03.228.

[140] H. Zhang, X. Guan, Y. Ding, and C. Liu, "Emergy analysis of Organic Rankine Cycle (ORC) for waste heat power generation," *J. Clean. Prod.*, vol. 183, pp. 1207–1215, 2018, doi: 10.1016/j.jclepro.2018.02.170.

[141] C. Sprouse and C. Depcik, "Review of organic Rankine cycles for internal combustion engine exhaust waste heat recovery," *Appl. Therm. Eng.*, vol. 51, no. 1–2, pp. 711–722, 2013, doi: 10.1016/j.applthermaleng.2012.10.017.

[142] T. Deethayat, T. Kiatsiriroat, and C. Thawonngamyingsakul, "Performance analysis of an organic Rankine cycle with internal heat exchanger having zeotropic working fluid," *Case Stud. Therm. Eng.*, vol. 6, pp. 155–161, 2015, doi:

10.1016/j.csite.2015.09.003.

[143] K. Darvish, M. A. Ehyaei, F. Atabi, and M. A. Rosen, "Selection of optimum working fluid for organic rankine cycles by exergy and exergy-economic analyses," *Sustain.*, vol. 7, no. 11, pp. 15362–15383, 2015, doi: 10.3390/su71115362.

[144] H. Yu, X. Feng, and Y. Wang, "A new pinch based method for simultaneous selection of working fluid and operating conditions in an ORC (Organic Rankine Cycle) recovering waste heat," *Energy*, vol. 90, pp. 36–46, 2015, doi: 10.1016/j.energy.2015.02.059.

[145] P. Colonna and S. Gabrielli, "Industrial trigeneration using ammonia-water absorption refrigeration systems (AAR)," *Appl. Therm. Eng.*, vol. 23, no. 4, pp. 381–396, 2003, doi: 10.1016/S1359-4311(02)00212-0.

[146] "Cycle-Tempo." http://www.asimptote.nl/software/cycle-tempo/ (accessed Aug. 27, 2018).

[147] O. W. Mohammed and G. Yanling, "Comprehensive Parametric Study of a Solar Absorption Refrigeration System to Lower Its Cut In / Off Temperature," *Energies*, vol. 10, p. 26, 2017, doi: 10.3390/en10111746.

[148] E. Conversion, M. Education, and T. Education, "Effect of heat exchangers on performance of absorption refrigeration systems," *Energy Convers. Manag.*, vol. 42, pp. 1699–1716, 2001.

[149] "Thermophysical Properties of Fluid Systems." https://webbook.nist.gov/chemistry/fluid/ (accessed Jul. 27, 2018).

[150] J. Wang, M. Diao, and K. Yue, "Optimization on pinch point temperature difference of ORC system based on AHP-Entropy method," *Energy*, vol. 141, pp. 97–107, 2017, doi: 10.1016/j.energy.2017.09.052.

[151] M. Ryms, T. Pyś, and E. Klugmann-Radziemska, "Adapting the pinch point analysis to improve the ORC design process," *Int. J. energy Res.*, vol. 38, no. 2014, pp. 29–40, 2014, doi: 10.1002/er.

[152] M. Khennich and N. Galanis, "Optimal design of ORC systems with a low-temperature heat source," *Entropy*, vol. 14, no. 2, pp. 370–389, 2012, doi: 10.3390/e14020370.

[153] F. A. Al-sulaiman, I. Dincer, and F. Hamdullahpur, "Energy and exergy analyses of a biomass trigeneration system using an organic Rankine Cycle," *Energy*, vol. 45, no. 1, pp. 975–985, 2016, doi: 10.1016/j.energy.2012.06.060.

[154] B. de Mena, D. Vera, F. Jurado, and M. Ortega, “Updraft gasifier and ORC system for high ash content biomass: A modelling and simulation study,” *Fuel Process. Technol.*, vol. 156, pp. 394–406, 2017, doi: 10.1016/j.fuproc.2016.09.031.

[155] Z. Yu, J. Han, H. Liu, and H. Zhao, “Theoretical study on a novel ammonia – water cogeneration system with adjustable cooling to power ratios,” *Appl. Energy*, vol. 122, pp. 53–61, 2014, doi: 10.1016/j.apenergy.2014.02.010.

[156] H. M. Sultan, O. N. Kuznetsov, and A. A. Z. Diab, “Site selection of large-scale grid-connected solar PV system in Egypt,” *Proc. 2018 IEEE Conf. Russ. Young Res. Electr. Electron. Eng. ElConRus 2018*, vol. 2018-Janua, pp. 813–818, 2018, doi: 10.1109/EIConRus.2018.8317214.

[157] A. A. Z. Diab, H. M. Sultan, and O. N. Kuznetsov, “Optimal sizing of hybrid solar/wind/hydroelectric pumped storage energy system in Egypt based on different meta-heuristic techniques,” *Environ. Sci. Pollut. Res.*, vol. 27, no. 26, pp. 32318–32340, 2020, doi: 10.1007/s11356-019-06566-0.

[158] H. M. Sultan, O. N. Kuznetsov, A. S. Menesy, and S. Kamel, “Optimal Configuration of a Grid-Connected Hybrid PV/Wind/Hydro-Pumped Storage Power System Based on a Novel Optimization Algorithm,” *Proc. 2nd 2020 Int. Youth Conf. Radio Electron. Electr. Power Eng. REEPE 2020*, 2020, doi: 10.1109/REEPE49198.2020.9059189.

[159] F. Porté-Agel, M. Bastankhah, and S. Shamsoddin, *Wind-Turbine and Wind-Farm Flows: A Review*, vol. 174, no. 1. Springer Netherlands, 2020. doi: 10.1007/s10546-019-00473-0.

[160] I. Firtina-Ertis, C. Acar, and E. Erturk, “Optimal sizing design of an isolated stand-alone hybrid wind-hydrogen system for a zero-energy house,” *Appl. Energy*, vol. 274, no. May, p. 115244, 2020, doi: 10.1016/j.apenergy.2020.115244.

[161] A. A. Al-Shamma’a and K. E. Addoweesh, “Optimum sizing of hybrid PV/wind/battery/diesel system considering wind turbine parameters using genetic algorithm,” *PECon 2012 - 2012 IEEE Int. Conf. Power Energy*, no. January 2015, pp. 121–126, 2012, doi: 10.1109/PECon.2012.6450190.

[162] International Electrotechnical Committee IEC, “Wind turbines – Part 1: Design requirements,” vol. 2005, no. 2, p. 88, 2005, doi: 10.4172/2155-9600.1000405.

[163] International Electrotechnical Committee IEC, “Wind Turbines - Part 3: Design requirements for offshore wind turbines,” *Eur. Comm. Electrotech. Stand.*, vol. 2009, pp. 1–132, 2009.

[164] Y. Sawle, S. C. Gupta, and A. K. Bohre, "Socio-techno-economic design of hybrid renewable energy system using optimization techniques," *Renew. Energy*, vol. 119, pp. 459–472, 2018, doi: 10.1016/j.renene.2017.11.058.

[165] M. Ray, R. Sheeran, E. Lewis, and J. Cavanagh, "THE CLIMATE CHANGE LEVY AND CLIMATE CHANGE AGREEMENTS A REVIEW BY THE NATIONAL AUDIT OFFICE," *Natl. Audit Off.*, no. August, 2007.

[166] M. A. Ashraf, Z. Liu, A. Alizadeh, S. Nojavan, K. Jermsittiparsert, and D. Zhang, "Designing an optimized configuration for a hybrid PV/Diesel/Battery Energy System based on metaheuristics: A case study on Gobi Desert," *J. Clean. Prod.*, vol. 270, p. 122467, 2020, doi: 10.1016/j.jclepro.2020.122467.

[167] A. Kashefi Kaviani, G. H. Riahy, and S. M. Kouhsari, "Optimal design of a reliable hydrogen-based stand-alone wind/PV generating system, considering component outages," *Renew. Energy*, vol. 34, no. 11, pp. 2380–2390, 2009, doi: 10.1016/j.renene.2009.03.020.

[168] A. Mills and S. Al-Hallaj, "Simulation of hydrogen-based hybrid systems using Hybrid2," *Int. J. Hydrogen Energy*, vol. 29, no. 10, pp. 991–999, 2004, doi: 10.1016/j.ijhydene.2004.01.004.

[169] H. R. Baghaee, M. Mirsalim, G. B. Gharehpetian, and H. A. Talebi, "Reliability/cost-based multi-objective Pareto optimal design of stand-alone wind/PV/FC generation microgrid system," *Energy*, vol. 115, pp. 1022–1041, 2016, doi: 10.1016/j.energy.2016.09.007.

[170] S. Vendoti, M. Muralidhar, and R. Kiranmayi, "Techno-economic analysis of off-grid solar/wind/biogas/biomass/fuel cell/battery system for electrification in a cluster of villages by HOMER software," *Environ. Dev. Sustain.*, vol. 23, no. 1, pp. 351–372, 2021, doi: 10.1007/s10668-019-00583-2.

[171] Y. Wang, B. Seo, B. Wang, N. Zamel, K. Jiao, and X. C. Adroher, "Fundamentals, materials, and machine learning of polymer electrolyte membrane fuel cell technology," *Energy AI*, vol. 1, p. 100014, 2020, doi: 10.1016/j.egyai.2020.100014.

[172] Y. Wang, K. S. Chen, J. Mishler, S. C. Cho, and X. C. Adroher, "A review of polymer electrolyte membrane fuel cells: Technology, applications, and needs on fundamental research," *Appl. Energy*, vol. 88, no. 4, pp. 981–1007, 2011, doi: 10.1016/j.apenergy.2010.09.030.

[173] M. A. Abdelkareem, K. Elsaid, T. Wilberforce, M. Kamil, E. T. Sayed, and A. Olabi,

"Environmental aspects of fuel cells: A review," *Sci. Total Environ.*, vol. 752, p. 141803, 2021, doi: 10.1016/j.scitotenv.2020.141803.

[174] M. M. Samy and S. H. Barakat, "biomass and fuel cells Multi-objective optimization of hybrid renewable energy system based on biomass and fuel cells," no. September, 2020, doi: 10.1002/er.5815.

[175] "MERRA - SoDa." https://www.soda-pro.com/web-services/meteo-data/merra?fbclid=IwAR2vTObCUaC3DpZev3PqLX0FwV-XATjk0E2qDqp1ZRCWIcVxBQBv6eeWTUA (accessed Jul. 01, 2022).

[176] "MERRA - SoDa."

[177] R. Mallipeddi, S. Jeyadevi, P. N. Suganthan, and S. Baskar, "Efficient constraint handling for optimal reactive power dispatch problems," *Swarm Evol. Comput.*, vol. 5, pp. 28–36, 2012, doi: 10.1016/j.swevo.2012.03.001.

[178] S. Kiranyaz, T. Ince, and M. Gabbouj, *Swarm Optimization for Machine Learning and*. 2014.

[179] I. Ahmadianfar, A. A. Heidari, A. H. Gandomi, X. Chu, and H. Chen, "RUN beyond the metaphor: An efficient optimization algorithm based on Runge Kutta method," *Expert Syst. Appl.*, vol. 181, no. January, p. 115079, 2021, doi: 10.1016/j.eswa.2021.115079.

[180] L. dos Santos Coelho, "A quantum particle swarm optimizer with chaotic mutation operator," *Chaos, Solitons & Fractals*, vol. 37, no. 5, pp. 1409–1418, 2008, doi: 10.1016/j.chaos.2006.10.028.

[181] M. Shadman Abid, H. J. Apon, K. A. Morshed, and A. Ahmed, "Optimal Planning of Multiple Renewable Energy-Integrated Distribution System With Uncertainties Using Artificial Hummingbird Algorithm," *IEEE Access*, vol. 10, pp. 40716–40730, 2022, doi: 10.1109/ACCESS.2022.3167395.

[182] A. Ramadan, M. Ebeed, S. Kamel, E. M. Ahmed, and M. Tostado-Véliz, "Optimal allocation of renewable DGs using artificial hummingbird algorithm under uncertainty conditions," *Ain Shams Eng. J.*, no. xxxx, p. 101872, 2022, doi: 10.1016/j.asej.2022.101872.

[183] B. S. Yildiz, P. Mehta, S. M. Sait, N. Panagant, S. Kumar, and A. R. Yildiz, "A new hybrid artificial hummingbird-simulated annealing algorithm to solve constrained mechanical engineering problems," *Mater. Test.*, vol. 64, no. 7, pp. 1043–1050, Jul. 2022, doi: 10.1515/mt-2022-0123.

[184] W. Zhao, L. Wang, and S. Mirjalili, “Artificial hummingbird algorithm: A new bio-inspired optimizer with its engineering applications,” *Comput. Methods Appl. Mech. Eng.*, vol. 388, p. 114194, 2022, doi: 10.1016/j.cma.2021.114194.

[185] I. Ahmadianfar, O. Bozorg-Haddad, and X. Chu, “Gradient-based optimizer: A new metaheuristic optimization algorithm,” *Inf. Sci. (Ny).*, vol. 540, pp. 131–159, 2020, doi: 10.1016/j.ins.2020.06.037.

[186] E. H. Houssein, B. E. Helmy, H. Rezk, and A. M. Nassef, “Engineering Applications of Artificial Intelligence An enhanced Archimedes optimization algorithm based on Local escaping operator and Orthogonal learning for PEM fuel cell parameter identification,” *Eng. Appl. Artif. Intell.*, vol. 103, no. February, p. 104309, 2021, doi: 10.1016/j.engappai.2021.104309.

[187] “Cycle-Tempo.” http://www.asimptote.nl/software/cycle-tempo/ (accessed May 09, 2018).

[188] S. M. Atnaw, S. A. Sulaiman, and S. Yusup, “Influence of Fuel Moisture Content and Reactor Temperature on the Calorific Value of Syngas Resulted from Gasification of Oil Palm Fronds,” *Sci. J.*, vol. 2014, 2014, doi: 10.1155/2014/121908.

[189] J. Dong *et al.*, “Effect of Operating Parameters and Moisture Content on Municipal Solid Waste Pyrolysis and Gasification To cite this version : HAL Id : hal-01609026 E ff ect of Operating Parameters and Moisture Content on Municipal Solid Waste Pyrolysis and Gasi fi catio,” *Energy & Fuels*, vol. 30, no. 5, pp. 3994–4001, 2016.

[190] D. Cocco, P. Deiana, and G. Cau, “Performance evaluation of small size externally fired gas turbine (EFGT) power plants integrated with direct biomass dryers,” *Energy*, vol. 31, pp. 1459–1471, 2006, doi: 10.1016/j.energy.2005.05.014.

[191] P. E. B. de Mello, S. Scuotto, F. dos Santos Ortega, and G. H. B. Donato, “Influence of Turbine Inlet Temperature on the Efficiency of Externally Fired Gas Turbines,” in *Progress in Sustainable Energy Technologies Vol II. Springer, Cham*, vol. II, 2014, pp. 79–95.

[192] S. Mirjalili, S. M. Mirjalili, and A. Lewis, “Grey Wolf Optimizer,” *Adv. Eng. Softw.*, vol. 69, pp. 46–61, 2014, doi: 10.1016/j.advengsoft.2013.12.007.

[193] S. Mirjalili, “SCA: A Sine Cosine Algorithm for solving optimization problems,” *Knowledge-Based Syst.*, vol. 96, pp. 120–133, 2016, doi: 10.1016/j.knosys.2015.12.022.

[194] S. Mirjalili and A. Lewis, “The Whale Optimization Algorithm,” *Adv. Eng. Softw.*, vol.

95, pp. 51–67, 2016, doi: 10.1016/j.advengsoft.2016.01.008.

[195] M. S. Hossain, A. Jahid, K. Z. Islam, and M. F. Rahman, “Solar PV and Biomass Resources-Based Sustainable Energy Supply for Off-Grid Cellular Base Stations,” *IEEE Access*, vol. 8, pp. 53817–53840, 2020, doi: 10.1109/ACCESS.2020.2978121.

[196] L. Abualigah, D. Yousri, M. Abd Elaziz, A. A. Ewees, M. A. A. Al-qaness, and A. H. Gandomi, “Aquila Optimizer: A novel meta-heuristic optimization algorithm,” *Comput. Ind. Eng.*, vol. 157, no. October 2020, p. 107250, 2021, doi: 10.1016/j.cie.2021.107250.

[197] F. A. Hashim, E. H. Houssein, K. Hussain, M. S. Mabrouk, and W. Al-Atabany, “Honey Badger Algorithm: New metaheuristic algorithm for solving optimization problems,” *Math. Comput. Simul.*, vol. 192, pp. 84–110, 2022, doi: 10.1016/j.matcom.2021.08.013.

[198] M. H. Qais, H. M. Hasanien, and S. Alghuwainem, “Transient search optimization: a new meta-heuristic optimization algorithm,” *Appl. Intell.*, vol. 50, no. 11, pp. 3926–3941, 2020, doi: 10.1007/s10489-020-01727-y.

[199] M. H. Hassan, E. H. Houssein, M. A. Mahdy, and S. Kamel, “An improved Manta ray foraging optimizer for cost-effective emission dispatch problems,” *Eng. Appl. Artif. Intell.*, vol. 100, no. January, p. 104155, 2021, doi: 10.1016/j.engappai.2021.104155.

[200] R. M. Rizk-Allah and A. A. El-Fergany, “Effective coordination settings for directional overcurrent relay using hybrid Gradient-based optimizer,” *Appl. Soft Comput.*, vol. 112, p. 107748, 2021, doi: 10.1016/j.asoc.2021.107748.

[201] S. Khalilpourazari, H. Hashemi Doulabi, A. Özyüksel Çiftçioğlu, and G. W. Weber, “Gradient-based grey wolf optimizer with Gaussian walk: Application in modelling and prediction of the COVID-19 pandemic,” *Expert Syst. Appl.*, vol. 177, no. March, pp. 0–2, 2021, doi: 10.1016/j.eswa.2021.114920.

[202] A. Ramadan, S. Kamel, M. H. Hassan, M. Tostado-Véliz, and A. M. Eltamaly, “Parameter estimation of static/dynamic photovoltaic models using a developed version of eagle strategy gradient-based optimizer,” *Sustain.*, vol. 13, no. 23, 2021, doi: 10.3390/su132313053.

[203] M. H. Hassan, S. Kamel, M. A. El-Dabah, and H. Rezk, “A novel solution methodology based on a modified gradient-based optimizer for parameter estimation of photovoltaic models,” *Electron.*, vol. 10, no. 4, pp. 1–23, 2021, doi: 10.3390/electronics10040472.

[204] Y. Fang, I. Ahmadianfar, A. Samadi-Koucheksaraee, R. Azarsa, M. Scholz, and Z. M. Yaseen, “An accelerated gradient-based optimization development for multi-reservoir hydropower systems optimization,” *Energy Reports*, vol. 7, pp. 7854–7877, 2021, doi: 10.1016/j.egyr.2021.11.010.

[205] M. Oszust, “Enhanced Marine Predators Algorithm with Local Escaping Operator for Global Optimization,” *Knowledge-Based Syst.*, vol. 232, p. 107467, 2021, doi: 10.1016/j.knosys.2021.107467.

[206] W. Zhao, L. Wang, and Z. Zhang, “Supply-Demand-Based Optimization: A Novel Economics-Inspired Algorithm for Global Optimization,” *IEEE Access*, vol. 7, pp. 73182–73206, 2019, doi: 10.1109/ACCESS.2019.2918753.

[207] I. Naruei and F. Keynia, *Wild horse optimizer: a new meta-heuristic algorithm for solving engineering optimization problems*, no. 0123456789. Springer London, 2021. doi: 10.1007/s00366-021-01438-z.

[208] S. Kaur, L. K. Awasthi, A. L. Sangal, and G. Dhiman, “Tunicate Swarm Algorithm: A new bio-inspired based metaheuristic paradigm for global optimization,” *Eng. Appl. Artif. Intell.*, vol. 90, no. February, p. 103541, 2020, doi: 10.1016/j.engappai.2020.103541.

Appendix

Short notes on Cycle-Tempo software

A. 1 Cycle-Tempo Overview

Cycle-Tempo is one of the few software packages that developed by TU Delft (Delft University of Technology) as a modern tool for the thermodynamic analysis and optimization of systems for the production of electricity, heat, and refrigeration. It is favorable for:

- Conventional power plants,
- Compression refrigeration and cooling systems
- Unconventional energy systems like:
  - Solar ORC power plants,
  - Tri-generation systems,
  - Absorption-cooling and refrigeration systems
  - Fuel cells,
  - Kalina-cycle power plants,
  - IGCC power plants

A. 2 The Main Screen Contents

Figure A.1 shows what the main screen of the software looks like. It is containing the following:

1. Menu bar

The Menu bar contains the commands that the user will need to perform all kinds of actions such as opening and printing files. When performing one of these commands from the Menu bar, the user will usually be offered another pull-down menu from which can select additional commands. If the status of the program is such that a specific command is not applicable or cannot be executed, the name of that command is dimmed.

2. Tool bar

The Tool bar contains a number of buttons for performing commands that are often used. All commands on the Tool bar can also be found in the Menu bar.

3. The working area

The working area comprises the larger part of the screen. The user can place one or several different windows in the working area as seen in Figure A.2.

4. Index-window

The index-window is designed to give the user an index of the data available while the user is working with the program. The index-window gives an overview of files that are open and what they contain. The data within a file include data concerning the diagram drawn as well as tables and graphs. Each of the windows referred to below can be opened by means of the index-window. Unlike other window types, index-windows can only be opened one at a time.

5. Status bar

The Status bar provides the user with information about the program. The Status bar also provides messages about the program, ranging from general information on this status of the program to error warnings or useful tips. Also, the Status bar will give a brief description of any particular command in the Tool Bar or Menu bar.

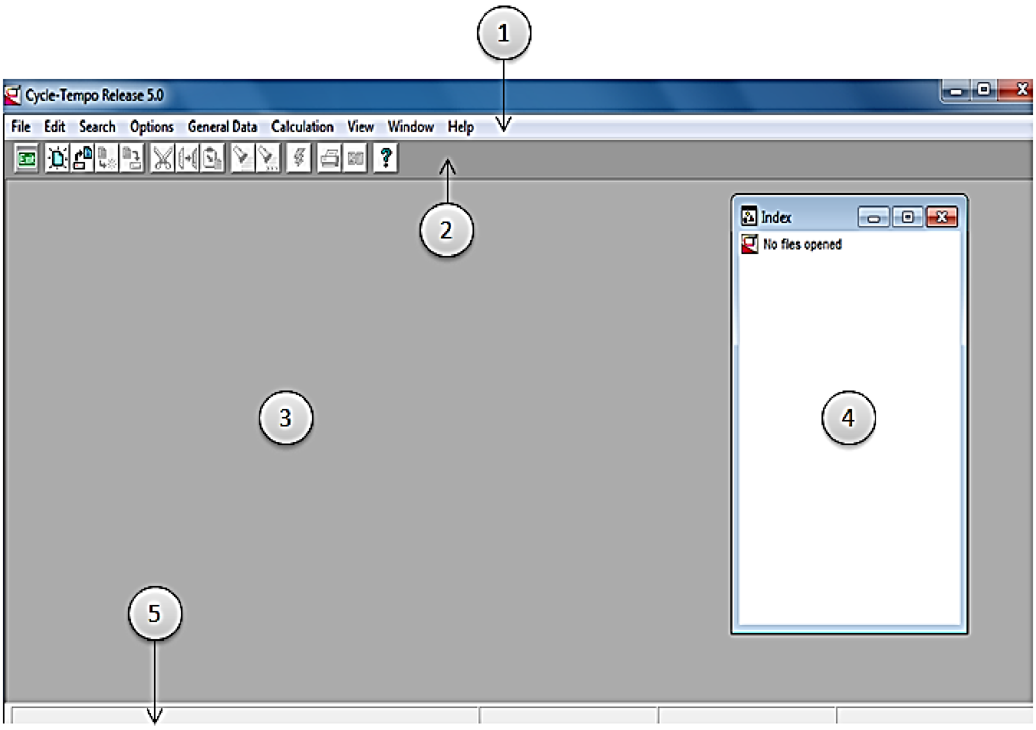

Figure A.1: The main window.

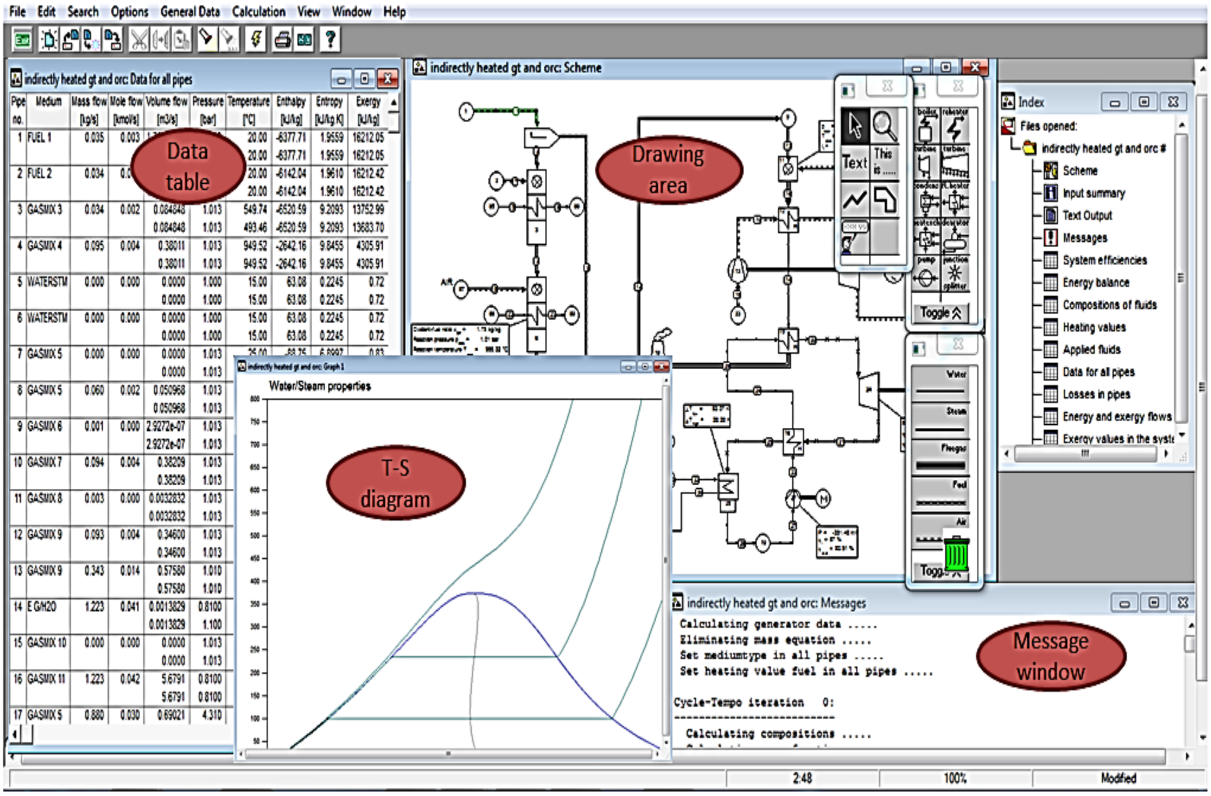

Figure A.2: Windows within the working area.

The diagram is created in a drawing window in Figure A.2. Within this area, you can draw apparatuses, and connect them with pipes. You can also add texts, and activate a properties - window for each object drawn. Results of calculations can also be displayed in this window. After finishing the simulation diagram, and to run it press the run button from the tool bar as shown in Figure A.3.

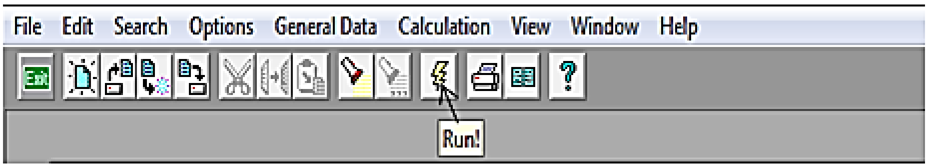

Figure A.3: the run button.

After that to present the results, press the view command from menu bar. Figure A.4 shows a variety of result options. The user can select the appropriate option to display it, then the results would be shown in anew window as shown in Figure A.2.

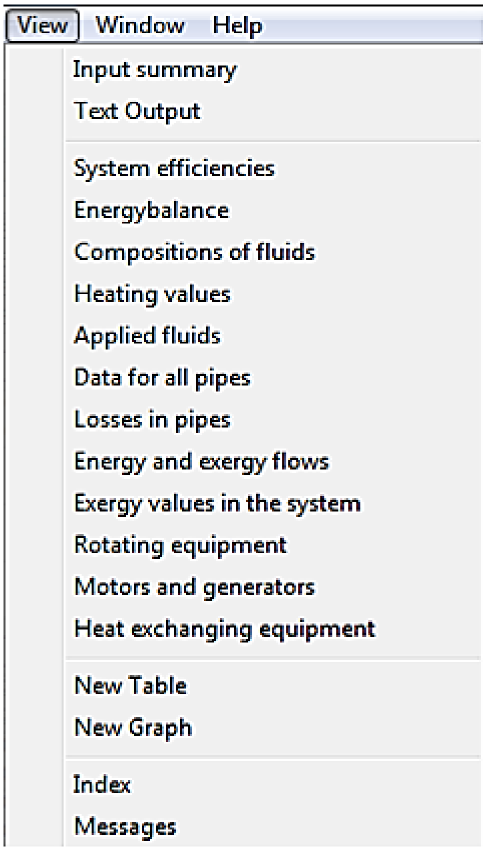

Figure A.4: the view command options.

الملخص العربى

ان استكشاف واستغلال موارد الطاقة المتجددة له أهمية خاصة لتعزيز أمن الطاقة لتقليل الاعتماد على الوقود الأحفوري ومن ثم تقليل آثار الاحتباس الحراري (تقليل انبعاثات الكربون). تعتبر الكتلة الحيوية واحدة من مصادر الطاقة المتجددة القليلة التي لا يعتمد توافرها على الظروف الجوية ويمكن تخزينها وفقًا للطلب ، وبالتالي ، يمكن التنبؤ بتوليد الكهرباء منها بدرجة كبيرة. كما ان الكتلة الحيوية هي مورد طاقة داخلي ويساهم الاستخدام المتزايد لطاقة الكتلة الحيوية في تأمين الإمداد (الموثوقية). يمكن تحويل الكتلة الحيوية إلى أشكال مختلفة من الطاقة باستخدام عمليات مختلفة ومن اهم هذه العمليات عمليه التغويز (Gasification process). حيث يعتبر التوليد الثلاثي للكتلة الحيوية (Trigeneration) مفهومًا جديدًا نسبيًا ، وله القدرة على تحسين اقتصاديات الطاقة الحيوية للمناطق ذات المناخ الدافئ. يمكن تطبيق هذا المفهوم مع تقنيات تحويل الطاقة المختلفة. أيضًا.

خلال هذه الرسالة، تم إجراء تقييم الأداء الأمثل على نظامين مختلفين من أنظمة التبريد والتدفئة والطاقة المشتركة (CCHP) لتقييم النظام المتكامل بدرجة عالية نسبيًا. يتكون نظام CCHP الأول من تكامل وحدة تغويز الطبقة الثابتة السفلية مع التوربينات الغازية الخارجية (EFGT) وهو نظام توليد الطاقة، وجهاز استرداد الحرارة ، ودورة التبريد بالامتصاص لإنتاج طاقة التبريد باستخدام حطب الذره (CS) كمادة وسيطة للكتلة الحيوية ، بينما يتكون النظام الثاني من وحدة احتراق مباشرة ، و التوربينات الغازية الخارجية ، ودورة رانكين عضوية (ORC) كوحدة لزيادة الكفاءة الكهربائية ، ووحدة تبريد بالامتصاص لإنتاج طاقة التبريد باستخدام تفل قصب السكر كمادة وسيطة للكتلة الحيوية.

على الرغم من التطور الكبير على نطاق عالمي في التقنيات المرتبطة بمصادر الطاقة المتجددة ، لا يزال نقص الكهرباء والتكلفة يمثلان مشكلة في المناطق المعزولة النائية وفي الجزر ذات الموارد المتجددة الوفيرة للطاقة. لذلك ، تقدم هذه الأطروحة أيضًا تصميمًا تقنيًا اقتصاديًا لسيناريوهات مختلفة لأنظمة الطاقة الهجينة المستقلة لمناطق مختلفه في مصر ، وتستند هذه النماذج المختلفة للنماذج التقنية والاقتصادية المثلى إلى دمج وحدات تغويز الكتلة الحيوية مع مصادر الاستدامة الأخرى مثل الطاقة الشمسية وطاقة الرياح وما إلى ذلك .

تم إجراء عمليات محاكاة التصميم باستخدام برنامج الديناميكا الحرارية Cycle-Tempo لحل تصميم الأداء الأمثل لنظام CCHP على نطاق صغير ، وخوارزميات التحسين الحديثة والمعدلة استنادًا إلى استخدام برنامج MATLAB لحل التحليل التقني والاقتصادي لشبكة دقيقة هجينة معزولة تتكون من نظام الكتلة الحيوية والألواح الكهروضوئية وتوربينات الرياح والبطاريات أو خلايا الوقود لتلبية الطلب على الكهرباء في القرى الصغيرة أو المناطق النائية في مصر.

الأنظمة الهجينة خارج الشبكة المقترحة التي تم مناقشتها خلال هذه الأطروحة للتحليل الاقتصاد التقني الأمثل هي كما يلي ؛

- نظام هجين مستقل مكون من وحدات الخلايا الشمسيه (PV) ، وتوربينات الرياح (WT) ، ونظام الكتلة الحيوية ، ووحدات البطارية في منطقة أبو منقر ، مصر.
- نظام هجين مستقل مكون من وحدات الخلايا الشمسيه (PV) ، وتوربينات الرياح (WT) ، ونظام الكتلة الحيوية ، ووحدات البطارية في قريه الراشدة بالواحات ، مصر.
- نظام هجين مستقل مكون من وحدات الخلايا الشمسيه (PV) ، ونظام الكتلة الحيوية ، ووحدات البطارية لتغذيه الاحمال بمدينة طيبة الجديدة ، شمال شرق مدينة الأقصر في مصر.
- نظام هجين مستقل مكون من وحدات الخلايا الشمسيه (PV) ، ونظام الكتلة الحيوية ، ، ووحدات خلايا الوقود (FC) ، ووحدات المحلل الكهربائي (ELE) ، ووحدات خزان الهيدروجين (HT) في منطقة أبو منقر ، مصر.

وتحتوي الرسالة علي سبعه أبواب:

الباب الأول وعنوانه **Introduction** :

يحتوي علي مقدمه عامة عن الطاقه المتجدده والكتلة الحيوية ووضعها الحالي .كما يعرض الأهداف الرئيسية للرسالة وتقسيماتها

الباب الثاني وعنوانه **Literature Review** :

يستعرض هذا الباب وضع الطاقة في مصر ومختلف مصادر الطاقة المتجددة (خاصة الكتلة الحيوية) والتوليد الموزع **(DG)** وطرق التحسين المستخدمه لحل المشكلات التقنيه والاقتصاديه المختلفه. كما ان هذا الفصل يقدم مسحًا شاملاً للحلول السابقة التي تم اقتراحها لحل التقنية الاقتصادية المثلى للأنظمة الهجينة المختلفة **(HRES).**

الباب الثالث وعنوانه **Development of CCHP System Based on Biomass Gasification** :

يناقش هذا الفصل نمذجة نظام ثلاثي الطاقه **(CCHP)** لتحويل الكتلة الحيوية إلى طاقة كهربائية وتبريدية وحرارية **.** يتم تحقيق هذا الهدف من خلال تطوير نظامين مختلفين ، يعتمد التكوين الأول على تكامل مغوِّز الطبقة الثابتة السفلية مع نظام التوربينات الخارجيه **(EFGT)** نظام توليد الطاقة ، وجهاز استرداد الحرارة ، ودورة التبريد بالامتصاص ، بينما يتكون النظام الثاني من وحده الحرق المباشر للكتلة الحيوية ، متصلة بنظام التوربينات الخارجيه ووحده توربينات **ORC** ونظام التبريد بالامتصاص.

الباب الرابع وعنوانه **Techno Economic Design of Hybrid Systems with Biomass Gasifier** :

في هذا الفصل ، تم تطوير سيناريوهات **HRPS** مختلفة لأداء الحجم الأمثل لنماذج التحسين الاقتصادي التقني لوحدات الكتلة الحيوية المتكاملة مع أنظمة الطاقة المتجددة الأخرى مثل **PV** و **WT** والبطاريات وخلايا الوقود **(FC)** . كما انه يحتوي علي وصف القيود الرئيسية والوظائف الموضوعية الخاصه بهذه الانظمه ومخطط لشرح عمليه تصميم هذه الانظمه المقترحه.

الباب الخامس وعنوانه **Recent and Developed Optimization Techniques for Optimal Techno Economic** :

في هذا الفصل ، تم اقتراح تقنيات تحسين مختلفة لحل مشكلة الحجم الأمثل والتحسين الاقتصادي لانظمه الطاقه الهجينه المختلفه **(HRPS)** ، كما تم اقتراح تحسينات وتعديلات مختلفة لتحسين أداء خوارزميات التحسين التقليدية.

الباب السادس وعنوانه **Results and Discussion** :

يعرض هذا الفصل مناقشه لنتائج النمذجه التي اجريت للحصول علي التحسين التقني والاقتصادي للحجم الأمثل لسيناريوهات **HRPS** المختلفة باستخدام طرق تحسين مختلفة . حيث تظهر النتائج قوة التقنيات المقترحة للعثور على أفضل حجم للمكونات الأمثل مع هدف تقليل سعر الطاقه **EC** وزيادة الموثوقية **LPSP** ، والتي تفي بالحمل المطلوب للمجتمعات المعزولة .تثبت النتائج التي تم الحصول عليها فعالية التقنيات المقترحة مقارنة بخوارزميات التحسين المعروفة والحديثة.

الباب السابع وعنوانه **Conclusions and Future Works** :

في هذا الباب تم عرض خلاصة للنتائج التي تم التوصل اليها خلال الدراسة ويعرض اقتراحات لدراسات مستقبلية مكملة لهذه الدراسة.

تصميم وتحليل تقني اقتصادي للمغوزات المختلفة لتطبيقات الطاقة الحيوية

مـقدمـة من

المهندسه / هدي عبد الستار حميد ابراهيم

للحصول علي درجة الدكتوراه

فى

الهندسة الكهربية

لجنة الاشراف على الرسالة

التوقيع

1. أ.د. لؤى سعد الدين نصرت - كلية الهندسة - جامعة أسوان ....
2. أ.د. فرانسسكو خورادو- جامعة خاين- أسبانيا ....
3. أ.م.د. صلاح محمد كامل - جامعة أسوان – مصر ....

لجنة المناقشة والحكم على الرسالة

		التوقيع
1. أ.د/ وليد على سيف الاسلام الختام	أستاذ بقسم الهندسة الكهربية - كلية الهندسة - جامعة عين شمس	....
2. أ.د/ عبد الله أحمد ابراهيم	أستاذ متفرغ بقسم الهندسة الكهربية -كلية الهندسة - جامعة أسوان	....
3. أ.د/ لؤى سعد الدين نصرت	أستاذ بقسم الهندسة الكهربية - كلية الهندسة - جامعة أسوان	....

جامعة اسوان

كليـة الهندسـة

تصميم وتحليل تقني اقتصادي للمغوزات المختلفة لتطبيقات الطاقة الحيوية

رسالة علمية مقدمة الى الدراسات العليا بكلية الهندسة

جامعة أسوان

كاستيفاء جزئي لمتطلبات الحصول على درجة الدكتوراه

في

الهندسة الكهربية

مـقدمـة من

المهندسة/ هدي عبد الستار حميد ابراهيم

ماجستير الهنـدسـة الكهربيـة – كلية الهندسة – جامعة أسوان

أكتوبر 2022